ENGINEERING *ESCHERICHIA COLI* TO CONTROL BIOFILM FORMATION, DISPERSAL, AND PERSISTER CELL FORMATION

A Dissertation

by

SEOK HOON HONG

Submitted to the Office of Graduate Studies of
Texas A&M University
in partial fulfillment of the requirements for the degree of

DOCTOR OF PHILOSOPHY

December 2011

Major Subject: Chemical Engineering

ENGINEERING *ESCHERICHIA COLI* TO CONTROL BIOFILM FORMATION, DISPERSAL, AND PERSISTER CELL FORMATION

A Dissertation

by

SEOK HOON HONG

Submitted to the Office of Graduate Studies of
Texas A&M University
in partial fulfillment of the requirements for the degree of

DOCTOR OF PHILOSOPHY

Approved by:

Chair of Committee,	Thomas K. Wood
Committee Members,	Arul Jayaraman
	Zhilei Chen
	Michael J. Benedik
Head of Department,	Charles J. Glover

December 2011

Major Subject: Chemical Engineering

ABSTRACT

Engineering *Escherichia coli* to Control Biofilm Formation, Dispersal,

and Persister Cell Formation. (December 2011)

Seok Hoon Hong, B.S., Seoul National University;

M.S., Seoul National University

Chair of Advisory Committee: Dr. Thomas K. Wood

Biofilms are formed in aquatic environments by the attachment of bacteria to submerged surfaces, to the air/liquid interface, and to each other. Although biofilms are associated with disease and biofouling, the robust nature of biofilms; for example, their ability to tolerate chemical and physical stresses, makes them attractive for beneficial biotechnology applications such as bioremediation and biofuels. Based on an understanding of diverse signals and regulatory networks during biofilm development, biofilms can be engineered for these applications by manipulating extracellular/intercellular signals and regulators.

Here, we rewired the global regulator H-NS of *Escherichia coli* to control biofilm formation using random protein engineering. H-NS variant K57N was obtained that reduces biofilm formation 10-fold compared with wild-type H-NS (wild-type H-NS increases biofilm formation whereas H-NS K57N reduces it) via its interaction with the nucleoid-associated proteins Cnu and StpA. H-NS K57N leads to enhanced excision of the defective prophage Rac and results in cell lysis through the activation of a host killing toxin HokD. We also engineered another global regulator, Hha, which interacts with H-NS, to disperse biofilms. Hha variant Hha13D6 was obtained that causes nearly complete biofilm dispersal by increasing cell death by the activation of proteases.

Bacterial quorum sensing (QS) systems are important components of a wide variety of engineered biological devices, since autoinducers are useful as input signals because they are small, diffuse freely in aqueous media, and are easily taken up by cells. To demonstrate that biofilms may be controlled for biotechnological applications such as biorefineries, we constructed a synthetic biofilm engineering circuit to manipulate biofilm formation. By using a population-driven QS switch based on the LasI/LasR system and biofilm dispersal proteins Hha13D6 and BdcAE50Q (disperses biofilms by titrating cyclic diguanylate), we displaced an existing biofilm and then removed the second biofilm.

Persisters are a subpopulation of metabolically-dormant cells in biofilms that are resistant to antibiotics; hence, understanding persister cell formation is important for controlling bacterial infections. Here, we engineered toxin MqsR with greater toxicity and demonstrated that the more toxic MqsR increases persistence by decreasing the ability of the cell to respond to antibiotic stress through its RpoS-based regulation of acid resistance, multidrug resistance, and osmotic resistance systems.

ACKNOWLEDGEMENTS

I would like to express my gratitude first to my advisor, Dr. Thomas K. Wood, for his excellent guidance, encouragement, and support during my Ph.D. study. I learned his enthusiasm and never-give-up spirit for the research.

I also would like to thank my committee members, Dr. Arul Jayaraman, Dr. Michael J. Benedik, and Dr. Zhilei Chen, for their splendid suggestions and comments for my research. I also thank Dr. Katy Kao for her kind help during my Ph.D. defense.

I thank everybody who has been working with me in Dr. Wood's lab and Dr. Jayaraman's lab. I am especially grateful to Dr. Jintae Lee, Dr. Xiaoxue Wang, and Dr. Younghoon Kim for their help and suggestions. Also, I would like to thank Dr. Jeongyun Kim, Dr. Manjunath Hegde, and Kyungoh Choi for their help.

I appreciate the strains provided by the National Institute of Genetics in Japan, and the support from the Texas Engineering Experiment Station, the National Science Foundation, the National Institutes of Health, and the Korean Government Scholarship.

I would like to express my sincere gratitude to my wife, Haejin, my two sons, Chanjin and Chanyoung, my parents, my brothers and sisters for their love, support, and prayers. None of this would have been possible without my family.

Lastly, I thank God for giving me the wisdom and the strength to challenge and overcome all of the difficulties in my Ph.D. study.

TABLE OF CONTENTS

CHAPTER Page

CHAPTER Page

CHAPTER Page

LIST OF FIGURES

FIGURE Page

LIST OF TABLES

CHAPTER I

INTRODUCTION

1.1 Background and motivation

A majority of bacteria exist in the natural world in sessile biofilm communities rather than as planktonic cells (Donlan and Costerton, 2002). More than 99% of all bacteria are present in biofilms (Navarre *et al.*, 2007), and over 80% of bacterial infections involve biofilms (Sauer *et al.*, 2007). The extracellular polymeric matrix including polysaccharides, proteins, lipids, and DNA holds cells together, forms a protective barrier, and makes biofilm cells more resistant to the host immune system during infection and tolerant to various antimicrobial agents such as disinfectants and antibiotics (Flemming and Wingender, 2010). In addition, biofilms cause biofouling and biocorrosion in industry (Beech *et al.*, 2005). However, biofilms are also beneficial for a wide range of applications including bioremediation, wastewater treatment, production of biofuels and chemicals, inhibition of corrosion, bioMEMS, pharmaceutical testing, and treatment of disease (Wood *et al.*, 2011). Hence, it is important to understand gene regulations in biofilms to both remove deleterious biofilms and to utilize beneficial biofilms.

There are six stages for biofilm development: movement to the surface (Wood *et al.*, 2006), initial reversible attachment, irreversible attachment, small aggregates, mature biofilm, and biofilm dispersal (van Houdt and Michiels, 2005). The biofilm development cycle is an ordered process involving environmental cues and specific gene regulation (Wood *et al.*, 2011). Therefore, to control biofilms, we can either block any of the first five stages or enhance the final dispersal stage based on understanding diverse signals and regulatory networks during biofilm development.

This dissertation follows the style of *Microbial Biotechnology*.

Persister formation in biofilms is the main culprit in the recalcitrance of chronic infections (Lewis, 2010). Persisters are a subpopulation of bacteria that are tolerant to antibiotics without inheritable genetic change (Lewis, 2010). Also, resistance to antibiotics involves *growth* due to mutation whereas persistence does not involve growth (Lewis, 2007). Bacterial toxin/antitoxin (TA) systems are responsible for persister cell formation, as TA genes are induced in biofilms (González Barrios *et al.*, 2006; Kim *et al.*, 2009) and in persister cells (Shah *et al.*, 2006), and the expression of TA modules are frequently linked to the dormant state (Lewis, 2008). Hence, understanding persisters through the study of TA systems may reveal the mechanisms of persister formation and provide insights to develop novel alternative drugs which overcome the limitations of antibiotics to treat chronic bacterial infections.

Directed evolution has been successfully used to engineer proteins for industrial applications as well as to explore natural evolutionary processes (Otten and Quax, 2005). Synthetic biology is also a powerful means to create new biological systems via assembling genetic modules for various applications (Fu, 2006). For example, *Pseudomonas aeruginosa* quorum sensing circuits were utilized in *Escherichia coli* to engineer a bidirectional communication (Brenner et al., 2007), to construct a predator-prey ecosystem (Balagaddé *et al.*, 2008), and to create a synthetic symbiotic ecosystem (Kambam *et al.*, 2008). Thus, genetic engineering may be a promising strategy for controlling biofilm formation and dispersal (Wood *et al.*, 2011).

1.2 Research objectives, importance, and novelty

Escherichia coli is the best-characterized bacterium in microbiology research. Single gene knockout mutants (Keio collection) (Baba *et al.*, 2006) and complementation plasmids (ASKA library) (Kitagawa *et al.*, 2005) provide ready-to-use templates to reveal insights into biological processes. Hence, we use *E. coli* as a model system in this study.

This study seeks to control biofilm formation and dispersal using protein engineering and synthetic biology and to discover biological insights for engineering applications. It also seeks to improve current knowledge about the mechanism of persister cell formation. The specific aims are to:

- Rewire global regulator H-NS to control biofilm formation and to determine how the engineered H-NS regulates biofilm formation.
- Engineer global regulator Hha to control biofilm dispersal as well as biofilm formation.
- Construct a synthetic biofilm circuit to control biofilm displacement via a population-driven QS switch coupled to engineered biofilm dispersal proteins (Hha13D6 and BdcAE50Q).
- Determine how *E. coli* cells become persisters through protein engineering of MqsR of the MqsR/MqsA TA system to increase its toxicity.

To increase the toolkit for manipulating biofilm formation, we have engineered regulator proteins which are known to repress or increase biofilm formation followed by diverse cellular mechanisms. First, we reconfigured *E. coli* quorum sensing regulator SdiA to control biofilm formation using protein engineering (Lee *et al.*, 2009b); SdiA1E11 reduced biofilm formation by 5 to 20 fold by producing 9-fold more indole compared to wild-type SdiA, and SdiA2D10 increased biofilm formation 7 fold in the presence of *N*-octanoyl-*DL*-homoserine lactone and *N*-(3-oxododecatanoyl)-*L*-homoserine lactone.

H-NS is also important in biofilm formation (White-Ziegler and Davis, 2009) since it regulates the transcription of many environmental responsive genes (Dorman, 2004). The goals of this study were to investigate how the global regulator H-NS influences biofilm formation and to determine whether H-NS may be evolved to reduce biofilm formation as well as to derive new insights into how H-NS functions. We identified an H-NS variant with a single amino acid

substitution in the N-terminal oligomerization domain that reduces biofilm formation as a result of its interaction with nucleoid-associated proteins Cnu and StpA, that induces Rac prophage excision, and that induces toxin HokD which leads to cell lysis.

Global regulator Hha was identified as one of the highly induced genes in *E. coli* biofilms relative to planktonic cells (Ren *et al.*, 2004a), and Hha decreases initial biofilm formation by repressing the transcription of rare codon tRNAs and by repressing transcription of fimbrial genes (García-Contreras *et al.*, 2008). Since controlling biofilm dispersal is as important as inhibiting biofilm formation, we engineered the global transcriptional regulator Hha to control biofilm dispersal and biofilm formation. In this study, we showed that the engineered Hha promotes biofilm dispersal by interacting with protease HslV.

Our group also identified and engineered biofilm dispersal protein BdcA which titrates cyclic diguanylate level by binding it (Ma *et al.*, 2011). Here, we devised a biofilm circuit that utilizes two dispersal proteins (Hha13D6 and BdcAE50Q) along with a population-driven LasI/LasR quorum sensing switch. Therefore, for the first time, we showed that the system may be utilized to selectively remove one type of cell from an existing biofilm, and then remove the second biofilm to create a surface ready for additional biofilms.

We also explored how the toxicity of MqsR is related to persistence by using protein engineering to increase the toxicity of MqsR. In this study, we found that MqsR increases persister cell formation by repressing acid resistance, multidrug resistance, and osmotic resistance, and that the general stress response master regulator RpoS is important for persister cell formation.

CHAPTER II

LITERATURE REVIEW*

2.1 Biofilm formation and dispersal

2.1.1 Overview

Biofilms are sessile bacterial communities formed on abiotic (minerals, air-water interfaces) and biotic (plants, animals) surfaces (Karatan and Watnick, 2009) by the production of microbial products including polysaccharides, proteins, lipids, and DNA (Flemming and Wingender, 2010). The vast majority of bacteria exist in biofilms rather than as planktonic cells (Donlan and Costerton, 2002) since the biofilm provides increased tolerance to stress, antibiotics, and host immunological defenses (Beloin *et al.*, 2008).

Biofilms consist of heterogeneous cells (Stewart and Franklin, 2008) that are the result of diverse signals and regulatory networks during biofilm development (Prüß *et al.*, 2006). Hundreds of genes are differentially controlled during the biofilm development process (Schembri *et al.*, 2003; Beloin *et al.*, 2004; Ren *et al.*, 2004a; Domka *et al.*, 2007); some of these regulation pathways include nutrient and metabolic cues, quorum sensing (QS) signals, and cyclic diguanylate (c-di-GMP) signals, while many regulation pathways remain unstudied (Karatan and Watnick, 2009).

Biofilm development is an ordered process involving environmental cues and specific gene regulation (Wood *et al.*, 2011). The biofilm development cycle has six stages: (i) movement of planktonic cells to a solid surface (Wood *et al.*, 2006), (ii) initial reversible attachment of planktonic cells to the surface by fluid stream or through motility, (iii) transition from reversible

---

* Parts of this chapter are reproduced with permission from "Engineering biofilm formation and dispersal" by Thomas K. Wood, Seok Hoon Hong, and Qun Ma, 2011, *Trends in Biotechnology* 29:87-94, Copyright 2011, Cell Press, DOI:10.1016/j.tibtech.2010.11.001.

to irreversible attachment by the production of extracellular polymers by the bacteria and/or by specific adhesins located on pili and fimbriae, (iv) early development of biofilm architecture, (v) development of microcolonies into a mature biofilm with pedestal-like structures, water channels and pores, and (vi) dispersial of cells from the biofilm into the surrounding environment to return cells to the planktonic state (van Houdt and Michiels, 2005).

Biofilm dispersal is an essential stage of the biofilm life cycle that contributes to bacterial survival and disease transmission upon changes of nutrient levels, oxygen tension, pH, and temperature (Kaplan, 2010). Like other stages of biofilm development, biofilm dispersal is a highly-regulated process involving numerous environmental signals, signal transduction pathways, and effectors (Karatan and Watnick, 2009). To date, little is known about the intracellular molecular mechanisms of bacterial biofilm dispersal (Kaplan, 2010); however, several biofilm dispersal signals have been identified including the auto-inducing peptide of the *agr* quorum signaling system of *Staphylococcus aureus* (Boles and Horswill, 2008), changes in carbon sources (Sauer *et al.*, 2004), reduction in the concentration of c-di-GMP (Ma *et al.*, 2011), surfactant (Boles *et al.*, 2005), *cis*-2-decenoic acid (Davies and Marques, 2009), as well as *D*-amino acids (Kolodkin-Gal *et al.*, 2010).

2.1.2 Gene regulation of biofilm formation

Whole-transcriptome profiling has provided robust insights into the biofilm mode of life (Wood, 2009). Stress-related genes are commonly induced in biofilms in DNA microarrays (Wood, 2009); in the temporal biofilm transcriptome study, 42 stress-related genes were induced in biofilms (Domka *et al.*, 2007), and five stress-response genes (*hslST*, *hha*, *soxS*, and *bhsA*) were identified in *E. coli* biofilm cells (Ren *et al.*, 2004a). Corroborating the biofilm transcriptome results and the importance of stress proteins, BhsA decreases biofilm formation and mediates the stress response in *E. coli* by increasing the cell resistance to acid, heat,

hydrogen peroxide and cadmium (Zhang *et al.*, 2007). Hha decreases initial biofilm formation by repressing the transcription of both rare codon tRNAs and fimbrial genes (García-Contreras *et al.*, 2008). In addition, the *ymg* locus is induced in biofilm in several microarrays (Ren *et al.*, 2004b; Herzberg *et al.*, 2006; Domka *et al.*, 2007; Lee *et al.*, 2007b). AriR (previously YmgB) represses biofilm formation in rich medium containing glucose, decreases cellular motility, and increases cell acid resistance via regulating *gadABC* and *hdeABD* (Lee *et al.*, 2007c). Critically, AriR is structurally homologous to Hha, while these two proteins have only 5% sequence identity (Lee *et al.*, 2007c). In addition, the envelope stress-response genes, such as *pspABCDE*, *cpxAR*, *rpoE* and *rseA*, are induced in *E. coli* 8-day-old biofilms cells compared with exponentially growing planktonic cells regardless of the presence of a conjugative plasmid (Beloin et al., 2004). Since these genes are regulated by RpoS, the sigma S factor which regulates a number of stress-related genes, RpoS is important during biofilm formation (Adnan *et al.*, 2010). Cold-shock genes *cspABFGI* and the heat-shock gene *htgA* were induced in a temporal fashion during biofilm formation (Domka *et al.*, 2007). Hence, stress tolerance is realted to biofilm formation and this insight was garnered via whole-transcriptome profiling.

2.1.3 Biofilm formation via cell signaling

Acyl homoserine lactones

Quorum sensing (QS) is a cell communication process in bacteria using the production and detection of extracellular chemicals named autoinducers (Ng and Bassler, 2009). QS allows bacteria to coordinate their gene expression in a population-driven manner (Ng and Bassler, 2009). Acyl homoserine lactones (AHLs) are a major autoinducer signal in Gram-negative bacteria for QS. AHLs consist of homoserine lactone rings carrying acylated chains of 4 to 18 carbons (Ng and Bassler, 2009). The LuxI/LuxR system of *Vibrio fischeri* is the prototypical AHL QS system; in *V. fischeri*, QS regulates light production (Karatan and Watnick, 2009).

Gram-positive bacteria use modified oligopeptides as autoinducers that are detected by membrane-bound two-component signaling proteins that transduce information via a series of phosphorylation events (Ng and Bassler, 2009). Cell signaling plays an important role in biofilm formation (Karatan and Watnick, 2009). In *V. cholerae* and *S. aureus*, increased cell density leads to inhibition of biofilm formation, while activation of QS circuits (two LuxI/R-type QS circuits, LasI/R and RhlI/R) in *Pseudomonas aeruginosa* stimulates biofilm formation (Karatan and Watnick, 2009). In *E. coli*, QS signal autoinducer-2 increases biofilm formation (González Barrios *et al.*, 2006). In addition, although *E. coli* does not produce AHLs since it lacks an AHL synthase, it senses AHL signals with the AHL receptor SdiA, a homologue of LuxR (van Houdt *et al.*, 2006). The addition of exogenous AHLs decreases *E. coli* biofilm formation and depends on SdiA (Lee *et al.*, 2007b).

Indole

Indole is an intercellular signal molecule (Lee *et al.*, 2007a) produced from tryptophan by tryptophanase (TnaA) (Lee *et al.*, 2007b). Indole plays diverse roles including spore formation (Stamm *et al.*, 2005), plasmid stability (Chant and Summers, 2007), drug resistance (Lee *et al.*, 2008b), biofilm formation (Lee *et al.*, 2007b), and virulence (Lee *et al.*, 2009a). In biofilm formation, indole was initially reported to enhance biofilm formation in *E. coli* S17-1, as deletion of *tnaA* in S17-1 reduced biofilm formation and indole restored the *tnaA* biofilm (Di Martino *et al.*, 2003). However, indole inhibits biofilm formation of nine nonpathogenic *E. coli* (Domka *et al.*, 2006; Lee *et al.*, 2007b; Zhang *et al.*, 2007) as well as pathogenic *E. coli* O157: H7 strain (Lee *et al.*, 2007a). Indole decreases *E. coli* biofilms by reducing motility (Domka *et al.*, 2006; Bansal *et al.*, 2007; Lee *et al.*, 2007b), repressing acid resistance genes (Lee *et al.*, 2007b), reducing chemotaxis (Bansal *et al.*, 2007), and reducing attachment to epithelial cells (Bansal *et al.*, 2007). Interestingly, the AHL signal receptor SdiA is also required for indole to

control biofilm formation (Lee *et al.*, 2007b; Lee *et al.*, 2008b). In addition, the effects of indole on biofilm formation, antibiotic resistance, cell division, and the ability to control gene expression are more significant at low temperature (below 37°C) (Lee *et al.*, 2008b).

Autoinducer-2

Autoinducer-2 (AI-2) is a species-nonspecific autoinducer produced by both Gram-negative and Gram-positive bacteria (Xavier and Bassler, 2003). It is synthesized by *S*-ribosylhomocysterine lyase (LuxS), which converts the *S*-ribosylhomocysteine to homocysteine and (*S*)-4,5-dihydroxy-2,3-pentanedione (DPD) then DPD simultaneously changes into AI-2 molecules (Wood, 2009).

TqsA (previously YdgG) was identified in biofilm transcriptome profiling (Ren *et al.*, 2004a) and is important for biofilm formation with the signal molecule AI-2 as TqsA enhances transport of AI-2. Deletion of *tqsA* increases intracellular concentrations of AI-2, which leads to a 7,000-fold increase in biofilm thickness and 574-fold increase in biomass in flow cells (Herzberg *et al.*, 2006). Consistent with these results, addition of AI-2 directly increases biofilm formation and motility (González Barrios *et al.*, 2006). MqsR regulates this AI-2-mediated motility and biofilm phenotype through the two-component motility regulatory system QseBC (González Barrios *et al.*, 2006). In addition, MqsR induces *mcbR* (previously *yncC*) expression (González Barrios *et al.*, 2006). McbR increases biofilm formation by repressing the production of colanic acid which is responsible for colony mucoidy and by repressing the predicted periplasmic protein-encoding gene *ybiM* (Zhang *et al.*, 2008).

c-di-GMP

c-di-GMP is a ubiquitous second messenger that exists in almost all bacteria; it is the central regulator of biofilm formation as it mediates the switch between motile and sessile forms in Gram-negative bacteria (Karatan and Watnick, 2009). c-di-GMP is synthesized from two

guanosine-5'-triphosphate molecules by diguanylate cyclases (DGCs) which contain GGDEF motifs, and is degraded into 5'-phosphoguanylyl-(3'-5')-guanosine and guanosine monophosphate by phosphodiesterases (PDEs) containing EAL or HD-GYP domains (Hengge, 2009). *E. coli* has 30 putative DGCs and PDEs including BdcA (Ma *et al.*, 2011). The redundancy of enzymatic activity of synthesizing or degrading c-di-GMP might be beneficial by allowing bacteria to respond to different environmental conditions (Wood *et al.*, 2011).

c-di-GMP helps biofilms mature by increasing exopolysaccharide production, cell size, and cell aggregation, while decreasing swimming motility and extracellular DNA production (Ma *et al.*, 2011). c-di-GMP binds to the PilZ domains of proteins to regulate exopolysaccharide synthesis, twitching motility, and flagella activity (Hengge, 2009). For example, c-di-GMP binds to the PilZ domain of YcgR of *E. coli* to decrease swimming motility by reducing flagella activity, and thereby increases biofilm formation. High levels of c-di-GMP increase biofilm formation whereas low levels reduce biofilm formation. In contrast, in biofilm dispersal, the decrease in c-di-GMP induces biofilm dispersal by decreasing exopolysaccharide production and by increasing motility (Kaplan, 2010).

2.1.4 Biofilms and disease

More than 99% of all bacteria are present in biofilms (Navarre *et al.*, 2007), and over 80% of human bacterial chronic inflammatory and infectious diseases (Sauer *et al.*, 2007) including periodontitis, native valve endocarditis, cystic fibrosis, otitis media, and chronic bacterial prostatitis are biofilm associated (Donlan and Costerton, 2002). Biofilms also colonize various medical devices such as prosthetic heart valves, central venous catheters, urinary catheters, contact lenses, intrauterine devices, and dental unit water lines (Donlan and Costerton, 2002). The economic costs to treat biofilms are high; for example, biofilms of uropathogenic *E. coli* cause urinary tract infections that result in 8 million annual trips to physicians in the United

States (Foxman, 2002), and enterohemorrhagic *E. coli* (EHEC) infections in the gastrointestinal (GI) tract are also important, as there are 73,000 EHEC-related illnesses annually in the United states, which leads to over 2,000 hospitalizations and 60 deaths, and the economic costs are up to $405 million (Frenzen *et al.*, 2005). The biofilm matrix formed by the microbial products (Flemming and Wingender, 2010), the induction of stress responsive genes in biofilms (Wood, 2009), and the non-metabolizing nature of some biofilm cells (Lewis, 2010) protect biofilm bacteria against from some antibiotic agents; biofilm cells are 1000-fold more resistant to various antibiotics than the same bacterium grown in planktonic culture (Davies, 2003). In addition, bacteria in biofilms gain tolerance to adverse environmental conditions such as chemicals, limited nutrition (Steinberger *et al.*, 2002) and improper temperatures (Kubota *et al.*, 2008). Hence is it important to discern the genetic basis of bacteria in biofilms to develop appropriate treatment strategies for bacterial infections.

2.2 Controlling biofilm formation and dispersal

2.2.1 Overview

The multicellular behavior of cells in biofilms makes it difficult to avoid bacterial infections during surgery (Bendouah *et al.*, 2006) as well as biofouling in industry (Beech *et al.*, 2005). Hence, it is important to control biofilm formation for engineering and medical applications such as reducing corrosion (Jayaraman *et al.*, 1999), facilitating remediation (Wood, 2008), and reducing disease (Jayaraman and Wood, 2008). Altering genetic circuits and cell signaling through genetic engineering and synthetic biology provides new methods for controlling biofilms for engineering applications (Wood *et al.*, 2011). Furthermore, compounds controlling the expression of virulence genes and QS are important for the design and development of

biofilm inhibiting compounds (Lesic et al., 2007), since effective biofilm inhibitors may be useful for various diseases (Cegelski *et al.*, 2008).

2.2.2 Genetic engineering to control biofilm formation and dispersal

Protein engineering and recombinant engineering are promising strategies for controlling biofilm formation as well as for promoting biofilm dispersal (Wood *et al.*, 2011). The first engineered biofilm utilized *Bacillus subtilis* to secrete the peptide antimicrobials indolicidin and bactenecin to inhibit the growth of sulfate-reducing bacteria in the biofilm (without harming the protective *B. subtilis* biofilm) and thereby decreased corrosion (Jayaraman *et al.*, 1999). An external stressor (UV light) also has been used to control the biofilm formation of a single *E. coli* strain through activation of the protease activity of RecA (Kobayashi *et al.*, 2004). In addition, the first synthetic circuit was created to control biofilm formation via an external signal by manipulating indole concentrations via toluene *o*-monooxygenase in a consortium of *Pseudomonas fluorescens* and *E. coli* (Lee *et al.*, 2007b). Furthermoe, protein engineering of the QS regulator SdiA enabled the control *E. coli* biofilm formation; upon addition of the extracellular signal AHLs, biofilm formation was increased with SdiA variant 2D10, and SdiA variant 1E11 increased the concentration of the biofilm inhibitor indole and thereby reduced biofilm formation (Lee *et al.*, 2009b).

To remove existing biofilms, BdcA (previously YjgI) has been engineered to cause biofilm dispersal by decreasing the concentration of second messenger c-di-GMP by binding it. Engineered BdcA induced nearly complete dispersal of biofilms via greater c-di-GMP binding without affecting initial biofilm formation (Ma *et al.*, 2011). Bacteriophages have also been engineered to control biofilm dispersal. Dispersin B from *Actinobacillus actinomycetemcomitans* is an enzyme that disrupts the glycosidic linkages of polymeric β-1,6-*N*-acetyl-*D*-glucosamine found in the biofilm matrix (Itoh *et al.*, 2005). *dspB* encoding dispersin B has been cloned into a

T7 bacteriophage under control of the T7φ10 promoter so it is transcribed during infection and resulted in nearly 100% dispersal of an *E. coli* biofilm (Lu and Collins, 2007). However, the use of bacteriophage has limitations fordispersing multi-species biofilms, since phages are usually very strain-specific (Wood *et al.*, 2011).

2.2.3 Synthetic biology and quorum sensing

Synthetic biology is an emerging field to create new biological systems that do not exist in nature by assembling genetic modules (Fu, 2006) including switches, cascades, pulse generators, time-delayed circuits, oscillators, spatial patterning, and logic formulas. These pieces can be utilized to control transcription, translation, and post-translational operations in order to tune gene expression, protein production, metabolism, and cell-cell communication (Purnick and Weiss, 2009). Synthetic biology may provide innovative methods for bioremediation, sustainable energy production, and biomedical therapies (Purnick and Weiss, 2009).

Bacterial QS systems have been important components of a wide variety of engineered biological devices (Hooshangi and Bentley, 2008), since autoinducers are useful as input signals because most are small, diffuse freely in aqueous media, and are easily imported by cells (Choudhary and Schmidt-Dannert, 2010). Because the engineered cells synthesize their own QS signals, they are able to monitor their cell density and modulate their activities (Ryan and Dow, 2008) without supervision. For example, LuxI from *Vibrio fischeri*, which produces *N*-(3-*oxo*-hexanoyl)-*L*-homoserine lactone (3*o*C6HSL) and AiiA from *Bacillus thuringiensis*, which degrades 3*o*C6HSL, were utilized to generate synchronized oscillations (Danino *et al.*, 2010). Also, the LuxI/LuxR QS system was coupled to the production of a toxin protein CcdB to induce cell death at high cell densities (You *et al.*, 2004).

The two best-characterized QS systems of *Pseudomonas aeruginosa* are the LasI/LasR and RhlI/RhlR systems, which regulate biofilm formation, virulence, swarming motility, and

antibiotic efflux pumps (Williams and Cámara, 2009). LasI produces autoinducer molecule, *N*-(3-*oxo*-dodecanoyl)-*L*-homoserine lactone (3*o*C12HSL), which is sensed by LasR (Pesci *et al.*, 1997). Likewise, RhlI produces *N*-butyryl-*L*-homoserine lactone (C4HSL) that is sensed by RhlR (Pesci *et al.*, 1997). The LasI/LasR and RhlI/RhlR QS systems have been used to engineer bidirectional communication to exhibit a consensus gene expression response in a biofilm consortium (Brenner et al., 2007), and the LasI/LasR QS system was used to both construct a predator-prey ecosystem showing extinction, coexistence, and oscillatory dynamics of the predator and prey populations (Balagaddé *et al.*, 2008) and create a synthetic symbiotic ecosystem in *E. coli* (Kambam *et al.*, 2008). Furthermore, the RhlI/RhlR QS system was utilized to demonstrate roles for self-organization and aggregation in a synthetic biofilm consortium (Brenner and Arnold, 2011). Hence, synthetic QS circuit systems have potential in that population-driven QS switches may be utilized to develop synthetic genetic networks for a variety of applications including controlling biofilm formation and dispersal.

2.2.4 Biofilm inhibitors

Furanone

Furanone produced by *Delisea pulchra* inhibits biofilm development by interfering with bacterial QS; furanone has a similar structure to AHLs (Nys *et al.*, 2006). Furanone and furanone derivatives possess antitumor, antiviral, anti-inflammatory, and antimicrobial activities (Kim *et al.*, 2008). Furanone inhibits the bioluminescence of *V. harveyi* (Manefield *et al.*, 2000). In *P. aeruginosa*, furanone represses biofilm formation infection in mice (Hentzer *et al.*, 2003), and pyoverdine production (Ren and Wood, 2005). Furanone also inhibits QS in *Serratia liquefaciens* MG1 (Rasmussen *et al.*, 2000) and the expression of virulence genes in *B. anthracis* (Jones *et al.*, 2005). In *E. coli*, furanone inhibits QS by masking AI-2 signaling and thereby

inhibits biofilm formation by repressing chemotaxis, flagellar synthesis, and motility genes (Ren *et al.*, 2004b).

7-hydroxyindole

Indole is readily converted into indigo, indirubin, hydroxyindole, and isatin (Rui *et al.*, 2005) via many bacterial oxygenases such as dioxygenases from *Pseudomonas putida* PpG7 (Ensley *et al.*, 1983), *Ralstonia picketti* PKO1 (Fishman *et al.*, 2005), and *Burkholderia cepacia* G4 (Rui *et al.*, 2005). Indole derivatives are important in bacterial virulence and biofilm formation. Indole-class compound CBR-4830 inhibits *P. aeruginosa* growth through MexAB-OprM multidrug efflux pump (Robertson *et al.*, 2007), and indole-3-acetic acid increases the virulence of *Agrobacterium tumefaciens* (Gafni *et al.*, 1995) and inhibits the expression of type III secretion system (Shen *et al.*, 2008). 7-hydroxyindole (7-HI) represses biofilm formation of *E. coli* K-12 and EHEC and induces the biofilm formation of *P. aeruginosa* without affecting the growth of planktonic cells, while isatin stimulates biofilm formation of EHEC (Lee *et al.*, 2007a). 7HI diminishes *P. aeruginosa* virulence by decreasing production of pyocyanin, rhamnolipid, PQS, and pyoverdine and by enhancing antibiotic resistance (Lee *et al.*, 2009a). In addition, 7-HI decreases pulmonary colonization of *P. aeruginosa* in guinea pigs (Lee *et al.*, 2009a).

5-fluorouracil

5-fluorouracil (5-FU) is a pyrimidine analog which is used in the treatment of a range of cancers including colorectal and breast cancers and cancers of the aerodigestive tract (Longley *et al.*, 2003). 5-FU represses biofilm formation, abolishes QS phenotypes, and reduces virulence in *P. aeruginosa* (Ueda et al. 2009). 5-FU is also a biofilm inhibitor of *Staphylococcus epidermis* (Hussain et al. 1992). In *E. coli*, uracil-related genes are repressed by the addition of indole at 30°C and are induced by the addition of AI-2 at 37°C (Lee *et al.*, 2008b), which gives an insight that uracil is important for *E. coli* biofilm formation. 5-FU decreases biofilm formation in a dose

dependent manner in *E. coli* K-12 through AriR, a global regulator that controls acid resistance, and represses the expression of virulence genes in EHEC (Attila *et al.*, 2009).

2.2.5 Biofilm dispersal signals

Nitric oxide

Nitric oxide (NO), a reactive nitrogen intermediate, is used widely in many signaling and regulatory pathways in biological systems (Nathan, 2003). NO has been shown to induce dispersal of *P. aeruginosa* biofilms (Barraud *et al.*, 2006). Addition of low levels of sodium nitroprusside, a NO donor, induces biofilm dispersal, and cells lacking nitrite reductase, the only enzyme capable of generating metabolic NO through anaerobic respiration, does not disperse. The mechanism of biofilm dispersal by NO is NO stimulates PDE activity to decrease in c-di-GMP levels, and thereby triggers planktonic growth by inducing cell motility (Barraud *et al.*, 2009b). NO is a promising dispersal agent not only for single-species biofilms including Gram-negative and Gram-positive bacteria and yeasts but also for multi-species biofilms of clinical and industrial relevance (Barraud *et al.*, 2009a).

cis-2-decenoic acid

Fatty acid derivatives mediate intra- and interkingdom cell- communication (Wang *et al.*, 2004) in several bacteria by regulating the production of extracellular proteases, exopolysaccharide production, aggregative behavior, biofilm formation, flagellum synthesis, resistance to toxins, activation of oxidative stress, and activation of aerobic respiration (Davies and Marques, 2009). Diffusible signal factor (DSF) identified as *cis*-11-methyl-2-dodecenoic acid (Wang *et al.*, 2004) is the best characterized fatty acid and regulates virulence in *Xanthomonas campestiris* (Barber *et al.*, 1997) and triggers biofilm dispersal by inducing the production of the enzyme endo-β-1,4-mannanase responsible for degrading biofilm matrix (Dow *et al.*, 2003). *P. aeruginosa* produces *cis*-2-decenoic acid which is structurally similar to DSF

(Davies and Marques, 2009). *cis*-2-decenoic acid induces biofilm dispersal and inhibits biofilm development (Davies and Marques, 2009) probably via the degradation of biofilm matrix (Dow *et al.*, 2003). This molecule also induces dispersal of biofilms of several bacteria including *E. coli*, *Klebsiella pneumoniae, Proteus mirabilis*, *Streptococcus pyogenes*, *B. subtilis*, *S. aureus*, as well as the yeast *Candida albicans* (Davies and Marques, 2009).

***D*-amino acid**

All biological systems predominantly synthesize and use *L*-amino acids, but *D*-amino acids such as *D*-alanine and *D*-glutamate are also produced by the action of racemases (Yoshimura and Esak, 2003) and accumulated at millimolar levels in bacteria (Lam *et al.*, 2009). *D*-amino acids have been shown to regulate stationary phase cell wall synthesis by contributing to peptidoglycan composition, amount, and strength (Lam *et al.*, 2009). In *B. subtilis*, *D*-amino acids induce the release of amyloid fibers in the biofilm matrix and trigger dispersal of biofilms and inhibit biofilm formation by *S. aureus* and *P. aeruginosa* (Kolodkin-Gal *et al.*, 2010). Hence, *D*-amino acids may be a cell survival strategy in environmental change (Lam *et al.*, 2009) through inducing biofilm dispersal (Kolodkin-Gal *et al.*, 2010).

2.3 Persister cell formation

2.3.1 Overview

Persisters comprise a subpopulation of bacteria that become highly tolerant to antibiotics and reach this state without undergoing genetic change (Lewis, 2010). Many chronic bacterial infections are associated with the formation of biofilms (Costerton *et al.*, 1999). Persister cells in biofilms appear to be responsible for the recalcitrance of chronic infections since antibiotics kill the majority of cells but persisters remain viable and repopulate biofilms when the level of antibiotics drops (Lewis, 2010). Persisters are less sensitive to antibiotics since the cells are not

undergoing cellular activities that antibiotics corrupt which results in tolerance. In contrast, resistance mechanisms arise from genetic changes that block antibiotic activity which results in resistance; i.e., cells grow in the presence of antibiotics when they are resistant whereas persister cells do not grow and are dormant (Lewis, 2007). Therefore, understanding persister cell formation is important to derive strategies for controlling bacterial infections. However, the genetic mechanism of persister cell formation is not fully understood.

2.3.2 Persistence vs. resistance

Persister cells are no more than 1% of stationary-phase cultures (Lewis, 2007). They survive elevated levels of antibiotics even though their offspring exhibit the same antibiotic sensitivity as the original population, demonstrating that the appearance of persisters is not a consequence of stable resistance-conferring mutations (De Groote et al., 2011). Persisters are dormant and have little or no cell-wall synthesis, translation or topoisomerase activity; hence, antibiotics are unable to corrupt the function of their target molecules (Lewis, 2007). Thus the persister cells survive but do not proliferate while the antibiotics are present (Lewis, 2007).

Resistance is the result of heritable genetic changes that allow the cells to grow in the presence of the antibiotic (Lewis, 2007). Bacteria rapidly evolve and develop resistance to antibiotics (De Groote et al., 2011). The main types of resistance are target modification by mutation or by specialized enzymatic changes, target substitution such as expressing an alternative target, antibiotic modification or destruction, antibiotic efflux, and restricted permeability to antibiotics (Lewis, 2007).

2.3.3 Gene regulation of persister cell formation

To investigate the mechanism of persister cell formation, an *E. coli* transposon insertion library was screened for reduced tolerance with kanamycin (Hu and Coates, 2005) and the Keio mutants were screened for reduced tolerance with ofloxacin (Hansen *et al.*, 2008). Although both

screens failed to find a single mutant completely lacking persisters, this failure provided an insight that persister cell formation has a high degree of redundancy (Lewis, 2010). The redundancy of persister formation is demonstrated in that the genes encoding global regulators such as DksA, DnaKJ, HupAB, and IhfAB and encoding nucleotide metabolism such as YgfA and YigB decrease the persister phenotype upon deletingthe genes and increase persistence upon producing the proteins (Hansen *et al.*, 2008). In addition, the SOS response induces persister formation when exposed to a DNA-damaging antibiotic, through the induction of toxin/antitoxin (TA) genes (Lewis, 2010). For example, deletion of *tisAB/istR* of *E. coli*, a particular SOS-TA locus, decreases persister formation dramatically (Dörr *et al.*, 2010). To perform a whole-transcriptome analysis, persister cells were isolated using a flow cytometer with a GFP-tagged *E. coli*; dormant cells are dim where active cells glow green (Shah *et al.*, 2006). Transcriptome results revealed that several TA modules (RelBE, MazEF, DinJYafQ, and MqsR/MqsA) are up-regulated in persister cells (Shah *et al.*, 2006).

2.3.4 Persisters and toxin/antitoxin system

Persister cell formation appears to be one of the main physiological roles of TA systems (Dörr *et al.*, 2010; Kim and Wood, 2010; Maisonneuve *et al.*, 2011; Wang and Wood, 2011), as TA modules induce dormancy (Lewis, 2008). TA systems are diverse and abundant in prokaryotic cells (Leplae *et al.*, 2011), and typically consist of two genes in one operon encoding a stable toxin that disrupts an essential cellular process and a labile antitoxin that neutralizes toxicity by binding to the protein or to the mRNA of the toxin (Wang and Wood, 2011). Since the role of TA systems in cell physiology is not well understood, nine possible roles have been proposed (Magnuson, 2007): addictive genomic debris, stabilization of genomic parasites, selfish alleles, gene regulation, growth control, persister cell formation, programmed cell arrest, programmed cell death, and anti-phage measures. Recently, two new roles of TA modules in cell

physiology have been discovered including influencing biofilm formation (González Barrios *et al.*, 2006; Kim *et al.*, 2009), and mediating the general stress response by controlling the stationary-phase sigma factor RpoS (Wang *et al.*, 2011).

Many bacterial chromosomes have several TA systems; for example, *E. coli* has 37 TA systems (Tan *et al.*, 2011), and *Mycobacterium tuberculosis* has at least 88 TA systems (Belitsky *et al.*, 2011). The various TA systems may allow the cell to respond to a specific stress or groups of stresses in a highly-regulated, elegant fashion (Wang and Wood, 2011). Hence, there are many TA systems involved in diverse regulatory pathways, but our understanding of these regulatory systems is far from complete.

Transcriptome analysis of persister cells demonstrates that several TA modules play an important role in persister formation (Shah *et al.*, 2006). Among *E. coli* TA loci, the MqsR/MqsA TA pair was the first to be shown to have a definitive role in persistence; deletion of the *mqsRA* locus or deletion of *mqsR* alone decreases persister cell formation and production of MqsR/MqsA increases the number of persisters (Kim and Wood, 2010). Furthermore, *mqsR* is the most-induced gene in persister cells compared to non-persisters (Shah *et al.*, 2006), and in whole-transcriptome studies to probe the impact of kanamycin on cell physiology, *mqsRA* was found to be one of the most-highly-induced operons (Kohanski *et al.*, 2007). MqsR was first identified in a whole-transcriptome study of biofilms cells as an induced gene (Ren *et al.*, 2004a), and MqsR/MqsA was linked to biofilm formation and motility via the autoinducer-2 quorum sensing system (González Barrios *et al.*, 2006). The three dimensional structure of MqsR/MqsA revealed that MqsR is an RNase similar to RelE and YoeB (Brown *et al.*, 2009) that cleaves mRNA at GCU sites (Yamaguchi *et al.*, 2009), and MqsR toxicity requires protease Lon and ClpXP (Kim *et al.*, 2010b; Wang *et al.*, 2011). Similar to MqsR, the TisAB/IstR-1 TA system of *E. coli* decreases persistence to ciprofloxacin upon deletion (Dörr *et al.*, 2010). Furthermore,

multiple deletions of TA loci decrease persister formation and the protease Lon-mediated degradation of antitoxin increases persister formation by inducing activity of RNase toxins (Maisonneuve *et al.*, 2011). Hence, TA systems are directly or indirectly associated with persister formation. We hope to determine how TA systems affect persistence by creating a toxin that has elevated toxicity.

CHAPTER III

CONTROLLING BIOFILM FORMATION, PROPHAGE EXCISION, AND CELL DEATH BY REWIRING GLOBAL REGULATOR H-NS OF *ESCHERICHIA COLI*[*]

3.1 Overview

The global regulator H-NS of *Escherichia coli* controls genes related to stress response, biofilm formation, and virulence by recognizing curved DNA and by silencing acquired genes. Here, we rewired H-NS to control biofilm formation using protein engineering; H-NS variant K57N was obtained that reduces biofilm formation 10-fold compared to wild-type H-NS (wild-type H-NS increases biofilm formation whereas H-NS K57N reduces it). Whole-transcriptome analysis revealed that H-NS K57N represses biofilm formation through its interaction with the nucleoid-associated proteins Cnu and StpA and in the absence of these proteins, H-NS K57N was unable to reduce biofilm formation. Significantly, H-NS K57N enhanced the excision of defective prophage Rac while wild-type H-NS represses excision, and H-NS controlled only Rac excision among the nine resident *E. coli* K-12 prophages. Rac prophage excision not only led to the change in biofilm formation but also resulted in cell lysis through the expression of toxin HokD. Hence, the H-NS regulatory system may be evolved through a single amino acid change in its N-terminal oligomerization domain to control biofilm formation, prophage excision, and apoptosis.

---

* Reprinted with permission from "Controlling biofilm formation, prophage excision, and cell death by rewiring global regulator H-NS of *Escherichia coli*" by Seok Hoon Hong, Xiaoxue Wang, and Thomas K. Wood, 2010, *Microbial Biotechnology* 3:344-356, Copyright 2010 Society for Applied Microbiology and Blackwell Publishing Ltd, DOI: 10.1111/j.1751-7915.2010.00164.x. S.H. Hong and X. Wang performed temporal biofilm measurement. S.H. Hong was responsible for the rest of the experiments.

3.2 Introduction

Biofilm formation converts single cells into a complex heterogeneous community (Stewart and Franklin, 2008) attached to a surface and requires precise regulation of many genes (Karatan and Watnick, 2009). For example, genes related to stress response, quorum sensing (QS), motility, fimbriae, metabolism, and transport are differentially regulated in *Escherichia coli* biofilms (Domka *et al.*, 2007). It is important to control biofilm formation for engineering and medical applications such as reducing corrosion (Jayaraman *et al.*, 1999), facilitating remediation (Wood, 2008), and reducing disease (Jayaraman and Wood, 2008).

The histone-like nucleoid structuring protein H-NS is widely conserved in Gram negative bacteria (Tendeng and Bertin, 2003) and is a global regulator that represses transcription (Dorman, 2004) by recognizing intrinsically curved DNA sequences (Rimsky, 2004). H-NS is a small protein (137 amino acids) that is very abundant with more than 20,000 copies per cell (Rimsky, 2004). H-NS regulates the transcription of many environmental responsive genes; for example, H-NS represses the locus of enterocyte effacement (LEE) in enteropathogenic and enterohemorrhagic *E. coli* by binding LEE regulatory DNA (Mellies *et al.*, 2007) and decreases resistance to high osmolarity and low pH in *E. coli* K-12 (Hommais *et al.*, 2001). H-NS consists of a N-terminal oligomerization domain (1-64 aa), a C-terminal DNA-binding domain (90-137 aa), and a flexible linker (65-89 aa) between both domains (Dorman, 2004). Interactions between the N-terminus of H-NS and other nucleoid-associated proteins enhance their activities (Fang and Rimsky, 2008) as H-NS increases repression by Hha of the hemolysin operon (Madrid *et al.*, 2007) and protects StpA from Lon-mediated proteolysis which results in increased viability of stationary phase cells (Johansson and Uhlin, 1999). To date, little is known about H-NS and its effect on biofilm formation; however, H-NS regulates genes related to biofilm formation in a temperature dependent manner (White-Ziegler and Davis, 2009), and the deletion of *hns*

decreases biofilm formation (Belik *et al.*, 2008).

H-NS also silences genes acquired from lateral transfer in that H-NS recognizes foreign DNA with AT-rich content compared to the resident genome (Navarre *et al.*, 2007). Prophage genes are obtained from lateral transfer and are common in most bacterial genomes contributing as much as 10-20% of a bacterium's genome (Casjens, 2003). *E. coli* K-12 has six cryptic prophage and three prophage-like elements (http://www.ecogene.org/) which have lost some functions essential for lytic growth such as excision, tail flagella formation, and the production of phage particles yet these loci retain some functional genes (Blattner *et al.*, 1997). H-NS completely or partially binds prophage and prophage-like DNA in *E. coli* (Oshima *et al.*, 2006), and the H-NS-Hha complex tightly silences foreign DNA (Baños *et al.*, 2009). However, the specific function of H-NS for prophage gene regulation remains unclear.

Previously we discovered that the global regulator Hha decreases biofilm formation and regulates the cryptic prophages CP4-57 and DLP12 (García-Contreras *et al.*, 2008). Deletions of single genes of these prophages increased or decreased biofilm formation significantly, and Hha induced excision of CP4-57 (Wang *et al.*, 2009). Although Hha decreases biofilm formation (García-Contreras *et al.*, 2008) and H-NS increases biofilm formation (Belik *et al.*, 2008), Hha can be functionally equivalent to the N-terminal domain of H-NS as demonstrated by a chimeric Hha-H-NS protein with Hha fused to the N-terminus of H-NS which complements some of the *hns*-induced phenotypes (Rodríguez *et al.*, 2005). Thus, both Hha and H-NS control prophage excision as well as influence biofilm formation.

Directed evolution is a useful tool to engineer proteins for industrial applications as well as to explore natural evolutionary processes (Otten and Quax, 2005). Since cell communication and biofilm formation are important for bacterial survival in microbial consortia (Jayaraman and Wood, 2008), bacteria may readily evolve global regulators for enhanced fitness. Illustrating this

concept, we evolved the *E. coli* QS regulator SdiA to control biofilm formation via the extracellular signals indole and *N*-acylhomoserine lactone (Lee *et al.*, 2009b).

The aims of this study were to investigate how the global regulator H-NS influences biofilm formation and to determine whether H-NS may be evolved to reduce biofilm formation as well as to derive new insights for how the structure of H-NS impacts its function. We identified an H-NS variant with a single amino acid substitution in the N-terminal oligomerization domain that reduces biofilm formation as a result of its interaction with nucleoid-associated proteins Cnu and StpA, that induces Rac prophage excision, and that induces toxin HokD which leads to cell lysis.

3.3 Results

3.3.1 Hha decreases biofilm formation and H-NS increases biofilm formation

Previously, we reported that Hha is highly induced in biofilm cells of *E. coli* (Ren *et al.*, 2004a) and that Hha decreases biofilm formation by repressing the transcription of rare codon tRNA and by repressing transcription of fimbrial genes (García-Contreras *et al.*, 2008). Deletion of *hns* decreases biofilm formation in *E. coli* (Belik *et al.*, 2008), though its deletion increases biofilm formation in *Actinobacillus pleuropneumoniae* (Dalai *et al.*, 2009). Consistently, we found that overexpressing Hha in BW25113 *hha hns* reduced biofilm formation after 24 h, while overexpressing H-NS in the same host increased biofilm formation. Overexpressing both Hha and H-NS resulted in an intermediate amount of biofilm formation (Fig. 3.1A).

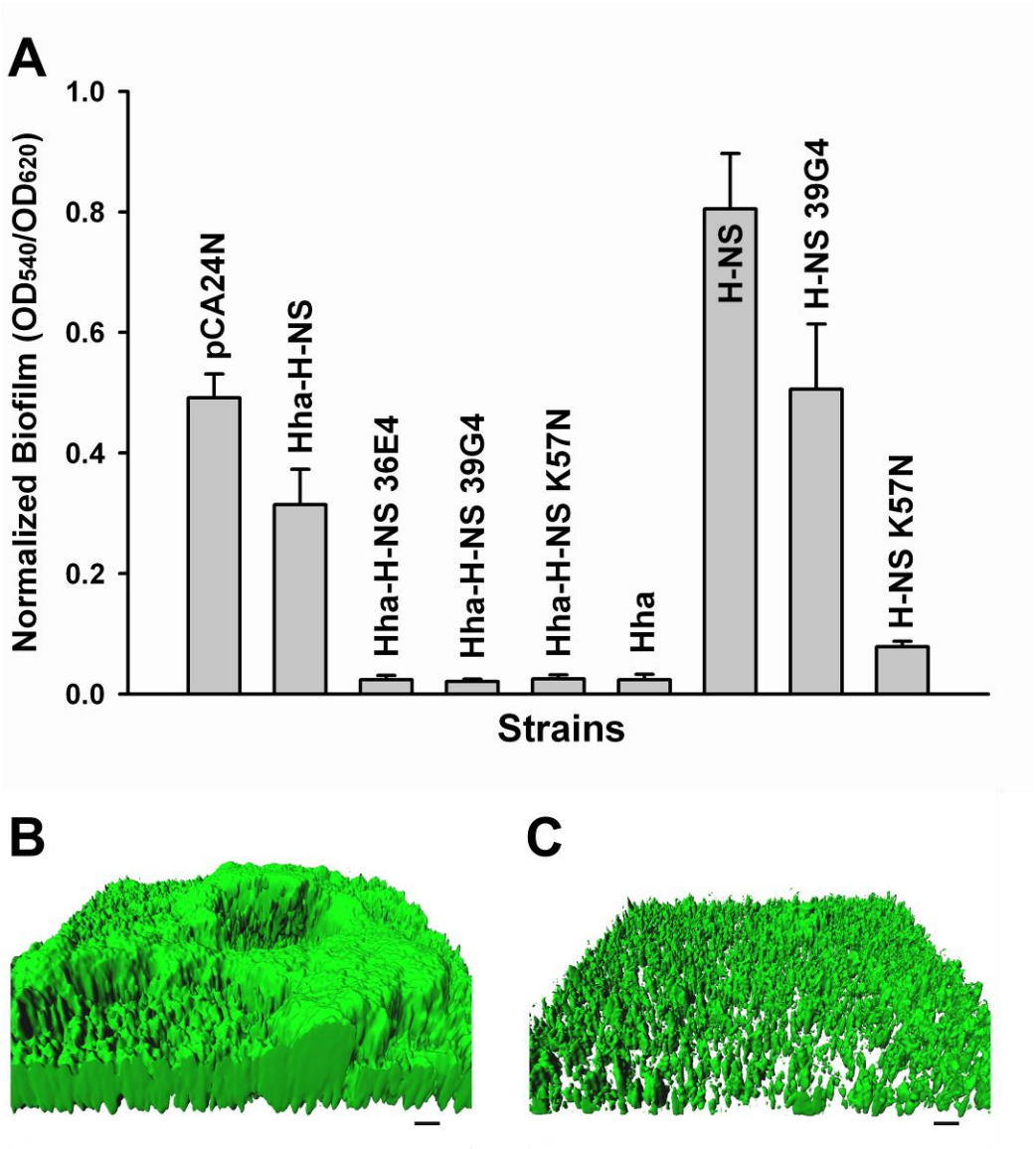

Figure 3.1 Biofilm formation with H-NS variants. Normalized biofilm formation for BW25113 *hha hns* cells producing the Hha-H-NS variants from pCA24N using 1 mM IPTG in 96-well polystyrene plates in LB at 37^{o}C after 24 h (A). Hha and H-NS amino acid substitutions are shown in Table 3.1 for Hha-H-NS 36E4, Hha-H-NS 39G4, and Hha-H-NS K57N. Hha-H-NS indicates simultaneous expression of both wild-type Hha and H-NS, Hha and H-NS indicate wild-type proteins expressed individually, H-NS 39G4 indicates expression of H-NS with H-NS amino acid substitution taken from Hha-H-NS 39G4, and H-NS K57N indicates expression of H-NS with the K57N substitution. Each data point is the average of at least twelve replicate wells from two independent cultures, and one standard deviation is shown. Biofilm formation of BW25113 *hha hns* cells producing wild-type H-NS (B) and H-NS K57N (C) from pCA24N using 1 mM IPTG on glass in flow-cells after 48 h in LB medium. Scale bars represent 10 μm.

3.3.2 Random mutagenesis of Hha-H-NS and biofilm screening

To reconfigure H-NS and Hha to control biofilm formation, we utilized the *hha hns* host so that there was no background Hha or H-NS in these cells since Hha and H-NS interact to control phenotypes (Madrid *et al.*, 2007). To mutagenize randomly both *hha* and *hns* via epPCR, a pCA24N-based vector was used to express *hha* and *hns* from a single promoter; hence, all the changes in phenotype were due to plasmid-encoded Hha-H-NS variants. The maximum error rate was determined to be 0.8% by sequencing three random colonies. A total of 2104 colonies were screened for altered biofilm formation which resulted in the identification of three variants that decreased biofilm formation more than 12-fold compared to wild-type Hha-H-NS (Fig. 3.1A).

Hha-H-NS 36E4 had three substitutions in Hha (Y11H, E25G, and L40Q) and four substitutions in H-NS (R12C, K57I, P72T, and D131V) (Table 3.1), whereas both Hha-H-NS 39G4 and Hha-H-NS K57N had completely inactivated Hha along with three substitutions and one substitution in H-NS, respectively (Table 3.1). Since active Hha was inactivated in two of the best mutants, the reduction in biofilm formation must be from changes in H-NS. To eliminate any possible chromosomal mutation effects, all the pCA24N-*hha hns* plasmids identified during the initial biofilm formation screens were re-transformed into BW25113 *hha hns*, and the changes in biofilm formation were confirmed; hence, the changes in biofilm formation are due to the changes in the *hha hns* genes on the plasmids.

Table 3.1 Protein sequences of the Hha-H-NS epPCR variants. Hha-H-NS 39G4 has a frameshift at Y33 in Hha due to the insertion of one base pair, and Hha-H-NS K57N has a frameshift at A2 in Hha due to the deletion of one base pair. X indicates termination.

Hha –H-NS variants	Substitutions
Hha-H-NS 36E4	Hha: Y11H, E25G, and L40Q
	H-NS: R12C, K57I, P72T, and D131V
Hha-H-NS 39G4	Hha: T23S, Y33 frame shift, and N38X
	H-NS: N9I, R12C, and T25M
Hha-H-NS K57N	Hha: A2 frame shift, and L6X
	H-NS: K57N

Table 3.2 COMSTAT analysis for flow-cell biofilms producing H-NS K57N. Biofilms of cells producing wild-type H-NS and H-NS K57N were formed in flow-cell in LB medium with 1 mM IPTG after 48 h at 37°C.

Strains	Biomass, $\mu m^3/\mu m^2$	Substratum coverage, %	Mean thickness, µm	Roughness coefficient
BW25113 *hha hns* /pCA24N *hns*/pHKT3	23 ± 2	54 ± 5	29 ± 3	0.25 ± 0.08
BW25113 *hha hns* /pCA24N *hns* K57N/pHKT3	2.4 ± 1.1	16 ± 9	4 ± 2	1.2 ± 0.3

To study the effects on H-NS alone, each mutation in *hns* that was found along with mutations in *hha* was introduced into pCA24N-*hns* to investigate whether the biofilm reduction of both Hha-H-NS 39G4 and Hha-H-NS K57N variants come from only the mutations in H-NS. Without Hha, H-NS 39G4 (H-NS N9I, R12C, and T25M) lost its biofilm reduction activity, but H-NS K57N maintained its significant reduction in biofilm formation (10-fold) compared to wild-type H-NS (Fig. 3.1A). Hence, these results show that the global regulator H-NS may be evolved to alter *E. coli* biofilm formation dramatically and switched from a protein that stimulates biofilm formation to one that reduces it.

To corroborate the static (96 well) biofilm results, we also conducted flow-cell biofilm experiments using cells expressing either wild-type H-NS (Fig. 3.1B) or H-NS K57N (Fig. 3.1C) in LB medium after 48 h. COMSTAT analysis (Table 3.2) shows biomass was decreased by 9.6-fold for H-NS K57N, and the mean biofilm thickness (7.1-fold) and substratum coverage were also decreased (3.3-fold) compared to cells expressing wild-type H-NS. Therefore, both static and flow-cell biofilm experiments confirm H-NS K57N reduces biofilm formation on glass (flow-cell) as well as polystyrene (96-well plate) surfaces.

3.3.3 Saturation mutagenesis at position K57 of H-NS

Since two of the three sets of mutations in *hns* involve the K57 codon and one mutant had only one amino acid substitution in H-NS (K57N) (Table 3.1), we investigated the importance of position K57 of H-NS for biofilm formation by substituting all possible amino acids via saturation mutagenesis. After screening 300 colonies to ensure with a probability of 99% that all possible codons were utilized (Rui *et al.*, 2004), we identified two variants (substitutions K57S and K57G) that show similar or less biofilm reduction relative to H-NS K57N but still decrease biofilm formation significantly compared to wild-type H-NS. Hence, it is clear that position K57 of H-NS is important for decreasing biofilm formation and that the K57N substitution is optimal.

3.3.4 H-NS K57N decreases biofilm formation via Cnu and StpA

To discern how H-NS K57N decreases biofilm formation, a whole-transcriptome study of biofilm cells of H-NS K57N versus wild-type H-NS was performed (*hha hns*/pCA24N-*hns* K57N vs. *hha hns*/pCA24N-*hns*), and *cnu* was identified as induced by overproducing H-NS K57N (Table 3.3). qRT-PCR of biofilm cells of H-NS K57N versus wild-type H-NS in BW25113 *hha hns* after 7 h confirmed that H-NS K57N induces *cnu* transcription by 5.7-fold ($\Delta\Delta C_T$ = -2.5 ± 0.2, where C_T is the threshold cycle of the target genes). Ori-C binding protein Cnu (YdgT) (Kim *et al.*, 2005) belongs to the Hha/YmoA family (Paytubi *et al.*, 2004), complements partially for some of the *hha*-induced phenotypes such as repression of the hemolysin operon (Paytubi *et al.*, 2004), and interacts with H-NS (Bae *et al.*, 2008). Therefore, we hypothesized that the reduction in biofilm formation from H-NS K57N was due to production of Cnu.

To determine the function of Cnu in biofilm formation, biofilm formation of the *cnu* deletion strain was tested. Deletion of *cnu* increased biofilm formation 12-fold compared to wild-type BW25113 strain after 7 h, and this phenotype was complemented in that *cnu* expression reduced biofilm formation more than 3-fold compared to the empty pCA24N control after 7 h (Fig. 3.2A). Thus, Cnu decreases biofilm formation like Hha. To see if H-NS K57N controls biofilm formation via Cnu, we compared biofilm formation with the *cnu* deletion (BW25113 *cnu*) and wild-type BW25113 in the presence of H-NS K57N after 7 h and 24 h (Fig. 3.2B). Without Cnu, H-NS K57N did not decrease biofilm formation, while it decreased biofilm formation for wild-type BW25113 after 24 h (Fig. 3.2B).

Table 3.3 Partial whole-transcriptome profiles to determine the impact of H-NS K57N on biofilm formation. List of differentially-expressed genes for biofilm cells of BW25113 *hha hns*/pCA24N-*hns* K57N vs. BW25113 *hha hns*/pCA24N-*hns*. Cells were grown in LB with 30 μg/mL chloramphenicol and 1 mM IPTG for 7 h at 37°C. Raw data for the two DNA microarrays are available using GEO series accession number GSE17853. Primarily, genes differentially-expressed above 2.7-fold are shown although some related genes are also shown.

Group and gene	b number	Fold change	Description
cnu	b1625	2.8	Hha paralog, OriC-binding protein
stpA	b2669	3.0	H-NS paralog, RNA chaperone and DNA-binding protein
Rac prophage			
intR	b1345	-2048.0	Putative Transposase/Integrase
ydaQ	b1346	-147.0	Putative Exisionase
ydaC	b1347	-2195.0	Function Unknown
lar	b1348	-831.7	Restriction alleviation
recT	b1349	-104.0	Recombinase, DNA Renaturation
recE	b1350	-891.4	Exonuclease VIII, ds DNA Exonuclease
racC	b1351	-3565.8	Function Unknown
kil	b1352	-4096.0	Kil Protein Of Lambdoid Prophage Rac
sieB	b1353	-2702.4	Phage Superinfection Exclusion Protein
-	b1354	-84.4	Function Unknown
ydaG	b1355	-548.7	Function Unknown
ydaR	b1356	-1176.3	Repressor
ydaS	b1357	-147.0	Repressor Protein
ydaT	b1358	-119.4	Function Unknown
ydaU	b1359	-97.0	Function Unknown
ydaV	b1360	-168.9	Putative DNA Replication Protein
ydaW	b1361	-59.7	Putative Transcriptional Regulator
rzpR	b1362	-59.7	Putative Prophage Lambda Endopeptidase
trkG	b1363	-445.7	Trk System Potassium Uptake
-	b1364	-1552.1	Function Unknown
ynaK	b1365	-337.8	Blue Light Induced, Function Unknown
ydaY	b1366	-2048.0	Function Unknown
-	b1367	-891.4	Function Unknown
ynaA	b1368	-55.7	Putative Tail Protein
lomR'	b1369	-42.2	Putative Outer Membrane Protein
trs5_5	b1370	-12.1	IS5Y Transposase
lomR	b1371	-68.6	Putative Outer Membrane Protein
stfR	b1372	-891.4	Putative Tail Fiber Protein
Other prophages			
insA	b0022	-3.5	IS1 protein; transposition function
ybcV	b0558	3.5	DLP12 prophage; putative envelope protein
intE	b1140	3.0	e14 prophage; integrase
ymfG	b1141	3.5	e14 prophage; putative exisionase
ymfJ	b1144	5.7	e14 prophage; function unknown

Table 3.3 Continued.

Group and gene	b number	Fold change	Description
dicC	b1569	4.6	Qin prophage; transcriptional repressor of cell division inhibition
dicF	b1574	4.6	Qin prophage; antisense sRNA, inhibits ftsZ
hokD	b1562	1.6	Qin prophage; small toxic membrane polypeptide
ydfO	b1549	5.3	Qin prophage; function unknown
ydfW	b1567	3.7	Qin prophage; integrase fragment
ydfX	b1568	4.0	Qin prophage; function unknown
Translation, Ribosomal structure and biogenesis			
rplB	b3317	-6.1	50S ribosomal subunit protein L2
rplC	b3320	-8.0	50S ribosomal subunit protein L3
rplD	b3319	-7.0	50S ribosomal subunit protein L4, regulates expression of S10 operon
rplK	b3983	-5.7	50S ribosomal subunit protein L11
rplN	b3310	-10.6	50S ribosomal subunit protein L14
rplP	b3313	-4.3	50S ribosomal subunit protein L16
rplR	b3304	-4.9	50S ribosomal subunit protein L18
rplV	b3315	-3.7	50S ribosomal subunit protein L22
rplW	b3318	-6.1	50S ribosomal subunit protein L23
rpsE	b3303	-6.1	30S ribosomal subunit protein S5
rpsG	b3341	-12.1	30S ribosomal subunit protein S7, initiates assembly
rpsH	b3306	-4.0	30S ribosomal subunit protein S8, and regulator
rpsK	b3297	-10.6	30S ribosomal subunit protein S11
rpsL	b3342	-10.6	30S ribosomal subunit protein S12
Transport and metabolism			
acpP	b1094	-4.3	acyl carrier protein
fabA	b0954	4.0	3-hydroxydecanoyl-[acyl-carrier-protein] dehydratase
fabH	b1091	3.2	3-oxoacyl-[acyl-carrier-protein] synthase III
glnH1	b0811	4.6	Glutamine-binding periplasmic protein precursor
iraM	b1160	3.5	RpoS stabilzer during Mg starvation, anti-RssB factor
sdaB	b2797	3.7	L-serine dehydratase 2
sdaC	b2796	3.5	Serine transporter
uhpT	b3666	4.3	Hexose phosphate transport protein
zntA	b3469	-3.2	Pb/Cd/Zn/Hg transporting ATPase (P-type ATPase family)
sodA	b3908	-3.2	Superoxide dismutase [Mn]
soxS	b4062	-4.6	Global transcription regulator for superoxide response; AraC family
pyrB	b4245	-3.2	Aspartate carbamoyltransferase catalytic chain
Information storage and processing			
nrdB	b2235	3.2	Ribonucleoside-diphosphate reductase 1, beta subunit
rmf	b0953	3.0	Binds 70S ribosome dimers to form 100S
Unknown			
ycdZ	b1036	-3.2	hypothetical protein
ycgX	b1161	5.3	hypothetical protein

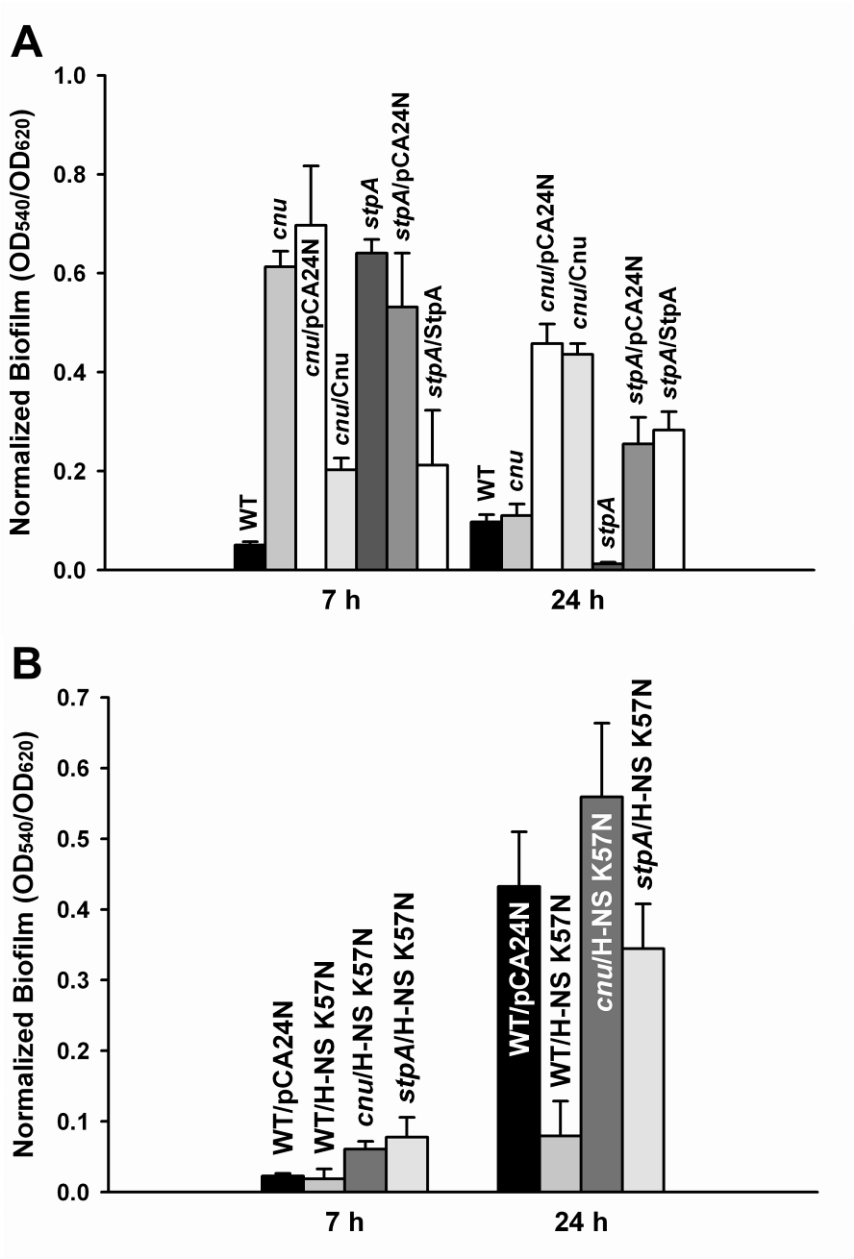

Figure 3.2 Biofilm formation with H-NS K57N with Cnu and StpA. Normalized biofilm formation in 96-well polystyrene plates in LB at 37°C after 7 h and 24 h for wild-type BW25113 (WT), *cnu* deletion (*cnu*), *cnu* complementation (*cnu*/Cnu), *stpA* deletion (*stpA*), complemented *stpA* (*stpA*/StpA), and *cnu* or *stpA* deletion with the empty pCA24N (*cnu*/pCA24N and *stpA*/pCA24N, respectively) (A), and for H-NS K57N with *cnu* deletion (*cnu*/H-NS K57N), with *stpA* deletion (*stpA*/pCA24N), for wild-type BW25113 (WT/H-NS K57N) and for wild-type BW25113 with the empty pCA24N (WT/pCA24N) (B). Each data point is the average of at least twelve replicate wells from two independent cultures, and one standard deviation is shown. H-NS K57N, Cnu, and StpA were expressed using 1 mM IPTG.

Moreover, *stpA*, which encodes a H-NS paralog (Zhang *et al.*, 1996), was induced 3-fold by H-NS K57N in the whole-transcriptome study (Table 3.3). Deletion of *stpA* decreases biofilm formation (Belik *et al.*, 2008) indicating StpA derepresses biofilm formation in *E. coli* K-12. We obtained similar biofilm results after 24 h in that the *stpA* deletion reduced biofilm formation (Fig. 3.2A) and this phenotype could be complemented at 24 h (Fig. 3.2A). However, deletion of *stpA* increased biofilm formation and StpA overproduction reduced biofilm formation after 7 h; thus, StpA controls biofilm formation differently according to the stage of biofilm development. To see whether H-NS K57N controls biofilm formation through StpA, we expressed H-NS K57N in the *stpA* mutant and compared biofilm formation in wild-type BW25113 with H-NS K57N and found, like Cnu, the absence of StpA abolished biofilm repression by H-NS K57N after 7 h and reduced the effect after 24 h (Fig. 3.2B). Therefore, StpA is necessary for H-NS K57N to repress biofilm formation. Taken together, these results indicate that H-NS K57N represses biofilm formation by interacting with nucleoid-associated proteins Cnu and StpA.

3.3.5 H-NS K57N induces Rac prophage excision through IntR and wild-type H-NS represses excision of Rac

The whole-transcriptome study also showed that H-NS K57N significantly repressed 28 genes in Rac prophage compared to wild-type H-NS (12- to 4100-fold, Table 3.3); hence, we hypothesized that H-NS K57N induced Rac excision so that these genes were no longer present which resulted in their low signal. To investigate the impact of H-NS on Rac prophage excision, pCA24N-*hns* K57N was expressed in BW25113 *hha hns* for 24 h and the chromosome was sequenced at the Rac prophage location. We found that Rac was excised by homologous recombination between two repeat DNA sequences (5'-TTGTTCAGGTTGTATTGTTCTTTCTT-3') flanking Rac prophage (Fig. 3.3A). Moreover, we quantified Rac excision by qPCR to find H-NS K57N induced Rac excision 11-fold after 7 h and

58-fold after 24 h compared to wild-type H-NS in planktonic cells (Fig. 3.3B). Similarly, H-NS K57N induced Rac excision 5.8 ± 0.0-fold after 7 h and 1.7 ± 0.2-fold after 24 h in biofilm cells.

Since H-NS represses genes obtained laterally (Navarre *et al.*, 2007), and since we used the double *hha hns* deletion strain as a host, we tested the excision of Rac in wild-type BW25113, BW25113 *hha*, BW25113 *hns*, and BW25113 *hha hns* without plasmids to see if *hn*s and *hha* control excision of Rac. As shown in Fig. 3.3C, *hns* deletion and *hha hns* double deletion induced the excision of Rac more than 13-fold compared to wild-type BW25113, while *hha* deletion did not increase Rac excision. This demonstrates that H-NS silences the excision of Rac which is one of gene locus acquired from lateral transfer. Hha induces the excision of another prophage, CP4-57, in *E. coli* (Wang *et al.*, 2009), but Hha does not control the excision of Rac (Fig. 3.3C). Therefore, the K57N substitution in H-NS enhances Rac excision from the *E. coli* K-12 chromosome (Fig. 3.3B), whereas wild-type H-NS represses Rac excision (Fig. 3.3C).

Integrase is required for lambdoid prophage excision by interacting with excisionase (Cho *et al.*, 2002), and its gene is usually placed adjacent to attachment site on the chromosome in order to interact with its DNA-target. Similarly, Rac *intR* is found next to Rac attachment site in *E. coli* K-12 (Casjens, 2003). To see whether H-NS K57N leads to Rac excision through IntR (recall there are eight other prophage elements in *E. coli* which may contribute), Rac excision by H-NS K57N was tested in the deletion of *intR*. Without IntR, Rac was not excised with H-NS K57N, and overexpressing IntR highly enhanced Rac excision, indicating IntR is necessary to excise Rac prophage and required by H-NS K57N (Fig. 3.3D).

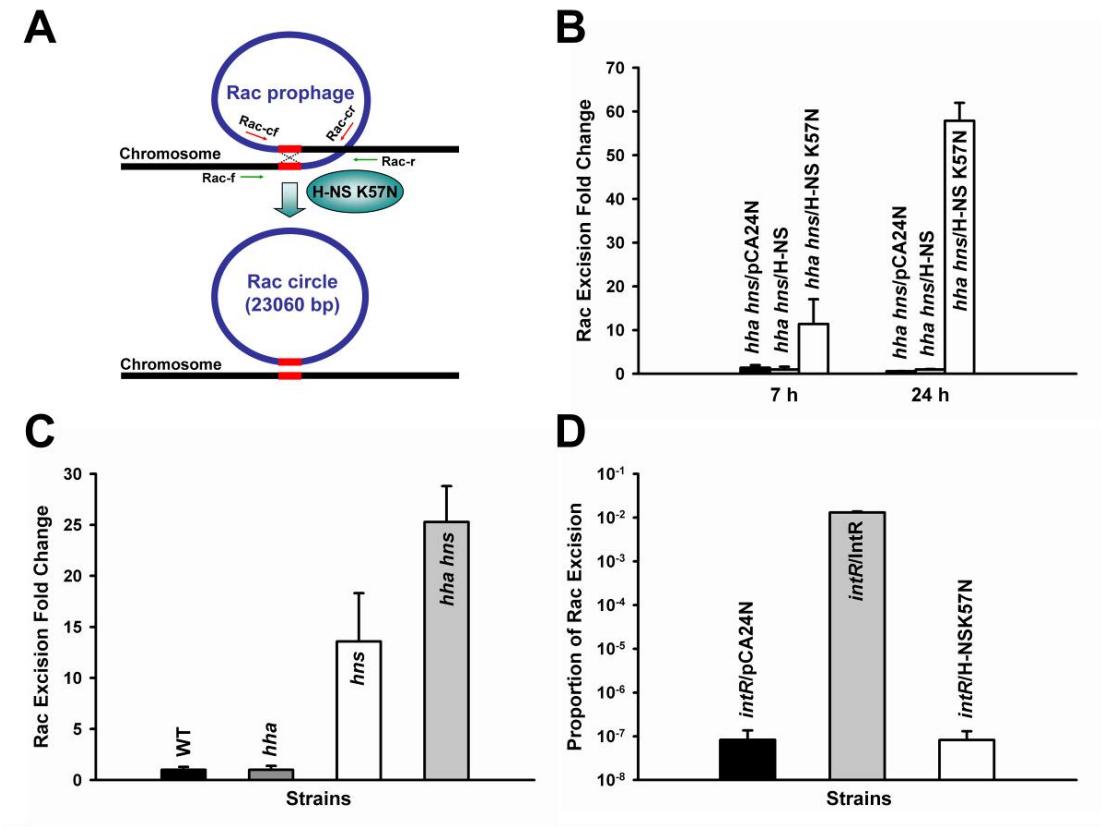

Figure 3.3 Excision of Rac prophage. Rac prophage in *E. coli* has two conserved attachment sites (5'-TTGTTCAGGTTGTATTGTTCTTTCTT-3', 26 bp) at the left and the right ends of Rac indicated as red lines (A). Rac excision is induced by H-NS K57N, and circularized to form a phage-like circle. Rac excision and phage-like circle were verified by DNA sequencing using primers Rac up and Rac down (Table 3.5) and by PCR using primer sets; green arrows indicate primers for Rac excision (Rac-f and Rac-r) and red arrows for Rac circle (Rac-cf and Rac-cr) (Table 3.5). Excision of Rac in LB at 37^{o}C for BW25113 *hha hns* cells expressing H-NS K57N, wild-type H-NS, and the empty pCA24N after 7 h and 24 h (B), for BW25113, BW25113 *hha*, BW25113 *hns*, and BW25113 *hha hns* without a plasmid after 15 h (C), and for BW25113 *intR* expressing H-NS K57N, IntR, and the empty pCA24N after 24 h (D). The number of chromosomes was quantified by qPCR using reference gene, *purA*, using primers purA-f and purA-r and the number of chromosomes devoid of Rac was quantified using primers Rac-f and Rac-r (Table 3.5). Each data point is the average of at least four replicates from each of two independent cultures, and one standard deviation is shown. H-NS K57N, H-NS, and IntR were expressed using 1mM IPTG.

3.3.6 Only Rac excision is controlled by H-NS and H-NS K57N

Since H-NS K57N increases Rac prophage excision, we investigated whether wild-type H-NS and H-NS K57N repress excision of the other five prophages (DLP12, e14, Qin, CPS-53, and CPZ-55) and three prophage-like elements (CP4-6, CP4-44, and CP4-57) in *E. coli* K-12 BW25113 using qPCR. Rac and e14 were highly excisable, while the other prophages were difficult to excise (Fig. 3.4A) since they lack excisionase activity; for example, DLP12 *xis* in *E. coli* K-12 is no longer functional (Lindsey *et al.*, 1989). Deletion of *hns* did not increase the excision of any prophage except Rac whose excision was increased by 13-fold (Fig. 3.4A). The Rac excision rate by cells producing wild-type H-NS in the *hha hns* double mutant (Fig. 3.4B) was not restored to that of the wild-type strain (Fig. 3.4A), probably due to the non-native promoter used to produce H-NS from pCA24N-*hns* (the *T5-lac* promoter) since H-NS functions as a repressor of its own transcription by interacting with its own promoter (Dersch *et al.*, 1993; Ueguchi *et al.*, 1993). Nevertheless, in the *hha hns* double mutant, only Rac excision among the nine prophages was enhanced significantly (58-fold) by H-NS K57N (Fig. 3.4B) relative to wild-type H-NS. Hence, wild-type H-NS represses only Rac excision in *E. coli* K-12, and the evolved H-NS can strongly induce only the excision of Rac prophage.

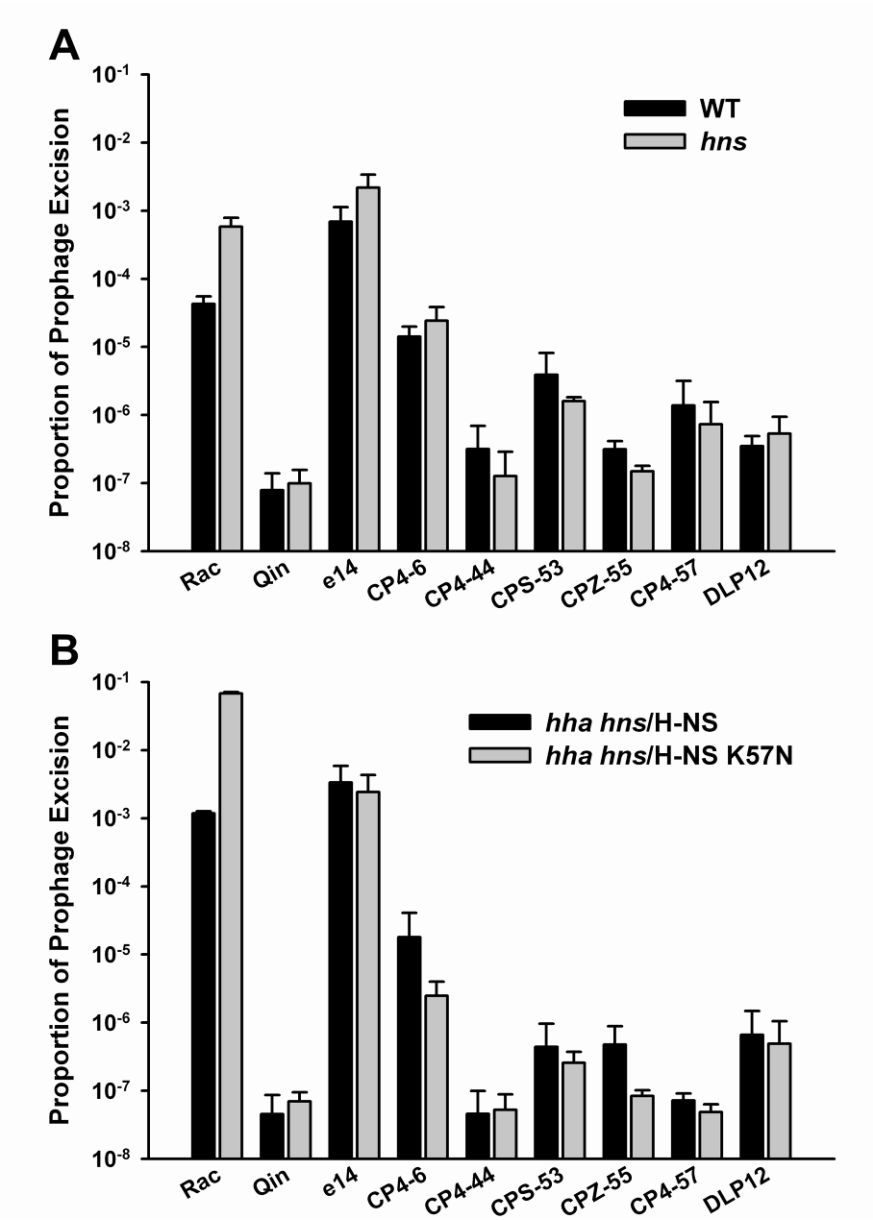

Figure 3.4 Excision of nine prophages. Comparison of nine prophage excision in LB at 37^{o}C upon deleting *hns* after 15 h (A) and for BW25113 *hha hns* cells expressing H-NS K57N and wild-type H-NS using 1mM IPTG after 24 h (B). The number of chromosomes was quantified by qPCR using reference gene, *purA*, via purA-f and purA-r primers and the number of chromosomes devoid of prophages was quantified using primers as described in Table 3.5. Each data point is the average of at least four replicates from each of two independent cultures, and one standard deviation is shown.

3.3.7 Rac prophage deletion changes biofilm formation

Previously, we discovered prophage CP4-57 controls biofilm formation (Wang *et al.*, 2009). To see the impact of Rac deletion on biofilm formation, we studied the effect of Rac deletion on temporal biofilm formation (Fig. 3.5). At early times (less than 18 h), Rac deletion (BW25113 Δ*rac*) increased biofilm formation up to 3-fold compared to wild-type BW25113, but at later times, biofilm formation was unchanged; these results are similar to the effect of cryptic prophage CP4-57 on biofilm formation (Wang *et al.*, 2009). Conversely, in the *hha hns* double deletion background, Rac deletion (BW25113 *hha hns* Δ*rac*) showed 2- to 3-fold less biofilm formation (Fig. 3.5).

3.3.8 Excision of Rac prophage by H-NS K57N enhances cell death and lysis

From the whole-transcriptome study of H-NS K57N biofilm cells versus wild-type H-NS biofilm cells, we observed that several ribosomal subunit genes (*rplBCDKNPRVW*, 50S ribosomal subunits; *rpsEGHKL*, 30S ribosomal subunits) were repressed by H-NS K57N (Table 3.3). To investigate how H-NS K57N affects cell growth, we measured the growth of cells during production of H-NS K57N and wild-type H-NS in BW25113 *hha hns* (Fig. 3.6A) and found that with H-NS K57N, growth was delayed compared to wild-type H-NS.

We hypothesized that this reduction in growth with H-NS K57N was due to increased cell lysis as a result of Rac prophage excision, so we measured cell lysis using eDNA as an indicator (Fig. 3.7). As a control, *hha hns*/pCA24N did not cause cell lysis, and wild-type H-NS (*hha hns*/pCA24N-*hns*) also showed very low cell lysis (0.8%); however, H-NS K57N (*hha hns*/pCA24N-*hns* K57N) increased cell lysis 28-fold vs. wild-type H-NS (to 23%). Therefore, H-NS K57N induces cell lysis, whereas wild-type H-NS does not.

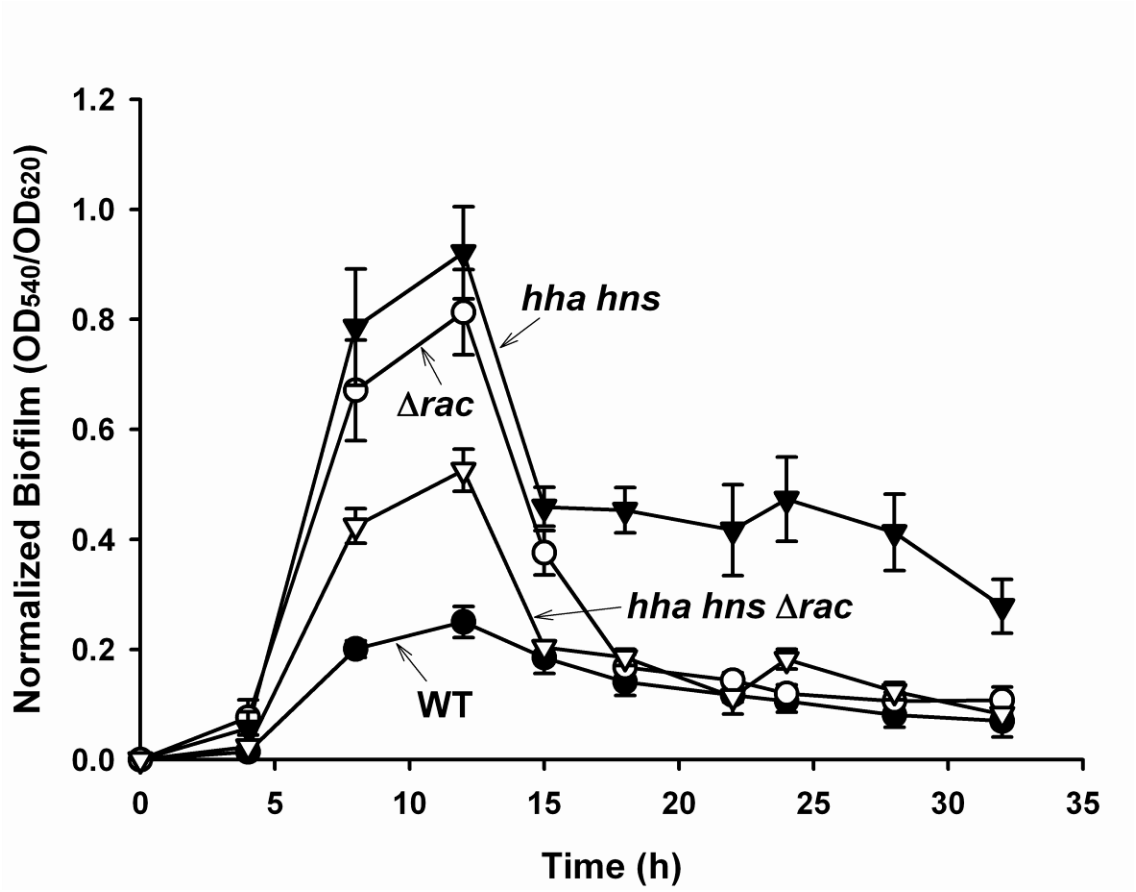

Figure 3.5 Temporal biofilm formation of Rac deletion mutants. Normalized biofilm formation upon deleting Rac prophage from wild-type BW25113 (WT) and BW25113 *hha hns* (*hha hns*) after 32 h in 96-well polystyrene plates in LB at 37^{o}C. Each data point is the average of at least twelve replicate wells from two independent cultures.

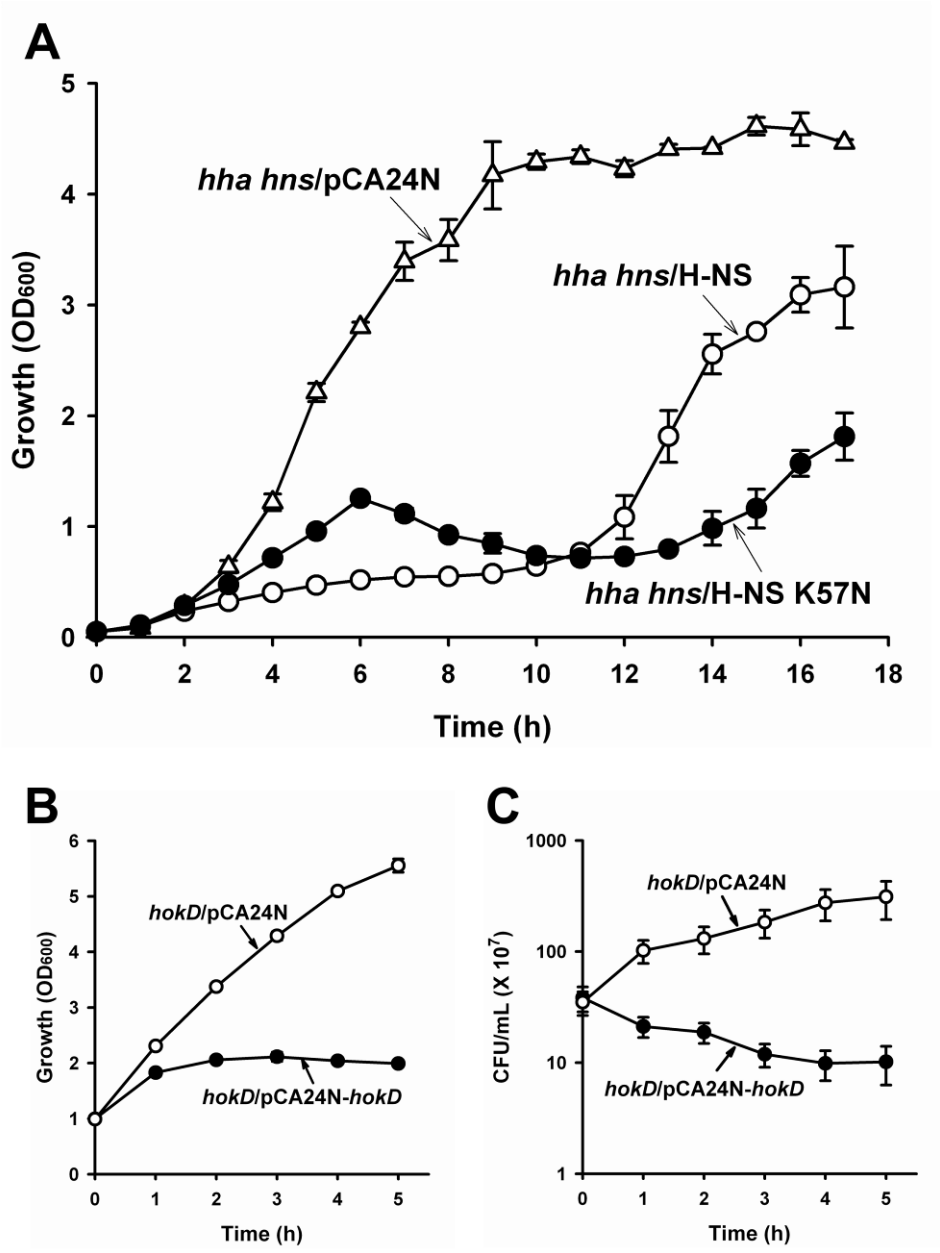

Figure 3.6 Growth during expression of H-NS K57N and toxicity of HokD. Growth in LB at 37°C for BW25113 *hha hns* cells expressing H-NS K57N (*hha hns*/H-NS K57N), wild-type H-NS (*hha hns*/H-NS), and empty pCA24N (*hha hns*/pCA24N) using 1 mM IPTG (A). Growth (B) and cell viability (CFU/mL) (C) for BW25113 *hokD* expressing HokD (*hokD*/HokD) and the empty pCA24N (*hokD*/pCA24N) using 1 mM IPTG at a turbidity of 1.0 at 600 nm. Each data point is the average of at least two independent cultures.

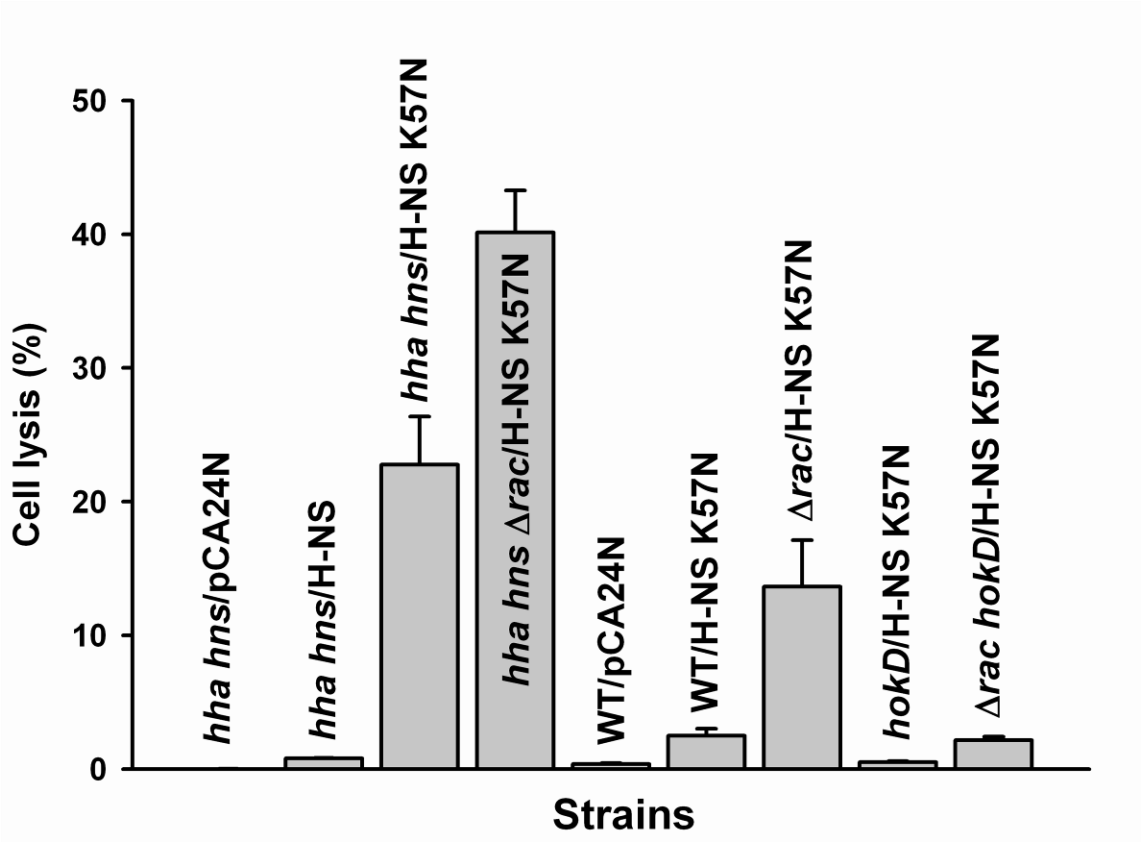

Figure 3.7 H-NS K57N induces cell lysis. Cell lysis by H-NS K57N in wild-type BW25113 (WT), BW25113 *hha hns* (*hha hns*), BW25113 Δ*rac* (Δ*rac*), BW25113 *hokD* (*hokD*), and BW25113 Δ*rac hokD* (Δ*rac hokD*) in LB at 37°C after 11 h. Extracellular DNA (eDNA) and intracellular DNA (iDNA) were quantified by qPCR using reference gene *purA* via the purA-f & purA-r primers. Cell lysis was calculated by dividing the amount of eDNA by the sum of eDNA and iDNA. Each data point is the average of at least four replicates from two independent cultures, and one standard deviation is shown. H-NS K57N and H-NS were expressed using 1mM IPTG.

We then investigated the role of Rac prophage for the increased lysis with H-NS K57N since some defective prophages such as DLP12 and Qin in *E. coli* K-12 retain a two-component cell lysis cassette (holin-endolysin) (Srividhya and Krishnaswamy, 2007), since excision of Rac prophage is increased dramatically by H-NS K57N (Fig. 3.3B), and since Rac prophage addition is lethal to a Rac^- host upon conjugative transfer due to expression of the Rac killing gene *kil* (Conter *et al.*, 1996). Surprisingly, we found production of H-NS K57N in the Rac deletion strain (*hha hns* Δ*rac*/pCA24N-*hns* K57N) was even more effective at causing cell lysis (increase of 1.8-fold relative to *hha hns*/pCA24N-*hns* K57N) (Fig. 3.7). Consistent results were obtained with BW25113 Δ*rac* with H-NS K57N vs. wild-type BW25113 with production of H-NS K57N (5.5-fold increase in cell lysis). Therefore, deletion of Rac prophage makes the cell more susceptible to lysis by H-NS K57N so as Rac is excised, the cell becomes more sensitive to H-NS K57N; this may explain the odd growth phenotype seen upon expressing H-NS K57N (Fig. 3.6A).

3.3.9 H-NS K57N induces cell death and lysis via HokD

To further examine the mechanism of cell lysis by H-NS K57N, we investigated other induced/repressed genes of the whole-transcriptome analysis results and found several genes inside Qin prophage that were induced (Table 3.3). Qin harbors important genes related to cell division and cell lysis; for example, *dicC* controls cell division inhibition proteins (Béjar *et al.*, 1986), *dicF* inhibits *ftsZ* (Faubladier and Bouché, 1994), and *hokD* (*relF*) induces cell death (Gerdes *et al.*, 1986). Since HokD has been identified as a homologue of the Hok (host killing) protein of R1 plasmid (Gerdes *et al.*, 1986), causes cell death by leading to loss of the cell membrane potential (Gerdes *et al.*, 1997), and was induced slightly (1.6-fold) by H-NS K57N in the whole-transcriptome analysis (Table 3.3), we focused on HokD to investigate cell lysis mechanism by H-NS K57N. HokD overexpression decreased cell growth (Fig. 3.6B) as well as

decreased cell viability (Fig. 3.6C), demonstrating HokD is toxic and finally leads to cell death. Moreover, when H-NS K57N was expressed in the absence of HokD using both *hokD*/pCA24N-*hns* K57N and Δ*rac hokD*/pCA24N-*hns* K57N, cell lysis by H-NS K57N was reduced (Fig. 3.7). Corroborating these cell lysis results, transcription of *hokD* was induced by 4.3-fold ($\Delta\Delta C_T$ = -2.1 ± 0.4) as shown by qRT-PCR with planktonic cells of H-NS K57N versus wild-type H-NS in BW25113 *hha hns* after 1 h by adding 1 mM IPTG at a turbidity of 0.5 at 600 nm. Furthermore, since Rac excision and deletion led to more cell lysis by H-NS K57N, HokD may be induced by H-NS K57N in the absence of Rac. As expected, qRT-PCR confirmed that *hokD* transcription is induced by 3.3-fold ($\Delta\Delta C_T$ = -1.7 ± 0.1) upon Rac deletion (BW25113 Δ*rac* vs. wild-type BW25113) as well as induced by 2.2-fold ($\Delta\Delta C_T$ = -1.1 ± 0.1) upon expressing H-NS K57N (*hha hns* Δ*rac*/pCA24N-*hns* K57N vs. *hha hns*/pCA24N-*hns* K57N) after 11 h. Hence, H-NS K57N induces expression of HokD along with Rac excision which results in cell lysis.

3.4 Discussion

In this study, we demonstrate that the global regulator H-NS of *E. coli* may be evolved to control three important cellular phenotypes: biofilm formation, Rac prophage excision, and cell lysis. We screened biofilm variants in the absence of endogenous Hha and H-NS and identified an H-NS variant with a single amino acid change, H-NS K57N, which reduces biofilm formation by 10-fold (Fig. 3.1). The mechanism by which H-NS K57N reduces biofilm formation is through its interaction with Cnu and StpA (Table 3.3 and Fig. 3.2AB). Cnu is a Hha paralog, and StpA is a H-NS paralog, and both are nucleoid-associated proteins. Here, we also show that Cnu reduces biofilm formation like Hha. Both Cnu and StpA have the ability to associate with H-NS by interacting with the N-terminus of H-NS (Bae *et al.*, 2008; Leonard *et al.*, 2009). Therefore, our results imply that the altered H-NS may interact closely with Cnu and StpA to reduce biofilm

reduction.

The N-terminus of H-NS includes three helical segments, H1 (1-8 aa), H2 (12-19 aa), and H3 (23-47 aa) (Fang and Rimsky, 2008) and plays an important role in forming homo- or hetero-oligomers of H-NS with Hha, Cnu, and StpA. In this study, the K57N substitution of H-NS occurred at a filament-like region in the N-terminus which is near a flexible linker, but not in the helical segments. This substitution replaces the positively-charged, long side chain of lysine with a neutrally-charged, short side chain of asparagine. The K57N substitution of H-NS may influence oligomerization of H-NS, cause a conformational change of the flexible linker, or cause a conformational change of the C-terminus, all of which would affect the DNA binding properties of H-NS. It is interesting that only a single amino acid substitution causes such dramatic physiological changes in the cell (biofilm formation, Rac prophage excision, and cell lysis).

The role of H-NS is to silence foreign DNA (Navarre *et al.*, 2007) by binding to curved DNA which is commonly found at promoters (Dorman, 2004). Prophages are genes laterally acquired that play an important role in the diversification of the genome (Oshima *et al.*, 2006), and repression of the Rac prophage excision by H-NS is the first report of this activity by H-NS (Fig. 3.4A). Moreover, we found that the reconfigured H-NS K57N protein induces Rac prophage excision which is opposite to wild-type H-NS (Fig. 3.3B). When Rac was deleted from the chromosome, it influenced biofilm formation by increasing biofilms as early as 18 h (BW25113 Δ*rac* vs. wild-type BW25113) and by decreasing biofilms with the deletion of *hha* and *hns* (BW25113 *hha hns* Δ*rac* vs. BW25113 *hha hns*) (Fig. 3.5). Also deletion of Rac enhanced cell lysis by H-NS K57N (Fig. 3.7). Note Rac is one of the most excisable prophages in *E. coli* (Fig. 3.4A). By regulating excision and integration of Rac prophage via H-NS, *E. coli* cells may enhance fitness in response to the environmental changes in terms of biofilm formation

and cell lysis.

H-NS K57N induces cell lysis by regulating a small toxic membrane protein HokD (Fig. 3.7). Previously, the function of HokD in *E. coli* was unclear, since the regulation element of the upstream part of *hokD* seems to be missing compared to *hok* in the R1 plasmid (Pedersen and Gerdes, 1999). However, our whole transcriptome study and qRT-PCR results show that HokD is induced by H-NS K57N (Table 3.3), that HokD is required for H-NS K57N to increase cell lysis (Fig. 3.7), and that *hokD* expression is related to Rac excision. Rac prophage may repress cell lysis by inhibiting HokD when Rac is in the chromosome, but if *E. coil* experiences some environmental stress, cells may kill themselves by expressing toxin proteins such as HokD that is induced due to Rac excision. The protein engineering of H-NS to form variant K57N thus represents one of the first examples of creating a global regulator to control prokaryotic apoptosis.

H-NS represses virulence genes in enterohemorrhagic *E. coli* (EHEC) (Mellies *et al.*, 2007), and several virulence genes are located in prophages; for example, Shiga toxin 1 (*stx1*) and 2 (*stx2*) genes are in cryptic prophage CP-933V and bacteriophage BP-933W in *E. coli* O157:H7 EDL933, respectively (Perna *et al.*, 2001). CP-933R in O157:H7 EDL933, Sp10 in O157 Sakai, and Rac in K-12 are located at identical positions in the three genomes and have identical attachment sites (Casjens, 2003). Our preliminary data show that transcription of virulence genes, *stx1A* in CP-933V, *stx2A* in BP-933W, and *espB* in LEE, are repressed up to 8-fold by producing wild-type H-NS, while *stx1A* is induced by producing H-NS K57N in EHEC. These results indicate that H-NS and the evolved H-NS influence expression of virulence genes in EHEC. Since wild-type H-NS represses the excision of Rac prophage (Fig. 3.4A) and H-NS K57N increases excision (Fig. 3.4B), it is possible that H-NS may affect virulence by controlling prophage excision in EHEC.

In this study, we demonstrate that a global regulator H-NS may be evolved readily which is similar to our results in which we evolved the QS signal regulator SdiA of *E. coli* to respond to homoserine lactones and to control indole concentrations (Lee *et al.*, 2009b). Evolution of global regulators may cause widespread changes in the regulatory system in bacteria including apoptosis, prophage excision, and biofilm formation as we show here; hence, this study implies that bacteria may evolve global regulators for the beneficial use of foreign genes that were originally introduced by prophage.

3.5 Experimental procedures

3.5.1 Bacterial strains and growth conditions

E. coli K-12 BW25113, its isogenic mutants, and the plasmids that were used in this study are listed in Table 3.4. We used the Keio collection (Baba *et al.*, 2006) for isogenic mutants and the ASKA library (Kitagawa *et al.*, 2005) for overexpressing genes. BW25113 *hha hns* was used as the host for screening plasmids containing *hha hns* alleles that were created via error-prone polymerase change reaction (epPCR) and was constructed using P1 transduction as described previously (Maeda *et al.*, 2008). The gene deletions were confirmed by PCR using primers hha up, hha down, hns up, and hns down (Table 3.5), which flank each gene of interest and confirm both the insertion and elimination of the Km^R gene. All strains were initially streaked from -80^{o}C glycerol stocks on Luria-Bertani (LB) agar plates and were cultured at 37^{o}C in LB (Sambrook *et al.*, 1989). Kanamycin (50 μg/mL) was used for pre-culturing isogenic knockout mutants, and chloramphenicol (30 μg/mL) was used for maintaining pCA24N-based plasmids. Genes were expressed from pCA24N using 1 mM isopropyl-β-D-thiogalactopyranoside (IPTG) (Sigma, St. Louis, MO, USA).

Table 3.4 *E. coli* K-12 bacterial strains and plasmids used in this study. Km^R, Cm^R, and Tet^R are kanamycin, chloramphenicol, and tetracycline resistance, respectively.

Strains and plasmids	Genotype/relevant characteristics	Source
Strains		
BW25113	*lacI*^{q} *rrnB*$_{T14}$ Δ*lacZ*$_{WJ16}$ *hsdR*514 Δ*araBAD*$_{AH33}$ Δ*rhaBAD*$_{LD78}$	(Baba *et al.*, 2006)
BW25113 *cnu*	BW25113 Δ*cnu* Ω Km^R	(Baba *et al.*, 2006)
BW25113 *hha*	BW25113 Δ*hha* Ω Km^R	(Baba *et al.*, 2006)
BW25113 *hns*	BW25113 Δ*hns* Ω Km^R	(Baba *et al.*, 2006)
BW25113 *hokD*	BW25113 Δ*hokD* Ω Km^R	(Baba *et al.*, 2006)
BW25113 *intR*	BW25113 Δ*intR* Ω Km^R	(Baba *et al.*, 2006)
BW25113 *stpA*	BW25113 Δ*stpA* Ω Km^R	(Baba *et al.*, 2006)
BW25113 *hha hns*	BW25113 Δ*hha* Δ*hns* Ω Km^R	This study
BW25113 Δ*rac*	BW25113 Δ*rac*	This study
BW25113 Δ*rac hokD*	BW25113 Δ*rac* Δ*hokD* Ω Km^R	This study
BW25113 *hha hns* Δ*rac*	BW25113 Δ*hha* Δ*hns* Δ*rac* Ω Km^R	This study
Plasmids		
pCA24N	Cm^R; *lacI*^{q}, pCA24N	(Kitagawa *et al.*, 2005)
pCA24N-*cnu*	Cm^R; *lacI*^{q}, pCA24N $P_{T5\text{-}lac}$::*cnu*$^+$	(Kitagawa *et al.*, 2005)
pCA24N-*hha*	Cm^R; *lacI*^{q}, pCA24N $P_{T5\text{-}lac}$::*hha*$^+$	(Kitagawa *et al.*, 2005)
pCA24N-*hns*	Cm^R; *lacI*^{q}, pCA24N $P_{T5\text{-}lac}$::*hns*$^+$	(Kitagawa *et al.*, 2005)
pCA24N-*hokD*	Cm^R; *lacI*^{q}, pCA24N $P_{T5\text{-}lac}$::*hokD*$^+$	(Kitagawa *et al.*, 2005)
pCA24N-*intR*	Cm^R; *lacI*^{q}, pCA24N $P_{T5\text{-}lac}$::*intR*$^+$	(Kitagawa *et al.*, 2005)
pCA24N-*hha hns*	Cm^R; *lacI*^{q}, pCA24N $P_{T5\text{-}lac}$::*hha*$^+$ *hns*$^+$	This study
pHKT3	Tet^R, RFP^+	(Tomlin *et al.*, 2004)

3.5.2 Construction of pCA24N-*hha hns*

hns was amplified using PCR from BW25113 chromosomal DNA using primers hns-SalI-f and hns-HindIII-r (Table 3.5), which were designed to have SalI and HindIII restriction recognition sites, respectively. The PCR product was cloned into pCA24N-*hha* using SalI and HindIII at the downstream region of *hha* in the plasmid. The *hha hns* transcriptional fusion in pCA24N was confirmed by DNA sequencing using primers seq-f1 and seq-f2 (Table 3.5).

3.5.3 epPCR for random mutagenesis

Both *hha* and *hns* from plasmid pCA24N-*hha hns* under the control of T5-*lac* promoter were mutated by epPCR as described previously (Fishman *et al.*, 2004) using primers epPCR-f and epPCR-r (Table 3.5). The epPCR product was cloned into pCA24N-*hha hns* using BseRI and HindIII after treating the plasmid with Antarctic phosphatase (New England Biolabs, Beverly, MA, USA). The ligation mixture was electroporated into BW25113 *hha hns* as described previously (Fishman *et al.*, 2004).

3.5.4 Biofilm screening of Hha-H-NS variants

Biofilm mutants were screened using polystyrene 96-well microtiter plates (Corning Costar, Cambridge, MA, USA) as described previously with crystal violet staining (Pratt and Kolter, 1998). The crystal violet dye stains both the air-liquid interface and bottom liquid-solid interface biofilm, and the total biofilm formation at both interfaces was measured at 540 nm whereas cell growth was measured at 620 nm. BW25113 *hha hns* colonies expressing Hha-H-NS variants from pCA24N-*hha hns* were grown overnight in 96-well plates with 200 μL of medium at 250 rpm, the overnight cultures were diluted (1:100) in 300 μL of LB containing 1 mM IPTG, and biofilm was formed for 24 h without shaking. To remove growth effects, biofilm formation was normalized by dividing total biofilm by cell growth for each strain. As controls, BW25113 *hha hns* with empty pCA24N and pCA24N-*hha hns* (wild-type *hha* and *hns*) were used.

Table 3.5 Primers used for error prone PCR, cloning, DNA sequencing, confirmation of the mutants, qPCR, and qRT-PCR. Underlined italic text indicates restriction enzyme recognition sites: SalI for hns-SalI-f, HindIII for hns-HindIII-r, and BglI for hns-39G4-f and hns-39G4-r. Underlined bold text indicates the site-directed mutation for the codon corresponding to K57 (5'-AAA to 5'-AAC for K57N) in hns-K57N-f and hns-K57N-r and indicates the saturation mutation of the codon corresponding to K57 (5'-NNS) in hns-K57sm-f and hns-K57sm-r (N is A, G, C, or T, and S is G or C).

Primer Name	Primer Sequence (listed 5' to 3')
error-prone PCR of *hha hns*	
epPCR-f	GCCCTTTCGTCTTCACCTCG
epPCR-r	GAACAAATCCAGATGGAGTTCTGAGGTCATT
Cloning *hns* to pCA24N-*hha*	
hns-SalI-f	CGCGCCG*GTCGAC*TATAAGTTTGAGATTACTACAATG
hns-HindIII-r	GCGCGTGC*AAGCTT*CAAAAGATTATTGCTTGATCAGG
Transferring mutations to pCA24N-*hns*	
hns-K57N-f	GAAGTTGAAGAGCGCACTCGT**AAC**CTGCAGCAATATC
hns-K57N-r	GATATTGCTGCAG**GTT**ACGAGTGCGCTCTTCAACTTC
hns-39G4-f	CGCGTCCG*GCCCTGAGGGC*CAGCGAAGCACTTAAAATTCTGATCA AC
hns-39G4-r	GCGCTG*GCCGCATAGGC*CTTGCTTGATCAGGAAATCGTCGAGGGA TTTAC
Saturation mutations at K57	
hns-K57sm-f	GAAGTTGAAGAGCGCACTCGT**NNS**CTGCAGCAATATCGCGAAATG
hns-K57sm-r	CATTTCGCGATATTGCTGCAG**SNN**ACGAGTGCGCTCTTCAACTTC
DNA Sequencing	
seq-f1	Same as epPCR-f
seq-f2	CTGTACGACAAGATCCCTTCCTCAGTATGG
Confirmation of deletions	
hha up	GGATGACACCTTTATGTTGTTCAG
hha down	GAGCGATACAACTCACCAGC
hns up	CTCACGTGCTGCGAAATCATCGGTG
hns down	ACCCTTGGCACGGAATTTAAAGCCT
cnu up	GTTGGTGATTGTCAGGGATAGTAAAG
cnu down	GGTGGTCATAGGTTCTCCAGAATAG
hokD up	GTGGTATGCCTGATTGTTACAAG
hokD down	GCGGTAATGACTAACAAGATTTCC
Rac up	GGTATCGCACAGATGCGACGGCACCAC
Rac down	GATCATCATTGCTTCCCATCGACCGG
intR-f	CAAACGAGTATCTCCTTTAGGTAAGC
intR-r	Same as Rac-f
Confirmation of Rac circle	
Rac-cf	GTAGCTTATTGTTGTCGCTGATG
Rac-cr	ATGACATGAACGACGAACAGATAG
qPCR	
Rac-f	CTCCAGCATGGTATAGCTGTCTTTAC
Rac-r	CAGATTTCTTATGCTGGGCGTTCCG
Qin-f	CGACAATACGCGCCACATAA
Qin-r	AACGGCGAGTAAGTAGTACGCA

Table 3.5 Continued.

Primer Name	Primer Sequence (listed 5' to 3')
e14-f	GTGCAAACATCGGTGACGAA
e14-r	TTCAGCAGCTTAGCGCCTTC
CP4-6-f	GCATCGCCCGGTTAGTTTTA
CP4-6-r	CACCTGCACTGCCTGATGTC
CP4-44-f	GAATTCACTGTCGGCGAAGG
CP4-44-r	TTGAAGCAATCCAGGGCATC
CPS-53-f	CGTACTTACCCCGCACTCCA
CPS-53-r	GGCAGTGGCCAAAAATTGAA
CPZ-55-f	AGCACATCCCCCGAACG
CPZ-55-r	TTGACGAAGTGATTGTCCGC
CP4-57-f	AAGCATGTAGTACCGAGGATGTAGG
CP4-57-r	TATGTCTCCTCACCGTCTGGTCGG
DLP12-f	CAAAAGCCATTGACTCAGCAAGG
DLP12-r	ACGGATAAGACGGGCATAAATGA
purA-f	GGGCCTGCTTATGAAGATAAAGT
purA-r	TCAACCACCATAGAAGTCAGGAT
qRT-PCR	
cnu-f	TATGGACCTTTTATGACTGTTCAGG
cnu-r	GCACGATACATATTGATCAGTTCC
hokD-f	ACAGGAGAAGCAGGCTATGAAG
hokD-r	TCAGGTTCGTAAGCTGTGAAGAC
rrsG-f	TATTGCACAATGGGCGCAAG
rrsG-r	ACTTAACAAACCGCTGCGT

Interesting biofilm mutants were re-analyzed by re-streaking the colonies on fresh LB plates and by performing another biofilm assay. Mutant *hha hns* alleles were sequenced using primers seq-f1 and seq-f2 (Table 3.5). Each data point was averaged from more than twelve replicate wells (six wells from two independent cultures).

3.5.5 Flow-cell biofilm experiments and image analysis

Strains were cultured in LB medium with chloramphenicol to retain the pCA24N-based plasmids and with tetracycline (20 µg/mL) to maintain pHKT3 (Tomlin *et al.*, 2004). Overnight cultures were diluted to a turbidity at 600 nm of 0.05 and pumped through the flow-cell (BST model FC81, Biosurface Technologies, Bozeman, MT) at 10 mL/h for 2 h, and then fresh LB medium with chloramphenicol, tetracycline, and 1 mM IPTG was pumped for 48 h. Since the red fluorescent protein via pHKT3 was weak in BW25113 *hha hns*, the flow-cell biofilms were stained for 30 min with 5 µL/mL SYTO 9 from the LIVE/DEAD *Bac*Light Bacterial Viability Kit (Molecular Probes, Carlsbad, CA) which causes both live and dead bacteria to fluoresce green (Cense *et al.*, 2006). The biofilms on the glass slides were visualized by exciting with an Ar laser at 488 nm (emission 510 to 530 nm) using a TCS SP5 scanning confocal laser microscope (Leica Microsystems, Wetzlar, Germany) with a 63x HCX PL FLUOTAR L dry objective. Six random positions were chosen, and 25 images were taken for each position. Simulated three-dimensional images were obtained using IMARIS software (BITplane, Zurich, Switzerland). Color confocal flow-cell images were converted to gray scale, and biomass, substratum coverage, mean thickness, and surface roughness were determined using COMSTAT image-processing software (Heydorn *et al.*, 2000).

3.5.6 Cloning of *hns* alleles to pCA24N-*hns*

To study the impact of the mutations in *hns* in the absence of *hha*, we transferred the mutations in *hns* of *hha hns* that give rise to alleles H-NS K57N and H-NS 39G4 to pCA24N-

hns. For introducing the K57N substitution to pCA24N-*hns*, site-directed mutagenesis was performed using a QuikChange® XL Site-directed Mutagenesis Kit (Stratagene, La Jolla, CA, USA) using primers hns-K57N-f and hns-K57N-r (Table 3.5). Since *hha hns* 39G4 has several mutations in *hns*, these mutations were introduced through cloning with restriction enzyme BglI. The PCR product using primers hns-39G4-f and hns-39G4-r (Table 3.5) on pCA24N-*hha hns* containing 39G4 allele was digested with BglI. The DNA fragments were ligated after treating the digested pCA24N-*hns* with Antarctic phosphatase (New England Biolabs, Beverly, MA, USA). The cloned plasmids were electroporated into BW25113 *hha hns*.

3.5.7 Saturation mutagenesis

The QuikChange® XL Site-directed Mutagenesis Kit (Stratagene, La Jolla, CA) was used to perform saturation mutagenesis of *hns* at the codon corresponding to position K57. Plasmid pCA24N-*hns* was used as a template. DNA primers hns-K57sm-f and hns-K57sm-r (Table 3.3) were designed to allow the substitution of all 20 amino acids using 32 possible codons (Rui *et al.*, 2004); the constructed plasmids were electroporated into BW25113 *hha hns*.

3.5.8 RNA isolation and whole-transcriptome studies

For the whole transcriptome study of BW25113 *hha hns*/pCA24N-*hns* K57N versus BW25113 *hha hns*/pCA24N-*hns*, cells were grown in 250 mL of LB containing 1 mM IPTG for 7 h with 10 g of glass wool (Corning Glass Works, Corning, NY, USA) in 1 L Erlenmeyer flasks to form a robust biofilm (Ren *et al.*, 2004a). Biofilm cells were obtained by rinsing and sonicating the glass wool in sterile 0.85% NaCl solution at 0°C and RNA*Later* buffer® (Applied Biosystems, Foster City, CA, USA) was added to stabilize RNA during the RNA preparation steps. Total RNA was isolated from biofilm cells as described previously (Ren *et al.*, 2004a) using a bead beater (Biospec, Bartlesville, OK, USA). cDNA synthesis, fragmentation, and hybridizations to the *E. coli* GeneChip Genome 2.0 array (Affymetrix, Santa Clara, CA, USA;

P/N 511302) described previously (González Barrios *et al.*, 2006). Genes were identified as differentially expressed if the expression ratio was higher (2.7-fold) than the standard deviation (1.4-fold) and if the *p*-value for comparing two chips was less than 0.05 (Ren *et al.*, 2004b). The whole-transcriptome data have been deposited in the NCBI Gene Expression Omnibus (http://www.ncbi.nlm.nih.gov/geo/) and are accessible through accession number GSE17853.

3.5.9 Quantitative real-time PCR (qPCR)

To determine the relative concentrations of specific DNA fragments, qPCR was used as described previously (Wang *et al.*, 2009). Total DNA (50 to 200 ng) isolated using the UltraClean™ Microbial DNA Isolation Kit (Mo Bio Laboratories, Carlsbad, CA, USA) was used as the template for the qPCR reaction using the Power *SYBR® Green RNA-to-*C_T™ 1-Step Kit (Applied Biosystems, Foster City, CA, USA). The reaction and analysis was carried out by the StepOnePlus™ Real-Time PCR System (Applied Biosystems, Foster City, CA, USA). A quantification method based on the relative amount of a target gene versus a reference gene was used (Pfaffl, 2001). The number of total chromosomes was quantified by a reference gene, adenylosuccinate synthase (*purA*). The number of chromosomes that are devoid of prophage was quantified using primers flanking each prophage (Table 3.5), which only give PCR products when the prophage is removed due to the size of the prophage.

3.5.10 Quantitative real-time reverse-transcription PCR (qRT-PCR)

To corroborate the DNA microarray data, qRT-PCR was used to quantify relative RNA concentrations using 100 ng as a template and included a complementary DNA synthesis step from RNA before the denaturation step. Primers for qRT-PCR of *cnu* and *hokD* are listed in Table 3.5. The housekeeping gene *rrsG* (16S rRNA gene) was used to normalize the gene expression data.

3.5.11 Construction of the Rac prophage deletion strain

To study the impact of the Rac prophage deletion on biofilm formation and cell lysis, we constructed Rac deletion strain from wild-type BW25113 and BW25113 *hha hns* by overexpressing H-NS K57N in LB with 1 mM IPTG for 24 h. The overnight culture was diluted (1:100) in LB containing 1 mM IPTG, and incubated for 24 h, single colonies were obtained by spreading the culture on LB agar plate, and Rac deletion strain was verified by PCR using primers (Table 3.5): Rac excision was verified by flanking primers Rac-f and Rac-r, removal of the Rac circle was verified by Rac-cf and Rac-cr, and complete deletion of Rac in the genome was confirmed by the absence of a PCR product using primers intR-f and intR-r that flank one Rac attachment site and the first gene of Rac, *intR*. pCA24N-*hns* K57N and the Rac circle were eliminated by incubating at 25°C for 24 h.

3.5.12 Cell lysis measurement

To quantify cell lysis, the DNA concentration in supernatants and in cells was measured by qPCR using reference gene *purA* with modifications (Ma and Wood, 2009). Cells were grown with 1 mM IPTG for 11 h then the culture (1 mL) centrifuged at 13,000 rpm for 5 min to obtain supernatant and cell pellet fractions. Extracellular DNA (eDNA) was obtained by filtering the supernatant (Vilain *et al.*, 2009) using a 0.22 µm-pore size Millex® (33 mm) PES membrane filter (Millipore, Billerica, MA, USA) and was diluted 100 times with dH_2O to eliminate the influence of LB on the qPCR reaction. Intracellular DNA (iDNA) was obtained from the cell pellet by resuspending the pellet in 1 mL of dH_2O, sonicating twice using a 60 Sonic Dismembrator (Fisher Scientific, Pittsburgh, PA, USA) at level 10 for 15 sec, centrifuging, filtering, and diluting 10 times with dH_2O. The amount of eDNA and iDNA was quantified using a standard curve produced by plotting serial dilution of genomic DNA of BW25113 versus its Ct value. The cell lysis percentage was calculated by dividing the amount of eDNA by total DNA.

CHAPTER IV

ENGINEERING GLOBAL REGULATOR HHA OF *ESCHERICHIA COLI* TO CONTROL BIOFILM DISPERSAL*

4.1 Overview

The global transcriptional regulator Hha of *Escherichia coli* controls biofilm formation and virulence. Previously we showed that Hha decreases initial biofilm formation; here, we engineered Hha for two goals: to increase biofilm dispersal and to reduce biofilm formation. Using random mutagenesis, Hha variant Hha13D6 (D22V, L40R, V42I, and D48A) was obtained that causes nearly complete biofilm dispersal (96%) by increasing apoptosis without affecting initial biofilm formation. Hha13D6 caused cell death probably by the activation of proteases ClpB, HslUV, Lon, and PrlC since Hha-mediated dispersal was dependent on protease HslV. Hha variant Hha24E9 was also obtained that decreased biofilm formation by inducing *gadW*, *glpT*, and *phnF* but that did not alter biofilm dispersal. Hence, Hha may be engineered to influence both biofilm dispersal and formation.

---

* Reprinted with permission from "Engineering global regulator Hha of *Escherichia coli* to control biofilm dispersal" by Seok Hoon Hong, Jintae Lee, and Thomas K. Wood, 2010, *Microbial Biotechnology* 3:717-728, Copyright 2010 Society for Applied Microbiology and Blackwell Publishing Ltd, DOI: 10.1111/j.1751-7915.2010.00220.x. S.H. Hong and J. Lee performed the biofilm screening, and S.H. Hong was responsible for the rest of the experiments.

4.2 Introduction

Hha (high hemolysin activity, 72 aa) belongs to the Hha-YmoA family of low-molecular-mass proteins (about 8 kDa) that regulate many genes in Gram-negative bacteria (Madrid *et al.*, 2007); Hha was identified as reducing hemolysin production by repressing the *hly* operon of *Escherichia coli* (Godessart *et al.*, 1988). However, Hha does not bind specific DNA sequences; instead, Hha has a protein partner, H-NS, and this complex binds specific sequences of the *hly* regulatory operon (Madrid *et al.*, 2002) as well as 162 genes controlled by the Hha-H-NS complex (Baños *et al.*, 2009). Hha also represses the pathogenicity locus of enterocyte effacement (LEE) set of operons in enterohemorrhagic *E. coli* by repressing transcription of *ler* which encodes the activator of LEE (Sharma *et al.*, 2005). We found that Hha is induced 30 fold in *E. coli* biofilms relative to planktonic cells (Ren *et al.*, 2004a) and that Hha decreases initial biofilm formation by repressing the transcription of rare codon tRNAs and by repressing transcription of fimbrial genes (García-Contreras *et al.*, 2008). Hha is also toxic and leads to cell lysis and biofilm dispersal due to activation of prophage lytic genes *appY* and *rzpD* of DLP12 and *alpA* and *yfjZ* of CP4-57, and due to the induction of protease ClpXP (García-Contreras *et al.*, 2008). In addition, Hha induces excision of prophages CP4-57 and DLP-12 of *E. coli* (Wang *et al.*, 2009). Hence, Hha is a global transcriptional regulator in modulating cell physiology.

Biofilms consist of a complex heterogeneity of cells (Stewart and Franklin, 2008) that are the result of diverse signals and regulatory networks during biofilm development (Prüß *et al.*, 2006). The final stage of the biofilm cycle is the dispersal of cells from the biofilm into the environment (Kaplan, 2010). Like other stages of biofilm development, biofilm dispersal is a highly-regulated process involving many sensory circuits (Karatan and Watnick, 2009). There have been several biofilm dispersal signals proposed including the auto-inducing peptide of the *agr* quorum-sensing system of *Staphylococcus aureus* that triggers biofilm detachment (Boles

and Horswill, 2008) and changes in carbon sources (Sauer *et al.*, 2004). To date, little is known about the intracellular molecular mechanisms of bacterial biofilm dispersal (Kaplan, 2010); however, phosphodiesterases can decrease concentrations of the secondary messenger cyclic diguanylate (c-di-GMP) (Karatan and Watnick, 2009) which results in increased motility (Kaplan, 2010), and surfactants such as rhamnolipid produced by *Pseudomonas aeruginosa* can cause dispersal of biofilms (Boles *et al.*, 2005). In addition, cell lysis may accompany the dispersal process; hence, biofilm dispersal in *P. aeruginosa* may be achieved through prophage-mediated cell death (Webb *et al.*, 2003) and in *Pseudoalteromonas tunicata* biofilm dispersal involves autolysis via AlpP (Mai-Prochnow *et al.*, 2006).

To control biofilm formation, nitric oxide was investigated as a dispersal agent not only for single-species biofilms including Gram-negative and Gram-positive bacteria and yeasts but also for multi-species biofilms of clinical and industrial relevance (Barraud *et al.*, 2009a). Also, T7 bacteriophage was engineered so that during bacteriophage infection dispersin B of *Actinobacillus actinomycetemcomitans* is produced to hydrolyze the glycosidic linkages of polymeric β-1,6-*N*-acetyl-*D*-glucosamine found in the biofilm matrix (Lu and Collins, 2007).

Protein engineering and recombinant engineering are promising strategies to control biofilm formation, but they have not been applied for promoting biofilm dispersal. Previously, we created the first synthetic circuit for controlling biofilm formation via an external signal by manipulating indole concentrations via toluene *o*-monooxygenase in a consortium of *Pseudomonas fluorescens* and *E. coli* (Lee *et al.*, 2007b). In addition, we controlled *E. coli* biofilm formation by rewiring the quorum-sensing regulator SdiA; upon addition of the extracellular signal *N*-acylhomoserine lactone, biofilm formation was increased with SdiA variant 2D10, and SdiA variant 1E11 increased concentrations of the biofilm inhibitor indole and thereby reduced biofilm formation (Lee *et al.*, 2009b). Furthermore, we engineered global

regulator H-NS to control biofilm formation via prophage excision and cell death (Hong *et al.*, 2010b); however, the engineered H-NS has no effect on biofilm dispersal. These results showed that bacterial biofilm formation may be controlled by manipulating key regulatory proteins and enzymes.

In this study, protein engineering was used to rewire the global transcriptional regulator Hha to control biofilms. The aims of this study were to engineer Hha to enhance biofilm dispersal, to engineer Hha to reduce biofilm formation, and to investigate the mechanism by which the Hha variants influence biofilm formation. Utilizing whole-transcriptome analyses, random mutagenesis, saturation mutagenesis, site-directed mutagenesis, double mutations, quantitative real-time reverse transcription PCR (qRT-PCR), and quantitative PCR (qPCR), we show Hha may be rewired to promote biofilm dispersal by interacting with protease HslV. We also show that Hha may be engineered to decrease biofilm formation.

4.3 Results

4.3.1 Random mutagenesis of Hha for biofilm dispersal

The *E. coli* BW25113 wild-type strain undergoes natural biofilm dispersal in 96-well plates after 31 h (results not shown), since the wild-type strain produces Hha from its chromosome. Here, as expected, biofilm cells that lack Hha (*hha*/pCA24N) did not disperse at all time points tested (24 h, 32 h, and 48 h) (Fig. 4.1A). Therefore, Hha is important for biofilm dispersal as we showed previously (García-Contreras *et al.*, 2008); however, wild-type Hha does not disperse biofilms after 32 and 48 h (Fig. 4.1A). Hence, we focused on creating Hha variants that could disperse biofilms from 24 to 48 h since wild-type Hha induced biofilm dispersal somewhat in early biofilms but not in mature biofilms (Fig. 4.1A).

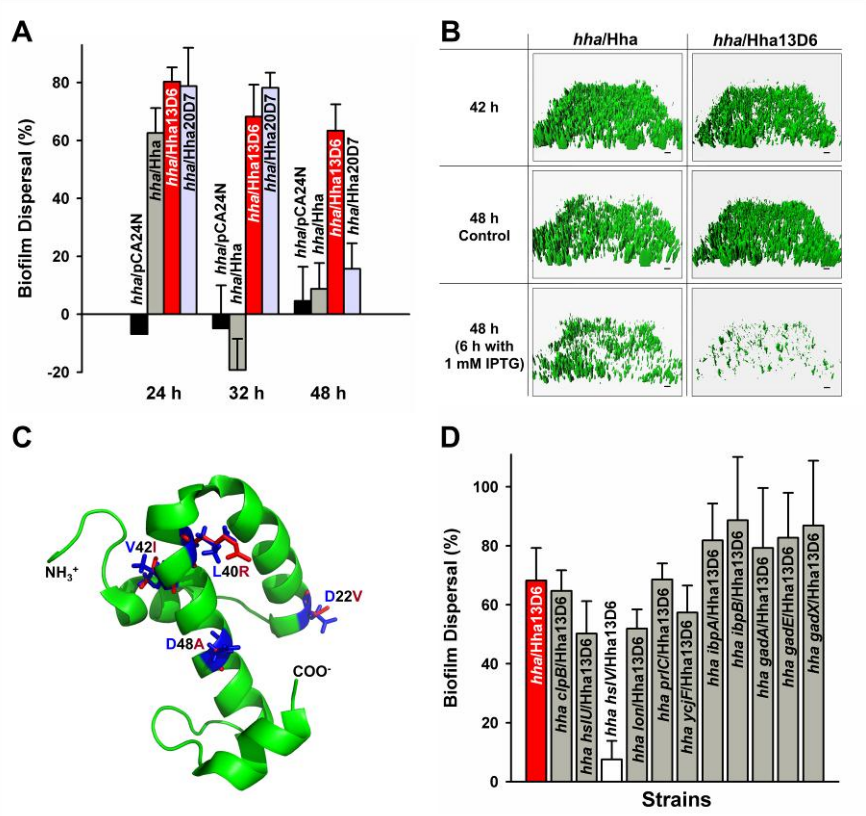

Figure 4.1 Biofilm dispersal with Hha13D6. Biofilm dispersal in 96-well plates for BW25113 *hha* producing Hha13D6 and Hha20D7 in LB glucose (0.2%) at 37°C (A). Biofilm dispersal was quantified by subtracting the normalized biofilm with Hha and its variants produced at 24 h, 32 h, and 48 h (8 h after adding 1 mM IPTG) from the normalized biofilm without Hha and its variants produced at 24 h, 32 h, and 48 h (no IPTG addition). Each data point is the average of at least two independent cultures, and one standard deviation is shown. Biofilm dispersal in flow-cells for BW25113 *hha* producing Hha13D6 from pCA24N (B). Biofilms were formed on glass surfaces in flow-cells for 42 h then 1 mM IPTG was added for 6 h to induce dispersal (control is no IPTG addition). Scale bar represents 10 μm. Modeled protein structure of Hha13D6 (C). Substituted residues of Hha13D6 (D22V, L40R, V42I, and D48A) are shown in red, while the original residues were shown in blue. Impact of ClpB, HslU, HslV, Lon, PrlC, YcjF, IbpA, IbpB, GadA, GadE, and GadX on Hha13D6-mediated biofilm dispersal (D)**.** Biofilm dispersal for cells producing Hha13D6 in LB glucose at 37°C after 32 h (8 h with 1 mM IPTG) in the following hosts: BW25113 *hha* (*hha*), BW25113 *hha clpB* (*hha clpB*), BW25113 *hha hslU* (*hha hslU*), BW25113 *hha hslV* (*hha hslV*), BW25113 *hha lon* (*hha lon*), BW25113 *hha prlC* (*hha prlC*), BW25113 *hha ycjF* (*hha ycjF*), BW25113 *hha ibpA* (*hha ibpA*), BW25113 *hha ibpB* (*hha ibpB*), BW25113 *hha gadA* (*hha gadA*), BW25113 *hha gadE* (*hha gadE*), and BW25113 *hha gadX* (*hha gadX*). Each data point is the average of at least two independent cultures, and one standard deviation is shown.

To engineer Hha for biofilm dispersal in the absence of effects related to wild-type Hha and the quorum sensing signal indole (Lee *et al.*, 2007a) produced by tryptophanase, we used a BW25113 *hha tnaA* double mutant for screening after error-prone PCR (epPCR) of *hha*. The average error rate was determined to be 0.8% by sequencing three random *hha* genes. A total of 2256 colonies were screened in polystyrene 96-well plates for robust biofilm formation in rich medium after 24 h followed by enhanced biofilm dispersal after 8 h of induction of *hha* with random mutations. Two Hha variants were identified with up to five-fold greater biofilm dispersal (wild-type Hha had 10% biofilm dispersal under these conditions). Hha dispersal variant Hha13D6 had four amino acid replacements at D22V, L40R, V42I, and D48A, and Hha20D7 had two replacements at D48G and R50C (Table 4.1). To eliminate any possible chromosomal mutation effects, all the pCA24N-*hha* plasmids identified during the initial screens were re-transformed into BW25113 *hha tnaA*, and the changes in biofilm dispersal were confirmed; hence, the phenotype changes in biofilm dispersal are due to the changes in the *hha* gene on the plasmids.

The dispersal variants were transformed into BW25113 *hha* for further study in only a *hha* deletion background. Corroborating the results with BW25113 *hha tnaA*, Hha20D7 in BW25113 *hha* had enhanced biofilm dispersal at 24 h and 32 h, and cells with Hha13D6 had enhanced biofilm dispersal at 24 h, 32 h, and 48 h whereas wild-type Hha caused little dispersal after 24 h (Fig. 4.1A). These results show that Hha may be rewired to enhance biofilm dispersal at both early and mature biofilms. Importantly, cells producing both the wild-type Hha and engineered Hha13D6 formed similar biofilms at 24 h (Fig. 4.2A); therefore, Hha13D6 does not affect biofilm formation but instead controls only biofilm dispersal.

Table 4.1 Protein sequences of the Hha variants from screening of altered biofilm dispersal and biofilm formation. X indicates termination.

Hha variants	Replacements
Hha dispersal variants	
Hha13D6	D22V, L40R, V42I, D48A
Hha20D7	D48G, R50C
Hha saturation mutagenesis variant	
HhaSM2C1	D22M, L40R, V42I, D48A
Hha biofilm variants	
Hha1D8	L6I, E34V, N38E, K58E, K62X
Hha1D9	E53X
Hha12H6	V67E
Hha13B3	Q19R, N57D
Hha24E9	K62X
Hha dispersal-biofilm combined variant	
Hha13D6-24E9	D22V, L40R, V42I, D48A, K62X

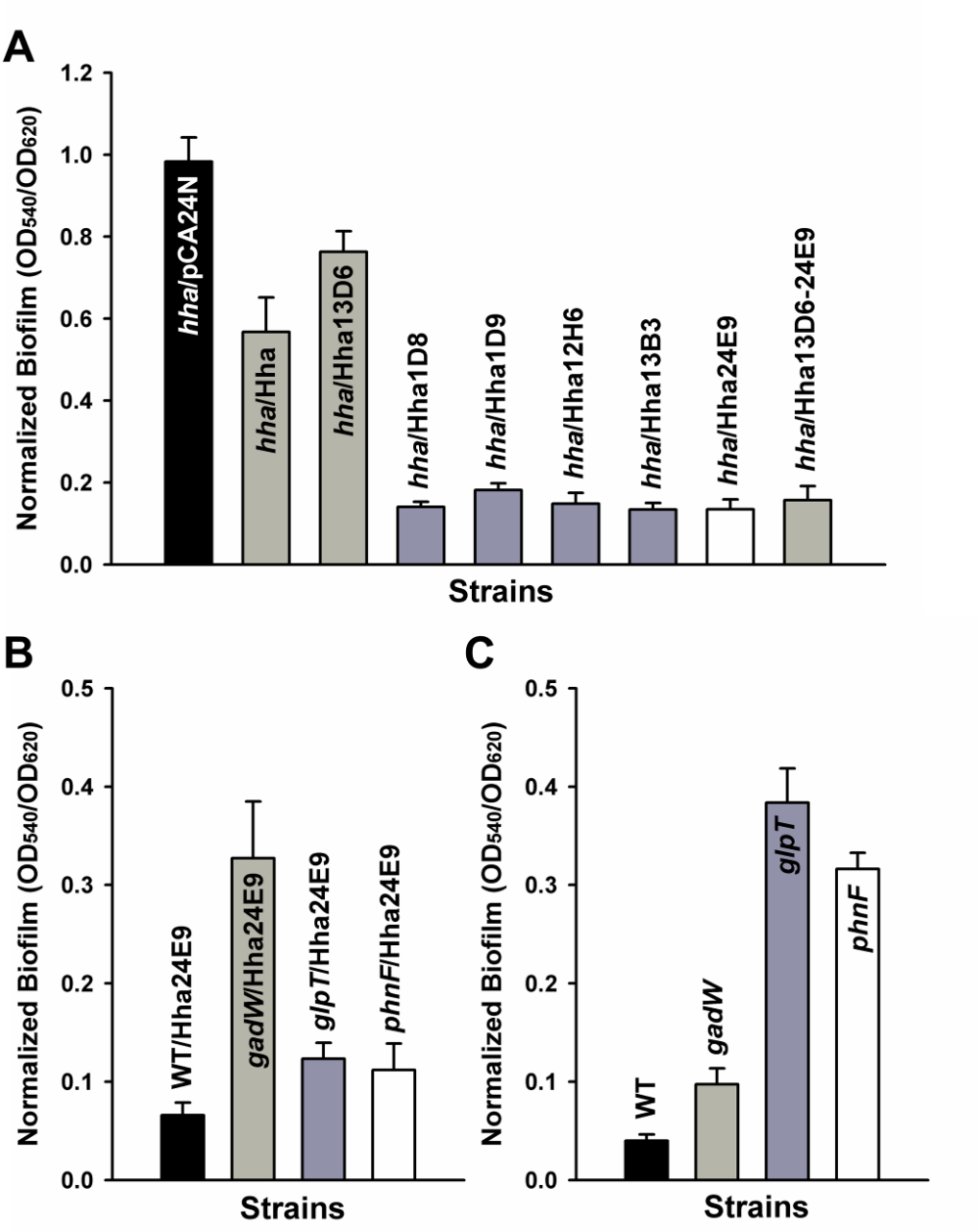

Figure 4.2 Engineering Hha for reduction in biofilm formation. Normalized biofilm formation for BW25113 *hha* (*hha*) producing Hha13D6, Hha1D8, Hha1D9, Hha12H6, Hha13B3, Hha24E9, and Hha13D6-24E9 from pCA24N using 1 mM IPTG in LB glucose after 24 h at 37°C (A), and for BW25113 (WT), BW25113 *gadW* (*gadW*), BW25113 *glpT* (*glpT*), BW25113 *phnF* (*phnF*) producing Hha24E9 after 24 h (B). Normalized biofilm formation for BW25113 *gadW*, BW25113 *glpT*, and BW25113 *phnF* after 7 h (C). Each data point is the average of at least twelve replicate wells from two independent cultures, and one standard deviation is shown.

To study biofilm dispersal by Hha13D6 in a more rigorous manner, we conducted flow-cell biofilm dispersal experiments in which biofilms were formed for 42 h followed by induction of Hha for 6 h. We chose 42 to 48 h for the flow cell work since we found wild-type BW25113 disperses naturally after 42 h (results not shown). As expected based on its enhanced biofilm dispersal in 96-well plates, Hha13D6 induced more biofilm dispersal in the flow-cell relative to wild-type Hha (Fig. 4.1B). COMSTAT statistical analysis (Table 4.2) shows that 97% of the biomass was removed with Hha13D6, and the mean thickness (96%) and the surface coverage (96%) were also reduced dramatically at 48 h with isopropyl-β-*D*-thiogalactopyranoside (IPTG) addition compared to 48 h biofilms without IPTG. Overproducing wild-type Hha removed 35% of the biofilms, and cells producing both Hha and Hha13D6 had similar amounts of biofilm initially at 42 h (Fig. 4.1B). Therefore, both static and flow-cell biofilm experiments confirm that Hha13D6 was engineered to enhance biofilm dispersal dramatically.

4.3.2 Saturation mutagenesis at position D22, L40, V42, and D48 of Hha

Since Hha13D6 has four amino acid replacements (D22V, L40R, V42I, and D48A) (Fig. 4.1C), each position was investigated for its role in the increased biofilm dispersal by substituting all possible amino acids via saturation mutagenesis using both wild-type Hha and Hha13D6. After screening 2256 colonies (282 colonies × 4 positions × 2 proteins) to ensure with a 99% probability that all possible codons were utilized at four positions (Rui *et al.*, 2004), we identified the D22M replacement (i.e., D22M along with L40R, V42I and D48A) that causes a 40 ± 10% increase in biofilm dispersal in the static biofilm assay compared to no IPTG addition (HhaSM2C1, Table 4.1); although, this variant causes the cells to undergo less dispersal than Hha13D6. We did not obtain any interesting biofilm dispersal variants using wild-type Hha. Therefore, the biofilm dispersal phenotype arises from the interaction of several amino acid replacements.

Table 4.2 COMSTAT analysis for flow-cell biofilms producing Hha13D6. Biofilm parameters of biofilms producing wild-type Hha (BW25113 *hha*/pC24N-*hha*/pCM18) and Hha13D6 (BW25113 *hha*/pC24N-*hha13D6*/pCM18) in flow cells were measured in LB glucose (0.2%) medium after 48 h (6 h with 1 mM IPTG or no IPTG addition as a control) at 37°C.

COMSTAT values	**Time**	***hha*/Hha**	***hha*/Hha13D6**
Biomass ($\mu m^3/\mu m^2$)	42 h	6 ± 1	5 ± 1
	48 h	4.0 ± 0.6	7 ± 3
	48 h (6 h with 1 mM IPTG)	3 ± 3	0.2 ± 0.2
Surface coverage (%)	42 h	16 ± 3	15 ± 5
	48 h	13 ± 4	19 ± 6
	48 h (6 h with 1 mM IPTG)	8 ± 7	0.8 ± 0.5
Mean thickness (μm)	42 h	10 ± 3	8 ± 2
	48 h	7 ± 1	11 ± 4
	48 h (6 h with 1 mM IPTG)	5 ± 4	0.4 ± 0.4
Roughness coefficient	42 h	1.1 ± 0.2	1.2 ± 0.2
	48 h	1.4 ± 0.1	1.1 ± 0.3
	48 h (6 h with 1 mM IPTG)	1.6 ± 0.3	1.95 ± 0.03

4.3.3 Hha13D6 increases cell lysis

Hha is toxic and is part of a putative toxin-antitoxin pair with antitoxin TomB (García-Contreras *et al.*, 2008). Therefore we assayed the toxicity of the engineered Hha three ways and found Hha13D6 is substantially more toxic than wild-type Hha. Hha13D6 repressed cell growth four fold (Fig. 4.3A), decreased cell viability by 10,000 fold (Fig. 4.3B), and increased cell lysis by an order of magnitude (Fig. 4.3C) at early times. Longer incubation times resulted in restoring both cell growth and viability for cells producing Hha13D6, which is probably due to an increase in resistance (Smith and Romesberg, 2007) to the Hha13D6 toxicity during the extended incubation.

4.3.4 HslV is important for biofilm dispersal with Hha13D6

Since whole-transcriptome profiling yields insights into the mechanism of biofilm formation and dispersal (Wood, 2009), we investigated how overproducing Hha13D6 regulates gene expression during biofilm dispersal. Glass wool has been used by us as a substratum for biofilm formation for whole-transcriptome analysis for *E. coli* (Ren *et al.*, 2004a; Domka *et al.*, 2007) and has been used for *P. aeruginosa* (Steyn *et al.*, 2001; Ueda and Wood, 2009), since it provides a large surface to volume ratio which promotes a large amount of biofilm biomass. The results from whole-transcriptome studies with glass wool have also been corroborated with 96-well plate assays (Domka *et al.*, 2007). Hence, in this experiment, biofilms were formed on glass wool for 16 h followed by 1 h of production of Hha13D6 and wild-type Hha, and gene expression was compared.

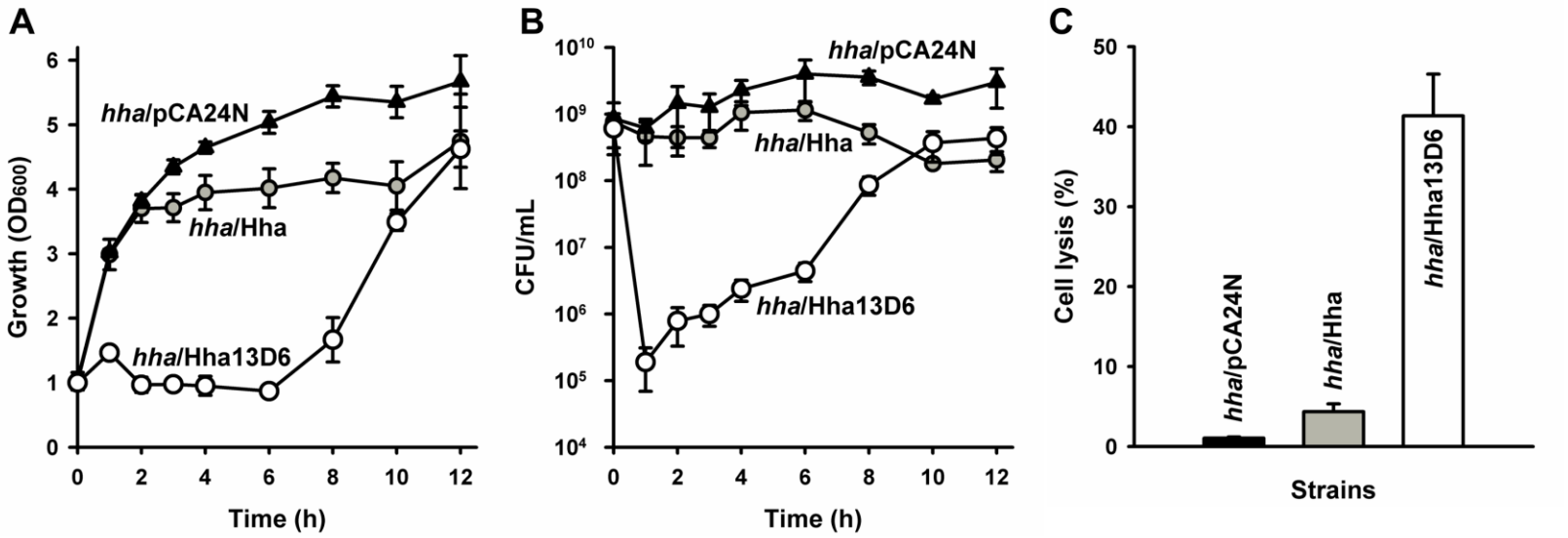

Figure 4.3 Hha13D6 causes cell lysis. Cell growth (A), CFU (B), and cell lysis (C) of Hha13D6 produced in BW25113 *hha*. Cells were grown in LB glucose at 37°C until a turbidity of 1, then 1 mM IPTG was added. Cell lysis was quantified by measuring eDNA at 4 h after 1 mM IPTG addition. Two independent cultures were used.

Hha13D6 induced acid resistance genes (*gadABCEX* and *hdeABD*) and several heat-shock genes including protease genes (*clpB, hslOR, hslUV, htpG, ibpAB, lon, prlC,* and *ycjF*) compared to wild-type Hha (Table 4.3). These results are consistent with our previous results with wild-type Hha in that it increased production of the proteases ClpXP and Lon (García-Contreras *et al.*, 2008). Corroborating these results, qRT-PCR confirmed that overproducing Hha13D6 induced the transcription of *gadA* by 1.6 fold, *gadE* by 1.7 fold, *gadX* by 1.5 fold, *clpB* by 9.2 fold, *hslU* by 3.3 fold, *hslV* by 1.6 fold, *ibpA* by 1.6 fold, *ibpB* by 2.7 fold, *lon* by 1.8 fold, *prlC* by 3.2 fold, and *ycjF* by 1.6 fold. ClpB refolds stress-damaged proteins with DnaK (Hsp70) (Mogk *et al.*, 2008) and has ATPase activity (Woo *et al.*, 1992), and IbpAB facilitate refolding of denatured proteins by forming a functional triad with ClpB and DnaK (Mogk *et al.*, 2003). ATP dependent proteases such as HslUV and Lon are responsible for the degradation of several regulatory proteins and abnormal proteins during stress which controls many cellular processes (Schmidt *et al.*, 2009). For example, overproduction of Lon inhibits translation in *E. coli* by degrading antitoxin YefM which results in induction of the toxin gene *yoeB* (Christensen *et al.*, 2004). PrlC cleaves peptides generated by proteases Lon, HslUV, and ClpAP (Jain and Chan, 2007), and YcjF is a heat shock protein (Rasouly and Ron, 2009). Therefore, Hha13D6 may have more toxicity via the activation of heat shock (ClpB, HslUV, Lon, PrlC, YcjF, IbpAB) and acid resistance (GadAEX) systems.

To test this hypothesis, we assayed biofilm dispersal via production of Hha13D6 in *hha* hosts that also lack *clpB, hslU, hslV, lon, prlC, ycjF, ibpA, ibpB, gadA, gadE,* and *gadX* (Fig. 4.1D). Deletion of *hslV* in the *hha* host reduced the level of biofilm dispersal by Hha13D6 by an order of magnitude whereas deletion of *clpB, lon, hslU, prlC,* or *ycjF* only partially decreased biofilm dispersal. In contrast, deletion of *ibpA, ibpB gadA, gadE,* or *gadX* did not reduce biofilm dispersal. Hence, HslV is important for the enhanced biofilm dispersal activity of Hha13D6. HslUV protease consists of two functional units, HslU ATPase and HslV peptidase, and although HslU stimulates proteolytic activity of HslV, HslV alone can digest certain unfolded proteins such as unfolded lactalbumin (Lee *et al.*, 2007d). Hence, Hha13D6 enhances biofilm dispersal via proteases, primarily through HslV.

4.3.5 Hha13D6 has little impact on c-di-GMP and swimming motility

Lower levels of c-di-GMP generally results in an increase in motility and induces biofilm dispersal (Kaplan, 2010). Since Hha13D6 induces biofilm dispersal, we measured swimming motility and c-di-GMP concentration using high performance liquid chromatography (HPLC) upon inducing wild-type Hha and Hha13D6. Production of Hha13D6 reduced slightly the swimming motility of the host (halo diameter 4 ± 1 cm with Hha13D6 vs. 5.6 ± 0.1 cm with wild-type Hha). In addition, cellular c-di-GMP concentrations were slightly decreased by Hha13D6 (c-di-GMP concentration 7 ± 3 nmol/g cells with Hha13D6 vs. 13 ± 2 nmol/g cells with wild-type Hha). Therefore, the decreased level of c-di-GMP by Hha13D6 may partially contribute to the greater biofilm dispersal, although Hha13D6 did not increase swimming motility. However, the small reduction in swimming motility with Hha13D6 confirms the whole-transcriptome results that indicated the flagella operons (*flgBCDEFG* and *fliACGHILN*) were repressed (Table 4.3).

Table 4.3 Partial whole-transcriptome profiles to determine the impact of Hha13D6 on biofilm dispersal. List of differentially-expressed genes for biofilm dispersal of BW25113 *hha*/pCA24N-*hha13D6* versus BW25113 *hha*/pCA24N-*hha* grown in LB glucose at 37°C for 16 h, and then 1 mM IPTG was added for 1 h. Raw data for the two DNA microarrays are available using GEO series accession number GSE21604.

Group and gene	b number	Fold change	Description
Stress response			
clpB	b2592	3.0	ATP-dependent protease, Hsp 100, part of multi-chaperone system with *dnaK*, *dnaJ*, and *grpE*
dnaK	b0014	-2.8	Chaperone Hsp70 in DNA biosynthesis/cell division
ftsJ	b3179	2.0	23S rRNA methyltransferase
gadA	b3517	2.6	Glutamate decarboxylase A subunit
gadC	b1492	2.3	Acid sensitivity protein, putative transporter
gadE	b3512	2.8	Transcriptional regulator of the *gadABC* operon
gadX	b3516	2.5	Transcriptional activator for *gadA* and *gadBC*
hdeA	b3510	2.0	Periplasmic chaperone of acid-denatured proteins
hdeB	b3509	2.1	Periplasmic chaperone of acid-denatured proteins
hdeD	b3511	2.0	Putative membrane transporter
hslO	b3401	2.5	Hsp33, oxidative stress-induced heat shock chaperone
hslR	b3400	2.1	Hsp15, a heat shock protein that binds free 50S subunits; binds RNA and DNA
hslU	b3931	2.6	ATPase component of the HslUV protease, also functions as molecular chaperone
hslV	b3932	3.7	Heat shock protein HslUV, proteasome-related peptidase subunit
htpG	b0473	3.0	Heat shock chaperone, HSP90 family
ibpA	b3687	2.0	Chaperone, heat-inducible protein of HSP20 family
ibpB	b3686	2.6	Chaperone, heat-inducible protein of HSP20 family
lon	b0439	2.6	DNA-binding ATP-dependent protease LA; heat shock K-protein
mopB	b4142	-4.6	GroES, 10 kDa chaperone binds to Hsp60 in pres. Mg-ATP, suppressing its atpase activity
prlC	b3498	2.0	Oligopeptidase A
ybbN	b0492	2.6	DnaK co-chaperone, thioredoxin-like protein
ycgF	b1163	-2.5	Anti-repressor for *ycgE*, blue light-responsive; cold shock gene, EAL domain
ycjF	b1322	3.5	Hypothetical protein
ycjX	b1321	3.5	Hypothetical protein
ynfN	b1551	-2.6	Cold shock gene, function unknown, Qin prophage
Motility and secretion			
flgB	b1073	-3.0	Flagellar biosynthesis, cell-proximal portion of basal-body rod
flgC	b1074	-3.2	Flagellar biosynthesis, cell-proximal portion of basal-body rod
flgD	b1075	-3.0	Flagellar biosynthesis, initiation of hook assembly
flgE	b1076	-2.8	Flagellar biosynthesis, hook protein
flgF	b1077	-3.5	Flagellar biosynthesis, cell-proximal portion of basal-body rod
flgG	b1078	-2.0	Flagellar biosynthesis, cell-distal portion of basal-body rod
fliA	b1922	-2.3	Flagellar biosynthesis; alternative sigma factor 28; regulation of flagellar operons
fliC	b1923	-2.5	Flagellar biosynthesis; flagellin, filament structural protein
fliG	b1939	-2.3	Flagellar biosynthesis, component of motor switching and energizing, enabling rotation and determining its direction

Table 4.3 Continued.

Group and gene	b number	Fold change	Description
fliH	b1940	-2.0	Flagellar biosynthesis; export of flagellar proteins
fliI	b1941	-2.0	Flagellum-specific ATP synthase
fliL	b1944	-2.3	Flagellar biosynthesis
fliN	b1946	-2.0	Flagellar biosynthesis, component of motor switch and energizing, enabling rotation and determining its direction
flu	b2000	-6.5	CP4-44 prophage; phase-variable outer membrane-associated fluffing protein, affects surface properties, piliation, colonial morphology
Transcription and translation			
cnu	b1625	2.3	Hha paralog, oriC-binding protein
csiE	b2535	2.0	Stationary phase inducible protein
dinG	b0799	-2.1	ATP-dependent DNA helicase, LexA-regulated (SOS) repair enzyme
insL	b0016	2.1	IS186 gene, transposition function
iscR	b2531	-2.0	Fe-S cluster-containing transcription factor
mfd	b1114	2.0	Transcription-repair ATP-dependent coupling factor
mlc	b1594	2.1	Putative NAGC-like transcriptional regulator
nusA	b3169	-2.5	Transcription pausing; L factor
obgE	b3183	-2.0	Putative GTP-binding factor
priB	b4201	-2.3	Primosomal replication protein N
queA	b0405	-2.0	S-adenosylmethionine: tRNA(m6t6A37) ribosyltransferase-isomerase
rhlE	b0797	-3.2	Putative ATP-dependent RNA helicase
rimM	b2608	-2.0	16S rRNA processing protein
rlmG	b3084	-2.0	23S rRNA m(2)G1835 methyltransferase
rmf	b0953	-8.6	Ribosome modulation factor
rnr	b4179	-2.3	Exoribonuclease R
rplB	b3317	-2.0	50S ribosomal subunit protein L2
rplC	b3320	-2.0	50S ribosomal subunit protein L3
rplD	b3319	-2.1	50S ribosomal subunit protein L4, regulates expression of S10 operon
rplN	b3310	2.5	50S ribosomal subunit protein L14
rplW	b3318	2.0	50S ribosomal subunit protein L23
rpmE	b3936	-2.0	50S ribosomal subunit protein L31
rpoD	b3067	2.6	RNA polymerase, sigma(70) factor; regulation of proteins induced at high temperatures
rpsF	b4200	-2.3	30S ribosomal subunit protein S6
rpsJ	b3321	-2.0	30S ribosomal subunit protein S10
rpsR	b4202	-2.1	30S ribosomal subunit protein S18
srmB	b2576	-2.0	ATP-dependent RNA helicase
typA	b3871	-2.0	GTP-binding elongation factor family protein
uvrA	b4058	-2.3	DNA excision repair enzyme subunit, with UvrBC
yhbY	b3180	-2.0	RNA binding protein, associated with pre-50S ribosomal subunits
zntR	b3292	2.3	Zn-responsive activator of *zntA* transcription
Transport and metabolism			
dctR	b3507	2.1	Probable repressor of *dctA* dicarboxylate transporter gene
ilvL	b3766	2.0	*ilvGEDA* operon leader peptide
ldhA	b1380	2.5	Fermentative *D*-lactate dehydrogenase, NAD-dependent
lipB	b0630	2.0	Protein of lipoate biosynthesis

Table 4.3 Continued.

Group and gene	b number	Fold change	Description
macB	b0879	2.8	ABC-type macrolide efflux transporter
mocA	b2877	2.0	Molybdopterin cytidylyltransferase
xylF	b3566	2.1	*D*-xylose transport protein
yhiD	b3508	2.5	Integral membrane protein related to MgtC
ynfM	b1596	2.1	Putative transporter
carA	b0032	-2.1	Carbamoyl phosphate synthetase, glutamine amidotransferase small subunit
cmk	b0910	-2.1	Cytidine monophosphate (CMP) kinase
cvpA	b2313	-2.8	Membrane protein required for colicin V production
cyoA	b0432	-2.1	Cytochrome o ubiquinol oxidase subunit II
cysK	b2414	-2.3	Cysteine synthase A, O-acetylserine sulfhydrolase A
glnA	b3870	-2.1	Glutamine synthetase
glnL	b3869	-2.1	Histidine protein kinase sensor for *glnG* regulator (nitrogen regulator II, NRII)
glnP	b0810	-2.0	Glutamine high-affinity transport system; membrane component
glnQ	b0809	-2.0	ATP-binding component of glutamine high-affinity transport system
hisC	b2021	-2.0	Histidinol phosphate aminotransferase
hisD	b2020	-2.3	*L*-histidinal:NAD+ oxidoreductase; *L*-histidinol:NAD+ oxidoreductase
iscS	b2530	-2.1	Cysteine desulfurase used in synthesis of Fe-S clusters and 4-thiouridine
iscU	b2529	-2.0	Involved in Fe-S biosynthesis
purE	b0523	-2.5	Phosphoribosylaminoimidazole carboxylase = AIR carboxylase, catalytic subunit
purH	b4006	-2.1	Bifunctional: IMP cyclohydrolase (N-terminal); phosphoribosylaminoimidazolecarboxamide formyltransferase (C-terminal)
purM	b2499	-3.2	Phosphoribosylaminoimidazole synthetase (AIR synthetase)
pyrL	b4246	-2.5	PyrBI operon leader peptide
suhB	b2533	-2.1	Inositol monophosphatase
upp	b2498	-2.1	Uracil phosphoribosyltransferase
ygeX	b2871	-2.0	2,3-diaminopropionate ammonia lyase
Cellular process			
cysP	b2425	-2.8	Thiosulfate binding protein
dniR	b0211	-2.0	Lytic murein transglycosylase C, membrane-bound
fxsA	b4140	3.7	Suppress F exclusion of bacteriophage T7
hybB	b2995	-2.0	Probable cytochrome Ni/Fe component of hydrogenase-2
rfaQ	b3632	-2.1	Glycosyltransferase needed for heptose region of LPS core
ssnA	b2879	-2.0	Soluble protein involved in cell viability at the beginning of stationary phase
tfaP	b1155	2.3	Predicted tail fiber assembly gene, e14 prophage
ydeH	b1535	-2.0	Diguanylate cyclase, GGDEF domain, required for *pgaD* induction

Table 4.3 Continued.

Group and gene	b number	Fold change	Description
Function unknown			
-	b4434	-2.3	Hypothetical protein
isrC	b4435	-4.0	Novel sRNA, function unknown, CP4-44 prophage
ycaO	b0905	-2.5	Hypothetical protein
ydjN	b1729	-2.6	Hypothetical protein
yeaD	b1780	2.6	Hypothetical protein
yhbE	b3184	-2.5	Hypothetical protein
yhdN	b3293	2.3	Hypothetical protein

4.3.6 Random mutagenesis of Hha for biofilm formation

In an effort to identify Hha variants that cause reduced biofilm formation (rather than increased biofilm dispersal), 2656 colonies for altered biofilm formation were screened using polystyrene 96-well plates, and five Hha variants were identified that decreased biofilm formation more than 4 fold compared to wild-type Hha (Table 4.1). Among the five Hha biofilm variants, three variants had truncations; hence, the amino-terminal region of Hha is most important for controlling biofilm formation.

Among the five best biofilm variants, Hha24E9 (K62X) decreased biofilm formation 4 fold compared to wild-type Hha in BW25113 *hha* (Fig. 4.2A). To investigate how Hha24E9 represses biofilm formation, a whole-transcriptome analysis was performed using biofilm cells of Hha24E9 vs. wild-type Hha in rich medium after 7 h (Table 4.4). Acid resistance (*gadAEW*), arginine metabolism (*astABD*), sulfate metabolism (*cysHJ*), glycerol-3-phosphate metabolism (*glpABCKQT*), phosphonate metabolism (*phnACEFGJL*), and outer membrane (*ompW*) genes were highly induced, and stress response (*cspF*, *cpxP*, and *bhsA*) and glucose phosphotransferase system (*ptsG*) genes were repressed by Hha24E9. Although indole related genes (*tnaABC*) were induced, indole production does not occur in this medium due to catabolic repression. Corroborating the whole-transcriptome results, Hha24E9 induced transcription of *gadW* by 26 fold ($\Delta\Delta C_T$ = -4.7 ± 0.2), *glpT* by 120 fold ($\Delta\Delta C_T$ = -6.9 ± 0.3), and *phnF* by 132 fold ($\Delta\Delta C_T$ = -7.0 ± 0.5).

Table 4.4 Partial whole-transcriptome profiles to determine the impact of Hha24E9 on biofilm formation. List of differentially-expressed genes for biofilm formation of BW25113 *hha*/pCA24N-*hha24E9* versus BW25113 *hha*/pCA24N-*hha* grown in LB glucose with 1 mM IPTG for 7 h at 37°C. Raw data for the two DNA microarrays are available using GEO series accession number GSE21604.

Group and gene	b number	Fold change	Description
Stress response			
cpxP	b3913	-7.5	Regulator, chaperone involved in resistance to extracytoplasmid stress
cspF	b1558	-5.3	Qin prophage; cold shock protein
gadA	b3517	11.3	Glutamate decarboxylase A subunit
gadE	b3512	16.0	Transcriptional regulator of the *gadABC* operon
gadW	b3515	11.3	Transcriptional activator of *gadA* and *gadBC* in absence of GadX; repressor of *gadX*
marR	b1530	-7.0	Multiple antibiotic resistance protein; repressor of mar operon
pspB	b1305	11.3	Stimulates PspC-mediated transcriptional activation of the *psp* operon; antitoxin of a PspC-PspB toxin-antitoxin pair
Indole related			
tnaA	b3708	12.1	*L*-cysteine desulfhydrase / tryptophanase
tnaB	b3709	18.4	TnaB tryptophan ArAAP transporter
tnaC	b3707	39.4	Tryptophanase leader peptide
Energy production and conversion			
glpA	b2241	34.3	Glycerol-3-phosphate-dehydrogenase, anaerobic
glpB	b2242	26.0	Glycerol-3-phosphate-dehydrogenase, anaerobic
glpC	b2243	32.0	Glycerol-3-phosphate-dehydrogenase, anaerobic
glpK	b3926	16.0	Glycerol kinase
glpQ	b2239	12.1	Glycerophosphoryl diester phosphodiesterase, periplasmic
glpT	b2240	55.7	Glycerol-3-P MFS transporter
hycB	b2724	29.9	Formate hydrogenlyase complex
lldD	b3605	14.9	*L*-lactate:quinone oxidoreductase
lldP	b3603	16.0	Lactate transporter
lldR	b3604	16.0	Transcriptional repressor
nrfC	b4072	13.0	Nitrite reductase complex
Transport and metabolism			
ackA	b2296	-5.3	Acetate kinase
acs	b4069	39.4	Putative hydroxycinnamate-CoA ligase / acetyl-CoA synthetase
actP	b4067	16.0	Acetate permease
ada	b2213	10.6	Ada transcriptional dual regulator / O-6-methylguanine-DNA methyltransferase
aldB	b3588	10.6	Putative aminobutyraldehyde dehydrogenase / aldehyde dehydrogenase B
alsC	b4086	13.9	Allose transport
alsE	b4085	13.9	Allulose-6-phosphate 3-epimerase
aslA	b3801	10.6	Arylsulfatase
asnA	b3744	-5.3	Asparagine synthetase A
astA	b1747	19.7	Arginine succinyltransferase
astB	b1745	12.1	Succinylarginine dihydrolase
astD	b1746	18.4	Succinylglutamic semialdehyde dehydrogenase
cadA	b4131	11.3	Lysine decarboxylase
cadB	b4132	10.6	Cadaverine/lysine APC exchanger / Transporter

Table 4.4 Continued.

Group and gene	b number	Fold change	Description
citC	b0618	12.1	Citrate lyase ligase
csiD	b2659	10.6	Carbon starvation induced gene
cstC	b1748	27.9	Acetylornithine transaminase, catabolic / succinylornithine transaminase
cysH	b2762	18.4	3'-phospho-adenylylsulfate reductase
cysJ	b2764	11.3	Sulfite reductase flavoprotein subunit
dppF	b3540	13.0	Dipeptide ABC transporter
ebgC	b3077	11.3	Evolved beta-*D*-galactosidase, beta subunit; cryptic gene
exbB	b3006	-4.9	Uptake of enterobactin; tonB-dependent uptake of B colicins
exbD	b3005	-4.9	Uptake of enterobactin; tonB-dependent uptake of B colicins
fabA	b0954	-4.9	Beta-hydroxydecanoyl thioester dehydrase (trans-2-decenoyl-ACP isomerase)
frwB	b3950	13.9	Putative fructose-like PTS system enzyme IIB
guaA	b2507	-5.7	GMP synthetase (glutamine aminotransferase)
guaB	b2508	-4.9	IMP dehydrogeanse
hisA	b2024	-4.9	*N*-(5'-phospho-*L*-ribosyl-formimino)-5-amino-1- (5'-phosphoribosyl)-4-imidazolecarboxamide isomerase
hisB	b2022	-5.3	Bifunctional: histidinol-phosphatase (N-terminal); imidazoleglycerol-phosphate dehydratase (C-terminal)
hisC	b2021	-5.3	Histidinol phosphate aminotransferase
hisD	b2020	-7.0	*L*-histidinal:NAD+ oxidoreductase; *L*-histidinol:NAD+ oxidoreductase
hisF	b2025	-4.6	Imidazole glycerol phosphate synthase subunit in heterodimer with HisH = imidazole glycerol phosphate synthase holoenzyme
hisG	b2019	-6.5	ATP phosphoribosyltransferase
hisH	b2023	-4.9	Glutamine amidotransferase subunit of heterodimer with HisF = imidazole glycerol phosphate synthase holoenzyme
hyuA	b2873	11.3	*D*-stereospecific phenylhydantoinase
mglA	b2149	13.0	Galactose ABC transporter
moaC	b0783	10.6	Molybdopterin biosynthesis, protein C
ndh	b1109	-10.6	Respiratory NADH dehydrogenase
nikA	b3476	16.0	Nickel ABC transporter / Transporters
norV	b2710	11.3	NO reductase
phnC	b4106	13.9	Alkylphosphonate ABC transporter
phnE	b4104	19.7	Alkylphosphonate ABC transporter
phnE'	b4103	11.3	Putative C terminus of split *phnE* gene product
phnF	b4102	12.1	Phosphonate utilization
phnG	b4101	13.9	Phosphonate metabolism
phnJ	b4098	16.0	Phosphonate metabolism
phnL	b4096	10.6	Carbon-phosphorus lyase complex subunit
potA	b1126	-4.6	ATP-binding component of spermidine/putrescine transport
potB	b1125	-4.3	Spermidine/putrescine transport protein (ABC superfamily, membrane)
potC	b1124	-4.3	Spermidine/putrescine transport protein (ABC superfamily, membrane)
potD	b1123	-4.6	Spermidine/putrescine periplasmic transport protein
proV	b2677	-7.5	ATP-binding component of transport system for glycine, betaine and proline

Table 4.4 Continued.

Group and gene	b number	Fold change	Description
proW	b2678	-8.0	Glycine/betaine/proline transport protein (ABC superfamily, membrane)
proX	b2679	-5.7	Glycine/betaine/proline transport protein (ABC superfamily, peri_bind)
prsA	b1207	-4.9	Phosphoribosylpyrophosphate synthetase
psuG	b2165	16.0	Pseudouridine 5'-phosphate glycosidase
ptsG	b1101	-6.5	Glucose phophotransferase enzyme IIBC(Glc)
speD	b0120	-5.3	S-adenosylmethionine decarboxylase
speE	b0121	-5.3	Spermidine synthase (putrescine aminopropyltransferase)
srlA	b2702	16.0	Split PTS system, glucitol/sorbitol-specific IIB component, see b2703
suhB	b2533	-5.3	Inositol monophosphatase
ybaS	b0485	13.9	Putative glutaminase
yeiT	b2146	13.0	Dihydropyrimidine dehydrogenase
yhjX	b3547	32.0	MFS transporter
Transciption and translation			
alaS	b2697	11.3	Alanyl-tRNA synthetase
apt	b0469	-4.6	Adenine phosphoribosyltransferase
cmk	b0910	-4.3	Cytidine monophosphate (CMP) kinase
dusB	b3260	-5.3	tRNA-dihydrouridine synthase B
fis	b3261	-6.1	DNA-binding protein for site-specific recombination and inversion, transcription of rRNA and tRNA operons, and DNA replication
melR	b4118	13.9	Melibiose transcriptional activator
mhpB	b0348	12.1	3-(2,3-dihydroxyphenyl)propionate dioxygenase
mhpR	b0346	12.1	Transcriptional activator of *mhp* operon
nrdA	b2234	-4.9	Ribonucleoside diphosphate reductase 1, alpha subunit
nrfF	b4075	10.6	Activator of formate-dependent nitrite reductase complex
obgE	b3183	-4.6	Putative GTP-binding factor
pheS	b1714	-4.6	Phenylalanine tRNA synthetase, alpha-subunit
pheT	b1713	-4.3	Phenylalanine tRNA synthetase, beta-subunit
priB	b4201	-5.3	Primosomal replication protein N
purB	b1131	-4.3	Adenylosuccinate lyase
pyrF	b1281	-4.9	Orotidine-5'-phosphate decarboxylase
rhlE	b0797	-4.6	Putative ATP-dependent RNA helicase
rlmH	b0636	-4.6	rRNA large-subunit methylation
rluB	b1269	-5.7	Hypothetical protein
rmf	b0953	-4.6	Ribosome modulation factor
rnpA	b3704	-4.6	RNase P, protein component; protein C5
rplB	b3317	-4.6	50S ribosomal subunit protein L2
rplI	b4203	-4.6	50S ribosomal subunit protein L9
rplM	b3231	-4.3	50S ribosomal subunit protein L13
rplV	b3315	-4.6	50S ribosomal subunit protein L22
rpmA	b3185	-4.3	50S ribosomal subunit protein L27
rpmC	b3312	-5.7	50S ribosomal subunit protein L29
rpmF	b1089	-5.3	50S ribosomal subunit protein L32
rpsC	b3314	-4.6	30S ribosomal subunit protein S3

Table 4.4 Continued.

Group and gene	b number	Fold change	Description
rpsF	b4200	-4.3	30S ribosomal subunit protein S6
rpsI	b3230	-6.1	30S ribosomal subunit protein S9
rpsU	b3065	-4.6	30S ribosomal subunit protein S21
rttR	b4425	-4.3	Repeat tyrT RNA; modulate stringent response
tgt	b0406	-4.9	tRNA-guanine transglycosylase
tpr	b1229	-6.5	Protamine like protein
upp	b2498	-4.6	Uracil phosphoribosyltransferase
ybeB	b0637	-4.6	Ribosome-associated protein
ychF	b1203	-4.9	Putative GTP-binding protein
ygjH	b3074	13.9	Putative tRNA synthetase
Cell wall/membrane and motility			
bhsA	b1112	-4.3	Influencing Biofilm through Hydrophobicity and Stress response
borD	b0557	-4.6	Lipoprotein in DLP12 prophage
gtrA	b2350	-4.3	CPS-53 (KpLE1) prophage; putative integral membrane protein
hflD	b1132	-4.3	Downregulates lambda lysogenization, peripheral membrane protein
mbhA	b0230	11.3	Putative motility protein
mdtN	b4082	12.1	Putative membrane protein
mdtO	b4081	10.6	PET family membrane translocase (MDR) of tripartite MdtNOP efflux pump
mipA	b1782	-4.3	MltA-interacting protein; outer membrane
mltD	b0211	-5.7	Lytic murein transglycosylase C, membrane-bound
ompW	b1256	24.3	Outer membrane protein
tig	b0436	-4.6	Peptidyl-prolyl cis/trans isomerase (trigger factor), molecular chaperone involved in cell division
yccA	b0970	-5.7	Membrane-associated protein that binds to FtsH(HflB) and HflKC proteins
ydcX	b1445	-4.3	Required for swarming phenotype
yeiP	b2171	-4.3	Putative elongation factor
yjfO	b4189	11.3	Hypothetical protein, probable lipoprotein
ykgI	b0303	10.6	Hypothetical protein, predicted periplasmic protein
Function unknown			
ybaE	b0445	11.3	Hypothetical protein
ybbV	b0510	18.4	Hypothetical protein
ycaO	b0905	-5.7	Hypothetical protein
yceD	b1088	-4.3	Hypothetical protein
yhbE	b3184	-6.1	Hypothetical protein
yjbL	b4047	13.9	Hypothetical protein
yjcH	b4068	21.1	Hypothetical protein
yjjM	b4357	11.3	Hypothetical protein
ymgG	b1172	-4.3	Hypothetical protein
yncE	b1452	-4.6	Hypothetical protein
yqeC	b2876	13.9	Hypothetical protein
yqgD	b2941	13.0	Hypothetical protein
-	b3004	10.6	Hypothetical protein
-	b3914	-8.0	Hypothetical protein

To determine if some of the proteins encoded by these genes are related to the ability of Hha24E9 to reduce biofilm formation, we checked biofilm formation with Hha24E9 in *gadW*, *glpT*, and *phnF* mutants and found Hha24E9 does not decrease biofilm formation in these mutants (Fig. 4.2B). Corroborating these results, deletion of *gadW*, *glpT*, and *phnF* increased biofilm formation considerably after 7 h (Fig. 4.2C); hence, GadW, GlpT, and PhnF decrease biofilm formation. Hence, the engineered Hha24E9 reduces biofilm formation by inducing acid resistance, glycerol-3-phosphate metabolism, and phosphonate metabolism.

4.3.7 Combining the Hha13D6 and Hha24E9 amino acid replacements decreases biofilm formation but does not induce biofilm dispersal

Hha variants Hha13D6 (D22V, L40R, V42I, and D48A) and Hha24E9 (K62X) were obtained with different phenotype screens; Hha24E9 does not induce biofilm dispersal (Fig. 4.4), and Hha13D6 does not decrease biofilm formation at 24 h (Fig. 4.2A) indicating that the Hha replacements necessary for biofilm dispersal are different from those that influence biofilm formation. To determine whether dispersal or biofilm formation could be enhanced by combining these amino acid replacements, truncation at K62 was introduced to Hha13D6 using site-directed mutagenesis. Hha13D6-24E9, the combined variant (Table 4.1), did not cause dispersal (Fig. 4.4) and reduced biofilm formation like Hha24E9 (Fig. 4.2A). These results indicate that the carboxy-terminal region of Hha is necessary for biofilm dispersal and the amino-terminal region is necessary for reducing biofilm formation.

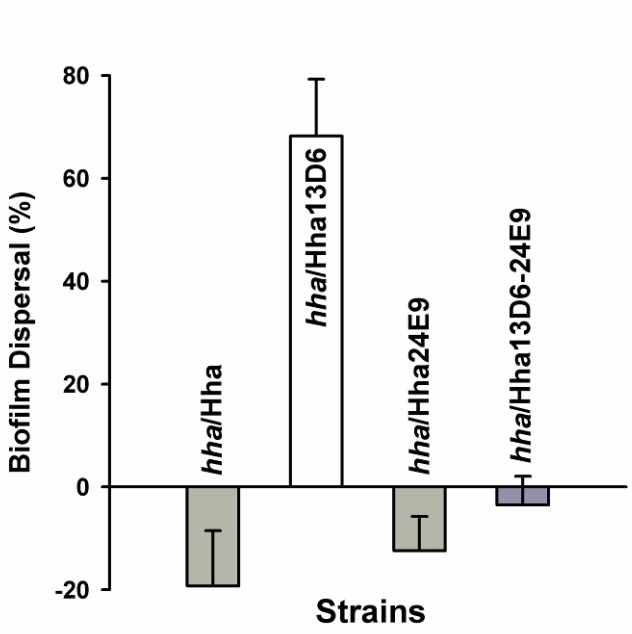

Figure 4.4 Biofilm dispersal with combined Hha13D6-24E9. Biofilm dispersal of BW25113 *hha* producing Hha13D6, Hha24E9, and Hha13D6-24E9 after 32 h (8 h with 1 mM IPTG) in LB glucose at 37°C. Each data point is the average of at least two independent cultures, and one standard deviation is shown.

4.4 Discussion

In this work, we show that the global transcriptional regulator Hha may be rewired to control biofilm dispersal, without affecting initial biofilm formation. In static biofilms, Hha13D6 removed 70% of the biofilm while there was little dispersal with wild-type Hha (Fig. 4.1A), and in flow-cells, the engineered Hha removed 96% of the biofilm (Fig. 4.1B), whereas wild-type Hha removed 35% of the biofilm (Fig. 4.1B). Hha13D6 increased biofilm dispersal by causing apoptosis (Fig. 4.3C) by activating proteases (Table 4.3); hence, we have created one of the first protein switches to control cell lysis. Biofilm dispersal by the engineered Hha requires protease HslV since adding the *hslV* mutation reduced the dispersal activity of Hha13D6 (Fig. 4.1D).

Cell death in biofilms is an important mechanism of dispersal since it leads to the creation of voids inside the biofilm which facilitates dispersal of the surviving cells (Webb *et al.*, 2003). Hence, programmed cell death is a social (altruistic) activity (Wood, 2009). Cell death in biofilms is mediated by prophage (Webb *et al.*, 2003) and autolysis proteins (Mai-Prochnow *et al.*, 2006). Since the biofilm matrix consists of structural proteins (Karatan and Watnick, 2009), protease activity is necessary for biofilm dispersal; for example, *agr*-mediated detachment in *Staphylococcus aureus* biofilms does not occur in the presence of a protease inhibitor and is induced by extracellular proteases (Boles and Horswill, 2008). Also, wild-type Hha disperses *E. coli* biofilms by inducing protease ClpXP that activates toxins by degrading antitoxins (García-Contreras *et al.*, 2008). Hence, induction of protease activity is a key mechanism of Hha13D6 to trigger biofilm dispersal by causing cell death and so by disrupting biofilm structure.

In addition to the evolution of Hha for biofilm dispersal, we also show that Hha may be reconfigured to control biofilm formation by inducing the activity of GadW, GlpT, and PhnF (Fig. 4.2B). We showed previously that biofilm formation is connected to the acid resistance system, showing increased biofilm formation in the absence of acid resistance genes such as

gadW, gadABC, and *hdeABD* (Domka *et al.*, 2007; Lee *et al.*, 2007c), and GadW is dual regulator with GadX of the glutamate-dependent decarboxylase acid-resistance system of *E. coli* (Sayed *et al.*, 2007). Hence, the engineered Hha24E9 uses the acid resistance regulatory system to inhibit biofilm formation.

We found the carboxy-terminus of Hha is important for controlling biofilm dispersal but not for biofilm formation. Hha is a non-specific DNA binding protein, but the Hha-H-NS complex allows specific binding to target DNA sequences to regulate transcription (Madrid *et al.*, 2002). Hha consists of four α-helices separated by a loop: helix 1 (8-16 aa), helix 2 (21-34 aa), helix 3 (37-55 aa), and helix 4 (65-69 aa), and all four helices interact with H-NS to cause conformational changes in Hha at both the surface and in the hydrophobic core (Madrid *et al.*, 2007). The dispersal variant Hha13D6 has amino acid replacements on helix 2 (D22V) and helix 3 (L40R, V42I, and D48A) (Fig. 4.1C), and all three residues on helix 3 are perturbed by the N-terminus H-NS (García *et al.*, 2005), suggesting that the replacements in Hha13D6 cause conformational change of Hha structure to interact with H-NS and results in the enhanced biofilm dispersal. However, loss of C-terminal 11 amino acids by truncation at K62 of Hha13D6 abolished the effect of the other four replacements. Since helix 4 also is highly affected by the binding of H-NS (García *et al.*, 2005), complete deletion of helix 4 of Hha may change the conformation of Hha and inhibit biofilm formation. In addition, whole-transcriptome profiles of Hha13D6 (Table 4.3) and Hha24E9 (Table 4.4) support that gene regulation pathways of Hha13D6 are quite different from those of Hha24E9.

Biofilm dispersal is an essential process of biofilm cycles for disseminating cells into the environment for their survival (Kaplan, 2010), and engineering approaches to disperse biofilms, like using engineered phage (Lu and Collins, 2007), are promising (Kaplan, 2010). The current study demonstrates that genetic switches exist for both biofilm formation and dispersal and once

they are discerned, as in the case of Hha (Ren *et al.*, 2004a; García-Contreras *et al.*, 2008), they may be manipulated to control bacterial activity. We envision that since biofilms are robust, i.e., biofilm cells withstand stress better than their planktonic counterparts (Singh *et al.*, 2006), biofilms will be used for diverse applications and some of these applications will involve controlling biofilm formation including replacing some existing engineered biofilms with other engineered strains; this will require control of biofilm dispersal. This capability is important for patterning biofilms in microdevices as well as for creating sophisticated reactor systems that will be used to form bio-refineries where various engineered strains produce a plethora of chemicals as function of position and depth in biofilms.

4.5 Experimental procedures

4.5.1 Bacterial strains and growth conditions

The bacterial strains and plasmids used in this study are listed in Table 4.3. We used the Keio collection (Baba *et al.*, 2006) for isogenic mutants and the ASKA library (Kitagawa *et al.*, 2005) for overexpressing genes. The gene deletions were confirmed by PCR using primers (Table 4.5). All strains were initially streaked from -80^{o}C glycerol stocks on Luria-Bertani (LB) (Sambrook *et al.*, 1989) agar plates and were cultured at 37^{o}C in LB glucose (0.2%). Kanamycin (50 μg/mL) was used for pre-culturing isogenic knockout mutants, and chloramphenicol (30 μg/mL) was used for maintaining pCA24N-based plasmids. Genes were expressed from pCA24N using 1 mM IPTG (Sigma, St. Louis, MO, USA).

4.5.2 epPCR for random mutagenesis

hha from plasmid pCA24N-*hha* under the control of T5-*lac* promoter was mutated by epPCR as described previously (Fishman *et al.*, 2004) using primers epPCR-f and epPCR-r (Table 4.5). The epPCR product was cloned into pCA24N-*hha* using BseRI and HindIII after

treating the plasmid with Antarctic phosphatase (New England Biolabs, Beverly, MA, USA). The ligation mixture was electroporated into BW25113 *hha tnaA* competent cells using the Gene Pulser/Pulse Controller (Bio-Rad, Hercules, CA, USA) at 1.25 kV/cm, 25 μF, and 200 Ω.

4.5.3 Crystal violet biofilm assay to measure biofilm formation and biofilm dispersal

Biofilm formation was assayed in 96-well polystyrene plates (Corning Costar, Cambridge, MA, USA) using 0.1% crystal violet staining (Fletcher, 1977). Briefly, each well was inoculated at an initial turbidity at 600 nm of 0.05 and grown without shaking for 24 h with 1 mM IPTG addition. The crystal violet dye stains both the air-liquid interface and bottom liquid-solid interface biofilm, and the total biofilm formation at both interfaces was measured at 540 nm, whereas cell growth was measured at 620 nm.

Biofilm formation was normalized by the bacterial growth for each strain (turbidity at 620 nm) to reduce growth effect. Similarly, for biofilm dispersal, biofilms were formed for 24 h without shaking. Then, 1 mM IPTG was added for 8 h to overproduce the Hha variants from the pCA24N vector, and biofilm formation was measured (total time 32 h). As a negative control, biofilm formation was also measured for no IPTG addition at 32 h. Biofilm dispersal was quantified by subtracting the normalized biofilm at 32 h (8 h after adding 1 mM IPTG) from the normalized biofilm at 32 h (no IPTG addition). Two independent cultures were used for each strain.

Table 4.5 Primers used for epPCR, DNA sequencing, saturation mutagenesis, site-directed mutagenesis, confirmation of the mutants, qPCR, and qRT-PCR. Underlined bold text indicates the saturation mutation of the codon corresponding to D22, L40, V42, and D48 (5'-NNS) (N is A, G, C, or T, and S is G or C). Underlined italic text indicates the site-directed mutation for the codon corresponding to truncation at K62 (5'-AAG to 5'-TAG for K62X) in hha-K62X-f and hha-K62X-r.

Primer Name	Primer Sequence (listed 5' to 3')
epPCR of *hha*	
epPCR-f	GCCCTTTCGTCTTCACCTCG
epPCR-r	GAACAAATCCAGATGGAGTTCTGAGGTCATT
Saturation mutations	
hha-D22sm-f	GCGTTTACGTCGTTGCCAGACAATT**NNS**ACGCTGGAGCGTG
hha-D22sm-r	CACGCTCCAGCGT**SNN**AATTGTCTGGCAACGACGTAAACGC
hha-L40sm-f	CGAATTATCAGATAATGAA**NNS**GCGGTATTTTACTCAGCCGCA GATCAC
hha-L40sm-r	GTGATCTGCGGCTGAGTAAAATACCGC**SNN**TTCATTATCTGATA ATTCG
hha-V42sm-f	CAGATAATGAACTGGCG**NNS**TTTTACTCAGCCGCAGATCACCG
hha-V42sm-r	CGGTGATCTGCGGCTGAGTAAAA**SNN**CGCCAGTTCATTATCTG
hha-D48sm-f	GGTATTTTACTCAGCCGCA**NNS**CACCGCCTCGCCGAATTGAG
hha-D48sm-r	GTCAATTCGGCGAGGCGGTG**SNN**TGCGGCTGAGTAAAATACC
Site-directed mutagenesis to truncate at K62 of Hha13D6	
hha-K62X-f	CATGAATAAACTGTACGAC*TAG*ATCCCTTCCTCAGTATG
hha-K62X-r	CATACTGAGGAAGGGAT*CTA*GTCGTACAGTTTATTCATG
DNA Sequencing	
seq-f1	Same as epPCR-f
Confirmation of deletions	
hha up	GGATGACACCTTTATGTTGTTCAG
hha down	GAGCGATACAACTCACCAGC
tnaA up	GTCGATCACCGCCCTTGATTTGCCCTTCTG
tnaA down	CTGTACCTGCTATAACCATAACACCCC
clpB up	TAACCTTGAATAATTGAGGGATGAC
clpB down	TTTCTTTGCTTTTCTCTGTTGAGATTC
hslU up	GACATTTGCATCTATACCAACCATTTC
hslU down	GCGAGGTTAGAAAGGATCTGTAATAG
hslV up	AAGGCTTTGACTCGAAAATCAC
hslV down	GATATTTTTCGGGGTCACTTCATG

Table 4.5 Continued.

Primer Name	Primer Sequence (listed 5' to 3')
lon up	CCCTTTAATTTTTCCTCTATTCTCG
lon down	AATTTATATCGCACTTGAATCCTTC
prlC up	ATTCACTACACTTAACCCCATGCTAC
prlC down	CCTGTTTCATCAATTAAGCAGATTTTC
ycjF up	CGGCATTATTGATGTTAACGGTGAG
ycjF down	TGCCTCTTAGCACGAGTAGATCGAG
ibpA-up	CAGACCCATTTTTACATCGTAGC
ibpA-down	GTTGAATCTCTAAATCTTCCTGACG
ibpB-up	CTAACCTGGTAAATGGTTTGCTG
ibpB-down	GCTATATCACTCATCGTCCATTTC
gadA-up	AGGATGTGGATGATATCGTAGC
gadA-down	TCGTGACATTAAAGGTAATCGCTAC
gadE-up	GACGTATTAGTTCACGAAGGGTAAAG
gadE-down	AGAGATATGAGGGATTTACAGACC
gadX-up	GTAGCGATTACCTTTAATGTCACG
gadX-down	AACTTACTGAGAGCACAAAGTTTCC
qPCR for cell lysis measurement	
purA-f	GGGCCTGCTTATGAAGATAAAGT
purA-r	TCAACCACCATAGAAGTCAGGAT
qRT-PCR	
clpB-f	AAGAGTCTGATGAAGCCAGTAAAAAAC
clpB-r	TCTCTGCTTTCCACTCTTCTTCTAAC
hslU-f	AGCGTTTAATGGAAGAGATTTCCTAC
hslU-r	ATAGGATAAAACGGCTCAGATCTTC
hslV-f	CAGAAAACGATCTTATTGCTATCG
hslV-r	AAATGGTTGGTATAGATGCAAATG
lon-f	CGTGCGTGATGAAGCGGAA
lon-r	AGGTAGTGGTCGCTGAACG
prlC-f	GTAGCTTCTACCTCGATCTGTATGC
prlC-r	GGTTGAAGTTACAAGTCAAATACGC
ycjF-f	TTTAAGCTGGTATTGCTGAATATCG
ycjF-r	CTCCATAGCTTTAATCCCGAGTC
ibpA-f	CTTTACCGTTCTGCTATTGGATTTG
ibpA-r	GTAATGGTTTTCGTCTACCAGTTC
ibpB-f	GTAACTTCGATTTATCCCCACTG
ibpB-r	GTAGTGGTTATCGTCGCTTTTCTC

Table 4.5 Continued.

Primer Name	Primer Sequence (listed 5' to 3')
gadA-f	GGTACAAATCTGCTGGCATAAATTC
gadA-r	ACTCATAGTTACCGGTGTAGGTCAC
gadE-f	GTTTTGGCACCTTATCACATCAG
gadE-r	GGGGCAAGTGTTTACCATAAG
gadX-f	CGAAGAAGAGACATCATATTCACAG
gadX-r	GTGATATCCACAGGATACTGCAAC
gadW-f	GAAAGAATGTATACCAGCGAGAGTC
gadW-r	AGTATGCAGAGGAATTTGACGTAAC
glpT-f	GATGGCCTGGTTCAATGACT
glpT-r	CAGCAGTTTGTTCGGCAGTA
phnF-f	GAAAAACTGCTTTCGGTATTGC
phnF-r	CGAAGTAGTGGTCGATTAAACAGAG
rrsG-f	TATTGCACAATGGGCGCAAG
rrsG-r	ACTTAACAAACCGCTGCGT

4.5.4 Biofilm and dispersal screening of Hha variants

In order to screen Hha variants for the altered biofilm formation, BW25113 *hha tnaA* strains expressing Hha variants from pCA24N-*hha* were grown overnight in 96-well plates with 200 μL of medium at 250 rpm, the overnight cultures were diluted (1:100) in 300 μL of LB glucose, and biofilms formation with 1 mM IPTG was measured after 24 h through the crystal violet biofilm assay. As controls, BW25113 *hha tnaA* with empty pCA24N and pCA24N-*hha* (wild-type *hha*) were used. For dispersal screening of mutant *hha* alleles, biofilms were formed for 24 h without shaking. Then, 1 mM IPTG was added for 8 h to overexpress the *hha* alleles from the pCA24N, and no IPTG was added as negative control. Interesting *hha* alleles were re-analyzed by re-streaking the colonies on fresh LB plates and by performing another biofilm or dispersal assay. Mutant *hha* alleles were sequenced using a primer seq-f1 (Table 4.5). Each data point was averaged from more than twelve replicate wells (six wells from two independent cultures).

4.5.5 Flow-cell biofilm experiments and image analysis

Strains were cultured with chloramphenicol (30 μg/mL) to retain the pCA24N-based plasmids and with erythromycin (300 μg/mL) to maintain pCM18 which produces green fluorescence protein (Hansen *et al.*, 2001). Overnight cultures were diluted to a turbidity at 600 nm of 0.05 and pumped through the flow-cell (BST model FC81, Biosurface Technologies, Bozeman, MT) at 10 mL/h for 2 h, and then fresh medium with chloramphenicol and erythromycin was pumped for 42 h, and 1 mM IPTG was added for 6 h to induce either wild-type Hha or Hha13D6 for biofilm dispersal. As a negative control, no IPTG was added. The biofilms on the glass slides were visualized by exciting with an Ar laser at 488 nm (emission 510 to 530 nm) using a TCS SP5 scanning confocal laser microscope (Leica Microsystems, Wetzlar, Germany) with a 63x HCX PL FLUOTAR L dry objective. Nine random positions were chosen, and 25 images were taken for each position. Simulated three-dimensional images were obtained

using IMARIS software (BITplane, Zurich, Switzerland). Color confocal flow-cell images were converted to gray scale, and biomass, surface coverage, mean thickness, and roughness coefficient were determined using COMSTAT image-processing software (Heydorn *et al.*, 2000).

4.5.6 Saturation and site-directed mutagenesis

Saturation mutagenesis was performed at the codons corresponding to positions D22, L40, V42, and D48 of Hha and Hha13D6. Saturation mutagenesis primers (Table 4.5) were designed to allow the replacement of all 20 amino acids using 32 possible codons with NNS (N is A, G, C, or T, and S is G or C) (Leungsakul *et al.*, 2006). Plasmid pCA24N-*hha* and pCA24N-*hha13D6* were used as templates. PCR was performed using *Pfu* DNA polymerase at 95°C for 1 min, with 20 cycles of 95°C for 1 min, 55°C for 50 seconds, and 68°C for 7 min, and a final extension of 68°C for 7 min. The constructed plasmids were electroporated into BW25113 *hha* after DpnI digestion of template plasmids. Similarly, site-directed mutagenesis was performed to create a truncation at K62 of Hha13D6 to make Hha13D6-24E9 using site-directed mutagenesis primers (Table 4.5).

4.5.7 RNA isolation and whole-transcriptome studies

For the whole-transcriptome study of BW25113 *hha*/pCA24N-*hha13D6* versus BW25113 *hha*/pCA24N-*hha* (biofilm dispersal), cells were grown in 250 mL for 16 h at 125 rpm with 10 g of glass wool (Corning Glass Works, Corning, NY, USA) in 1 L Erlenmeyer flasks to form a robust biofilm (Ren *et al.*, 2004a) and incubated additional 1 h with 1 mM IPTG to induce wild-type Hha and Hha13D6. Similarly, for the whole transcriptome study of BW25113 *hha*/pCA24N-*hha24E9* versus BW25113 *hha*/pCA24N-*hha* (biofilm formation), cells were grown in 250 mL containing 1 mM IPTG for 7 h at 250 rpm with 10 g of glass wool to form biofilms. Biofilm cells were obtained by rinsing and sonicating the glass wool in sterile 0.85% NaCl solution at 0°C, and RNA*Later* buffer® (Applied Biosystems, Foster City, CA, USA) was

added to stabilize RNA during the RNA preparation steps. Total RNA was isolated from biofilm cells as described previously (Ren *et al.*, 2004a) using a bead beater (Biospec, Bartlesville, OK, USA). cDNA synthesis, fragmentation, and hybridizations to the *E. coli* GeneChip Genome 2.0 array (Affymetrix, Santa Clara, CA, USA; P/N 511302) were described previously (González Barrios *et al.*, 2006). Genes were identified as differentially expressed if the expression ratio was higher than the standard deviation: 2.0 fold (induced and repressed) cutoff for Hha13D6 DNA microarrays (standard deviation 1.3 fold) and 10 fold (induced) or 4 fold (repressed) for Hha24E9 DNA microarrays (standard deviation 4 fold), and if the *p*-value for comparing two chips was less than 0.05 (Ren *et al.*, 2004b). The whole-transcriptome data have been deposited in the NCBI Gene Expression Omnibus (http://www.ncbi.nlm.nih.gov/geo/) and are accessible through accession number GSE21604.

4.5.8 qRT-PCR

To corroborate the DNA microarray data, qRT-PCR was used to quantify relative RNA concentrations using 100 ng as a template using the Power *SYBR Green RNA-to-*C_T™ 1-Step Kit (Applied Biosystems, Foster City, CA, USA). The reaction and analysis was carried out by the StepOne™ Real-Time PCR System (Applied Biosystems, Foster City, CA, USA). The housekeeping gene *rrsG* was used to normalize the gene expression data. The annealing temperature was 60°C for all the genes in this study. Primers for qRT-PCR are listed in Table 4.5.

4.5.9 Cell lysis assay

To quantify cell lysis, the DNA concentration in supernatants and in cells was measured by qPCR using primers for *purA* (encodes the subunit of adenylosuccinate synthetase) (Ma and Wood, 2009). BW25113 *hha*/pCA24N-*hha* and BW25113 *hha*/pCA24N-*hha13D6* were grown until a turbidity of 1.0 at 600 nm and incubated 4 h with 1 mM IPTG to induce wild-type Hha

and Hha13D6. Then total DNA which is all genomic DNA released by sonication and extracellular DNA (eDNA) in the supernatant were isolated as described previously (Ma and Wood, 2009). The percentage of cell lysis was calculated as the ratio of eDNA relative to the total DNA. This experiment was performed with two independent cultures for each strain.

4.5.10 Quantification of c-di-GMP

c-di-GMP was quantified using HPLC as described previously (Ueda and Wood, 2009). BW25113 *hha*/pCA24N-*hha* and BW25113 *hha*/pCA24N-*hha13D6* were grown from overnight cultures in 1 L of LB glucose (0.2%) medium with 30 μg/mL chloramphenicol until a turbidity of 1.0 at 600 nm and incubated 4 h with 1 mM IPTG to induce wild-type Hha and Hha13D6. Briefly, formaldehyde (0.18%) was used to inactivate degradation of c-di-GMP, then cell pellets were boiled for 10 min, and nucleotides were extracted in 65% ethanol. HPLC (Waters 515 with a photodiode array detector, Milford, MA, USA) was used to detect nucleotides at 254 nm with a reverse-phase column (Nova-Pak® C18 column; Waters, 3.9×150 mm, 4 μm). Synthetic c-di-GMP (BIOLOG Life Science Institute, Bremen, Germany) was used as the standard, and the c-di-GMP peak was verified by spiking the samples with the synthetic c-di-GMP. *E. coli* AG1/pCA24N-*yddV,* which has elevated c-di-GMP concentrations (Mendez-Ortiz *et al.*, 2006), was used as a positive control along with AG1/pCA24N.

4.5.11 Gene deletions

BW25113 *hha tnaA*, BW25113 *hha clpB*, BW25113 *hha hslU*, BW25113 *hha hslV*, BW25113 *hha lon*, BW25113 *hha prlC*, BW25113 *hha ycjF*, BW25113 *hha ibpA*, BW25113 *hha ibpB*, BW25113 *hha gadA*, BW25113 *hha gadE*, and BW25113 *hha gadX* were constructed as described previously using the rapid gene knockout procedure with P1 transduction (Maeda *et al.*, 2008) by using plasmid pCP20 (Cherepanov and Wackernagel, 1995) to eliminate the kanamycin resistance (Km^R) gene. Mutations were confirmed by PCR with primers (Table 4.5).

4.5.12 Protein modeling

The amino acid sequences of the Hha13D6 were modeled into the known three-dimensional structure of the *E. coli* Hha (residues 1 to 72; Protein Data Bank accession code 1jw2) (Yee *et al.*, 2002). The three dimensional model was obtained using the SWISS-MODEL server (http://swissmodel.expasy.org/) (Schwede *et al.*, 2003). The molecular visualization program PyMOL (http://pymol.sourceforge.net/) was utilized to make the protein image of the molecular model.

CHAPTER V

SYNTHETIC QUORUM SENSING CIRCUIT TO CONTROL CONSORTIAL BIOFILM FORMATION AND DISPERSAL IN A MICROFLUIDIC DEVICE*

5.1 Overview

Bacteria grow primarily as biofilms, and to utilize them for chemical transformations in biorefineries, they periodically need to be replaced. Previously, we engineered global regulator Hha and cyclic diguanylate-binding BdcA to create proteins that enable biofilm dispersal. Here, we devise a biofilm circuit that utilizes these two dispersal proteins along with a population-driven quorum sensing switch. With this synthetic circuit, in a novel microfluidic channel, we (i) formed an initial colonizer biofilm, (ii) introduced a second cell type (dispersers) into this existing biofilm, (iii) formed a robust dual-species biofilm, (iv) displaced the initial colonizer cells in the biofilm with an extra-cellular signal from the disperser cells, and (v) removed the disperser biofilm with a chemically-induced switch. Therefore, for the first time, cells have been engineered that are able to displace an existing biofilm and then be removed on command allowing one to control consortial biofilm formation for various applications.

---

* The manuscript of "Synthetic quorum sensing circuit to control consortial biofilm formation and dispersal in a microfluidic device" by Seok Hoon Hong, Manjunath Hegde, Jeongyun Kim, Arul Jayaraman, and Thomas K. Wood is in revision in *Nature Communications* at the time of this dissertation submission. S.H. Hong constructed synthetic circuit, measured cell growth and 3*o*C12HSL concentration. M. Hegde and J. Kim performed microfluidic biofilm displacement experiment. S.H. Hong, M. Hegde, and J. Kim contributed equally to this work.

5.2 Introduction

Biofilms are groups of cells at an interface cemented together by polysaccharides, protein, DNA, and lipids (Flemming and Wingender, 2010). Biofilms are related to most bacterial chronic inflammatory and infectious diseases (Sauer *et al.*, 2007) as well as involved in biocorrosion (Beech and Sunner, 2004) and biofouling (Dobretsov *et al.*, 2009) in diverse areas. They also may be used for beneficial applications such as bioremediation and hold much potential for chemical transformations in biorefineries (Wood *et al.*, 2011). For these applications, compared to monocultures, mixed populations have the advantages of being able to perform more complex transformations (e.g., those requiring multiple steps), and they are more resistant to environmental stress (Brenner *et al.*, 2008). For these reasons, consortia have been heralded as the new frontier in synthetic biology (Brenner *et al.*, 2008). However, to date, it has not been possible to control consortial biofilm formation.

Based on an understanding of signals and regulatory networks during biofilm development (Prüß *et al.*, 2006), biofilms have been engineered by manipulating extracellular/intercellular signals and regulators (Wood *et al.*, 2011). The first engineered biofilm was a consortium where *Bacillus subtilis* was engineered to secrete the peptide antimicrobials indolicidin and bactenecin to inhibit the growth of sulfate-reducing bacteria and thereby decrease corrosion (Jayaraman *et al.*, 1999). Also, the first synthetic signaling circuit to control biofilm formation was developed for *Escherichia coli* and *Pseudomonas fluorescens* by manipulating the extracellular concentration of the signal indole produced by *E. coli* (Lee *et al.*, 2007b); indole is a biofilm inhibitor for *E. coli*. In addition, using directed evolution, SdiA was reconfigured to decrease biofilm formation by increasing indole (Lee *et al.*, 2009b), and the global regulator H-NS was evolved to decrease biofilm formation via prophage excision and cell death (Hong *et al.*, 2010b).

To remove existing biofilms, T7 bacteriophage was engineered to produce dispersin B of

Actinobacillus actinomycetemcomitans to disrupt the glycosidic linkages of polymeric β-1,6-*N*-acetyl-*D*-glucosamine found in the biofilm matrix during bacteriophage infection (Lu and Collins, 2007). In addition, global transcriptional regulator Hha was engineered using protein engineering to enhance biofilm dispersal primarily by inducing protease HslV (Hong *et al.*, 2010a), and BdcA, which increases biofilm dispersal by decreasing the concentration of the second messenger cyclic diguanylate (c-di-GMP) by binding it, was engineered for nearly complete dispersal of biofilms (Ma *et al.*, 2011). Therefore, new genetic modules are available for manipulating biofilms (Wood *et al.*, 2011).

Synthetic biology is an emerging field to develop biological systems that perform novel functions by assembling genetic modules (Fu, 2006). The genetic modules include switches, cascades, pulse generators, time-delayed circuits, oscillators, spatial patterning, and logic formulas, and they can be utilized to control transcription, translation, and post-translational operations in order to tune gene expression, protein production, metabolism, and cell-cell communication (Purnick and Weiss, 2009). Among these genetic modules, bacterial quorum sensing (QS) systems are becoming important components of a wide variety of engineered biological devices (Hooshangi and Bentley, 2008), since autoinducers are useful as input signals because most are small, diffuse freely in aqueous media, and are easily imported by cells (Choudhary and Schmidt-Dannert, 2010). Because the engineered cells synthesize their own QS signals, they are able to monitor their cell density and modulate their activities (Ryan and Dow, 2008) accordingly without supervision. Hence, QS based circuits have a wide range of potential engineering applications such as production of biochemicals, tissue engineering, and mixed-species fermentations as well as developing biosensors and controlling biofouling (Choudhary and Schmidt-Dannert, 2010). For example, LuxI from *Vibrio fischeri*, which produces *N*-(3-*oxo*-hexanoyl)-*L*-homoserine lactone (3*o*C6HSL) and AiiA from *Bacillus thuringiensis*, which

degrades 3*o*C6HSL, were utilized to generate synchronized oscillations (Danino *et al.*, 2010). Also, the LuxI/LuxR QS system was coupled to the production of a toxin protein CcdB to induce cell death at high cell densities (You *et al.*, 2004).

The two best-characterized QS systems of *Pseudomonas aeruginosa* are the LasI/LasR and RhlI/RhlR systems, which regulate biofilm formation, virulence, swarming motility, and antibiotic efflux pumps (Williams and Cámara, 2009). LasI produces autoinducer molecule, *N*-(3-*oxo*-dodecanoyl)-*L*-homoserine lactone (3*o*C12HSL), which is sensed by LasR (Pesci *et al.*, 1997). Likewise, RhlI produces *N*-butyryl-*L*-homoserine lactone (C4HSL) that is sensed by RhlR (Pesci *et al.*, 1997). The LasI/LasR and RhlI/RhlR QS systems have been used to engineer bidirectional communication(Brenner *et al.*, 2007), and the LasI/LasR QS system was used to both construct a predator-prey ecosystem (Balagaddé *et al.*, 2008) and create a synthetic ecosystem in *E. coli* (Kambam *et al.*, 2008). Furthermore, the RhlI/RhlR QS system was utilized to demonstrate roles for self-organization and aggregation in a synthetic biofilm consortium (Brenner and Arnold, 2011). Hence, synthetic QS circuit systems have potential in that population-driven QS switches may be utilized to develop synthetic genetic networks for a variety of applications.

Since biofilm formation and dispersal are ultimately genetic processes, they may be manipulated like other genetic systems (Wood *et al.*, 2011) using the tools of synthetic biology (Purnick and Weiss, 2009) and directed evolution. In this work, our goal was to control biofilm displacement via a population-driven QS switch coupled to engineered biofilm dispersal proteins. Controlling biofilm dispersal creates a synthetic biological platform for sophisticated patterning of biofilms for engineering applications. The LasI/LasR QS module of *P. aeruginosa* was combined with engineered Hha (Hong *et al.*, 2010a) and BdcA (Ma *et al.*, 2011) biofilm dispersal proteins, and the system was utilized to selectively remove one type of cell from an

existing biofilm, and then remove the second biofilm to create a surface ready for additional biofilms.

5.3 Results

5.3.1 Microfluidic biofilm engineering (μBE) circuit

The μBE signaling circuit was constructed in *E. coli* using two engineered biofilm-dispersing proteins, Hha13D6 (Hong *et al.*, 2010a) and BdcAE50Q (Ma *et al.*, 2011), along with the *P. aeruginosa* LasI/LasR QS system (Fig. 5.1A). *E. coli hha* (Baba *et al.*, 2006) was used as the host since deletion of *hha* increases biofilm formation (García-Contreras *et al.*, 2008) and provides a background in which there is no wild-type Hha. Lactococcal promoter CP25 (Hansen *et al.*, 2001) was used as the strong constitutive promoter for two of the three proteins on each plasmid. To obtain high concentrations of intercellular signal 3*o*C12HSL and regulator LasR, a synthetic ribosomal binding site (RBS II) (Hansen *et al.*, 2001) was first utilized. However, high expression of *lasI* or *lasR* was deleterious; thus, we used the native RBS of these genes. All the cloned genes for the two cell types were placed on a single plasmid (pCA24N derivative, Fig. 5.2) to avoid plasmid instability and so that a single antibiotic could be used to maintain the key plasmid during growth of the consortia.

In the μBE circuit, disperser cells (*lasI*$^+$, *hha13D6*$^+$, *gfp*$^+$ via *E. coli hha/*pHha13D6-*gfp-lasI*) produce constitutively green fluorescent protein (GFP) and the quorum-sensing signal 3*o*C12HSL and have *hha13D6* induced upon addition of isopropyl-β-D-thiogalactopyranoside (IPTG) (Fig. 5.1A). The initial colonizer cells (*lasR*$^+$, *bdcAE50Q*$^+$, *rfp*$^+$ via *E. coli hha/*pBdcAE50Q-*rfp-lasR*) produce constitutively red fluorescent protein (RFP) and regulator LasR, the receptor of 3*o*C12HSL. The initial colonizer cells also have *bdcAE50Q* under the

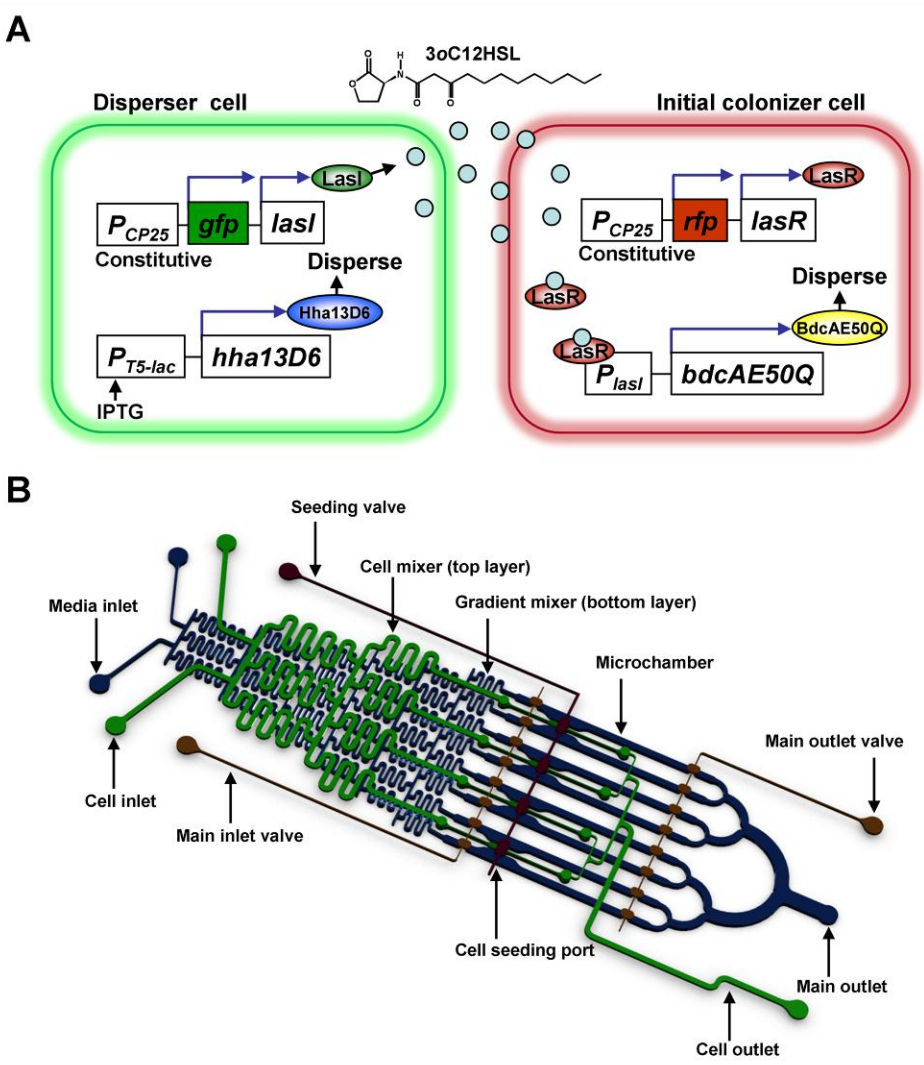

Figure 5.1 µBE metabolic circuit and microfluidic device. (A) The two *E. coli* cell types communicate by using the LasI/LasR QS module. In the disperser cell, the LasI protein is constitutively produced and synthesizes 3*o*C12HSL. 3*o*C12HSL freely diffuses into the initial colonizer cell and makes a complex with LasR, and the 3*o*C12HSL + LasR complex induces biofilm dispersal protein BdcAE50Q by activating the *lasI* promoter. The biofilm dispersal protein Hha13D6 in the disperser cell is induced upon adding IPTG. Plasmid maps for the synthetic µBE circuit are shown in Fig. 5.2. (B) The novel microfluidic device is shown with its two PDMS layers, a bottom layer with a diffusive-mixer and eight microchambers, and a top layer containing a second diffusive mixer and the pneumatic elements to control microvalves. The diffusive mixer in the bottom layer was used to generate different concentrations of dispersal signals (e.g., IPTG for removing disperser cells and 3*o*C12HSL for dispersing initial colonizer cells) and to perfuse growth media into the biofilm microchambers. The mixer in the top layer was used to introduce bacteria into the microchambers at different cell densities.

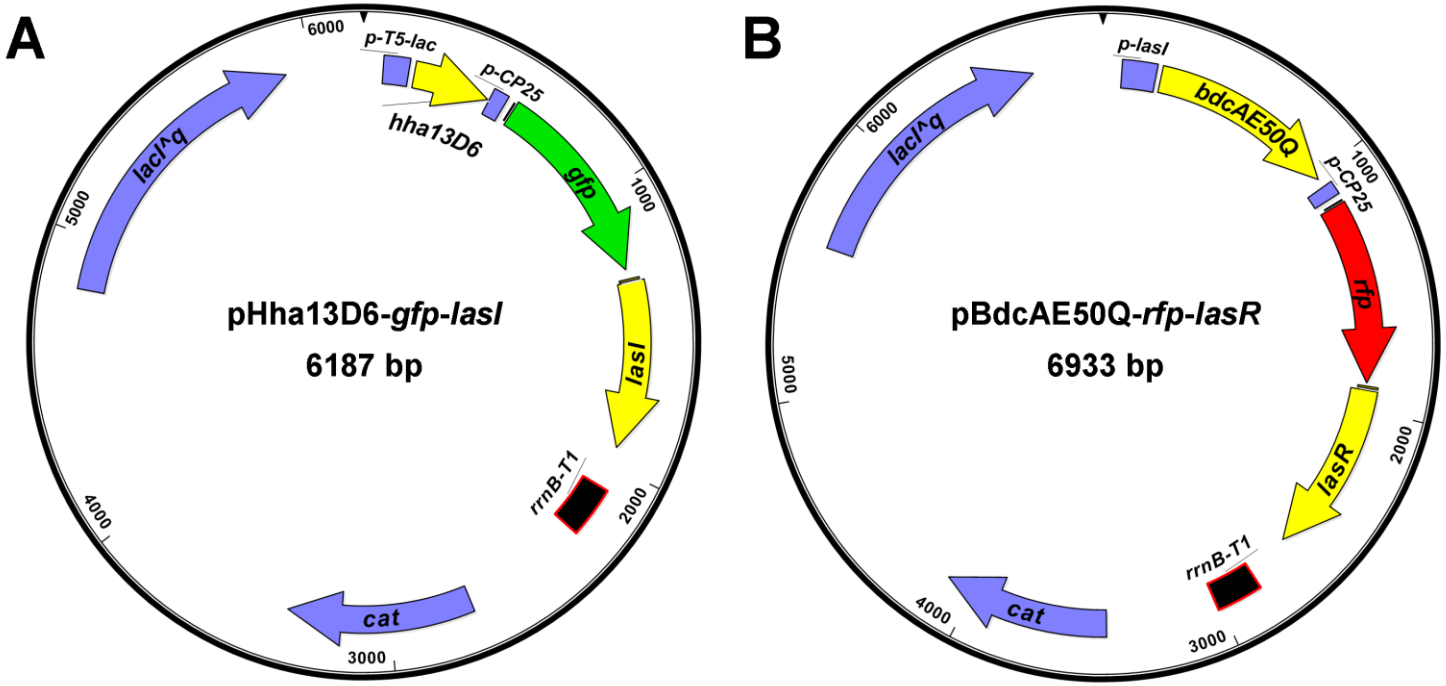

Figure 5.2 Plasmid maps of the disperser plasmid and the initial colonizer plasmid that are used to create the µBE circuit. (A) pHha13D6-*gfp-lasI* with *hha13D6* under control of the *T5-lac* promoter and *gfp* and *lasI* under control of the constitutive CP25 promoter. (B) pBdcAE50Q-*rfp-lasR* with *bdcAE50Q* under control of the *lasI* promoter and *rfp* and *lasR* under control of the constitutive CP25 promoter. *cat* encodes chloramphenicol acetyltransferase, *lacI^q* encodes a repressor mutant of the *lac* operator, and *rrnB-T1* indicates the *rrnB* T1 transcription termination sequence.

control of the *lasI* promoter which is activated via the 3*o*C12HSL + LasR complex (Seed *et al.*, 1995) (Fig. 5.1A). Thus, disperser cells produce the signaling molecule 3*o*C12HSL, and the initial colonizer biofilm-forming cells sense it and disperse when the disperser cells reach a quorum.

Since we desire the disperser cells to supplant the initial colonizer cells, we checked the specific growth rates of the two strains to see if they are comparable; the disperser cells grew 14% slower than initial colonizer cells in rich medium (LB glucose, $\mu_{disperser} = 1.13 \pm 0.08\ h^{-1}$ and $\mu_{initial\ colonizer} = 1.31 \pm 0.05\ h^{-1}$). The slower growth of the disperser cells is most likely due to leaky expression of toxin *hha13D6* from the *T5-lac* promoter (Kitagawa *et al.*, 2005). Corroborating this difference in cell growth, disperser cells formed biofilms more slowly compared to initial colonizer cells: the biomass of initial colonizer cells after 9 h was 5.7 ± 0.1 $\mu m^3/\mu m^2$ (Fig. 5.3A) while the biomass of the disperser cells after 9 h was 4.1 ± 0.1 $\mu m^3/\mu m^2$ (Fig. 5.3B).

5.3.2 Disperser cells produce 3*o*C12HSL

To confirm the disperser μBE circuit synthesizes 3*o*C12HSL, we measured the 3*o*C12HSL concentration of the disperser cells (*E. coli hha/*pHha13D6-*gfp-lasI*) in the biofilm using a *lacZ* reporter (*lasB-lacZ* translational fusion) that is activated by 3*o*C12HSL (Pearson *et al.*, 1994). In flow-cells, disperser cells in biofilms produced 13-fold higher concentrations of 3*o*C12HSL compared to the planktonic cells in the effluent (6.7 ± 3 μM vs. 0.5 ± 0.2 μM) and produced 48-fold higher concentrations of 3*o*C12HSL compared to planktonic cells in shake flasks (0.1 ± 0.1 μM). The negative control (no *lasI*) had no detectable 3*o*C12HSL. These results confirm that autoinducer concentrations in biofilms are higher than in planktonic cultures (Charlton *et al.*, 2000) and compare well to levels of 3*o*C12HSL produced in *P. aeruginosa* biofilms (1 (Flickinger *et al.*, 2011) to 600 μM (Charlton *et al.*, 2000)).

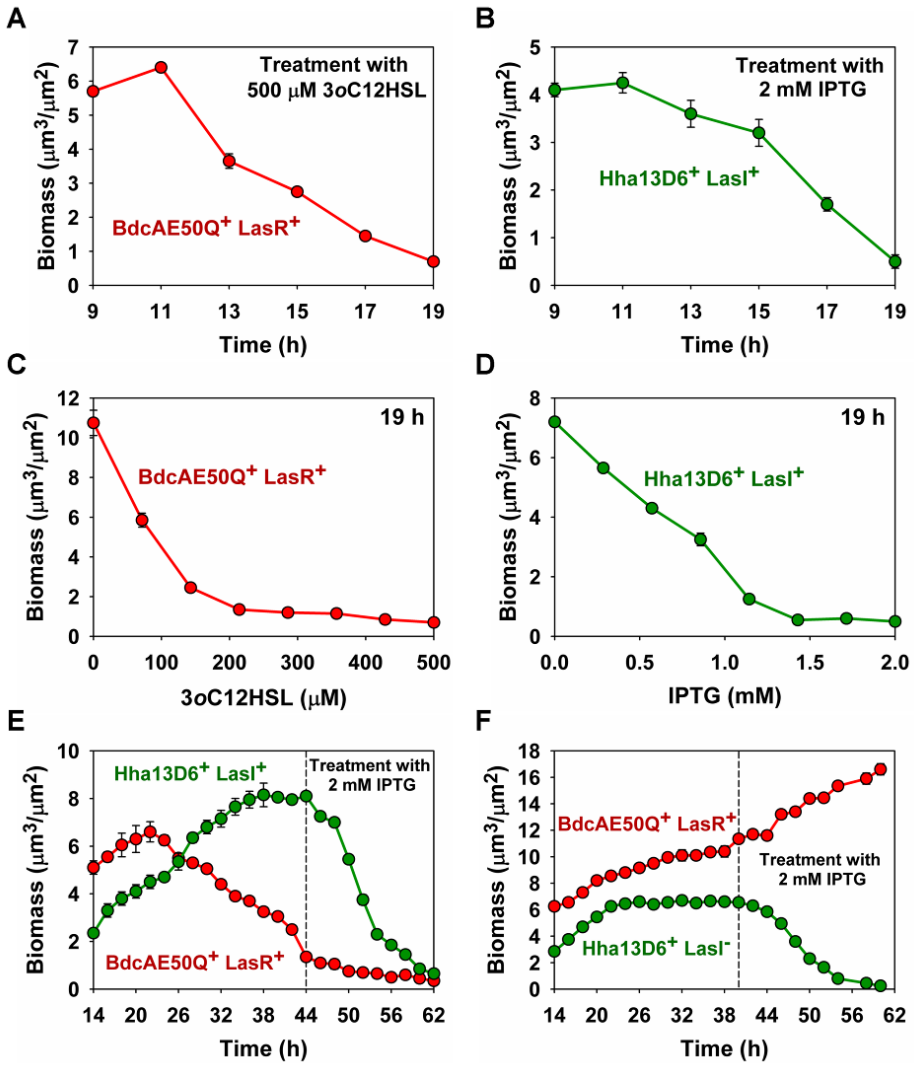

Figure 5.3 Biomass of initial colonizer and disperser biofilms. (A) Biomass of initial colonizer biofilms (BdcAE50Q$^+$, LasR$^+$) with 500 μM of 3*o*C12HSL for 10 h. (B) Biomass of disperser biofilms (Hha13D6$^+$, LasI$^+$) with 2 mM of IPTG for 10 h. (C) Biomass after 19 for the initial colonizer biofilms with different concentrations of 3*o*C12HSL (0, 71, 143, 214, 286, 357, 429, and 500 μM for 10 h). (D) Biomass after 19 h for the disperser biofilms with different concentrations of IPTG (0, 0.3, 0.6, 0.9, 1.1, 1.4, 1.7, and 2.0 μM for 10 h). Robust biofilms at 9 h were formed by seeding the initial colonizer or the disperser cells into microchambers for (A), (B), (C), and (D). (E) Biomass of the initial colonizer (BdcAE50Q$^+$, LasR$^+$) and disperser (Hha13D6$^+$, LasI$^+$) biofilms. After 44 h, 2 mM of IPTG was added to remove the disperser biofilm for an additional 18 h. (F) Biomass of the initial colonizer (BdcAE50Q$^+$, LasR$^+$) and the no LasI disperser control (Hha13D6$^+$, LasI$^-$) biofilms. After 40 h, 2 mM of IPTG was introduced to disperse the no LasI disperser control biofilm for an additional 20 h. The initial colonizer biofilms were formed by seeding for 9 h, then disperser cells were seeded for 5 h to form both initial colonizer and disperser biofilms for (E) and (F).

Since maximum activity of the *lasI* promoter is obtained with 0.1 µM of 3*o*C12HSL with LasR (Seed *et al.*, 1995), 3*o*C12HSL production in the disperser biofilms should induce the *lasI* promoter in the initial colonizer cells to express *bdcAE50Q* to disperse the initial colonizer biofilms. Moreover, since 3*o*C12HSL diffusion is significantly slower compared to C4HSL diffusion (Pearson *et al.*, 1999), local concentrations of 3*o*C12HSL in biofilms may be much higher than the 3*o*C12HSL concentration measured here.

5.3.3 3*o*C12HSL disperses the initial colonizer biofilm

To demonstrate that 3*o*C12HSL disperses biofilms produced by the initial colonizer cells (*E. coli hha/*pBdcAE50Q-*rfp-lasR*) by binding LasR and inducing *bdcAE50Q*, exogenous 3*o*C12HSL at different concentrations was added to biofilms formed by the initial colonizer cells in microfluidic channels. As expected, the initial colonizer biofilms were dispersed upon adding 3*o*C12HSL in a dose-dependent manner (Fig. 5.3C); nearly complete biofilm dispersal was obtained at 500 µM of 3*o*C12HSL (Fig. 5.4A). In contrast, there was no dispersal in the absence of 3*o*C12HSL (Fig. 5.4B), and the initial colonizer cells formed thick biofilms (10.8 ± 0.6 $\mu m^3/\mu m^2$) (Fig. 5.3C). Hence, initial colonizer cells recognize 3*o*C12HSL and this signal may be used to disperse initial colonizer biofilms.

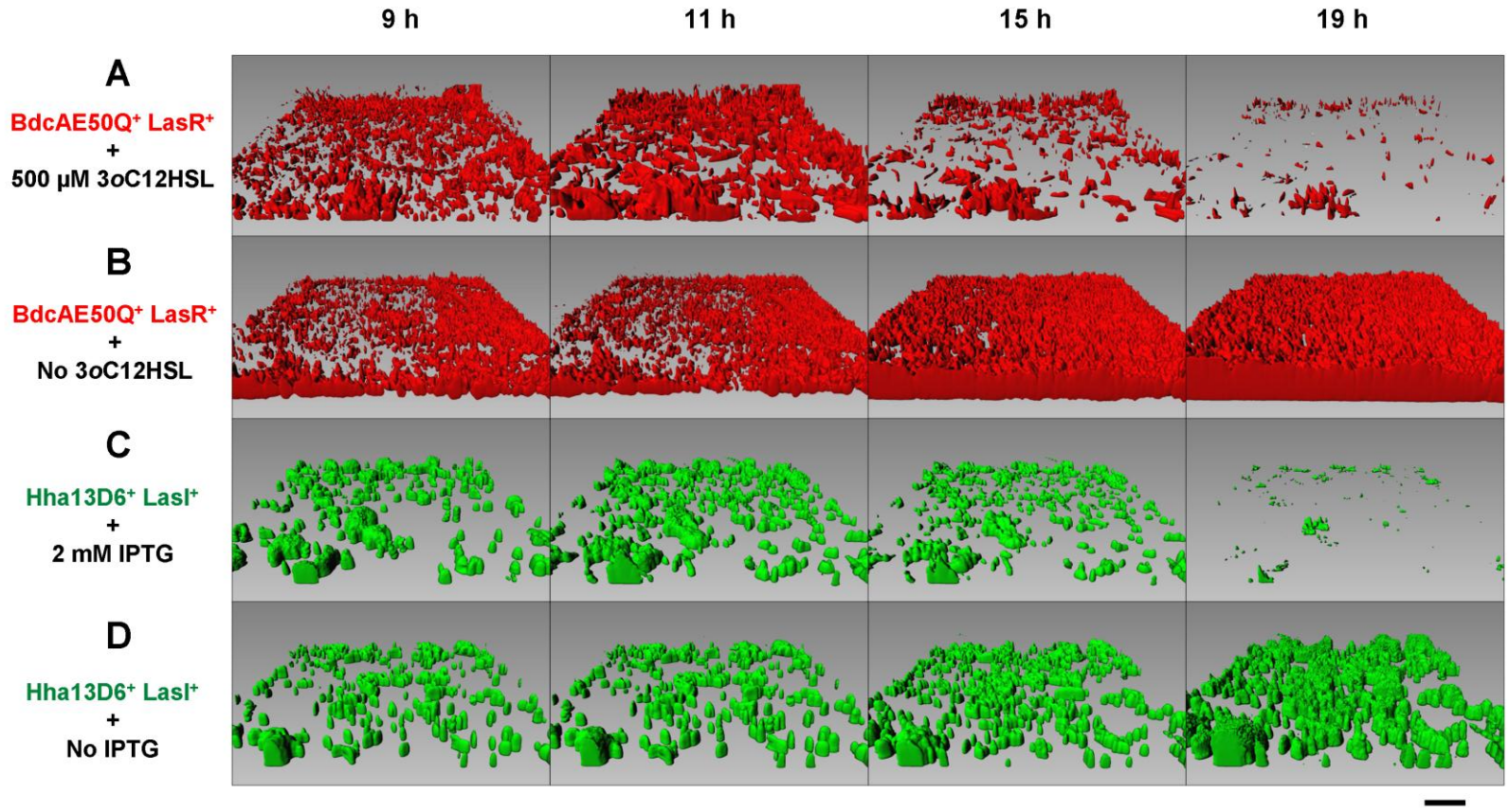

Figure 5.4 Dispersal of mono-species biofilms. Initial colonizer biofilms (BdcAE50Q^{+}, LasR^{+}) were formed by seeding for 9 h, then 3*o*C12HSL (500 µM) was added for 10 h to induce biofilm dispersal (A) or not added (B). Disperser biofilms (Hha13D6^{+}, LasI^{+}) were formed by seeding disperser cells for 9 h, then 2 mM of IPTG was added for 10 h to induce biofilm dispersal (C) or not added (D). Scale bar indicates 20 µm.

5.3.4 IPTG removes the disperser biofilm

To demonstrate that IPTG disperses biofilms produced by disperser cells by inducing *hha13D6*, exogenous IPTG at different concentrations was added to biofilms formed by disperser cells in microfluidic channels. As expected, disperser biofilms were dispersed upon adding IPTG in a dose-dependent manner (Fig. 5.3D) with nearly complete biofilm dispersal at 2 mM IPTG (Fig. 5.4C); hence, we used 2 mM IPTG in subsequent experiments. In contrast, there was no dispersal in the absence of *hha13D6* (Fig. 5.4D). Thus, the disperser cell produces 3*o*C12HSL at concentrations adequate to disperse the initial colonizer biofilm and has active *hha13D6* to disperse its own biofilm upon IPTG addition. Taken together, both disperser and initial colonizer cells were constructed to allow us to manipulate biofilm dispersal using a population-driven switch.

5.3.5 Engineered BdcA and Hha are necessary for biofilm dispersal

To confirm that the biofilm dispersal upon addition of 3*o*C12HSL and IPTG is the result of production of the engineered biofilm dispersal proteins, we performed dispersal experiments of initial colonizer cells that lack *bdcAE50Q* and disperser cells that lack *hha13D6*. As expected, initial colonizer biofilms formed without *bdcAE50Q* (via *E. coli hha/*pRFP-*lasR*) did not disperse in the presence of 3*o*C12HSL (Fig. 5.5A), while initial colonizer biofilms formed with *bdcAE50Q* dispersed with 3*o*C12HSL (Fig. 5.4A). Similarly, disperser biofilms formed without *hha13D6* (via *E. coli hha/*pGFP-*lasI*) did not disperse upon addition of IPTG (Fig. 5.5B), while disperser biofilms formed with *hha13D6* dispersed with IPTG (Fig. 5.4C). Taken together, BdcAE50Q and Hha13D6 are necessary to disperse the initial colonizer and disperser biofilms, respectively.

5.3.6 Disperser cells displace initial colonizer biofilms

Having verified the disperser and initial colonizer cell elements of the µBE signaling circuit, we combined both cell types to form a consortial biofilm and investigated whether the disperser cells could displace the initial colonizer cells. First, robust biofilms of initial colonizer cells were formed for 9 h, and then disperser cells were added to the initial colonizer biofilms for 5 h to form the biofilm consortium (Fig. 5.6A). Since disperser cells synthesize 3*o*C12HSL constitutively, 3*o*C12HSL should bind to LasR when the concentration of 3*o*C12HSL is increased as the disperser biofilms mature. Then, the 3*o*C12HSL + LasR complex should induce dispersal of initial colonizer biofilms by switching on *bdcAE50Q* under control of the *lasI* promoter. As expected, the initial colonizer biofilms were displaced from the surface as the disperser cells grew (Fig. 5.6A). After 44 h, 80% of the maximum initial colonizer biofilm formed was removed (Fig. 5.3E and Fig. 5.6A). The displacement of the initial colonizer cells by the disperser cells was accomplished by the production of 3*o*C12HSL from the disperser biofilms not by shear force since the disperser biofilms that lack LasI did not reduce initial colonizer biofilms; i.e., both no *lasI* disperser and initial colonizer biofilms grew when 3*o*C12HSL was not produced (Fig. 5.6B), and the biofilm became essentially that of the faster-growing initial colonizer cells after 40 h (Fig. 5.3F and Fig. 5.6B). Hence, the disperser cells completely displaced the initial colonizer biofilm via the population-driven synthetic µBE systems.

The second key element of our design was the removal of the disperser biofilm; we found we could remove the disperser biofilm by inducing Hha13D6 with IPTG (Fig. 5.6A). After 62 h (18 h with 2 mM IPTG), 92% of the maximum disperser biofilm was removed (Fig. 5.3E).

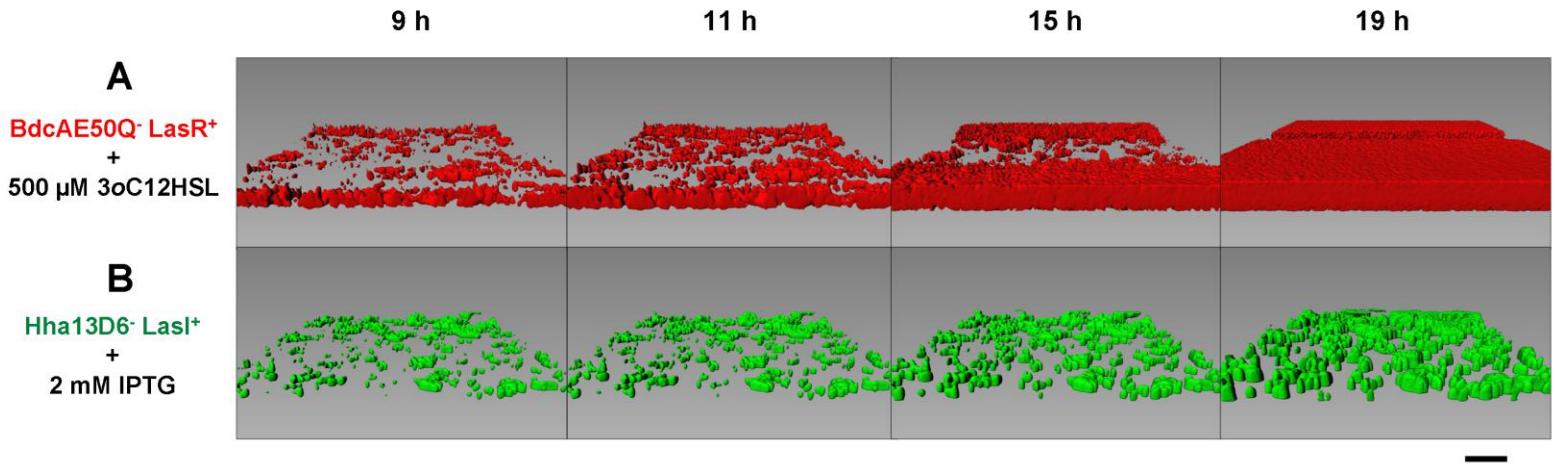

Figure 5.5 Biofilms formed by cells that lack their respective biofilm dispersal proteins in the presence of 3*o*C12HSL or IPTG. (A) Initial colonizer biofilms that lack BdcA (BdcAE50Q$^-$, LasR$^+$ via *E. coli hha/*pRFP-*lasR*) with 500 µM of 3*o*C12HSL for 10 h. (B) Disperser biofilms that lack Hha (Hha13D6$^-$, LasI$^+$ via *E. coli hha/*pGFP-*lasI*) with 2 mM of IPTG for 10 h. Robust biofilms at 9 h were formed by seeding initial colonizer or disperser cells into microchambers. Scale bar indicates 20 µm.

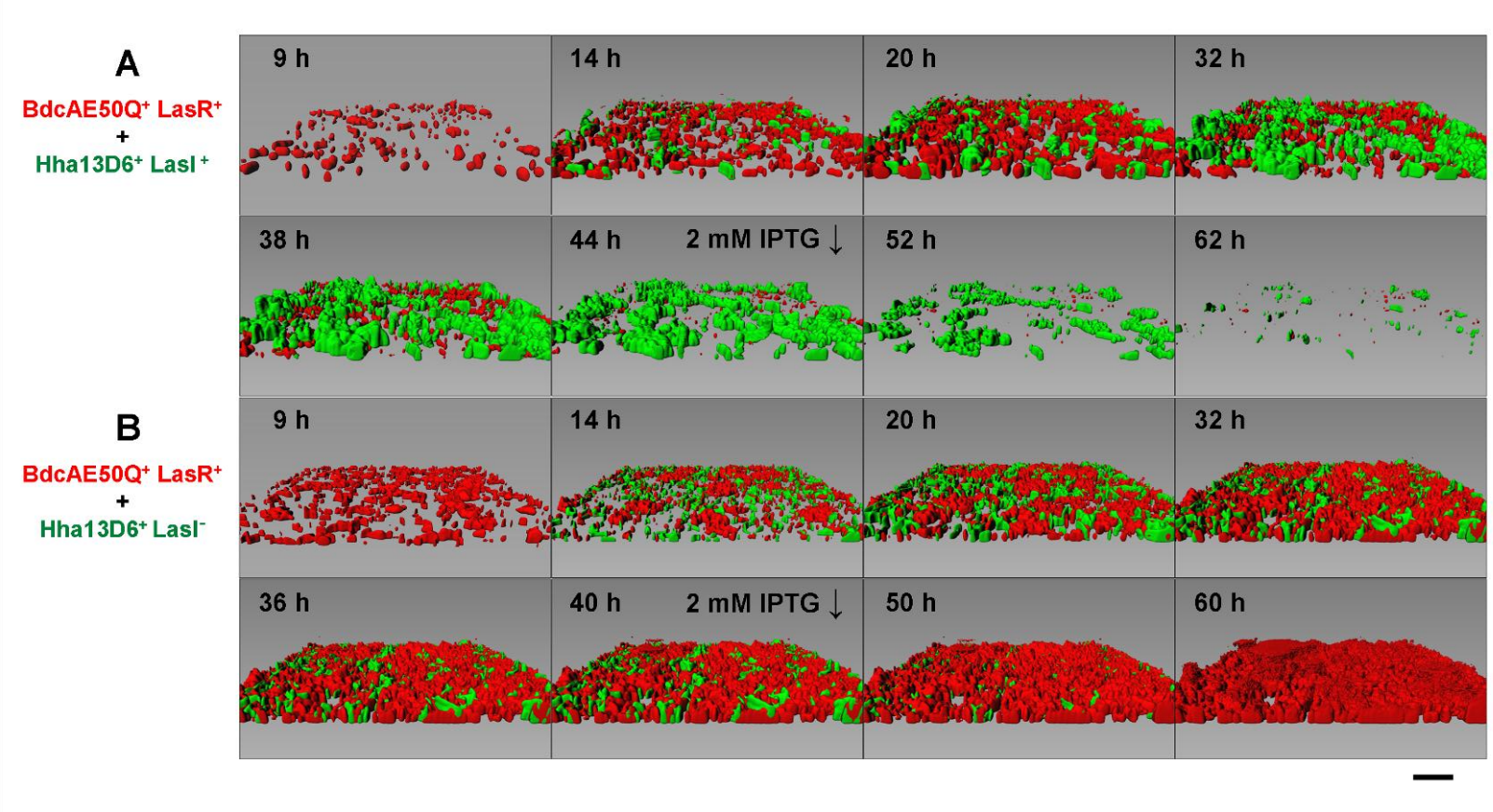

Figure 5.6 Dispersal of dual-species biofilms. (A) An initial colonizer biofilm (BdcAE50Q$^+$, LasR$^+$) was formed by seeding for 9 h (red), then disperser cells (green) were seeded for 5 h to form both initial colonizer and disperser biofilms. After 44 h, 2 mM of IPTG was added for an additional 18 h to remove the disperser biofilm. (B) Initial colonizer biofilms (BdcAE50Q$^+$, LasR$^+$) were formed by seeding for 9 h, then control disperser cells which lack LasI were seeded for 5 h to form both initial colonizer and control disperser biofilms. After 40 h, 2 mM of IPTG was introduced for an additional 20 h to try to disperse the no *lasI* disperser biofilms. Scale bar indicates 20 µm.

5.4 Discussion

We developed a synthetic μBE system by combining a QS signaling module with two engineered biofilm dispersal proteins. With this synthetic circuit, in a microfluidic channel, we (i) formed an initial colonizer biofilm with cells tagged red, (ii) introduced a second cell type (dispersers, tagged green) into this existing biofilm, (iii) created a means of communication between the two cell types, (iv) formed a robust biofilm with the disperser cells in an existing initial colonizer biofilm, (v) displaced the initial colonizer cells in the biofilm with a QS signal from the disperser cells, and (vi) removed the disperser cells with a chemically-induced switch. Our work demonstrates that biofilms can be formed, that new cells may be engineered to integrate and then replace the initial colonizer biofilm and that both cell types may be removed which is a promising strategy for applications requiring different kinds of engineered cells such as creating a biorefinery.

Although some of the biofilm may be dispersed naturally upon changes in environmental conditions (e.g., nutrition level and oxygen depletion) (Kaplan, 2010), it is a significant challenge to remove biofilms (Bardouniotis *et al.*, 2001; del Pozo and Patel, 2007) since cells in biofilms are cemented in place by the secreted polymer matrix consisting of polysaccharide, protein, DNA, and lipids (Flemming and Wingender, 2010). The matrix holds bacterial cells together and forms a protective barrier conferring resistance to killing by nonspecific and specific host defenses during infection and conferring tolerance to various antimicrobial agents such as disinfectants and antibiotics (Flemming and Wingender, 2010). Thus, the defensive nature of the biofilm colony makes most biofilms difficult or impossible to eradicate (Kaplan, 2010); hence, our demonstration that both the initial colonizer and disperser biofilms may be nearly completely removed is highly significant.

To preferentially remove one type of cell in a biofilm, in our system it requires that the

second cell elicit robust growth such that it can attach to an existing biofilm and propagate, that it flourishes, that it communicates to another cell as the QS signals generated within the biofilm must be perceived at a relatively high local concentration compared to planktonic cultures (Charlton *et al.*, 2000), and that it displaces the existing biofilm without itself being displaced but instead it forms a strong biofilm. Here, we produced the QS signal in the biofilm itself to remove the initial colonizer cells. As the signal accumulated, the engineered BdcA in the initial colonizer cells reduces c-di-GMP levels which results in a cascade of events, such as an increase in motility and reduction in adhesion production, that allows the initial colonizer cells to disperse (Ma *et al.*, 2011).

As the initial colonizer cells disperse, the disperser cells must form a robust biofilm. After the disperser biofilm is formed, the engineered Hha protein must be able to cause dispersal since it induces cell lysis which leads to dispersal (Hong *et al.*, 2010a). Therefore, our synthetic µBE system provides a useful platform for the removal of existing deleterious biofilms via generating signaling molecules *in situ*. In addition, since the disperser cells grow more slowly than the initial colonizer ones, the disperser cells cannot displace the initial colonizer biofilm based on a difference in growth rates. This demonstrates clearly that QS circuit was required to complete this feat of progressive biofilm development/dispersal. Since, several biofilm dispersal signals have been identified including the auto-inducing peptide of the *agr* QS system of *Staphylococcus aureus* (Boles and Horswill, 2008), changes in carbon sources (Sauer *et al.*, 2004), reduction in the concentration of c-di-GMP (Ma *et al.*, 2011) (as utilized here with BdcA), surfactant (Boles *et al.*, 2005), *cis*-2-decenoic acid (Davies and Marques, 2009), as well as *D*-amino acids (Kolodkin-Gal *et al.*, 2010), we envision that other biofilm dispersal mechanisms may also be utilized to control biofilms.

The µBE device described here offers several advantages over the commercially available

BioFlux device developed by Benoit *et al.* (Benoit *et al.*, 2010) and other microfluidic devices used for biofilm study (Lee *et al.*, 2008a). With our device, we can (i) precisely control the development of biofilm by intermittent flow of nutrients, (ii) completely isolate the biofilm from the media inlet and gradient generating channels using the pneumatic valves, and (iii) sequentially introduce different kinds of cell into the biofilm chamber. Of course, the ability to study a range of concentrations simultaneously with the eight channels (e.g., Fig. 5.3CD) was instrumental in analyzing the effect of various concentrations of 3*o*C12HSL and IPTG.

Bacterial QS systems have the attractive design features that they utilize diffusible signals (Choudhary and Schmidt-Dannert, 2010). Here we show, for the first time, that a QS system may be utilized with biofilm dispersal proteins to control consortial biofilm formation; i.e., that an existing biofilm may be formed and then replaced by another biofilm which then may be removed. These types of synthetic QS circuits may be used to pattern biofilms by facilitating the re-use of platforms and to create sophisticated reactor systems that will be used to form bio-refineries. Furthermore, these systems may be adopted in industrial and clinical processing as an alternative strategy to overcome the current limitations of biofilm control.

5.5 Experimental procedures

5.5.1 Bacterial strains and growth conditions

The bacterial strains and plasmids used in this study are listed in Table 5.1 and were cultured at 37^{o}C. LB (Sambrook *et al.*, 1989) with 0.2% glucose (LB-glucose) was used in all of the non-microfluidic experiments, and both M9 (Sambrook *et al.*, 1989) supplemented with 0.2% glucose (M9-glucose) and LB glucose were used in the microfluidic device. Kanamycin (50 µg/mL) was used for overnight cultures, chloramphenicol (100 µg/mL) was used for maintaining the pCA24N-based plasmids, and erythromycin (300 µg/mL) was used for maintaining the pCM18-

Table 5.1 Strains and plasmids used in this study. Km^R, Cm^R, Em^R, and Ap^R are kanamycin, chloramphenicol, erythromycin, and ampicillin resistance, respectively.

Strains and plasmids	Genotype/relevant characteristics	Source
Strains		
E. coli hha	BW25113 Δ*hha* Ω Km^R	(Baba *et al.*, 2006)
E. coli MG4/pKDT17	Ap^R, P_{lasB}::*lasB*$^+$-*lacZ*$^+$ translational fusion, P_{lac}::*lasR*$^+$	(Pearson *et al.*, 1994)
P. aeruginosa PAO1	Wild-type	T. McDermott
Plasmids		
pCA24N-*hha13D6*	Cm^R; *lacI*^{q}, pCA24N $P_{T5\text{-}lac}$::*hha13D6*$^+$	(Hong *et al.*, 2010a)
pHha13D6-*gfp*	Cm^R; *lacI*^{q}, pCA24N $P_{T5\text{-}lac}$::*hha13D6*$^+$ P_{CP25}::*gfp*$^+$	This study
pHha13D6-*gfp-lasI*	Cm^R; *lacI*^{q}, pCA24N $P_{T5\text{-}lac}$::*hha13D6*$^+$ P_{CP25}::*gfp*$^+$-*lasI*$^+$	This study
pCA24N-*bdcAE50Q*	Cm^R; *lacI*^{q}, pCA24N $P_{T5\text{-}lac}$::*bdcAE50Q*$^+$	(Ma *et al.*, 2011)
pBdcAE50Q	Cm^R; *lacI*^{q}, pCA24N P_{lasI}::*bdcAE50Q*$^+$	This study
pBdcAE50Q-*rfp-lasR*	Cm^R; *lacI*^{q}, pCA24N P_{lasI}::*bdcAE50Q*$^+$ P_{CP25}::*rfp*$^+$-*lasR*$^+$	This study
pCM18	Em^R, P_{CP25}::*gfp*$^+$	(Hansen *et al.*, 2001)
pGFP-*lasI*	Em^R, P_{CP25}::*gfp*$^+$-*lasI*$^+$	This study
pCM18-X	Em^R, *gfp*-disrupted	This study
pRFP-*lasR*	Em^R, P_{CP25}::*rfp*$^+$-*lasR*$^+$	This study
pDsRed-Express	Ap^R, P_{lac}::*rfp*$^+$	Clontech
pDsRed-*lasR*	Ap^R, P_{lac}::*rfp*$^+$-*lasR*$^+$	This study
pDsRed-BlpIX-*lasR*	Ap^R, P_{lac}::*rfp*$^+$-*lasR*$^+$ (BlpI site disrupted)	This study

based plasmids.

5.5.2 Plasmid construction

All primers used for cloning are listed in Table 5.2. Plasmid pHha13D6-*gfp-lasI* (Fig. 5.2A) encodes *hha13D6* (Hong *et al.*, 2010a) under the control of the IPTG-inducible *T5-lac* promoter, as well as *gfp* and *lasI* under the control of constitutive CP25 promoter. To form this plasmid, *gfp* was amplified by three rounds of PCR: the first PCR with primers gfp-F3 and gfp-R and template pCM18 (Hansen *et al.*, 2001) was to amplify *gfp* with the same RBS of *rfp*, and the second PCR with primers gfp-F2 and gfp-R using the first PCR product as a template and the third PCR with primers gfp-F1 and gfp-R using the second PCR product as a template were performed to include the constitutive CP25 promoter of pCM18. pHha13D6-*gfp* was constructed by cloning the third PCR product into pCA24N-*hha13D6* (Hong *et al.*, 2010a) using the NotI and BlpI restriction sites after *hha13D6* sequence. The final construct pHha13D6-*gfp-lasI* was formed by cloning *lasI* with its native RBS from the *P. aeruginosa* PAO1 chromosome by using the lasI-F and lasI-R primers; the PCR product was cloned into pHha13D6-*gfp* using the BlpI restriction site. As a control plasmid for producing GFP and LasI but not producing Hha13D6, pGFP-*lasI* was constructed by inserting *lasI* into pCM18 using lasI-F and las-R primers.

Plasmid pBdcAE50Q-*rfp-lasR* (Fig. 5.2B) encodes *bdcAE50Q*(Ma *et al.*, 2011) under the control of the *lasI* promoter, as well as *rfp* and *lasR* under the control of the constitutive CP25 promoter. pBdcAE50Q was constructed by replacing the *T5-lac* promoter in pCA24N-*bdcAE50Q* (Ma *et al.*, 2011) with the *lasI* promoter from *P. aeruginosa* using the plasI-F and plasI-R primers; the PCR fragment was cloned into the Ava1 and BseRI restriction sites. Plasmid pDsRed-*lasR* was constructed by inserting *lasR* and its native RBS into the NotI site downstream of the *rfp* sequence in pDsRed-Express (Clontech, CA, USA) using the lasR-F and lasR-R primers. Since a BlpI restriction site lies within *lasR* but was required for the next cloning steps,

the BlpI site in pDsRed-*lasR* was disrupted by site-directed mutagenesis(Hong *et al.*, 2010a) (5'-GCTGAGC to 5'-TCTGAGC) using the BlpIX-F and BlpIX-R primers (this mutation did not change the aa sequence), to form pDsRed-BlpIX-*lasR*. *rfp* and *lasR* were amplified from pDsRed-BlpIX-*lasR* by two rounds of PCR to include the constitutive CP25 promoter of pCM18: the first PCR was performed using the rfp-lasR-F2 and rfp-lasR-R primers and the second PCR was performed using the rfp-lasR-F1 and rfp-lasR-R primers with the first PCR product. The final construct pBdcAE50Q-*rfp-lasR* was formed by inserting the *rfp* and *lasR* PCR products into the BlpI site downstream of *bdcAE50Q* in pBdcAE50Q. As a control plasmid for producing RFP and LasR but not producing BdcAE50Q, pRFP-*lasR* was constructed by inserting *rfp* and *lasR* using the rfp-lasR-F3 and rfp-lasR-R primers into pCM18-X in which *gfp* was disrupted by introducing a truncation at Y66 of GFP using the gfpX-F and gfpX-R primers in pCM18. All plasmids were confirmed by PCR and DNA sequencing.

5.5.3 Microfluidic device

The poly(dimethyl)siloxane (PDMS)-based μBE device (Fig. 5.1B) was fabricated in the Materials Characterization Facility at Texas A&M University using conventional soft lithographic techniques as described previously (Kim *et al.*, 2010a). The μBE device consists of a glass slide and two layers, a bottom layer with a diffusive-mixer and eight microchambers, and a top layer which contains the pneumatic elements for controlling microvalves and a second diffusive mixer. The diffusive mixer in the bottom layer was used to generate different concentrations of dispersal signals (e.g., IPTG for removing disperser cells) and to perfuse growth media into the biofilm microchambers. The mixer in the top layer was used to introduce bacteria into the microchambers at different cell densities (Fig. 5.1B). The dimensions of the

Table 5.2 Primers used for constructing plasmids for the µBE circuit. Underlined italic text indicates the restriction enzyme sites: AvaI in plasI-F, BlpI in lasI-F, lasI-R, rfp-lasR-F1, rfp-lasR-F3, and rfp-lasR-R, BseRI in plasI-R, and NotI in gfp-F1. Italicized bold text indicates the site-directed mutation for disruption of the BlpI restriction site (5'-GCTGAGC to 5'-TCTGAGC) in BlpI-X-F and BlpI-X-R. Underlined bold text indicates the site-directed mutation site for the codon corresponding to truncation at GFP Y66 (5'-TAT to 5'-TA**A** for Y66X) in gfpX-F and gfpX-R.

Primer Name	Primer Sequence (listed 5' to 3')
Construction of the plasmid for the disperser circuit (pHha13D6-*gfp-lasI*)	
gfp-F1	GGACTC*GCGGCCGC*TAAGGGCTTTGGCAGTTTATTCTTGACATGTA GTGAGGGGGCTGGT
gfp-F2	ACATGTAGTGAGGGGGCTGGTATAATAAAATAGTACTGTTCGGGT GAGCGGATAACAATT
gfp-F3	TTCGGGTGAGCGGATAACAATTTCACACAGGAAACAGCTATGCGT AAAGGAGAAGAACTT
lasI-F	CCTGCA*GCTGAGC*TTCTTCAGCTTCCTATTTGGAGGAAGTG
lasI-R	GCTCGACG*GCTCAGC*AGGTCCCCGTCATGAAACCGCCAGTCGC
Construction of the plasmid for the initial colonizer circuit (pBdcAE50Q-*rfp-lasR*)	
plasI-F	CGACGCCG*CTCGAG*GGGCTGTGTTCTCTCGTGTG
plasI-R	GCCGTGC*ATAGTTAATTTCTCCTC*TTTAATGGAAGCTGAAGAATTTA TGC
BlpI-X-F	GTGCTCGCGGCGAACTCGGCGC***TCTGAGC***CTCAGCGTGGAAGCGG
BlpI-X-R	CCGCTTCCACGCTGAG***GCTCAGA***GCGCCGAGTTCGCCGCGAGCAC
BlpI-X-seq-F	GAACGCCTTCATCGTCGGCAACTACC
rfp-lasR-F1	GGACTC*GCTGAGC*GCTTTGGCAGTTTATTCTTGACATGTAGTGAGG GGGCTGGTATAATA
rfp-lasR-F2	GTGAGGGGGCTGGTATAATAAAATAGTACTGTTCGGGTGAGCGGA TAACAATTTCACAC
rfp-lasR-F3	CCGGACTC*GCTGAGC*ATAACAATTTCACACAGGAAACAGCTATGA CCATGATTACGC
rfp-lasR-R	GCTCGACG*GCTCAGC*AGGTCCCGCTCAGAGAGTAATAAGACCC
gfpX-F	CAACACTTGTCACTACTTTCGGT**TAA**GGTGTTCAATGCTTTGCGAG ATAC
gfpX-R	GTATCTCGCAAAGCATTGAACACC**TTA**ACCGAAAGTAGTGACAAG TGTTG

diffusive mixers in both the top and bottom layers were 100 µm (width) × 150 µm (height) and 200 µm (width) × 200 µm (height) respectively, and the biofilm microchambers were 600 µm (width) × 150 µm (height). All pneumatic channels were 200 µm thick. The two layers were fabricated separately and assembled by sequential oxygen plasma treatment and bonding (100 mTorr, 100 W, 40 s) in a reactive ion etcher. The top pneumatic layer was first aligned and bonded to the bottom diffusive-mixer/microchamber membrane layer followed by bonding of the combined PDMS layer to a cover glass (22 x 50 mm). Tygon tubing (0.01" ID × 0.03" OD, Saint Gobain performance plastics, OH, USA) was used for all fluidic connections. Two PicoPlus 11 syringe pumps (Harvard Apparatus, MA, USA) were used for each experiment to separately control fluid flow rates in the two layers. A temperature controlled micro-incubator was used to maintain the temperature of the device at 37^{o}C. Moist air flowed continuously over the device in order to maintain humidity and avoid bubble formation inside the microchambers. The opening and closing of valves were pneumatically controlled by introducing vacuum or compressed air through the solenoid valves. The operation of solenoid valves and syringe pumps were remotely controlled through programs developed in-house for the LabVIEW platform (National Instruments, TX, USA).

5.5.4 Microfluidic biofilm experiments

For mono-species biofilm dispersal experiments, overnight cultures were washed and resuspended in M9 medium supplemented with glucose (0.2%) at a turbidity at 600 nm of ~1.0. The bacterial suspension was introduced into the eight biofilm microchambers through the top layer in the PDMS device (Fig. 5.1B). During this process, the main inlet valves (Fig. 5.1B) remained closed to prevent cells from entering and forming biofilm in the gradient mixing channels and to ensure proper mixing of dispersal signals before they enter the microchambers. The main outlet valves and seeding valves were then closed, and the culture was maintained

without flow for 2 h to enable attachment of bacteria to the glass surface (seeding). After 2 h, both main inlet and outlet valves were opened, unattached cells were removed, and the attached bacteria were allowed to grow by flowing LB-glucose at 2 µL/min. After 3 h, the medium was switched from LB-glucose to M9-glucose for 3 h because we found that a sudden depletion of nutrients promoted rapid development of biofilms. The biofilm was then developed for another 3 h by introducing LB-glucose into the chambers in a semi-batch mode (55 min static and 5 min flow). Thus, within 9 h after seeding, a robust and mature biofilm was formed. To disperse the biofilm, LB-glucose and LB-glucose containing a single concentration of the dispersal signal (IPTG for disperser cells and 3*o*C12HSL for initial colonizer cells) was introduced through the two media inlets and allowed to mix in the serpentine gradient generating channels to form eight concentrations of the dispersal signal in LB-glucose medium. Each stream leaving the diffusive mixer was used to perfuse a specific biofilm microchamber for 10 h.

For dual-species biofilm dispersal experiments, initial colonizer cell biofilm was developed uniformly across all eight microchambers for 9 h as for mono-species biofilms. During this 9 h period, unattached initial colonizer cells were continuously removed from the cell mixer and connecter tubing through the cell outlet by flowing M9 medium at 8 µL/min. After formation of the initial colonizer biofilm, disperser cells (turbidity at 600 nm of 2.0 in M9-glucose) were continuously perfused into the microchamber for 5 h to allow disperser cells to colonize the initial colonizer biofilm as well as the glass surface in vacant regions. After 5 h, LB-glucose was introduced into the microchamber in semi-batch mode (55 min static and 5 min flow) for 28-30 h. The static condition ensured biofilm development and build-up of 3*o*C12HSL needed for induction of the BdcAE50Q dispersal protein in initial colonizer cells. To remove the disperser cell biofilm, LB-glucose containing 2 mM IPTG was introduced in semi-batch mode for 18 to 20 h.

5.5.5 Confocal microscopy

Images were taken every 1 to 2 h using a 40X/0.85 NA dry objective with a TCS SP5 scanning confocal laser microscope (Leica Microsystems, Wetzlar, Germany) (Lee *et al.*, 2007b). Z-stack images were taken at a zoom level of 2 such that the image covered 90% of width of the microchamber. Two individual positions per microchamber covering a total of 70% of the channel length were chosen for imaging. Using the confocal z-stack images, 3-D reconstruction of the biofilm architecture was performed using IMARIS 3D and 4D Real-Time Interactive Data Visualization software (Bitplane Inc., CT, USA). Biomass and average biofilm height were obtained using COMSTAT image-processing software (Heydorn *et al.*, 2000).

5.5.6 Flow-cell biofilm experiments and biofilm volume analysis

Overnight cultures were diluted to a turbidity at 600 nm of 0.05 in LB-glucose and pumped through the flow-cell (BST model FC81, Biosurface Technologies, MT, USA) at 10 mL/h for 2 h, then LB-glucose was pumped for 48 h to form biofilms. The biofilms on the glass slides were visualized after robust biofilms were formed (48 h) using a confocal microscope. COMSTAT was used to analyze the biofilms formed at 13 positions. Biofilm volume was calculated by multiplying biofilm biomass and the surface area (1400 mm^2) of the flow-cell.

5.5.7 3*o*C12HSL assay in biofilms

The flow-cell was disassembled, and biofilms samples were collected by wiping the coverslip, glass slides, and four sides of the flow-cell with paper towels (Kimwipes, 1.5 cm × 1.5 cm). This was repeated three times to ensure all biofilm cells were collected. The biofilm cells were resuspended in 5 mL of dH_2O, mixed, and centrifuged. The biofilm cells were resuspended in 3 mL of dH_2O and sonicated twice using a 60 Sonic Dismembrator (Fisher Scientific, PA, USA) at level 10 for 15 sec. 3*o*C12HSL was extracted as described previously (Erickson *et al.*, 2002) with slight modifications. The samples were extracted three times with a half volume of dichloromethane. The aqueous residue was removed after freezing the samples for 3 h at -20ºC. The solvent was evaporated via rotary evaporation, and the residue was resuspended in 200 µL of ethyl acetate. *E. coli* MG4/pKDT17 was used to assay the 3*o*C12HSL levels (Pearson *et al.*, 1994). This reporter strain contains a copy of the *lasR* gene as well as a *lasB*::*lacZ* fusion. β-galactosidase activity was measured as described previously (Wood and Peretti, 1991). Synthetic 3*o*C12HSL (Sigma-Aldrich, MO, USA) was used as the standard (Fig. 5.7), and planktonic cultures of *E. coli hha*/pHha13D6-*gfp*, which does not produce 3*o*C12HSL, was used as a negative control. As additional controls, effluent from the flow-cell and planktonic cultures were used to compare with 3*o*C12HSL concentrations from the biofilm.

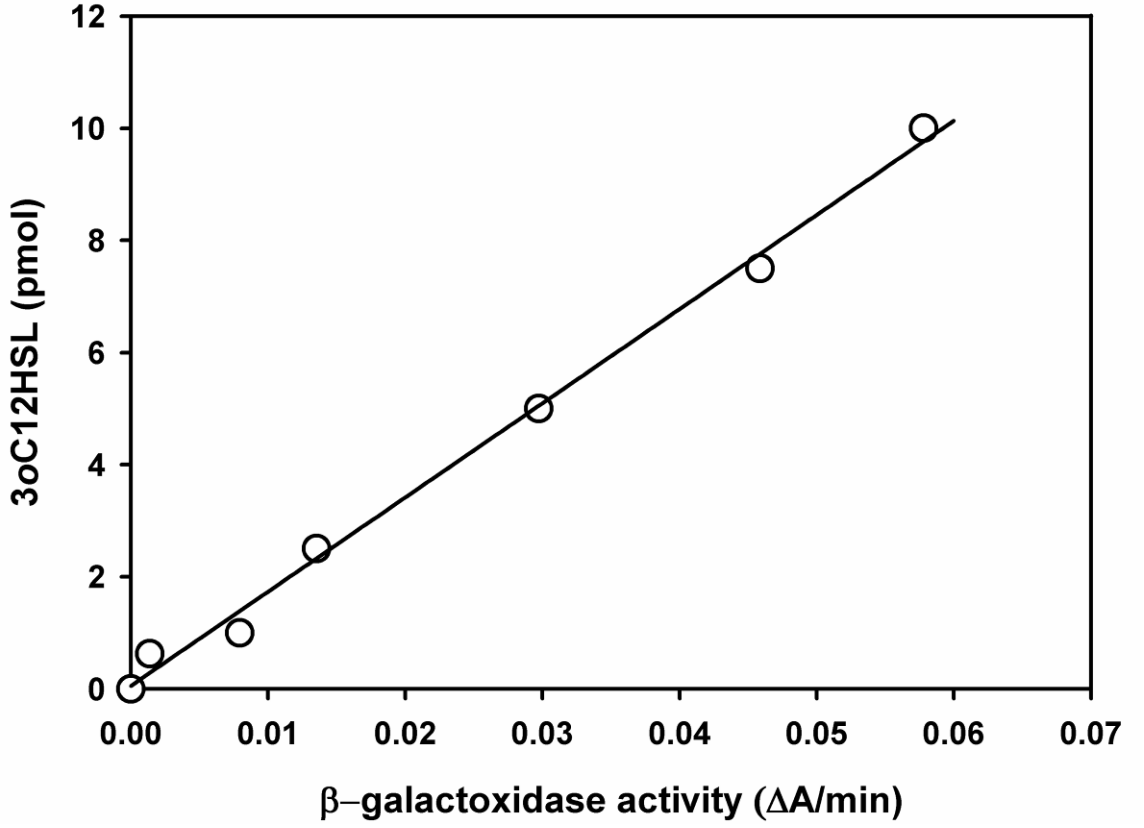

Figure 5.7 Standard curve for determining 3*o*C12HSL concentrations. β-galactosidase activity was measured using reporter *E. coli* MG4/pKDT17 upon adding different amounts of 3*o*C12HSL.

CHAPTER VI

BACTERIAL PERSISTENCE INCREASES AS ENVIRONMENTAL FITNESS DECREASES

6.1 Overview

Persisters are a subpopulation of metabolically-dormant cells in biofilms that are resistant to antibiotics; hence, understanding persister cell formation is important for controlling bacterial infections. Previously we discerned that toxin MqsR of the MqsR/MqsA toxin/antitoxin pair of *Escherichia coli* influences persister cell production. Here, to gain more insights into the origin of persisters, we used protein engineering to increase the toxicity of toxin MqsR by reasoning it would be easier to understand the effect of this toxin if it were more toxic. We found two mutations, K3N and N31Y, that increase the toxicity four fold and increase persistence 73 fold compared to native MqsR by making the protein more stabile. A whole transcriptome study revealed that the MqsR variant represses acid resistance genes (*gadABCEWX* and *hdeABD*), multidrug resistance genes (*mdtEF*), and osmotic resistance genes (*osmEY*). Corroborating these microarray results, deletion of *rpoS* as well as the genes that the master stress response regulator RpoS controls, *gadB*, *gadX*, *mdtF*, and *osmY,* increased persister formation dramatically to the extent that nearly the whole population became persistent. Furthermore, wild-type cells stressed by prior treatment to acid or hydrogen peroxide increased persistence 12,000-fold. Therefore, the more toxic MqsR *increases* persistence by *decreasing* the ability of the cell to respond to antibiotic stress through its RpoS-based regulation of acid resistance, multidrug resistance, and osmotic resistance systems.

6.2 **Introduction**

Persisters comprise a subpopulation of bacteria that become highly tolerant to antibiotics and reach this state without undergoing genetic change (Lewis, 2010). Persister cells in biofilms appear to be responsible for the recalcitrance of chronic infections since antibiotics kill the majority of cells but persisters remain viable and repopulate biofilms when the level of antibiotics drops (Lewis, 2010). Persisters are less sensitive to antibiotics since the cells are not undergoing cellular activities that antibiotics corrupt which results in tolerance (i.e., no growth and slow death). In contrast, resistance mechanisms arise from genetic changes that block antibiotic activity which results in resistance; i.e., cells grow in the presence of antibiotics when they are resistant whereas persister cells do not grow and are dormant (Lewis, 2007). Therefore, understanding persister cell formation is important to derive strategies for controlling bacterial infections. However, the genetic mechanism of persister cell formation is not fully understood.

Bacterial toxin/antitoxin (TA) systems appear to be the most likely genetic basis of persister cell formation, since the expression of TA modules are frequently linked to the dormant state (Lewis, 2008; Kim and Wood, 2010; Maisonneuve *et al.*, 2011; Wang and Wood, 2011). TA systems are diverse and abundant in prokaryotic cells (Leplae *et al.*, 2011), and typically consist of two genes in one operon encoding a stable toxin that disrupts an essential cellular process and a labile antitoxin that neutralizes toxicity by binding to the protein or to the mRNA of the toxin (Wang and Wood, 2011). Since the role of TA systems in cell physiology is not well understood, nine possible roles have been proposed (Magnuson, 2007): addictive genomic debris, stabilization of genomic parasites, selfish alleles, gene regulation, growth control, persister cell formation, programmed cell arrest, programmed cell death, and anti-phage measures. Recently, three new roles of TA modules in cell physiology have been discovered including influencing biofilm formation (González Barrios *et al.*, 2006; Kim *et al.*, 2009), mediating the general stress

response by controlling the stationary-phase sigma factor RpoS (Wang *et al.*, 2011), and regulating gene expression at a post-transcriptional level by differential mRNA decay (DMD) (González Barrios *et al.*, 2006; Amitai *et al.*, 2009; Wang and Wood, 2011).

Many bacterial chromosomes have several TA systems; for example, *Escherichia coli* has 37 TA systems (Tan *et al.*, 2011), and *Mycobacterium tuberculosis* has at least 88 TA systems (Ramage *et al.*, 2009). The various TA systems may allow the cell to respond to a specific stress or groups of stresses in a highly-regulated, elegant fashion (Wang and Wood, 2011). Hence, there are many TA systems involved in diverse regulatory pathways, but our understanding of these regulatory systems is far from complete.

Among *E. coli* TA loci, the MqsR/MqsA TA pair was the first to be shown to have a definitive role in persistence; deletion of the *mqsRA* locus or deletion of *mqsR* alone decreases persister cell formation and production of MqsR increases the number of persisters (Kim and Wood, 2010). Furthermore, *mqsR* is the most-induced gene in persister cells compared to non-persisters (Shah *et al.*, 2006). MqsR was first identified in a whole-transcriptome study of biofilms cells as an induced gene (Ren *et al.*, 2004a), and MqsR/MqsA was linked to biofilm formation and motility via the autoinducer-2 quorum sensing system (González Barrios *et al.*, 2006). The three dimensional structure of MqsR/MqsA revealed that MqsR is an RNase similar to RelE and YoeB (Brown *et al.*, 2009) that cleaves mRNA at GCU sites (Yamaguchi *et al.*, 2009), and MqsR toxicity requires protease Lon and ClpXP (Kim *et al.*, 2010b; Wang *et al.*, 2011). The MqsR/MqsA TA system was the first TA system to affect persistence upon deletion (Kim and Wood, 2010). Similarly, the TisAB/IstR-1 TA system of *E. coli* decreases persistence to ciprofloxacin upon deletion (Dörr *et al.*, 2010). Thus, MqsR toxicity is directly or indirectly associated with persister formation.

As a specific RNase, toxin MqsR is a global regulator that controls protein expression by

enriching specific mRNAs that either lack the GCU cleavage sites or are protected from degradation by secondary structure or bound proteins (Wang and Wood, 2011). This specific RNase activity may dictate whether the cell responds to the stress by being able to rapidly form new proteins to cope with the stress while forming a biofilm or whether the cell becomes dormant (i.e., a persister cell) in a biofilm (Wang *et al.*, 2011). Previously, we identified eight proteins (CspD, ClpX, ClpP, Lon, YfjZ, RelB, RelE, and HokA) that are involved in MqsR DMD where three of these are related to the degradation of the antitoxin MqsA (ClpX, ClpP, and Lon) (Kim *et al.*, 2010b). In addition, deletion of *mqsR* induces 76 genes, and MqsR production induces 132 genes (Kim *et al.*, 2010b); these initial results indicated stress-associated proteins CstA, CspD, RpoS, ClpP, ClpB, and Dps are produced when MqsR is activated which linked MqsR to the stress response although the mechanism was not clear. Similarly, toxin MazF is a specific RNase whose activity results in the production of a pool of small proteins that are necessary both for toxicity and for survival (Amitai *et al.*, 2009).

In this study, we explored how the toxicity of MqsR is related to persistence by using protein engineering (Wood *et al.*, 2011) to increase the toxicity of MqsR; we reasoned that the genetic basis for persistence would be easier to study if a toxin related to persistence had enhanced activity without a change in catalytic function. Utilizing a systems biology approach (transcriptome analysis) along with quantitative real time-polymerase chain reaction (qRT-PCR) and cell survival studies, we found that MqsR increases persister cell formation by repressing acid resistance, multidrug resistance, and osmotic resistance, and that the general stress response master regulator RpoS is important for persister cell formation. Together with the result that wild-type cells that are stressed prior to antibiotic treatment increase 12,000 fold in persistence, we concluded that stressed cells become more persistent than those that are not stressed.

6.3 Results

6.3.1 Random mutagenesis of MqsR for increased toxicity

Previously, we demonstrated that producing MqsR is toxic (Zhang *et al.*, 2008)and that MqsR forms a toxin/antitoxin pair with antitoxin MqsA (Brown *et al.*, 2009; Kim *et al.*, 2010b). To explore how toxicity affects persister cell formation, we engineered MqsR for increased toxicity. Using error prone PCR (epPCR) of *mqsR* with a 0.8% error rate confirmed by sequencing three random *mqsR* genes, a MqsR variant library was constructed and a total of 2160 colonies were screened for reduced colony growth on LB agar plates (*mqsR* expression and the inherent toxicity of MqsR was turned off prior to screening by using glucose). The interesting MqsR variants were confirmed with their reduced cell growth in LB culture in shake flasks. Two MqsR variants were identified with up to four-fold repression of cell growth compared to native MqsR (Fig. 6.1A) indicating that these MqsR variants are more toxic than native MqsR. As a control, producing native MqsR repressed cell growth compared to empty pBS(Kan) (Fig. 6.1A) as expected (Zhang *et al.*, 2008). MqsR variant 2-1 had two amino acid replacements at K3N and N31Y, and MqsR 20-14 had three replacements at R9C, L35F, and V70I (Table 6.1); there were no changes to the promoter or ribosome-binding site regions. Hence, MqsR was engineered to increase toxicity.

6.3.2 MqsR 2-1 is more stable than native MqsR

Amino acid residues K56, Q68, Y81, and K96 of MqsR are key residues for catalysis in MqsR-mediated toxicity by alanine-scanning mutagenesis of evolutionarily and structurally conserved residues (Brown *et al.*, 2009). Since the two amino acid substitutions K3N and N31Y in MqsR 2-1 are distant from the active site residues and residues involved in binding MqsA (Fig. 6.1B), these substitutions probably do not affect catalytic activity of MqsR (Brown *et al.*, 2009). It is also possible that the MqsR 2-1 aa substitutions may affect MqsR binding with

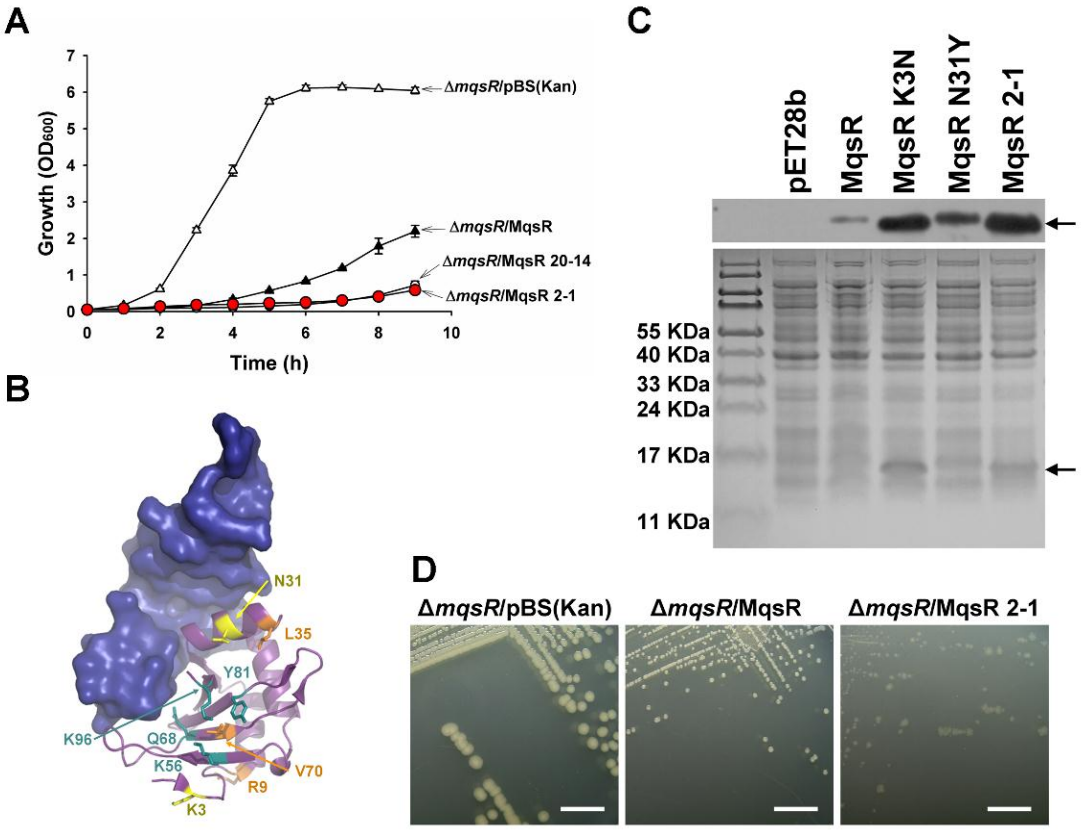

Figure 6.1 Growth, stability, and colony morphology of MqsR variants. (**A**) Growth curves in LB medium with 1 mM IPTG induction at 37°C for BW25113 Δ*mqsR* strains containing pBS(Kan) (empty plasmid control), pBS(Kan)-*mqsR*, pBS(Kan)-*mqsR* 2-1, and pBS(Kan)-*mqsR* 20-14. Error bars indicate standard deviation (n = 3). (**B**) Structure of MqsR in ribbon representation with MqsA in surface representation (based on Protein Data Bank accession code 3HI2). Cyan indicates MqsR active site residues (K56, Q68, Y81, and K96), yellow indicates the residues (K3 and N31) where the substitutions occur in MqsR 2-1 (K3N and N31Y), and orange indicates the residues (R9, L35, and V70) where the substitutions occur in MqsR 20-14 (R9C, L35F, and V70I). (**C**) Protein stability of native MqsR and the MqsR variants (MqsR K3N, MqsR N31Y, and MqsR 2-1). Western blot (upper panel) and SDS-PAGE show the protein levels of His-MqsR and variants detected by a His-tagged antibody. MqsR and the variants were induced from pET28a-based plasmids in *E. coli* BL21 (DE3) via 1 mM IPTG. Arrows indicate the MqsR proteins. (**D**) Colony morphology of BW25113 Δ*mqsR* strains containing pBS(Kan) (empty plasmid), pBS(Kan)-*mqsR*, and pBS(Kan)-*mqsR* 2-1 grown on LB agar plates at 37°C after 24 h. Scale bars indicate 1 cm. Representative images are shown. (**E**) Observation of BW25113 Δ*mqsR* strains containing pBS(Kan) (empty plasmid control), pBS(Kan)-*mqsR*, and pBS(Kan)-*mqsR* 2-1. IPTG was added to LB for 2 h to produce native MqsR and MqsR 2-1 (middle row), while glucose (0.2%) was added to LB to repress MqsR production (upper row). Lower row shows the result of Live/Dead staining after producing MqsR and MqsR 2-1. Live cells are stained in green, and dead cells are stained in red. Scale bars indicate 10 μm. Representative images are shown.

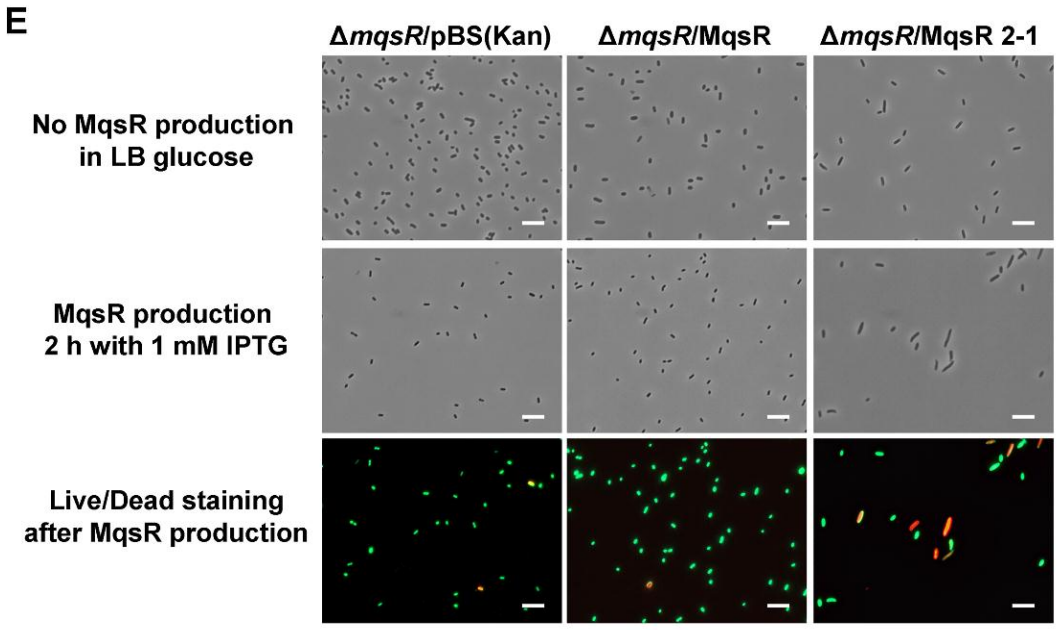

Figure 6.1 Continued.

Table 6.1 Protein sequences of the MqsR variants from screening for increased toxicity and from site-directed mutagenesis.

MqsR variants	Amino acid replacements
MqsR 2-1	K3N, N31Y
MqsR 20-14	R9C, L35F, V70I
MqsR K3N	K3N
MqsR N31Y	N31Y

MqsA which might change MqsA-mediated gene regulation based on its palindrome recognition site (Wang *et al.*, 2011).

To investigate this further, Western blot analysis and SDS-PAGE were used (Fig. 6.1C); these results showed that MqsR 2-1 is more than an order of magnitude more stable than native MqsR without altering the promoter or ribosome binding sequence; hence, the increase in activity of MqsR 2-1 is due to its increased stability. Furthermore, each amino acid substitution (K3N and N31Y) of MqsR 2-1 increased the stability of MqsR (8 fold and 4 fold, respectively) compared to native MqsR; the combination of both amino acid replacements of MqsR 2-1 act synergistically to increase the protein level of MqsR 2-1. Therefore, the increase in toxicity of MqsR 2-1 is due to the dramatic increase in stability and therefore quantity of the protein, as it is easier to increase protein stability while maintaining high function than to change function while maintaining high stability (Bloom *et al.*, 2004).

6.3.3 MqsR 2-1 reduces colony size and enhances cell death

The increased toxicity of MqsR 2-1 was also visible by the changes in colony morphology. Cells producing MqsR 2-1 formed colonies that were non-uniform, translucent, and thin compared to those of cells producing native MqsR (Fig. 6.1D); similar colony morphology was observed with MqsR 20-14. Furthermore, producing MqsR 2-1 made the cell elongate 2.7 fold (Fig. 6.1E) and lyse (Fig. 6.1E) compared to native MqsR. After 2 h of induction, 17% of the cells producing MqsR 2-1 were dead (Fig. 6.1E); most dead cells were the elongated, thus the increase in cell size by MqsR 2-1 is indicative of cell death. For comparison, only 3% of cells died upon producing native MqsR. Taken together, MqsR 2-1 induces cell death and lysis via its increased toxicity when it is produced from a high copy number plasmid.

6.3.4 MqsR 2-1 increased toxicity induces persister cell formation

We investigated whether the MqsR variants with enhanced toxicity enhance persister cell formation with ampicillin as a representative antibiotic since non-persister cells die within 15 min with this antibiotic (Keren *et al.*, 2004). MqsR increases persistence while deletion of *mqsR* reduces persistence (Kim and Wood, 2010). Consistent with these previous results, producing native MqsR in a cell which lacks a chromosomal copy of *mqsR* increased cell survival more than 200 fold under antibiotic stress compared to the empty plasmid control (Fig. 6.2). Producing MqsR 2-1 increased persister cell formation another 73 fold compared to producing native MqsR, and so overall a 14,000 fold increase in persistence was obtained by MqsR 2-1 compared to no MqsR (Fig. 6.2). Similar results were observed with two other concentrations of ampicillin. Therefore, the increased toxicity of MqsR dramatically enhances persister cell formation.

6.3.5 MqsR 2-1 reduces production of stress response proteins

To discern how the increase in toxicity of MqsR 2-1 increases persister production, we performed a whole-transcriptome analysis of cells producing MqsR 2-1 versus native MqsR. Unlike a traditional DNA microarray, apparent induction of gene expression in this experiment is due to greater degradation of other transcripts by MqsR 2-1, so the induced genes are those that are enriched.

Under antibiotic stress, MqsR 2-1 led to the enrichment of 78 transcripts by more than 4.0 fold (Table 6.2). MqsR 2-1 production enriched the master motility regulator transcripts (*flhDC*), which was confirmed by the higher swimming motility of cells producing MqsR 2-1 relative to native MqsR which had no motility (halo diameter 0.8 ± 0.1 cm for MqsR 2-1 vs. 0.0 ± 0.0 cm for native MqsR).

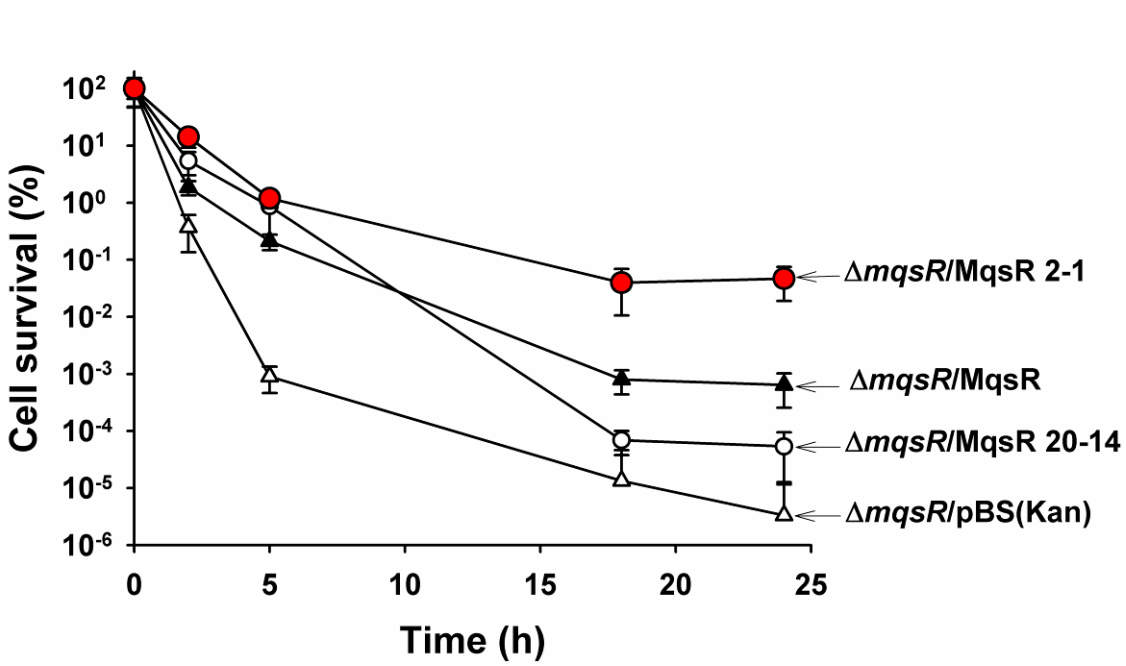

Figure 6.2 Persister cell formation of MqsR variants. BW25113 Δ*mqsR* strains containing pBS(Kan) (empty plasmid control), pBS(Kan)-*mqsR*, pBS(Kan)-*mqsR* 2-1, and pBS(Kan)-*mqsR* 20-14 were grown to a turbidity of 0.5 at 600 nm in LB with 1 mM IPTG at 37°C, adjusted to a turbidity of 1, and exposed to 26 μg/mL ampicillin with 1 mM IPTG for 24 h. Error bars indicate the standard deviation (n = 3).

Table 6.2 Partial whole-transcriptome profiles to determine the impact of MqsR 2-1 on persister formation. List of differentially-enriched and differentially-degraded genes of BW25113 Δ*mqsR*/pBS(Kan)-*mqsR* 2-1 vs. BW25113 Δ*mqsR*/pBS(Kan)-*mqsR* for cells exposed to ampicillin (20 µg/mL) in LB with 1 mM IPTG at 37°C for 1 h. Strains were grown to a turbidity of 0.5 at 600 nm in LB with 1 mM IPTG and adjusted to a turbidity of 1 before ampicillin treatment. Raw data for the two DNA microarrays are available using GEO series accession number GSE31054.

Group and gene	b number	Fold change	Description
Stress response			
bdm	b1481	-9.8	Biofilm-dependent modulation protein
gadA	b3517	-19.7	Glutamate decarboxylase A, isozyme
gadB	b1493	-36.8	Glutamate decarboxylase isozyme
gadC	b1492	-18.4	Acid sensitivity protein, putative transporter
gadE	b3512	-18.4	Transcriptional activator of the *gadABC* operon
gadW	b3515	-6.1	Transcriptional repressor of the *gadABC* operon
gadX	b3516	-6.5	Transcriptional activator for *gadA* and *gadBC*
hdeA	b3510	-13.9	Periplasmic chaperone of acid-denatured proteins
hdeB	b3509	-19.7	Periplasmic chaperone of acid-denatured proteins
hdeD	b3511	-12.1	Putative membrane transporter
kaeE	b1732	-8.6	Hydroperoxidase II
mdtE	b3513	-9.8	Multidrug resistance protein (lipoprotein)
mdtF	b3514	-7.5	Multidrug transport protein, RpoS-dependent
osmE	b1739	-7.0	Osmotically inducible protein
osmY	b4376	-4.9	Hyperosmotically inducible periplasmic protein
ychH	b1205	4.6	Stress-induced protein, involved in cadmium and peroxide resistance
ydjM	b1728	4.9	LexA regulated gene, possible SOS response
yggE	b2922	-4.3	Oxidative stress defense
ygiW	b3024	-4.6	Stress-induced protein, involved in cadmium and peroxide resistance
yhbO	b3153	-4.6	Stress-resistance protein
yodD	b1953	-4.9	Stress-induced protein, involved in peroxide and acid resistance
Motility			
flhC	b1891	5.7	Regulator of flagellar biosynthesis, acting on class 2 operons
flhD	b1892	5.7	Regulator of flagellar biosynthesis, acting on class 2 operons
Transport and metabolism			
cstA	b0598	6.5	peptide transporter induced by carbon starvation
fadA	b3845	4.3	3-ketoacyl-CoA thiolase; in complex with FadB catalyzes
fadB	b3846	7.0	Multifunctional fatty acid oxidation complex subunit alpha
fbaB	b2097	-9.8	Fructose-bisphosphate aldolase class I
frdA	b4154	-5.7	Fumarate reductase, anaerobic, catalytic and NAD/flavoprotein subunit
frdB	b4153	-6.1	Fumarate reductase, anaerobic, Fe-S subunit
frdC	b4152	-5.7	Fumarate reductase, anaerobic, membrane anchor polypeptide
frdD	b4151	-4.6	Fumarate reductase, anaerobic, membrane anchor polypeptide

Table 6.2 Continued.

Group and gene	b number	Fold change	Description
gatA	b2094	13.9	PTS family enzyme IIA, galactitol-specific
gatB	b2093	18.4	PTS family enzyme IIB, galactitol-specific
gatC	b2092	9.8	PTS family enzyme IIC, galactitol-specific
gatD	b2091	26.0	Galactitol-1-phosphate dehydrogenase
gatY	b2096	7.5	Tagatose 6-phosphate aldolase 2, subunit with GatZ
gatZ	b2095	9.2	Putative tagatose 6-phosphate kinase 1
glpQ	b2239	6.5	Glycerophosphodiester phosphodiesterase, periplasmic
glpT	b2240	19.7	Glycerol-3-P MFS transporter
ilvB	b3671	8.6	Acetolactate synthase I, large subunit, valine-sensitive
ilvN	b3670	6.1	Acetolactate synthase I, small subunit
livG	b3455	4.3	Leucine ABC transporter
livH	b3457	4.9	Leucine ABC transporter
livK	b3458	4.9	High-affinity branched-chain amino acid transport protein
lldD	b3605	4.6	*L*-lactate dehydrogenase
lldP	b3603	11.3	*L*-lactate permease
lldR	b3604	7.0	Putative transcriptional repressor for *L*-lactate utilization
mglA	b2149	7.5	Galactose ABC transporter
mglB	b2150	10.6	Galactose ABC transporter
mglC	b2148	5.3	Galactose ABC transporter
otsA	b1896	-9.8	Trehalose-6-phosphate synthase
otsB	b1897	-10.6	Trehalose-6-phosphate phophatase, biosynthetic
paoA	b0286	-9.2	PaoABC aldehyde oxidoreductase, 2Fe-2S subunit
paoB	b0285	-8.0	PaoABC aldehyde oxidoreductase, FAD-binding domain
paoC	b0284	-5.3	PaoABC aldehyde oxidoreductase, molybdemum cofactor-binding subunit
paoD	b0283	-4.3	Molybdemum cofactor insertion for PaoABC aldehyde oxidoreductase
rbsA	b3749	11.3	Ribose ABC transporter
rbsC	b3750	6.1	Ribose ABC transporter
rbsD	b3748	13.0	*D*-ribose utilization
sdhA	b0723	4.3	Succinate dehydrogenase, catalytic and NAD/flavoprotein subunit
sdhB	b0724	4.9	Succinate dehydrogenase, Fe-S protein
sdhC	b0721	6.5	Succinate dehydrogenase, cytochrome b556
sdhC	b0721	4.9	Succinate dehydrogenase, cytochrome b556
sdhD	b0722	4.9	Succinate dehydrogenase, hydrophobic subunit
slp	b3506	-8.6	Outer membrane protein induced after carbon starvation
srlA	b2702	24.3	PTS family enzyme IIC, glucitol/sorbitol-specific
srlB	b2704	14.9	PTS family enzyme IIA, glucitol/sorbitol-specific
srlD	b2705	10.6	Glucitol (sorbitol)-6-phosphate dehydrogenase
srlE	b2703	21.1	PTS family enzyme IIBC, glucitol/sorbitol-specific
sufA	b1684	-7.5	Scaffold protein for iron-sulfur cluster assembly
sufB	b1683	-7.0	Component of SufB-SufC-SufD cysteine desulfurase (SufS) activator complex
sufC	b1682	-7.0	ATPase component of SufB-SufC-SufD cysteine desulfurase (SufS) activator complex

Table 6.2 Continued.

Group and gene	b number	Fold change	Description
sufD	b1681	-6.5	Component of SufB-SufC-SufD cysteine desulfurase (SufS) activator complex
tnaA	b3708	6.5	Tryptophanase
tnaC	b3707	9.2	Tryptophanase leader peptide
yhiD	b3508	-11.3	Putative Mg(2+) transport ATPase
ynfG	b1589	-6.5	Oxidoreductase, Fe-S subunit paralog of DmsB
Cellular process			
glgS	b3049	-4.3	Glycogen biosynthesis, RpoS dependent
grxB	b1064	-4.6	Glutaredoxin 2, regulated by RpoS and ppGpp
iraM	b1160	4.6	RpoS stabilzer during Mg starvation
ivbL	b3672	4.6	*ilvB* operon leader peptide
mokB	b1420	4.3	Regulatory peptide whose translation enables *hokB* expression
nmpC	b0553	18.4	DLP12 prophage; outer membrane porin
ompW	b1256	-12.1	Outer membrane protein W; colicin S4 receptor; putative transport protein
oxyS	b4458	7.5	OxyS sRNA activates genes that detoxify oxidative damage
pspB	b1305	6.5	Antitoxin of a PspC-PspB toxin-antitoxin pair
rpoS	b2741	-1.1	Master stress response regulator RpoS
Fuction unknown			
yccJ	b1003	-11.3	Hypothetical protein

Also, *tnaC* encoding the tryptophanase leader peptide was enriched by MqsR 2-1. *tnaC* is one of the 14 MqsR-resistant mRNAs that lack the MqsR specific GCU sequences (Yamaguchi *et al.*, 2009). Carbon starvation (*cstA*), glycerol-3-phosphate metabolism (*glpQT*), galactitol metabolism (*gatABCDYZ*), ribose transport (*rbsACD*), and glucitol/sorbitol metabolism (*srlABDE*) transcripts were also enriched by MqsR 2-1. Enrichment of these transcripts during MqsR 2-1 production was confirmed using quantitative real-time reverse transcription polymerase chain reaction (qRT-PCR) using independent cultures. Corroborating the DNA microarray data, MqsR 2-1 enriched transcripts of *tnaC* (0 GCU sites), *cstA* (62 GCU sites), *glpT* (30 GCU sites), *rbsA* (27 GCU sites), and *srlA* (10 GCU sites) by 3 to 5 fold (Table 6.3). Glycerol-3-phosphate metabolism might be related to MqsR toxicity and persister formation (Kim *et al.*, 2010b) since producing GlpD induced tolerance to ampicillin and ofloxacin, while deletion of *glpD* repressed the persister production (Spoering *et al.*, 2006). Moreover, enrichment of transcripts related to galactitol metabolism may also be linked to persister cell formation as the genes for galactitol metabolism are highly regulated in biofilms (Domka *et al.*, 2007) in which persister frequencies are elevated (Lewis, 2010).

Critically, MqsR 2-1 also differentially degraded 94 transcripts by more than 4 fold compared to native MqsR (Table 6.2). Primarily, MqsR 2-1 degraded transcripts related to acid resistance (*gadABCEWX* and *hdeABD*), multidrug resistance (*mdtEF*), osmotic resistance (*osmEY*), and oxidative stress related (*yggE, ygiW,* and *yodD*) genes. Corroborating the whole-transcriptome results, qRT-PCR confirmed that MqsR 2-1 differentially degraded transcripts of *gadA, gadB, gadE, gadW, gadX, hdeA, hdeB, mdtE, mdtF,* and *osmY* by 3 to 89 fold (Table 6.3).

Table 6.3 qRT-PCR confirmation of DNA microarray. qRT-PCR results of differentially-enriched and differentially-degraded genes of BW25113 Δ*mqsR*/pBS(Kan)-*mqsR* 2-1 vs. BW25113 Δ*mqsR*/pBS(Kan)-*mqsR* for cells exposed to ampicillin (20 µg/mL) in LB with 1 mM IPTG at 37°C for 1 h. Standard deviation is shown for $\Delta\Delta C_T$ (n = 3). C_T is the threshold cycle of the target genes.

Gene	qRT-PCR		DNA microarray
	$\Delta\Delta C_T$	Fold change	Fold change
Differentially-enriched			
cstA	-1.6 ± 0.8	2.9	6.5
gatD	-2.3 ± 0.6	4.8	26.0
glpT	-2.4 ± 0.6	5.3	19.7
rbsA	-1.8 ± 0.5	3.5	11.3
srlA	-1.4 ± 1.5	2.7	24.3
tnaC	-2.3 ± 0.5	4.8	9.2
Differentially-degraded			
gadA	4.9 ± 0.5	-29.5	-19.7
gadB	4.5 ± 0.7	-23.3	-36.8
gadE	3.8 ± 0.4	-13.6	-18.4
gadW	2.7 ± 0.4	-6.6	-6.1
gadX	2.0 ± 0.5	-4.0	-6.5
hdeA	6.5 ± 0.7	-89.0	-13.9
hdeB	6.2 ± 0.7	-71.4	-19.7
mdtE	1.8 ± 0.6	-3.6	-9.8
mdtF	1.5 ± 0.6	-2.8	-7.5
osmY	3.3 ± 0.6	-9.8	-4.9
rpoS	1.5 ± 0.7	-2.9	-1.1

Corroborating these results, *hdeAB* and *osmE* are repressed in *E. coli* persister cells isolated using a flow cytometer compared to non-persisters (Shah *et al.*, 2006). Hence, the increased MqsR toxicity during antibiotic stress degraded transcripts of multiple stress response loci including acid resistance, osmotic resistance, oxidative stress resistance, and multidrug resistance. These results suggest that the stress response transcripts that are degraded by MqsR 2-1 are closely connected to persister cell production.

6.3.6 Deletion of *gadB, gadX, mdtF,* and *osmY* increase persistence

To investigate whether the stress-related genes that were identified in the whole-transcriptome experiment are important for persister cell formation, cell survival of isogenic deletion strains of each stress gene was measured under antibiotic stress. Deletion of *gadB* significantly increased persister production (43,000 fold) compared to BW25113 wild-type to the extent that 55% of the cells were persistent (Fig. 6.3A); by comparison, the wild-type had only 0.001% persister cells. *gadB* encodes glutamate decarboxylase and confers resistance to extreme acid conditions (Waterman and Small, 2003). *gadB* expression is also increased in ampicillin-resistant *E. coli* (Adam *et al.*, 2008) and the cell appears to use GadB to thwart the action of ampicillin, since glutamate decarboxylase may remove the carboxyl group from ampicillin, thereby inactivating it (Adam *et al.*, 2008). Therefore, deletion of *gadB* dramatically increases persistence.

Along with the increased persistence of *gadB* deletion, the *gadX* deletion also resulted in a large increase in persisters (10,000 fold increase and 13% persist) (Fig. 6.3). GadX is a transcriptional activator of the *gadBC* operon (Tramonti *et al.*, 2002). Also, deletion of *mdtF* encoding a component of the multidrug efflux pump MdtEF (Nishino and Yamaguchi, 2001), increased persistence by 4,000 fold and increased the percentage of persisters to 5% (Fig. 6.3A).

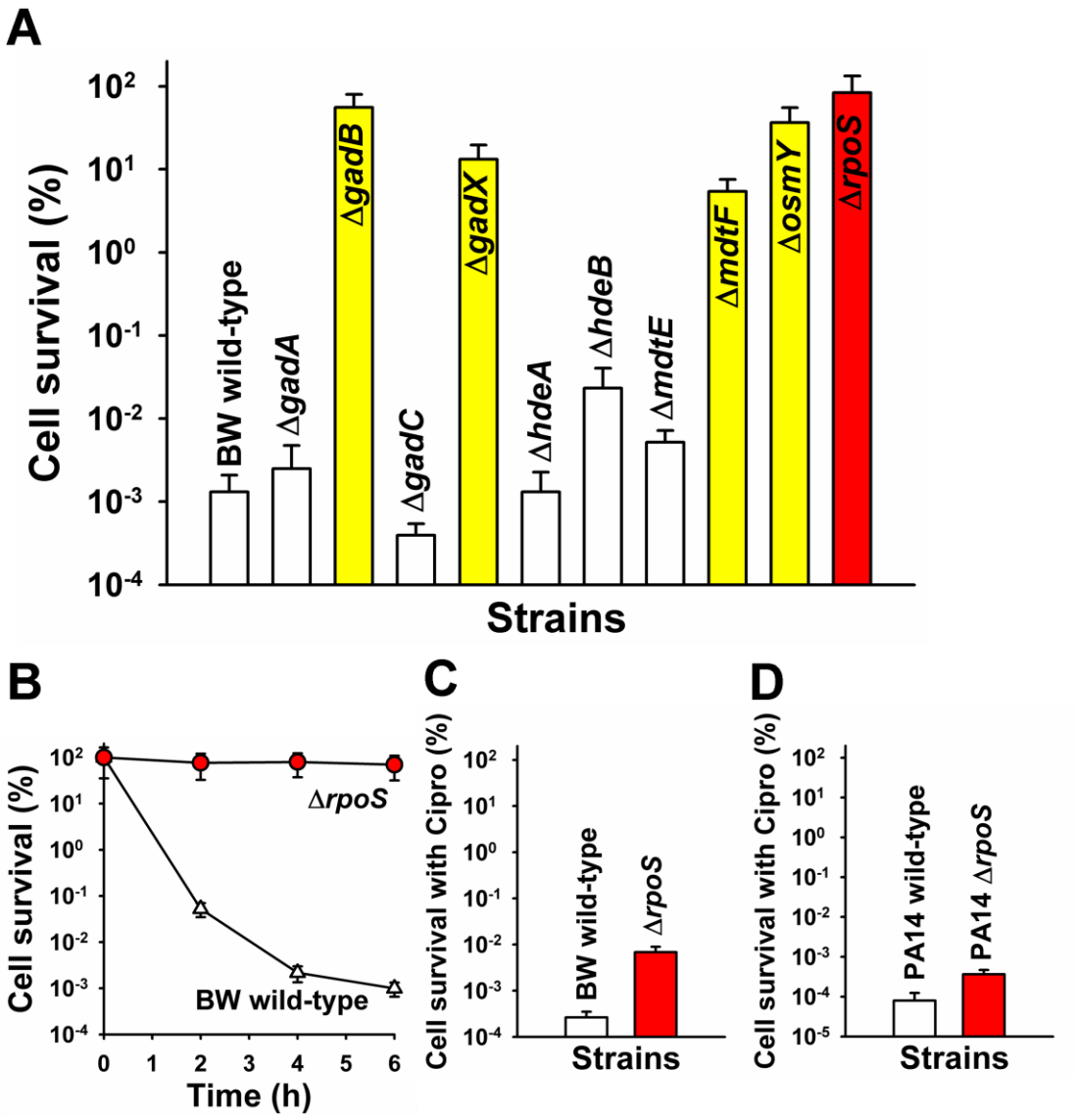

Figure 6.3 Effect of isogenic mutations on persister cell formation. BW25113 and its isogenic Δ*gadA*, Δ*gadB*, Δ*gadC*, Δ*gadX*, Δ*hdeA*, Δ*hdeB*, Δ*mdtE*, Δ*mdtF*, Δ*osmY*, and Δ*rpoS* mutants were grown to a turbidity of 1 in LB at 37°C and exposed to 20 μg/mL ampicillin for 5 h (A). Time-course of persister formation of BW25113 Δ*rpoS* exposed to 20 μg/mL ampicillin for 6 h (B). Persister formation of BW25113 Δ*rpoS* exposed to 1 μg/mL ciprofloxacin (Cipro) for 5 h (C). Persister formation of PA14 Δ*rpoS* exposed to 1 μg/mL Cipro for 5 h (D). Error bars indicate the standard deviation (n = 3).

Deletion of *osmY* encoding hyperosmotic resistance protein (Yim and Villarejo, 1992) enhanced persistence 28,000 fold and increased the percentage of persisters to 37% (Fig. 6.3A). This change in persistence could be complemented since overproducing OsmY reduced the persistence level to that of wild-type strain (Fig. 6.4). Hence, MqsR 2-1 reduces acid resistance, multidrug resistance, and osmotic resistance systems which injure the cells and make them enter a dormant state.

6.3.7 RpoS is important for persister formation

Since the general stress response master regulator RpoS (Hengge-Aronis, 1996) positively regulates *gadB* (Waterman and Small, 2003), *gadX* (Tramonti *et al.*, 2002), *osmY* (Vijayakumar *et al.*, 2004), and *mdtF* (Nishino *et al.*, 2008), directly or indirectly, we hypothesized that MqsR 2-1 may represses *rpoS* and thereby control all of these stress-response genes. Hence, cells less able to respond to stress more readily become persisters. Using qRT-PCR, we found that Mqsr 2-1 degraded *rpoS* by 2.9 fold (Table 6.3) compared to native MqsR. The *rpoS* transcript has 26 GCU sites in 1558 nt for possible cleavage by MqsR. Although *E. coli* K-12 BP792, the parent strain of BW25113, has an amber mutation in *rpoS*, this mutation was removed from BW25113 (Baba *et al.*, 2006), and we confirmed that there is no amber mutation in *rpoS* gene by sequencing the *rpoS* coding region. Hence, RpoS from BW25113 strain is active, and deletion of *rpoS* makes cells more sensitive to stress.

Consistent with our model, cells that lack *rpoS* dramatically increased persister production by 64,000 fold (84% of cell survival after 5 h) compared to BW25113 wild-type with ampicillin stress (Fig. 6.3A). Furthermore, the *rpoS* deletion strain maintained high persistence during ampicillin treatment (2, 4, and 6 h) while the wild-type strain continuously decreased cell survival (Fig. 6.3B). Hence, the high cell survival was not due to ampicillin resistance as there was no growth, only persistence. Since we found that *rpoS* in pCA24N plasmid from ASKA

library (Kitagawa *et al.*, 2005) lacks 117 nt encoding N-terminal 39 aa of RpoS, we constructed the plasmid which has full *rpoS* sequence to investigate *rpoS* complementation in persistence. The change in persistence could be complemented since overproducing RpoS reduced the persistence level to that of wild-type strain (Fig. 6.4). Furthermore, since growth of the *rpoS* deletion strain in rich medium was only 15% less than that of the wild-type strain (1.30 ± 0.01 h^{-1} for Δ*rpoS* vs. 1.52 ± 0.01 h^{-1} for BW25113), the dramatic increase in persistence of the *rpoS* mutant is not due to persister cell formation prior to antibiotic addition. Hence, the antibiotic treatment itself is responsible for generating the persister cells.

To test our hypothesis further that cells less able to respond to stress generate greater numbers of persister cells, we tested persistence with another antibiotic, ciprofloxacin. Ciprofloxacin inhibits DNA replication by interfering DNA gyrase, while ampicillin inhibits cell wall synthesis by binding to penicillin-binding proteins (Kohanski *et al.*, 2010). As expected, deletion of *rpoS* increased persister formation by 26 fold compared to the wild-type strain in the presence of ciprofloxacin (Fig. 6.3C). Since RpoS regulates virulence factors as well as the stress responses in *Pseudomonas aeruginosa* (Suh *et al.*, 1999), we tested the effect of *rpoS* mutation in persister formation of *P. aeruginosa*. Mutation of *rpoS* in *P. aeruginosa* PA14 increased persister formation by 5 fold compared to PA14 wild-type strain in the presence of ciprofloxacin (Fig. 6.3D). Therefore, persister cell formation is controlled by RpoS levels that regulate many stress response genes.

6.3.8 Persistence increases when cells are damaged by oxidative and acid stresses

Since deletion of *rpoS* as well as the other stress-resistance genes (*gadB*, *gadX*, *mdtF*, and *osmY*) dramatically increased persister cell formation (Fig. 6.3), we hypothesized that cells damaged by stress have increased persister cell formation compared to the cells without stress.

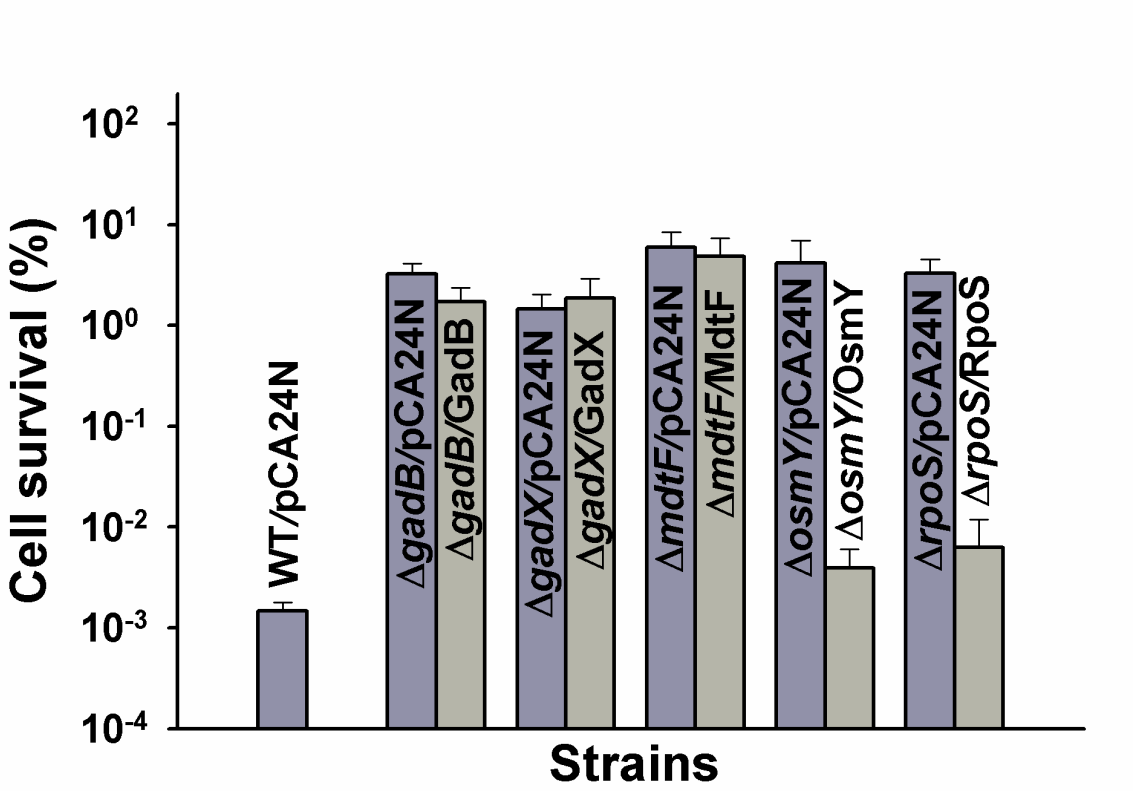

Figure 6.4 Persister cell formation in isogenic mutants with stress-related deletions (blue bars). Grey bars show persister cells after producing proteins from pCA24N-based plasmids. Strains were grown in LB at 37°C for 2 h, 1 mM IPTG was added except the cell producing RpoS protein with 0.1 mM IPTG, cells were grown to a turbidity of 1 at 600 nm, and cells were exposed to 20 μg/mL ampicillin for 5 h. Error bars indicate the standard deviation (n = 2).

To test this hypothesis, we first measured cell survival after oxidative (H_2O_2) and acid (pH 2.5) stress in the *rpoS* deletion strain to ensure that the cells were less viable. As expected, cells that lacked the ability to respond to stress through RpoS were more sensitive to oxidative stress (80-fold less survival than wild-type) (Fig. 6.5A) as well as acid stress (930-fold less survival than wild-type) (Fig. 6.5B). Similarly, deleting *gadA* and *hdeB* decreased viability 10-fold compared to the wild-type strain (Fig. 6.5B). Hence, cells lacking stress response-genes are more sensitive to stress.

Then we investigated persister cell formation after stress in order to test whether the damaged cells become more persistent than intact cells. As deletion of *rpoS* already has high persistence (Fig. 6.3A), we measured persister formation of the wild-type strain after exposing the cells to H_2O_2 prior to antibiotic treatment. We found that wild-type cells that received oxidative stress prior to antibiotic treatment had 11,000-fold increase in persister cell formation compared to the cells with no stress (Fig. 6.5C). This increase is not just a percentage increase in that the total number of wild-type cells that persist was 9.8×10^7 cells/mL when cells were stressed first with hydrogen peroxide vs. 9.8×10^3 cells/mL that persist without hydrogen peroxide (both samples originally had roughly 5×10^8 cells/mL). Hence, a 25% reduction in viability leads to an extraordinary increase in persistence. Similarly, persister cell formation of the wild-type strain increased 13,000-fold with acid stress (Fig. 6.5C). Furthermore, both *gadA* and *hdeB* knockout strains which did not increase persister cell formation (Fig. 6.3A) also increased persister cell formation 1,400 and 700 fold with acid stress, respectively, compared to no stress condition (Fig. 6.5C). Taken together, persister cell formation increases dramatically if cells are stressed prior to antibiotic addition.

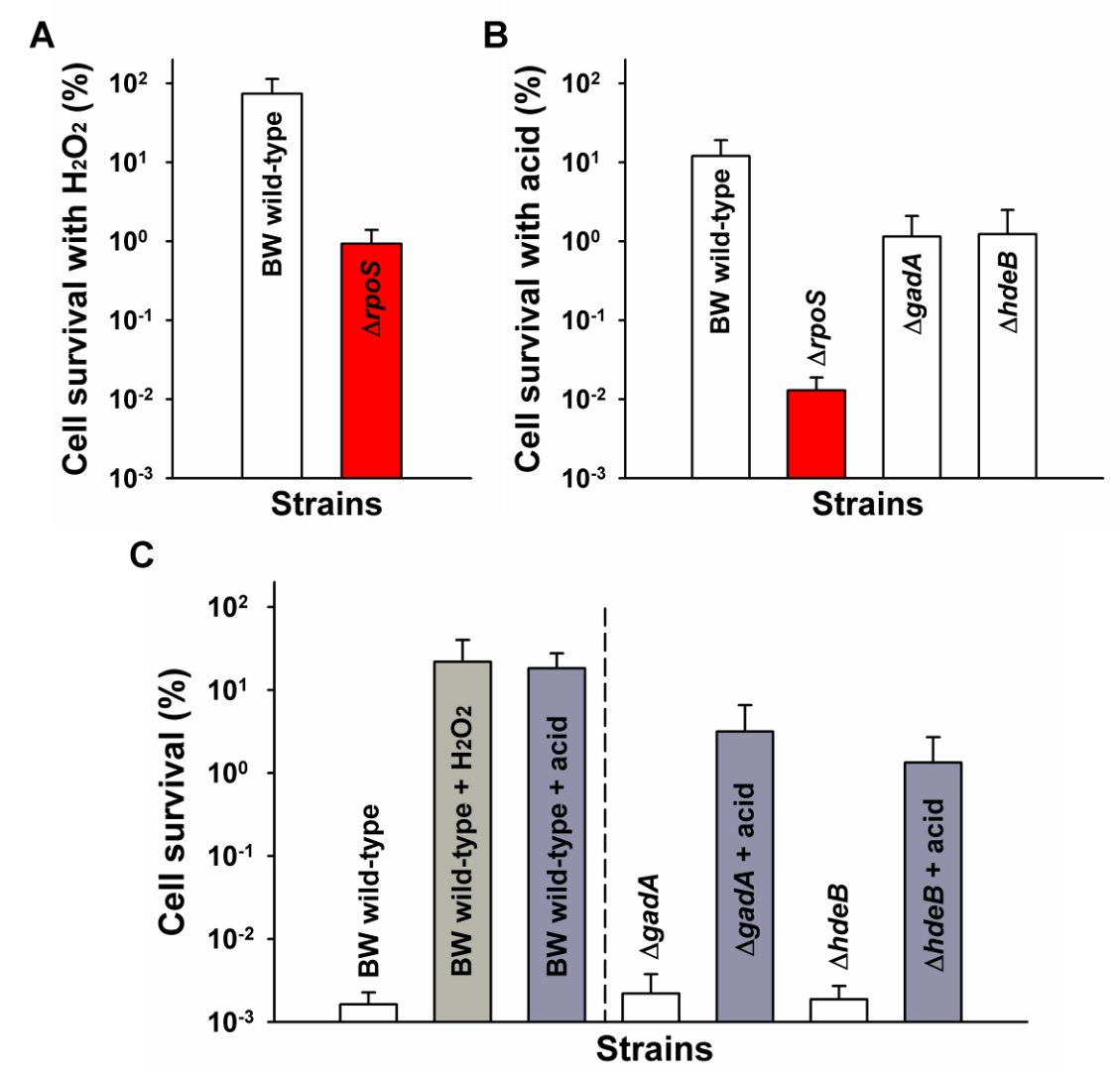

Figure 6.5 Persister formation after oxidative and acid stresses. Cell survival (%) with oxidative stress (20 mM H_2O_2) for 10 min (**A**) and with acid stress (pH 2.5) for 2 min (**B**). BW25113 and its isogenic Δ*gadA*, Δ*hdeB*, and Δ*rpoS* mutants were grown to a turbidity of 1 in LB at 37°C and exposed to H_2O_2 or pH 2.5. Persister cell formation of BW25113 and its isogenic Δ*gadA* and Δ*hdeB* mutants exposed to 20 μg/mL ampicillin for 5 h after oxidative or acid stresses (**C**). Error bars indicate the standard deviation (n = 3).

6.4 Discussion

Persister cell formation appears to be one of the main physiological roles of TA systems (Lewis, 2008; Kim and Wood, 2010; Maisonneuve *et al.*, 2011; Wang and Wood, 2011), as TA modules induce dormancy (Lewis, 2008). In this study, we showed that toxin MqsR may be engineered for enhanced toxicity (Fig. 6.1) and that this increased toxicity leads to increased persister cell formation (Fig. 6.2). The increase in persistence resulted from a reduction in transcripts for the stress response cascades including acid resistance, multidrug resistance, and osmotic resistance systems all regulated by RpoS, as shown in whole-transcriptome results and by the dramatic increase in persistence upon deleting *gadB*, *gadX*, *mdtF*, *osmY,* and *rpoS* (Fig. 6.3A). Hence, we identified part of the genetic basis of persister cell formation by using the tools of protein engineering and systems biology. This is the first report that differential degradation of *rpoS* transcripts leads to persister cell formation by down-regulating stress responsive genes. This result was corroborated by showing a reduction in transcripts of genes controlled by RpoS also led to an increase in persistence via *gadB*, *gadX*, *mdtF*, and *osmY*, and this is the first report of the influence of these acid resistance, antibiotic resistance, and osmolarity resistance on persister cell formation. This is also the first report of exceptionally high levels of persister cells; normally they are no more than 1% of stationary-phase cultures (Lewis, 2007) but their concentration reaches 80% here (Fig. 6.3A). Hence we have determined a new mechanism for increasing persistence. Furthermore, since we can enhance persister cell formation dramatically using knockout strains of stress resistance genes or pre-exposing cells to stresses prior to antibiotic treatment, isolating persister cells may be achieved far easier than in previous efforts where persister cells were isolated using a flow cytometer with a GFP-tagged *E. coli*; dormant cells are dim where active cells glow green (Shah *et al.*, 2006). Therefore, using our new tool for increasing persistence, further studies for persisters will be facilitated for determining what

proteins are expressed during persistence and what proteins are required to wake these sleeping cells (these experiments are underway).

In most cases, when genes are deleted, mutant cells become more sensitive to antibiotics, as shown in antibiotic hypersensitivity screening of nearly 4,000 single-gene-knockouts in *E. coli* (Tamae *et al.*, 2008). Thus, it is interesting that deletion of stress resistance genes increases persister cell formation, which indicates the persistence mechanism is quite different from the resistant mechanisms. Previously, labs had searched unsuccessfully (Hu and Coates, 2005; Hansen *et al.*, 2008) for deletions that would make cells less persistent when in fact key, deletions in the stress response make the cell more persistent (Fig. 6.3). Sigma factor RpoS regulation is one of the main stress resistant mechanisms in the cell since RpoS regulates many stress-responsive genes (Vijayakumar *et al.*, 2004) that allow the cell to survive various stresses including UV exposure, acid shock, heat shock, oxidative stress, and starvation (Dong and Schellhorn, 2009). Antitoxin MqsA represses *rpoS,* while upon stress, RpoS is induced via degradation of MqsA by Lon protease (Wang *et al.*, 2011). Thus deletion of *rpoS* makes cells more sensitive to stresses (Fig. 6.5AB), but the damaged cells become dramatically more persistent to the antibiotic (Fig. 6.5C).

Hence, our results show cells behave somewhat counter intuitively: in terms of persistence, it is better for cells to have less fitness for environmental stress; i.e., it is better for persistence for the cell to be more sensitive to stress which likely activates toxins. It appears cells may have two different survival mechanisms upon external stresses (Fig. 6.6): stress turns on the stress-responsive gene cascades, and most cells combat the stress while keeping cellular metabolism relatively active. Alternatively, environmental stress may induce Lon-mediated degradation of antitoxins (Maisonneuve *et al.*, 2011; Wang *et al.*, 2011), and the activated toxins then degrade most mRNA transcripts (Wang and Wood, 2011) including stress responsive genes and make the

cell dormant. Therefore, persister cells are generated in response to stresses rather than preexisting heterogeneity in bacterial populations (Balaban *et al.*, 2004). The decision whether the cell actively combats the stress or becomes persistent may depend on intensity and type of stresses.

Deletion of *mqsR* decreases persister cell formation using *E. coli* BW25113 (Kim and Wood, 2010), and this result was verified by an independent group (Luidalepp *et al.*, 2011). Using different strains (e.g., *E. coli* MG1655) and different conditions, others have found that the *mqsR* deletion does not affect persistence (Shah *et al.*, 2006; Maisonneuve *et al.*, 2011) unless multiple TA loci are deleted (Maisonneuve *et al.*, 2011). In addition, the age of the inoculum strongly influences persister cell development in that the lower persister frequencies of cells such as *glpD*, *dnaJ*, and *surA* knockout strains were elevated to the level of the wild-type when inocula aged (Luidalepp *et al.*, 2011). In contrast, persister cell formation by production of MqsR is consistent when MqsR is produced (Shah *et al.*, 2006; Kim and Wood, 2010) because of its RNase activity. In this study, we engineered MqsR for much greater toxicity and persistence by two amino acid replacements (K3N and N31Y) that increase protein stability (Fig. 6.1C) probably without affecting binding affinity with MqsA and catalytic activity (Fig. 6.1B).

In summary, we demonstrate that toxicity may increase persister cell formation and that cells may enter non-metabolizing state through the repression of stress resistance modules. Hence, TA systems have a vital role in cell physiology especially in the formation of persister cells. Understanding protein targets for maintaining persisters is important for discovery of drugs for effectively treating chronic infections (Lewis, 2010) and here we provide some new targets and strategies for combating persister cells.

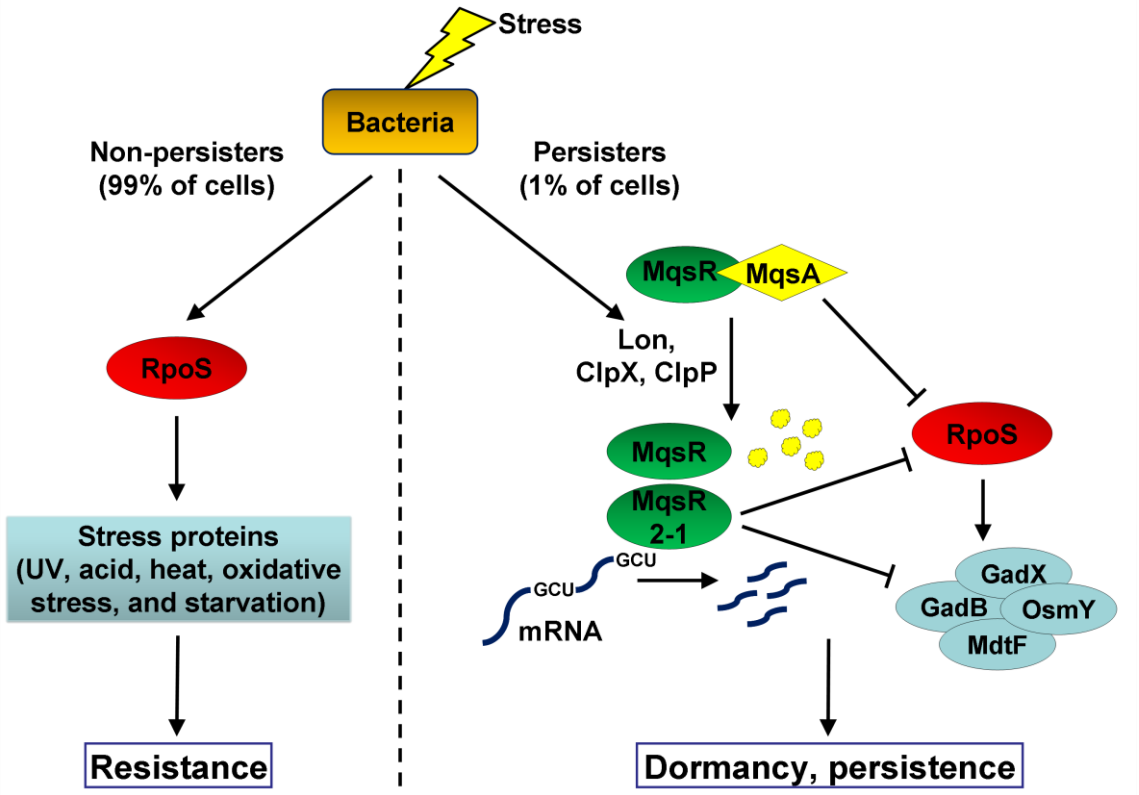

Figure 6.6 Schematic of the persistence and resistance with *rpoS*. Upon stresses such as UV exposure, acid shock, heat shock, oxidative stress, starvation, most cells induce resistance mechanism by RpoS regulation (left panel). Stresses also increase persister formation (right panel). MqsA is degraded by proteases (ClpXP and Lon). MqsR 2-1 with enhanced toxicity degrades mRNA transcripts including stress responsive mRNAs. The degradation of *rpoS* by the toxin leads to down-regulation of acid (*gadB*, *gadX*) osmotic (*osmY*), multidrug (*mdtF*) resistance systems. Then, upon antibiotic treatment, cells enter a dormant state. → indicates induction, and ⊥ indicates repression.

6.5 Experimental procedures

6.5.1 Bacterial strains and growth conditions

The bacterial strains and plasmids used in this study are listed in Table 6.4. We used the Keio collection (Baba *et al.*, 2006) for isogenic mutants and pBS(Kan) plasmid (Canada *et al.*, 2002) for overexpressing genes of *E. coli*. The gene deletions of *mqsR*, *gadB*, *gadX*, *mdtF*, *osmY*, and *rpoS* were confirmed by PCR using primers (Table 6.5). All strains were initially streaked from -80^{o}C glycerol stocks on Luria-Bertani (LB) (Sambrook *et al.*, 1989) with glucose (0.2%) agar plates and were cultured at 37^{o}C in LB. Kanamycin (50 µg/mL) was used for pre-culturing isogenic knockout mutants and for maintaining pBS(Kan)-based and pET28a-based plasmids, chloramphenicol (30 µg/mL) was used for maintaining pCA24N-based plasmids, and gentamycin (15 µg/mL) was used for pre-culturing PA14 Δ*rpoS* mutant. Genes were expressed by adding 1 mM isopropyl-β-D-thiogalactopyranoside (IPTG) (Sigma, St. Louis, MO, USA).

6.5.2 epPCR for random mutagenesis

mqsR from plasmid pBS(Kan)-*mqsR* under the control of *lac* promoter was mutated by epPCR as described previously (Fishman *et al.*, 2004) using primers ep-pBS(Kan)-f and ep-pBS(Kan)-r (Table 6.5). The epPCR product was cloned into pBS(Kan)-*mqsR* using BamHI and XbaI after treating the plasmid with Antarctic phosphatase (New England Biolabs, Beverly, MA, USA). The ligation mixture was electroporated into BW25113 *mqsR* competent cells using the Gene Pulser/Pulse Controller (Bio-Rad, Hercules, CA, USA) at 1.25 kV/cm, 25 µF, and 200 Ω.

Table 6.4 Strains and plasmids used in the persistence study. Km^R, Gm^R, and Cm^R are kanamycin, gentamycin, and chloramphenicol resistance, respectively.

Strains and plasmids	Genotype/relevant characteristics	Source
Strains		
BL21 (DE3)	F^- *ompT hsdS*$_B$ (*r*$_B^-$*m*$_B^-$) *gal dcm* λ(DE3) Ω P_{lacUV5}:: T7 polymerase	Novagen
BW25113	*lacI*^{q} *rrnB*$_{T14}$ Δ*lacZ*$_{WJ16}$ *hsdR*514 Δ*araBAD*$_{AH33}$ Δ*rhaBAD*$_{LD78}$	(Baba *et al.*, 2006)
BW25113 Δ*mqsR*	BW25113 Δ*mqsR*	(Kim *et al.*, 2010b)
BW25113 Δ*gadA*	BW25113 Δ*gadA* Ω Km^R	(Baba *et al.*, 2006)
BW25113 Δ*gadB*	BW25113 Δ*gadB* Ω Km^R	(Baba *et al.*, 2006)
BW25113 Δ*gadC*	BW25113 Δ*gadC* Ω Km^R	(Baba *et al.*, 2006)
BW25113 Δ*gadX*	BW25113 Δ*gadX* Ω Km^R	(Baba *et al.*, 2006)
BW25113 Δ*hdeA*	BW25113 Δ*hdeA* Ω Km^R	(Baba *et al.*, 2006)
BW25113 Δ*hdeB*	BW25113 Δ*hdeB* Ω Km^R	(Baba *et al.*, 2006)
BW25113 Δ*rpoS*	BW25113 Δ*rpoS* Ω Km^R	(Baba *et al.*, 2006)
BW25113 Δ*mdtE*	BW25113 Δ*mdtE* Ω Km^R	(Baba *et al.*, 2006)
BW25113 Δ*mdtF*	BW25113 Δ*mdtF* Ω Km^R	(Baba *et al.*, 2006)
BW25113 Δ*osmY*	BW25113 Δ*osmY* Ω Km^R	(Baba *et al.*, 2006)
PA14	PA14 wild-type strain	(Liberati *et al.*, 2006)
PA14 Δ*rpoS*	PA14_17480 Ω *Mar2xT7*, Gm^R	(Liberati *et al.*, 2006)
Plasmids		
pBS(Kan)	Km^R, pBS(Kan)	(Canada *et al.*, 2002)
pBS(Kan)-*mqsR*	Km^R, pBS(Kan) P_{lac}::*mqsR*$^+$	(Kim *et al.*, 2010b)
pET28b*	Km^R, pET28b	Novagen
pET28a-*mqsR*	Km^R, pET28a P_{T7}::*mqsR*$^+$	(Brown *et al.*, 2009)
pCA24N	Cm^R; *lacI*^{q}, pCA24N	(Kitagawa *et al.*, 2005)
pCA24N-*gadB*	Cm^R; *lacI*^{q}, pCA24N $P_{T5\text{-}lac}$::*gadB*$^+$	(Kitagawa *et al.*, 2005)
pCA24N-*gadX*	Cm^R; *lacI*^{q}, pCA24N $P_{T5\text{-}lac}$::*gadX*$^+$	(Kitagawa *et al.*, 2005)
pCA24N-*mdtF*	Cm^R; *lacI*^{q}, pCA24N $P_{T5\text{-}lac}$::*mdtF*$^+$	(Kitagawa *et al.*, 2005)
pCA24N-*osmY*	Cm^R; *lacI*^{q}, pCA24N $P_{T5\text{-}lac}$::*osmY*$^+$	(Kitagawa *et al.*, 2005)
pCA24N-full *rpoS*	Cm^R; *lacI*^{q}, pCA24N $P_{T5\text{-}lac}$:: *rpoS*$^+$	This study

*pET28b is identical to pET28a except for 1 bp that is deleted near BamHI in the multiple cloning site.

Table 6.5 Primers used for epPCR, site-directed mutagenesis, *rpoS* cloning, DNA sequencing, confirmation of the mutants, and qRT-PCR. Underlined italic text indicates the site-directed mutation for the codon corresponding to amino acid replacement for K3N (5'-AAA to 5'-AAC) in mqsR-K3N-f and mqsR-K3N-r and for N31Y (5'-AAT to 5'-TAT) in mqsR-N31Y-f and mqsR-N31Y-r. Underlined bold text indicates the BseRI restriction site in rpoS-BseRI-f2 and SalI restriction site in rpoS NS-r.

Primer Name	Primer Sequence (listed 5' to 3')
epPCR of *mqsR*	
ep-pBS(Kan)-f	AGGAAACAGCTATGACCATGATTAC
ep-pBS(Kan)-r	ATACGACTCACTATAGGGCGAATTG
Site-directed mutagenesis	
mqsR K3N-f	CGCGGCAGCCATATGGAA*AAC*CGCACACCACATACACGTTTGAG
mqsR K3N-r	CTCAAACGTGTATGTGGTGTGCG*GTT*TTCCATATGGCTGCCGCG
mqsR N31Y-f	GTACAACACGTAGTGCCCTGTTA*TAT*GCAGATGAGTTAGGTTTGG
mqsR N31Y-r	CCAAACCTAACTCATCTGC*ATA*TAACAGGGCACTACGTGTTGTAC
Cloning *rpoS* into pCA24N	
rpoS-BseRI-f	ACCATCACCATCACCATACGGATCCGGCCCTGAGGGCCAGTCAGAATACGCTGAAAGTTC
rpoS-BseRI-f2	TTCATTAAA**GAGGAGAAATTAACTAT**GAGAGGATCTCACCATCACCATCACCATACG
rpoS-NS-r	GGCTGCAG**GTCGAC**CCTTAGCGGCCGCATAGGCCCTCGCGGAACAGCGCTTCGATATTC
DNA sequencing	
T7-f	TAATACGACTCACTATAGGG
T7-ter-r	GCTAGTTATTGCTCAGCGG
pCA24N-seq-f	GCCCTTTCGTCTTCACCTCG
pCA24N-seq-r	GAACAAATCCAGATGGAGTTCTGAGGTCATT
Confirmation of deletions	
mqsR up	GCCACTTTCTTATATGGTCAATCAC
mqsR down	GACACAATATAAACCGTGGATACCT
gadB up	TACGTGATAATTCAGGAGACACAGA
gadB down	AGCAGGAAGAAGACTAATGAAAAGC
gadX up	CCGTAGAACATCACACATTATCATC
gadX down	CGCACAGCGTATAGCTTATGTTTAT

Table 6.5 Continued.

Primer Name	Primer Sequence (listed 5' to 3')
mdtF up	GTACAGCTCAATCTGGAAAATGGTA
mdtF down	TGGGATTATTAAGCTGACAATTCAT
osmY up	ATAACTGATTCAGAGGCTGTAATGG
osmY down	AGTTAATGTCACCGCTTGATATGAG
rpoS up	AAGGCTTTGACTCGAAAATCAC
rpoS down	GATATTTTTCGGGGTCACTTCATG
qRT-PCR	
cstA-RT-f	GGGCACCGTACTTTGACTTTAC
cstA-RT-r	TTTCAGGAAGGTAGAGAGGTAGTCA
gadA-RT-f	GGTACAAATCTGCTGGCATAAATTC
gadA-RT-r	ACTCATAGTTACCGGTGTAGGTCAC
gadB-RT-f	TGGTACTTTTGCCATCAACTTCTC
gadB-RT-r	GTAAGAGGCGTTCTGTACTTTGGTA
gadE-RT-f	GTTTTGGCACCTTATCACATCAG
gadE-RT-r	GGGGCAAGTGTTTACCATAAG
gadW-RT-f	GAAAGAATGTATACCAGCGAGAGTC
gadW-RT-r	AGTATGCAGAGGAATTTGACGTAAC
gadX-RT-f	CGAAGAAGAGACATCATATTCACAG
gadX-RT-r	GTGATATCCACAGGATACTGCAAC
gatD-RT-f	GTTATCGGCAGTTGGATGAACTACT
gatD-RT-r	ATTAATGGCTCCAGGCTTAACTTAC
glpT-RT-f	GATGGCCTGGTTCAATGACT
glpT-RT-r	CAGCAGTTTGTTCGGCAGTA
hdeA-RT-f	AGTATTAGGCGTTATTCTTGGTGGT
hdeA-RT-r	AAATCTTCACAGGTCCAGGAGTT
hdeB-RT-f	ATGAATCCGCTAAAGATATGACCTG
hdeB-RT-r	AACGGTATCGCCACCTTTATATACT
mdtE-RT-f	GATTTCTTACGCATGAAAGAAGAGG
mdtE-RT-r	CTGTAGCGTTTACCATTTTCCAGAT
mdtF-RT-f	CAAGTCTGAAGACGGTTTATCCTTA
mdtF-RT-r	AAAACAGATACATGACCAGGAAGAC

Table 6.5 Continued.

Primer Name	Primer Sequence (listed 5' to 3')
osmY-RT-f	GTCGATAGCTCTATGAATAAAGTCG
osmY-RT-r	TTACAGAGATATCGGTGCTCTTGAT
rbsA-RT-f	CATGTCAGTAAAAGAGAACATGTCG
rbsA-RT-r	ACAGACGAATGAAATCACTCACAG
rpoS-RT-f	AGAGTAACTTGCGTCTGGTGGTAAA
rpoS-RT-r	ATAGTACGGGTTTGGTTCATAATCG
srlA-RT-f	GTTACCTACTGTTACCGTGCATTG
srlA-RT-r	ATTCATTGAGTGGCAGCTATAAGAG
tnaC-RT-f	ATCTTACATATATGTGTGACC
tnaC-RT-r	AGGGCGGTGATCGACAATTTTG
rrsG-RT-f	TATTGCACAATGGGCGCAAG
rrsG-RT-r	ACTTAACAAACCGCTGCGT

6.5.3 Toxicity screening of MqsR variants

In order to screen MqsR variants for the increased toxicity, each single colony of BW25113 Δ*mqsR* producing MqsR variants from pBS(Kan)-*mqsR* was transferred on fresh LB agar plates by touching with a toothpick, and incubated for 24 h to select colonies with reduced cell growth (i.e., small colony). As controls, BW25113 Δ*mqsR* with empty pBS(Kan) and pBS(Kan)-*mqsR* (native MqsR) were used. Interesting *mqsR* alleles were re-analyzed by measuring cell growth in LB culture in a shake flask after re-electroporation the plasmids; overnight culture was diluted to a turbidity of 0.05 at 600 nm in LB medium, incubated in a shake flask for 9 h, cell growth was measured at OD 600 nm every 1 h. Mutant *mqsR* alleles were sequenced using a primer ep-pBS(Kan)-f (Table 6.5). Each data point was averaged from two independent cultures.

6.5.4 Site-directed mutagenesis

Site-directed mutagenesis was performed at the codons corresponding to positions at K3 and N31 of MqsR using plasmid pET28a-*mqsR* as a template with site-directed mutagenesis primers (Table 6.5). PCR was performed using *Pfu* DNA polymerase at 95°C for 1 min, with 20 cycles of 95°C for 1 min, 55°C for 50 seconds, and 68°C for 9 min, and a final extension of 68°C for 7 min. The constructed plasmids were electroporated into BL21 (DE3) after DpnI digestion of template plasmids. Mutations were confirmed by sequencing the constructed plasmids using the T7-f and T7-ter-r primers (Table 6.5).

6.5.5 Cloning full *rpoS* into pCA24N plasmid

Since *rpoS* in pCA24N plasmid from ASKA library (Kitagawa *et al.*, 2005) lacks 117 nt encoding N-terminal 39 aa of RpoS, we constructed the plasmid which has full *rpoS* sequence. Full *rpoS* sequence was amplified from *E. coli* BW25113 chromosome using rpoS-BseRI-f and rpoS-NS-r primers (Table 6.5) and then 2nd PCR on the 1st PCR template with rpoS-BseRI-f2 and rpoS-NS-r primers was performed to obtain N-terminal histag and BseRI restriction site with

rpoS. pCA24N empty plasmid was used as a vector to insert full *rpoS* gene into it using BseRI and SalI restriction sites. Full *rpoS* insertion was confirmed by sequencing using pCA24N-seq-f, pCA24N-seq-r, and rpoS-RT-f primers (Table 6.5)**.**

6.5.6 Persister assay

To determine the number of persister cells with MqsR variants, cells were inoculated in LB medium and grown to a turbidity of 0.5 (to obtain 3 to 7×10^8 CFU/mL of viable cells) at 600 nm with 1 mM IPTG. Cells were washed with same amount of 0.85% NaCl solution, adjusted to a turbidity of 1, and were exposed to 20, 26, or 40 μg/mL ampicillin with 1 mM IPTG for 24 h. Cells were diluted by 10^2–10^7 via 10-fold serial dilution steps in 0.85% NaCl solution and applied as 10 μL drops on LB agar with kanamycin to determine persister cell viability (Donegan *et al.*, 1991). For isogenic mutants, cells were grown to a turbidity of 1 at 600 nm and exposed to 20 μg/mL ampicillin with 1 mM IPTG for 5 h. Two independent cultures were used for each strain for each ampicillin concentration.

6.5.7 RNA isolation and whole-transcriptome studies

For the whole-transcriptome study of BW25113 Δ*mqsR*/pBS(Kan)-*mqsR 2-1* versus BW25113 Δ*mqsR*/pBS(Kan)-*mqsR*, planktonic cells were grown to a turbidity of 0.5 at 600 nm in LB medium with 1 mM IPTG at 37 °C, adjusted the turbidity to 1, and exposed to 20 μg/mL ampicillin with 1 mM IPTG for 1 h. Cells were isolated by centrifuging at 0°C, and RNA*Later*® buffer (Applied Biosystems, Foster City, CA, USA) was added to stabilize RNA during the RNA preparation steps. Total RNA was isolated from cell pellets as described previously (Ren *et al.*, 2004a) using a bead beater (Biospec, Bartlesville, OK, USA). cDNA synthesis, fragmentation, and hybridizations to the *E. coli* GeneChip Genome 2.0 array (Affymetrix, Santa Clara, CA, USA; P/N 511302) were described previously (González Barrios *et al.*, 2006). Genes were identified as differentially expressed if the expression ratio was higher than the standard

deviation: 4.0 fold (induced and repressed) cutoff for the DNA microarrays (standard deviation 1.3 fold), and if the *p*-value for comparing two chips was less than 0.05 (Ren *et al.*, 2004c). The whole-transcriptome data have been deposited in the NCBI Gene Expression Omnibus (http://www.ncbi.nlm.nih.gov/geo/) and are accessible through accession number GSE31054.

6.5.8 qRT-PCR

To corroborate the DNA microarray data, qRT-PCR was used to quantify relative RNA concentrations using 100 ng as a template using the Power *SYBR Green RNA-to-*C_T™ 1-Step Kit (Applied Biosystems, Foster City, CA, USA). The reaction and analysis was carried out by the StepOne™ Real-Time PCR System (Applied Biosystems, Foster City, CA, USA). The housekeeping gene *rrsG* was used to normalize the gene expression data. The annealing temperature was 60°C for all the genes in this study. Primers for qRT-PCR are listed in Table 6.5.

6.5.9 Western blot analysis and SDS-PAGE

To investigate MqsR protein levels, Western blot and SDS-PAGE was performed. BL21 (DE3) strains containing pET28b, pET28a-*mqsR*, pET28a-*mqsR* K3N, pET28a-*masR* N31Y, and pET28a-*mqsR* 2-1 were grown to a turbidity of 0.2, then 1 mM ITPG was added to produce MqsR and the MqsR variants. When the turbidity reached 0.5, cells were washed with TE buffer, and protease inhibitor cocktail (Sigma-Aldrich, USA) was added to protect proteins. Samples were sonicated using a 60 Sonic Dismembrator (Fisher Scientific, Pittsburgh, PA, USA) at level 4 for 30 sec twice. Total protein was quantified using a Pierce BCA Protein Assay kit (Fisher Scientific, Pittsburgh, PA, USA). 2X SDS sample buffer was added and Protein was denatured at 95°C for 5 min. The Western blot was performed using 2.5 μg protein of each sample with primary antibodies raised against a His tag (Cell Signaling Technology, Danvers, MA, USA) and horseradish peroxidase-conjugated goat anti-mouse secondary antibodies (Millipore, Billerica, MA, USA). CL-Xposure film (Thermo Scientific, Rockford, IL USA) was used after a 30 sec

exposure. We confirmed that the same amount of total cell protein was loaded for each sample by over-exposing the Western blot for 2 min. For SDS-PAGE, 25 μg protein of each sample was loaded, and the gel was stained with Coomassie blue.

6.5.10 Oxidative and acid stress assays

Overnight cultures were diluted to a turbidity of 0.05 and grown to a turbidity of 1 at 600 nm. Cells were centrifuged and resuspended in LB and exposed to either 20 mM H_2O_2 for 10 min or pH 2.5 for 2 min.

6.5.11 Live/dead staining

The ratio of live and dead cells was quantified using a Live/Dead *Bac*Light® kit (Invitrogen). Cells were grown to a turbidity of 0.5 with 2 h induction of MqsR 2-1 and native MqsR by adding 1mM IPTG, diluted 10 times, and washed with 0.85% NaCl. Live/Dead staining dye mixture (3 μL of a 1:1 mix of Component A and B) was added to 1 mL of washed culture and incubated at room temperature in a dark room for 15 min. Stained culture (1 μL) was observed using a 40X/0.75 Plan-NEOFLUAR dry objective with an Axiovert 200 M microscope (Carl Zeiss, Berlin, Germany). A FITC filter (excitation 490 nm and emission 525 nm) was used to observe cells stained green (live cells), and a Nile Red filter (excitation 515~530 nm and emission 525~605 nm) was used to observe cells stained red (dead cells). Three images were taken for each sample to quantify the average cell size (40 cells) and percentage of dead cells (more than 300 cells).

CHAPTER VII

CONCLUSIONS AND RECOMMENDATIONS

7.1 Conclusions

We show herein that the global regulator H-NS of *E. coli* may be engineered to control three important cellular phenotypes: biofilm formation, Rac prophage excision, and cell lysis. We screened biofilm variants in the absence of endogenous Hha and H-NS and identified an H-NS variant with a single amino acid change, H-NS K57N, which reduces biofilm formation by 10-fold through its interaction with Cnu and StpA. Cnu is a Hha paralog, and StpA is a H-NS paralog, and both are nucleoid-associated proteins. Here, we also show that Cnu reduces biofilm formation like Hha. Therefore, our results imply that the altered H-NS may interact closely with Cnu and StpA to reduce biofilm reduction. The N-terminus of H-NS includes three helical segments, H1 (1-8 aa), H2 (12-19 aa), and H3 (23-47 aa) (Fang and Rimsky, 2008) and plays an important role in forming homo- or hetero-oligomers of H-NS with Hha, Cnu, and StpA. The K57N substitution of H-NS may influence oligomerization of H-NS, cause a conformational change of the flexible linker, or cause a conformational change of the C-terminus, all of which would affect the DNA binding properties of H-NS. It is interesting that only a single amino acid substitution causes such dramatic physiological changes in the cell. This study implies that evolution of global regulators may cause widespread changes in the regulatory system in bacteria.

We also show that the global transcriptional regulator Hha may be rewired to control biofilm dispersal, without affecting initial biofilm formation. In static biofilms, Hha13D6 removed 96% of the biofilm in a flow-cell, whereas wild-type Hha removed 35% of the biofilm. Hha13D6 increased biofilm dispersal by causing cell death by activating proteases; hence, we have created one of the first protein switches to control cell lysis. Biofilm dispersal by the engineered Hha

requires protease HslV since adding the *hslV* mutation reduced the dispersal activity of Hha13D6. Cell death in biofilms is an important mechanism of dispersal since it leads to the creation of voids inside the biofilm which facilitates dispersal of the surviving cells (Webb *et al.*, 2003) implying that programmed cell death is a social (altruistic) activity (Wood, 2009). Hence, induction of protease activity is a key mechanism of Hha13D6 to trigger biofilm dispersal by causing cell death and so by disrupting biofilm structure. In addition to the evolution of Hha for biofilm dispersal, we show that Hha24E9 represses biofilm formation by inducing the activity of GadW, GlpT, and PhnF. However, according to the whole-transcriptome profiles of Hha13D6 and Hha24E9, the gene regulation pathways of Hha13D6 are quite different from those of Hha24E9. This study demonstrates that genetic switches exist for both biofilm formation and dispersal and once they are discerned, as in the case of Hha (Ren *et al.*, 2004a; García-Contreras *et al.*, 2008), they may be manipulated to control bacterial activity.

We envision that biofilms will be used for diverse applications and biofilms will have to be controlled; hence, we developed a synthetic μBE system by combining a QS signaling module with two engineered biofilm dispersal proteins: Hha13D6 and BdcAE50Q. With this synthetic circuit, in a microfluidic channel, we (i) formed an initial colonizer biofilm with cells tagged red, (ii) introduced a second cell type (dispersers, tagged green) into this existing biofilm, (iii) created a means of communication between the two cell types, (iv) formed a robust biofilm with the disperser cells in an existing initial colonizer biofilm, (v) displaced the initial colonizer cells in the biofilm with a QS signal from the disperser cells, and (vi) removed the disperser cells with a chemically-induced switch. The defensive nature of the biofilm colony makes most biofilms difficult or impossible to eradicate (Kaplan, 2010); hence, our demonstration that both the initial colonizer and disperser biofilms may be nearly completely removed is highly significant. Here we show, for the first time, that a QS system may be utilized with biofilm dispersal proteins to

control consortial biofilm formation; i.e., that an existing biofilm may be formed and then replaced by another biofilm which then may be removed. These types of synthetic QS circuits may be used to pattern biofilms by facilitating the re-use of platforms and to create sophisticated reactor systems that will be used to form bio-refineries.

We demonstrate that toxin MqsR may be engineered for enhanced toxicity and that this increased toxicity leads to increased persister cell formation. The increase in persistence resulted from a reduction in transcripts for the stress response cascades including acid resistance, multidrug resistance, and osmotic resistance systems all regulated by RpoS, as shown in whole-transcriptome results and by the dramatic increase in persistence upon deleting *gadB, gadX*, *mdtF, osmY,* and *rpoS*. Hence, we identified part of the genetic basis of persister cell formation by using the tools of protein engineering and systems biology. This is the first report that differential degradation of *rpoS* transcripts leads to persister cell formation by down-regulating stress responsive genes. In terms of persistence, it may be better for cells to have less fitness (more sensitive to stress which likely activates toxins) for environmental stress. We show that toxicity may increase persister cell formation and that cells may enter non-metabolizing state through the repression of stress resistance modules, which provides critical insights to develop strategies for combating persister cells.

7.2 Recommendations

Global regulators are important for virulence in pathogenic *E. coli* (Mellies *et al.*, 2007). H-NS represses virulence genes in enterohemorrhagic *E. coli* (EHEC) (Mellies *et al.*, 2007), and several virulence genes are located in prophages; for example, Shiga toxin 1 (*stx1*) and 2 (*stx2*) genes are in cryptic prophage CP-933V and bacteriophage BP-933W in *E. coli* O157:H7 EDL933, respectively (Perna *et al.*, 2001). CP-933R in O157:H7 EDL933, Sp10 in O157 Sakai,

and Rac in K-12 are located at identical positions in the three genomes and have identical attachment sites (Casjens, 2003). Our preliminary data show that transcription of virulence genes, *stx1A* in CP-933V, *stx2A* in BP-933W, and *espB* in the pathogenicity locus of enterocyte effacement (LEE), are repressed up to 8-fold by producing wild-type H-NS, while *stx1A* is induced by producing H-NS K57N in EHEC. These results indicate that H-NS and the evolved H-NS influence expression of virulence genes in EHEC. Since wild-type H-NS represses the excision of Rac prophage and H-NS K57N increases excision, it is possible that H-NS may affect virulence by controlling prophage excision in EHEC and that the evolved H-NS may further repress virulence factors in pathogenic *E. coli*.

Hha also represses LEE set of operons in EHEC by repressing transcription of *ler* which encodes the activator of LEE (Sharma *et al.,* 2005). EHEC infections cause 73,000 illnesses annually in the United states, which leads to over 2,000 hospitalizations and 60 deaths, and the economic costs of the illnesses are $405 million (Frenzen *et al.*, 2005). Hence, Hha may be engineered to disperse EHEC as well as to repress LEE to control EHEC infections. Also, utilizing an animal model such as *Caenorhabditis elegans* for testing virulence of EHEC (Anyanful *et al.*, 2005) with the engineered Hha will be a promising approach corroborating to measure transcription level of virulence genes.

We have demonstrated that a synthetic QS circuit utilizing biofilm dispersal proteins may be used to displace an existing biofilm as well as remove the second biofilm. Several biofilm dispersal signals have been identified including the auto-inducing peptide of the *agr* QS system of *Staphylococcus aureus* (Boles and Horswill, 2008), changes in carbon sources (Sauer *et al.*, 2004), reduction in the concentration of c-di-GMP (Ma *et al.,* 2011) (as utilized here with BdcA), surfactant (Boles *et al.,* 2005), *cis*-2-decenoic acid (Davies and Marques, 2009), and *D*-amino acids (Kolodkin-Gal *et al.,* 2010). Hence, other biofilm dispersal mechanisms may be

utilized to construct additional synthetic circuits for controlling biofilms. Controlling biofilms by engineering genetic circuits of cells may be utilized to produce bioenergy such as bio-ethanol and bio-diesel and to create bio-refineries by allowing sophisticated biofilm reactor systems (Wood *et al.*, 2011).

Persister frequency is no more than 1% at stationary-phase cultures (Lewis, 2007), but we have determined a new mechanism for increasing persistence by using knockout strains of stress resistance genes (e.g., *rpoS* mutant increases persistence up to 80%) and by pre-exposing cells to stresses prior to antibiotic treatment. Isolating persister cells may be achieved far easier than in previous efforts where persister cells were isolated using a flow cytometer with a GFP-tagged *E. coli*; dormant cells are dim where active cells glow green (Shah *et al.*, 2006). Therefore, using our new tool for increasing persistence, further studies for persisters will be facilitated for whole-transcriptome profiles determining what proteins are involved during persistence and what proteins are required to wake these sleeping cells and for screening alternative drug candidates to eradicate persisters. In addition, RpoS regulates virulence factors as well as the stress responses in several Gram-negative bacteria including *P. aeruginosa* (Suh *et al.*, 1999), Hence the importance of *rpoS* in persister formation should be investigated in other strains which cause chronic infections.

REFERENCES

Adam, M., Murali, B., Glenn, N., and Potter, S. (2008) Epigenetic inheritance based evolution of antibiotic resistance in bacteria. *BMC Evol Biol* **8**: 1-12.

Adnan, M., Morton, G., Singh, J., and Hadi, S. (2010) Contribution of *rpoS* and *bolA* genes in biofilm formation in *Escherichia coli* K-12 MG1655. *Mol Cell Biochem* **342**: 207-213.

Amitai, S., Kolodkin-Gal, I., Hananya-Meltabashi, M., Sacher, A., and Engelberg-Kulka, H. (2009) *Escherichia coli* MazF leads to the simultaneous selective synthesis of both "death proteins" and "survival proteins". *PLoS Genet* **5**: e1000390.

Anyanful, A., Dolan-Livengood, J.M., Lewis, T., Sheth, S., DeZalia, M.N., Sherman, M.A. *et al.* (2005) Paralysis and killing of *Caenorhabditis elegans* by enteropathogenic *Escherichia coli* requires the bacterial tryptophanase gene. *Mol Microbiol* **57**: 988-1007.

Attila, C., Ueda, A., and Wood, T.K. (2009) 5-Fluorouracil reduces biofilm formation in *Escherichia coli* K-12 through global regulator AriR as an antivirulence compound. *Appl Microbiol Biotechnol* **82**: 525-533.

Béjar, S., Cam, K., and Bouché, J.-P. (1986) Control of cell division in *Escherichia coli*. DNA sequence of *dicA* and of a second gene complementing mutation *dicA1*, *dicC*. *Nucl Acids Res* **14**: 6821-6833.

Baños, R.C., Vivero, A., Aznar, S., García, J., Pons, M., Madrid, C., and Juárez, A. (2009) Differential regulation of horizontally acquired and core genome genes by the bacterial modulator H-NS. *PLoS Genet* **5**: e1000513.

Baba, T., Ara, T., Hasegawa, M., Takai, Y., Okumura, Y., Baba, M. *et al.* (2006) Construction of *Escherichia coli* K-12 in-frame, single-gene knockout mutants: the Keio collection. *Mol Syst Biol* **2**: 2006.0008.

Bae, S.-H., Liu, D., Lim, H.M., Lee, Y., and Choi, B.-S. (2008) Structure of the nucleoid-associated protein Cnu reveals common binding sites for H-NS in Cnu and Hha. *Biochemistry* **47**: 1993-2001.

Balaban, N.Q., Merrin, J., Chait, R., Kowalik, L., and Leibler, S. (2004) Bacterial persistence as a phenotypic switch. *Science* **305**: 1622-1625.

Balagaddé, F.K., Song, H., Ozaki, J., Collins, C.H., Barnet, M., Arnold, F.H. *et al.* (2008) A synthetic *Escherichia coli* predator-prey ecosystem. *Mol Syst Biol* **4**: 187.

Bansal, T., Englert, D., Lee, J., Hegde, M., Wood, T.K., and Jayaraman, A. (2007) Differential effects of epinephrine, norepinephrine, and indole on *Escherichia coli* O157:H7 chemotaxis, colonization, and gene expression. *Infect Immun* **75**: 4597-4607.

Barber, C.E., Tang, J.L., Feng, J.X., Pan, M.Q., Wilson, T.J.G., Slater, H. *et al.* (1997) A novel regulatory system required for pathogenicity of *Xanthomonas campestris* is mediated by a small diffusible signal molecule. *Mol Microbiol* **24**: 555-566.

Bardouniotis, E., Huddleston, W., Ceri, H., and Olson, M.E. (2001) Characterization of biofilm growth and biocide susceptibility testing of *Mycobacterium phlei* using the MBEC™ assay system. *FEMS Microbiol Lett* **203**: 263-267.

Barraud, N., Hassett, D.J., Hwang, S.-H., Rice, S.A., Kjelleberg, S., and Webb, J.S. (2006) Involvement of nitric oxide in biofilm dispersal of *Pseudomonas aeruginosa*. *J Bacteriol* **188**: 7344-7353.

Barraud, N., Michael, V.S., Moore, Z.P., Webb, J.S., Rice, S.A., and Kjelleberg, S. (2009a) Nitric oxide-mediated dispersal in single- and multi-species biofilms of clinically and industrially relevant microorganisms. *Microb Biotechnol* **2**: 370-378.

Barraud, N., Schleheck, D., Klebensberger, J., Webb, J.S., Hassett, D.J., Rice, S.A., and Kjelleberg, S. (2009b) Nitric oxide signaling in *Pseudomonas aeruginosa* biofilms mediates phosphodiesterase activity, decreased cyclic di-GMP levels, and enhanced Dispersal. *J Bacteriol* **191**: 7333-7342.

Beech, I.B., and Sunner, J. (2004) Biocorrosion: towards understanding interactions between biofilms and metals. *Curr Opin Biotechnol* **15**: 181-186.

Beech, I.B., Sunner, J.A., and Hiraoka, K. (2005) Microbe–surface interactions in biofouling and biocorrosion processes. *Int Microbiol* **8**: 157-168.

Belik, A.S., Tarasova, N.N., and Khmel, I.A. (2008) Regulation of biofilm formation using *Escherichia coli* K12: effect of mutations in the genes HNS, StpA, Lon, RpoN. *Mol Gen Microbiol Virol* **23**: 159–162.

Belitsky, M., Avshalom, H., Erental, A., Yelin, I., Kumar, S., London, N. *et al.* (2011) The *Escherichia coli* extracellular death factor EDF induces the endoribonucleolytic activities of the toxins MazF and ChpBK. *Mol Cell* **41**: 625-635.

Beloin, C., Valle, J., Latour-Lambert, P., Faure, P., Kzreminski, M., Balestrino, D. *et al.* (2004) Global impact of mature biofilm lifestyle on *Escherichia coli* K-12 gene expression. *Mol Microbiol* **51**: 659-674.

Beloin, C., Roux, A., and Ghigo, J.-M. (2008) *Escherichia coli* biofilms. In *Bacterial Biofilms*. Romeo, T. (ed). Berlin: Springer-Verlag, pp. 249-289.

Bendouah, Z., Barbeau, J., Hamad, W.A., and Desrosiers, M. (2006) Biofilm formation by *Staphylococcus aureus* and *Pseudomonas aeruginosa* is associated with an unfavorable evolution after surgery for chronic sinusitis and nasal polyposis. *Otolaryngol Head Neck Surg* **134**: 991-996.

Benoit, M.R., Conant, C.G., Ionescu-Zanetti, C., Schwartz, M., and Matin, A. (2010) New device for high-throughput viability screening of flow biofilms. *Appl Environ Microbiol* **76**: 4136-4142.

Blattner, F.R., Guy Plunkett, I., Bloch, C.A., Perna, N.T., Burland, V., Riley, M. *et al.* (1997) The complete genome sequence of *Escherichia coli* K-12 *Science* **277**: 1453-1462.

Bloom, J.D., Wilke, C.O., Arnold, F.H., and Adami, C. (2004) Stability and the evolvability of function in a model protein. *Biophys J* **86**: 2758-2764.

Boles, B.R., Thoendel, M., and Singh, P.K. (2005) Rhamnolipids mediate detachment of *Pseudomonas aeruginosa* from biofilms. *Mol Microbiol* **57**: 1210-1223.

Boles, B.R., and Horswill, A.R. (2008) *agr*-mediated dispersal of *Staphylococcus aureus* biofilms. *PLoS Pathog* **4**: e1000052.

Brenner, K., Karig, D.K., Weiss, R., and Arnold, F.H. (2007) Engineered bidirectional communication mediates a consensus in a microbial biofilm consortium. *Proc Natl Acad Sci U S A* **104**: 17300-17304.

Brenner, K., You, L., and Arnold, F.H. (2008) Engineering microbial consortia: a new frontier in synthetic biology. *Trends Biotechnol* **26**: 483-489.

Brenner, K., and Arnold, F.H. (2011) Self-organization, layered structure, and aggregation enhance persistence of a synthetic biofilm consortium. *PLoS ONE* **6**: e16791.

Brown, B.L., Grigoriu, S., Kim, Y., Arruda, J.M., Davenport, A., Wood, T.K. *et al.* (2009) Three dimensional structure of the MqsR:MqsA complex: a novel toxin:antitoxin pair comprised of a toxin homologous to RelE and an antitoxin with unique properties. *PLoS Pathog* **5**: e1000706.

Canada, K.A., Iwashita, S., Shim, H., and Wood, T.K. (2002) Directed evolution of toluene *ortho*-monooxygenase for enhanced 1-naphthol synthesis and chlorinated ethene degradation. *J Bacteriol* **184**: 344-349.

Casjens, S. (2003) Prophages and bacterial genomics: what have we learned so far? *Mol Microbiol* **49**: 277-300.

Cegelski, L., Marshall, G.R., Eldridge, G.R., and Hultgren, S.J. (2008) The biology and future prospects of antivirulence therapies. *Nat Rev Micro* **6**: 17-27.

Cense, A.W., Peeters, E.A.G., Gottenbos, B., Baaijens, F.P.T., Nuijs, A.M., and van Dongen, M.E.H. (2006) Mechanical properties and failure of *Streptococcus mutans* biofilms, studied using a microindentation device. *J Microbiol Methods* **67**: 463-472.

Chant, E.L., and Summers, D.K. (2007) Indole signalling contributes to the stable maintenance of *Escherichia coli* multicopy plasmids. *Mol Microbiol* **63**: 35-43.

Charlton, T.S., De Nys, R., Netting, A., Kumar, N., Hentzer, M., Givskov, M., and Kjelleberg, S. (2000) A novel and sensitive method for the quantification of *N*-3-oxoacyl homoserine lactones using gas chromatography–mass spectrometry: application to a model bacterial biofilm. *Environ Microbiol* **2**: 530-541.

Cherepanov, P.P., and Wackernagel, W. (1995) Gene disruption in *Escherichia coli*: Tc^R and Km^R cassettes with the option of Flp-catalyzed excision of the antibiotic-resistance determinant. *Gene* **158**: 9-14.

Cho, E.H., Gumport, R.I., and Gardner, J.F. (2002) Interactions between integrase and excisionase in the phage lambda excisive nucleoprotein complex. *J Bacteriol* **184**: 5200-5203.

Choudhary, S., and Schmidt-Dannert, C. (2010) Applications of quorum sensing in biotechnology. *Appl Microbiol Biotechnol* **86**: 1267-1279.

Christensen, S.K., Maenhaut-Michel, G., Mine, N., Gottesman, S., Gerdes, K., and Van Melderen, L. (2004) Overproduction of the Lon protease triggers inhibition of translation in *Escherichia coli*: involvement of the *yefM-yoeB* toxin-antitoxin system. *Molecular Microbiology* **51**: 1705-1717.

Conter, A., Bouché, J.-P., and Dassain, M. (1996) Identification of a new inhibitor of essential division gene *ftsZ* as the *kil* gene of defective prophage Rac. *J Bacteriol* **178**: 5100-5104.

Costerton, J.W., Stewart, P.S., and Greenberg, E.P. (1999) Bacterial biofilms: a common cause of persistent infections. *Science* **284**: 1318-1322.

Dörr, T., Vulić, M., and Lewis, K. (2010) Ciprofloxacin causes persister formation by inducing the TisB toxin in *Escherichia coli*. *PLoS Biol* **8**: e1000317.

Dalai, B., Zhou, R., Wan, Y., Kang, M., Li, L., Li, T. *et al.* (2009) Histone-like protein H-NS regulates biofilm formation and virulence of *Actinobacillus pleuropneumoniae*. *Microb Pathog* **46**: 128-134.

Danino, T., Mondragón-Palomino, O., Tsimring, L., and Hasty, J. (2010) A synchronized quorum of genetic clocks. *Nature* **463**: 326-330.

Davies, D. (2003) Understanding biofilm resistance to antibacterial agents. *Nat Rev Drug Discov* **2**: 114-122.

Davies, D.G., and Marques, C.N.H. (2009) A fatty acid messenger is responsible for inducing dispersion in microbial biofilms. *J Bacteriol* **191**: 1393-1403.

De Groote, V.N., Fauvart, M., Kint, C.I., Verstraeten, N., Jans, A., Cornelis, P., and Michiels, J. (2011) *Pseudomonas aeruginosa* fosfomycin resistance mechanisms affect non-inherited fluoroquinolone tolerance. *J Med Microbiol* **60**: 329-336.

del Pozo, J.L., and Patel, R. (2007) The challenge of treating biofilm-associated bacterial infections. *Clin Pharmacol Ther* **82**: 204-209.

Dersch, P., Schmidt, K., and Bremer, E. (1993) Synthesis of the *Escherichia coli* K-12 nucleoid-associated DNA-binding protein H-NS is subjected to growth-phase control and autoregulation. *Mol Microbiol* **8**: 875-889.

Di Martino, P., Fursy, R., Bret, L., Sundararaju, B., and Phillips, R.S. (2003) Indole can act as an extracellular signal to regulate biofilm formation of *Escherichia coli* and other indole-producing bacteria. *Can J Microbiol* **49**: 443-449.

Dobretsov, S., Teplitski, M., and Paul, V. (2009) Mini-review: quorum sensing in the marine environment and its relationship to biofouling. *Biofouling* **25**: 413 - 427.

Domka, J., Lee, J., and Wood, T.K. (2006) YliH (BssR) and YceP (BssS) regulate *Escherichia coli* K-12 biofilm formation by influencing cell signaling. *Appl Environ Microbiol* **72**: 2449-2459.

Domka, J., Lee, J., Bansal, T., and Wood, T.K. (2007) Temporal gene-expression in *Escherichia coli* K-12 biofilms. *Environ Microbiol* **9**: 332-346.

Donegan, K., Matyac, C., Seidler, R., and Porteous, A. (1991) Evaluation of methods for sampling, recovery, and enumeration of bacteria applied to the phylloplane. *Appl Environ Microbiol* **57**: 51-56.

Dong, T., and Schellhorn, H. (2009) Global effect of RpoS on gene expression in pathogenic *Escherichia coli O157:H7* strain EDL933. *BMC Genomics* **10**: 349.

Donlan, R.M., and Costerton, J.W. (2002) Biofilms: survival mechanisms of clinically-relevant microorganisms. *Clin Microbiol Rev* **15**: 167-193.

Dorman, C.J. (2004) H-NS: a universal regulator for a dynamic genome. *Nat Rev Micro* **2**: 391-400.

Dow, J.M., Crossman, L., Findlay, K., He, Y.-Q., Feng, J.-X., and Tang, J.-L. (2003) Biofilm dispersal in *Xanthomonas campestris* is controlled by cell–cell signaling and is required for full virulence to plants. *Proc Natl Acad Sci U S A* **100**: 10995-11000.

Ensley, B.D., Ratzkin, B.J., Osslund, T.D., Simon, M.J., Wackett, L.P., and Gibson, D.T. (1983) Expression of Naphthalene Oxidation Genes in *Escherichia coli* Results in the Biosynthesis of Indigo. *Science* **222**: 167-169.

Erickson, D.L., Endersby, R., Kirkham, A., Stuber, K., Vollman, D.D., Rabin, H.R. *et al.* (2002) *Pseudomonas aeruginosa* quorum-sensing systems may control virulence factor expression in the lungs of patients with cystic fibrosis. *Infect Immun* **70**: 1783-1790.

Fang, F.C., and Rimsky, S. (2008) New insights into transcriptional regulation by H-NS. *Curr Opin Microbiol* **11**: 113-120.

Faubladier, M., and Bouché, J.-P. (1994) Division inhibition gene *dicF* of *Escherichia coli* reveals a widespread group of prophage sequences in bacterial genomes. *J Bacteriol* **176**: 1150-1156.

Fishman, A., Tao, Y., Bentley, W., and Wood, T.K. (2004) Protein engineering of toluene 4-monooxygenase of *Pseudomonas mendocina* KR1 for synthesizing 4-nitrocatechol from nitrobenzene. *Biotechnol Bioeng* **87**: 779-790.

Fishman, A., Tao, Y., Rui, L., and Wood, T.K. (2005) Controlling the regiospecific oxidation of aromatics via active site engineering of toluene *para*-monooxygenase of *Ralstonia pickettii* PKO1. *J Biol Chem* **280**: 506-514.

Flemming, H.-C., and Wingender, J. (2010) The biofilm matrix. *Nat Rev Micro* **8**: 623-633.

Fletcher, M. (1977) The effects of culture concentration and age, time, and temperature on bacterial attachment to polystyrene. *Can J Microbiol* **23**: 1-6.

Flickinger, S.T., Copeland, M.F., Downes, E.M., Braasch, A.T., Tuson, H.H., Eun, Y.-J., and Weibel, D.B. (2011) Quorum sensing between *Pseudomonas aeruginosa* biofilms accelerates cell growth. *J Am Chem Soc* **133**: 5966–5975.

Foxman, B. (2002) Epidemiology of urinary tract infections: incidence, morbidity, and economic costs. *Am J Med* **113**: 5-13.

Frenzen, P.D., Drake, A., Angulo, F.J., and Group, T.E.I.P.F.W. (2005) Economic cost of illness fue to *Escherichia coli* O157 infections in the United States. *J Food Prot* **68**: 2623-2630.

Fu, P. (2006) A perspective of synthetic biology: assembling building blocks for novel functions. *Biotechnol J* **1**: 690-699.

Gafni, Y., Icht, M., and Rubinfeld, B.Z. (1995) Stimulation of *Agrobacterium tumefaciens* virulence with indole-3-acetic-acid. *Lett Appl Microbiol* **20**: 98-101.

García-Contreras, R., Zhang, X.-S., Kim, Y., and Wood, T.K. (2008) Protein translation and cell death: The role of rare tRNAs in biofilm formation and in activating dormant phage killer genes. *PLoS ONE* **3**: e2394.

García, J., Cordeiro, T.N., Nieto, J.M., Pons, I., Juárez, A., and Pons, M. (2005) Interaction between the bacterial nucleoid associated proteins Hha and H-NS involves a conformational change of Hha. *Biochem J* **388**: 755-762.

Gerdes, K., Bech, F.W., Jørgensen, S.T., Løbner-Olesen, A., Rasmussen, P.B., Atlung, T. *et al.* (1986) Mechanism of postsegregational killing by the *hok* gene product of the *parB* System of plasmid R1 and its homology with the RelF gene product of the *E. coli relB* operon. *EMBO J* **5**: 2023-2029.

Gerdes, K., Gultyaev, A.P., Franch, T., Pedersen, K., and Mikkelsen, N. (1997) Antisense RNA-regulated programmed cell death. *Annual Review of Genetics* **31**: 1-31.

Godessart, N., Munoa, F.J., Regue, M., and Juaerez, A. (1988) Chromosomal mutations that increase the production of a plasmid-encoded haemolysin in *Escherichia coli*. *J Gen Microbiol* **134**: 2779-2787.

González Barrios, A.F., Zuo, R., Y. Hashimoto, Yang, L., Bentley, W.E., and Wood, T.K. (2006) Autoinducer 2 controls biofilm formation in *Escherichia coli* through a novel motility quorum-sensing regulator (MqsR, B3022). *J Bacteriol* **188**: 305-306.

Hansen, M.C., Palmer, R.J., Jr, Udsen, C., White, D.C., and Molin, S. (2001) Assessment of GFP fluorescence in cells of *Streptococcus gordonii* under conditions of low pH and low oxygen concentration. *Microbiology* **147**: 1383-1391.

Hansen, S., Lewis, K., and Vulić, M. (2008) Role of global regulators and nucleotide metabolism in antibiotic tolerance in *Escherichia coli*. *Antimicrob Agents Chemother* **52**: 2718-2726.

Hengge-Aronis, R. (1996) Back to log phase: sigma S as a global regulator in the osmotic control of gene expression in Escherichia coli. *Mol Microbiol* **21**: 887-893.

Hengge, R. (2009) Principles of c-di-GMP signalling in bacteria. *Nat Rev Microbiol* **7**: 263-273.

Hentzer, M., Wu, H., Anderson, J.B., Riedel, K., Rasmussen, T.B., Bagge, N. *et al.* (2003) Attenuation of *Pseudomonas aeruginosa* biofilm virulence by quorum sensing inhibitors. *EMBO J* **22**: 3803-3815.

Herzberg, M., Kaye, I.K., Peti, W., and Wood, T.K. (2006) YdgG (TqsA) controls biofilm formation in *Escherichia coli* K-12 by enhancing autoinducer 2 transport. *J Bacteriol* **188**: 587-598.

Heydorn, A., Nielsen, A.T., Hentzer, M., Sternberg, C., Givskov, M., Ersbøll, B.K., and Molin, S. (2000) Quantification of biofilm structures by the novel computer program COMSTAT. *Microbiology* **146**: 2395-2407.

Hommais, F., Krin, E., Laurent-Winter, C., Soutourina, O., Malpertuy, A., Caer, J.-P.L. *et al.* (2001) Large-scale monitoring of pleiotropic regulation of gene expression by the prokaryotic nucleoid-associated protein, H-NS. *Mol Microbiol* **40**: 20-36.

Hong, S.H., Lee, J., and Wood, T.K. (2010a) Engineering global regulator Hha of *Escherichia coli* to control biofilm dispersal. *Microb Biotechnol* **3**: 717-728.

Hong, S.H., Wang, X., and Wood, T.K. (2010b) Controlling biofilm formation, prophage excision, and cell death by rewiring global regulator H-NS of *Escherichia coli*. *Microb Biotechnol* **3**: 344-356.

Hooshangi, S., and Bentley, W.E. (2008) From unicellular properties to multicellular behavior: bacteria quorum sensing circuitry and applications. *Curr Opin Biotechnol* **19**: 550-555.

Hu, Y., and Coates, A.R.M. (2005) Transposon mutagenesis identifies genes which control antimicrobial drug tolerance in stationary-phase *Escherichia coli*. *FEMS Microbiol Lett* **243**: 117-124.

Itoh, Y., Wang, X., Hinnebusch, B.J., Preston, J.F., III, and Romeo, T. (2005) Depolymerization of β-1,6-N-acetyl-D-glucosamine disrupts the integrity of diverse bacterial biofilms. *J Bacteriol* **187**: 382-387.

Jain, R., and Chan, M.K. (2007) Support for a potential role of *E. coli* oligopeptidase A in protein degradation. *Biochem Biophys Res Commun* **359**: 486-490.

Jayaraman, A., Mansfeld, F.B., and Wood, T.K. (1999) Inhibiting sulfate-reducing bacteria in biofilms by expressing the antimicrobial peptides indolicidin and bactenecin. *J Ind Microbiol Biotechnol* **22**: 167-175.

Jayaraman, A., and Wood, T.K. (2008) Bacterial quorum sensing: signals, circuits, and implications for biofilms and disease. *Annu Rev Biomed Eng* **10**: 145-167.

Johansson, J., and Uhlin, B.E. (1999) Differential protease-mediated turnover of H-NS and StpA revealed by a mutation altering protein stability and stationary-phase survival of *Escherichia coli*. *Proc Natl Acad Sci U S A* **96**: 10776-10781.

Jones, M.B., Jani, R., Ren, D., Wood, T.K., and Blaser, M.J. (2005) Inhibition of *Bacillus anthracis* growth and virulence gene expression by inhibitors of quorum-sensing. *J Infect Dis* **191**: 1881-1888.

Kambam, P.K.R., Henson, M.A., and Sun, L. (2008) Design and mathematical modelling of a synthetic symbiotic ecosystem. *IET Syst Biol* **2**: 33-38.

Kaplan, J.B. (2010) Biofilm dispersal: mechanisms, clinical implications, and potential therapeutic uses. *J Dent Res* **89**: 205-218.

Karatan, E., and Watnick, P. (2009) Signals, regulatory networks, and materials that build and break bacterial biofilms. *Microbiol Mol Biol Rev* **73**: 310-347.

Keren, I., Shah, D., Spoering, A., Kaldalu, N., and Lewis, K. (2004) Specialized persister cells and the mechanism of multidrug tolerance in *Escherichia coli*. *J Bacteriol* **186**: 8172-8180.

Kim, C., Kim, J., Park, H.-Y., Park, H.-J., Lee, J., Kim, C., and Yoon, J. (2008) Furanone derivatives as quorum-sensing antagonists of *Pseudomonas aeruginosa*. *Appl Microbiol Biotechnol* **80**: 37-47.

Kim, J., Hegde, M., and Jayaraman, A. (2010a) Co-culture of epithelial cells and bacteria for investigating host-pathogen interactions. *Lab Chip* **10**: 43-50.

Kim, M.S., Bae, S.-H., Yun, S.H., Lee, H.J., Ji, S.C., Lee, J.H. *et al.* (2005) Cnu, a novel *oriC*-binding protein of *Escherichia coli*. *J Bacteriol* **187**: 6998-7008.

Kim, Y., Wang, X., Ma, Q., Zhang, X.-S., and Wood, T.K. (2009) Toxin-antitoxin systems in *Escherichia coli* influence biofilm formation through YjgK (TabA) and fimbriae. *J Bacteriol* **191**: 1258-1267.

Kim, Y., Wang, X., Zhang, X.-S., Grigoriu, S., Page, R., Peti, W., and Wood, T.K. (2010b) *Escherichia coli* toxin/antitoxin pair MqsR/MqsA regulate toxin CspD. *Environ Microbiol* **12**: 1105-1121.

Kim, Y., and Wood, T.K. (2010) Toxins Hha and CspD and small RNA regulator Hfq are involved in persister cell formation through MqsR in *Escherichia coli*. *Biochem Biophys Res Commun* **391**: 209-213.

Kitagawa, M., Ara, T., Arifuzzaman, M., Ioka-Nakamichi, T., Inamoto, E., Toyonaga, H., and Mori, H. (2005) Complete set of ORF clones of *Escherichia coli* ASKA library (a complete set of *E. coli* K-12 ORF archive): unique resources for biological research. *DNA Res* **12**: 291-299.

Kobayashi, H., Kærn, M., Araki, M., Chung, K., Gardner, T.S., Cantor, C.R., and Collins, J.J. (2004) Programmable cells: interfacing natural and engineered gene networks. *Proc Natl Acad Sci U S A* **101**: 8414-8419

Kohanski, M.A., Dwyer, D.J., Hayete, B., Lawrence, C.A., and Collins, J.J. (2007) A common mechanism of cellular death induced by bactericidal antibiotics. *Cell* **130**: 797 - 810.

Kohanski, M.A., Dwyer, D.J., and Collins, J.J. (2010) How antibiotics kill bacteria: from targets to networks. *Nat Rev Micro* **8**: 423-435.

Kolodkin-Gal, I., Romero, D., Cao, S., Clardy, J., Kolter, R., and Losick, R. (2010) D-amino acids trigger biofilm disassembly. *Science* **328**: 627-629.

Kubota, H., Senda, S., Nomura, N., Tokuda, H., and Uchiyama, H. (2008) Biofilm formation by lactic acid bacteria and resistance to environmental stress. *J Biosci Bioeng* **106**: 381-386.

Lam, H., Oh, D.-C., Cava, F., Takacs, C.N., Clardy, J., de Pedro, M.A., and Waldor, M.K. (2009) *D*-amino acids govern stationary phase cell wall remodeling in bacteria. *Science* **325**: 1552-1555.

Lee, J.-H., Kaplan, J., and Lee, W. (2008a) Microfluidic devices for studying growth and detachment of *Staphylococcus epidermidis* biofilms. *Biomed Microdevices* **10**: 489-498.

Lee, J., Bansal, T., Jayaraman, A., Bentley, W.E., and Wood, T.K. (2007a) Enterohemorrhagic *Escherichia coli* biofilms are inhibited by 7-hydroxyindole and stimulated by isatin. *Appl Environ Microbiol* **73**: 4100-4109.

Lee, J., Jayaraman, A., and Wood, T.K. (2007b) Indole is an inter-species biofilm signal mediated by SdiA. *BMC Microbiol* **7**: 42.

Lee, J., Page, R., García-Contreras, R., Palermino, J.-M., Zhang, X.-S., Doshi, O. *et al.* (2007c) Structure and function of the *Escherichia coli* protein YmgB: a protein critical for biofilm formation and acid resistance. *J Mol Biol* **373**: 11-26.

Lee, J., Zhang, X.-S., Hegde, M., Bentley, W.E., Jayaraman, A., and Wood, T.K. (2008b) Indole cell signaling occurs primarily at low temperatures in *Escherichia coli*. *ISME J* **2**: 1007-1023.

Lee, J., Attila, C., Cirillo, S.L., Cirillo, J.D., and Wood, T.K. (2009a) Indole and 7-hydoxyindole diminish *Pseudomonas aeruginosa* virulence. *Microb Biotechnol* **2**: 75-90.

Lee, J., Maeda, T., Hong, S.H., and Wood, T.K. (2009b) Reconfiguring the quorum-sensing regulator SdiA of *Escherichia coli* to control biofilm formation via indole and *N*-acylhomoserine lactones. *Appl Environ Microbiol* **75**: 1703-1716.

Lee, J.W., Park, E., Bang, O., Eom, S.-H., Cheong, G.-W., Chung, C.H., and Seol, J.H. (2007d) Nucleotide triphosphates inhibit the degradation of unfolded proteins by HslV peptidase. *Mol Cells* **23**: 252-257.

Leonard, P.G., Ono, S., Gor, J., Perkins, S.J., and Ladbury, J.E. (2009) Investigation of the self-association and hetero-association interactions of H-NS and StpA from *Enterobacteria*. *Mol Microbiol* **73**: 165-179.

Leplae, R., Geeraerts, D., Hallez, R., Guglielmini, J., Drèze, P., and Van Melderen, L. (2011) Diversity of bacterial type II toxin–antitoxin systems: a comprehensive search and functional analysis of novel families. *Nucleic Acids Res* **39**: 5513-5525.

Lesic, B., Lépine, F., Déziel, E., Zhang, J., Zhang, Q., Padfield, K. *et al.* (2007) Inhibitors of pathogen intercellular signals as selective anti-infective compounds. *PLoS Pathog* **3**: 1229-1239.

Leungsakul, T., Johnson, G.R., and Wood, T.K. (2006) Protein engineering of the 4-methyl-5-nitrocatechol monooxygenase from *Burkholderia* sp. strain DNT for enhanced degradation of nitroaromatics. *Appl Environ Microbiol* **72**: 3933-3939.

Lewis, K. (2007) Persister cells, dormancy and infectious disease. *Nat Rev Micro* **5**: 48-56.

Lewis, K. (2008) Multidrug tolerance of biofilms and persister cells. In *Bacterial Biofilms*. Romeo, T. (ed). Berlin: Springer-Verlag, pp. 107-131.

Lewis, K. (2010) Persister cells. *Annu Rev Microbiol* **64**: 357-372.

Liberati, N.T., Urbach, J.M., Miyata, S., Lee, D.G., Drenkard, E., Wu, G. *et al.* (2006) An ordered, nonredundant library of *Pseudomonas aeruginosa* strain PA14 transposon insertion mutants. *Proc Natl Acad Sci U S A* **103**: 2833-2838.

Lindsey, D.F., Mullin, D.A., and Walker, J.R. (1989) Characterization of the cryptic lambdoid prophage DLP12 of *Escherichia coli* and overlap of the DLP12 integrase gene with the tRNA gene *argU*. *J Bacteriol* **171**: 6197-6205.

Longley, D.B., Harkin, D.P., and Johnston, P.G. (2003) 5-Fluorouracil: mechanisms of action and clinical strategies. *Nat Rev Cancer* **3**: 330-338.

Lu, T.K., and Collins, J.J. (2007) Dispersing biofilms with engineered enzymatic bacteriophage. *Proc Natl Acad Sci U S A* **104** 11197-11202.

Luidalepp, H., Jõers, A., Kaldalu, N., and Tenson, T. (2011) Age of inoculum strongly influences persister frequency and can mask effects of mutations implicated in altered persistence. *J Bacteriol* **193**: 3598-3605.

Ma, Q., and Wood, T.K. (2009) OmpA influences *Escherichia coli* biofilm formation by repressing cellulose production through the CpxAR two-component system. *Environ Microbiol* **11**: 2735-2746.

Ma, Q., Yang, Z., Pu, M., Peti, W., and Wood, T.K. (2011) Engineering a novel c-di-GMP-binding protein for biofilm dispersal. *Environ Microbiol* **13**: 631-642.

Madrid, C., Nieto, J.M., Paytubi, S., Falconi, M., Gualerzi, C.O., and Juarez, A. (2002) Temperature- and H-NS-dependent regulation of a plasmid-encoded virulence operon expressing *Escherichia coli* hemolysin. *J Bacteriol* **184**: 5058-5066.

Madrid, C., Balsalobre, C., García, J., and Juárez, A. (2007) The novel Hha/YmoA family of nucleoid-associated proteins: use of structural mimicry to modulate the activity of the H-NS family of proteins. *Mol Microbiol* **63**: 7-14.

Maeda, T., Sanchez-Torres, V., and Wood, T.K. (2008) Metabolic engineering to enhance bacterial hydrogen production. *Microb Biotechnol* **1**: 30-39.

Magnuson, R.D. (2007) Hypothetical functions of toxin-antitoxin systems. *J Bacteriol* **189**: 6089-6092.

Mai-Prochnow, A., Webb, J.S., Ferrari, B.C., and Kjelleberg, S. (2006) Ecological advantages of autolysis during the development and dispersal of *Pseudoalteromonas tunicata* biofilms. *Appl Environ Microbiol* **72**: 5414-5420.

Maisonneuve, E., Shakespeare, L.J., Jørgensen, M.G., and Gerdes, K. (2011) Bacterial persistence by RNA endonucleases. *Proc Natl Acad Sci U S A* **108**: 13206-13211.

Manefield, M., Harris, L., Rice, S.A., de Nys, R., and Kjelleberg, S. (2000) Inhibition of luminescence and virulence in the black tiger prawn (*Penaeus monodon*) pathogen *Vibrio harveyi* by intercellular signal antagonists. *Appl Environ Microbiol* **66**: 2079-2084.

Mellies, J.L., Barron, A.M.S., and Carmona, A.M. (2007) Enteropathogenic and enterohemorrhagic *Escherichia coli* virulence gene regulation. *Infect Immun* **75**: 4199-4210.

Mendez-Ortiz, M.M., Hyodo, M., Hayakawa, Y., and Membrillo-Hernandez, J. (2006) Genome-wide transcriptional profile of *Escherichia coli* in response to high levels of the second messenger 3',5'-cyclic diguanylic acid. *J Biol Chem* **281**: 8090-8099.

Mogk, A., Deuerling, E., Vorderwülbecke, S., Vierling, E., and Bukau, B. (2003) Small heat shock proteins, ClpB and the DnaK system form a functional triad in reversing protein aggregation. *Mol Microbiol* **50**: 585-595.

Mogk, A., Haslberger, T., Tessarz, P., and Bukau, B. (2008) Common and specific mechanisms of AAA+ proteins involved in protein quality control. *Biochem Soc Trans* **036**: 120-125.

Nathan, C. (2003) Specificity of a third kind: reactive oxygen and nitrogen intermediates in cell signaling. *J Clin Invest* **111**: 769-778.

Navarre, W.W., McClelland, M., Libby, S.J., and Fang, F.C. (2007) Silencing of xenogeneic DNA by H-NS—facilitation of lateral gene transfer in bacteria by a defense system that recognizes foreign DNA. *Genes Dev* **21**: 1456-1471.

Ng, W.-L., and Bassler, B.L. (2009) Bacterial quorum-sensing network architectures. *Ann Rev Genet* **43**: 197-222.

Nishino, K., and Yamaguchi, A. (2001) Analysis of a complete library of putative drug transporter genes in *Escherichia coli*. *J Bacteriol* **183**: 5803-5812.

Nishino, K., Senda, Y., and Yamaguchi, A. (2008) The AraC-family regulator GadX enhances multidrug resistance in *Escherichia coli* by activating expression of *mdtEF* multidrug efflux genes. *J Infect Chemother* **14**: 23-29.

Nys, R., Givskov, M., Kumar, N., Kjelleberg, S., and Steinberg, P.D. (2006) Furanones. In *Antifouling Compounds*. Fusetani, N., and Clare, A.S. (eds). Berlin: Springer, pp. 55-86.

Oshima, T., Ishikawa, S., Kurokawa, K., Aiba, H., and Ogasawara, N. (2006) *Escherichia coli* histone-like protein H-NS preferentially binds to horizontally acquired DNA in association with RNA polymerase. *DNA Res* **13**: 141-153.

Otten, L.G., and Quax, W.J. (2005) Directed evolution: selecting today's biocatalysts. *Biomol Eng* **22**: 1-9.

Paytubi, S., Madrid, C., Forns, N., Nieto, J.M., Balsalobre, C., Uhlin, B.E., and Juárez, A. (2004) YdgT, the Hha paralogue in *Esherichia coli*, forms heteromeric complexes with H-NS and StpA. *Mol Microbiol* **54**: 251-263.

Pearson, J.P., Gray, K.M., Passador, L., Tucker, K.D., Eberhard, A., Iglewski, B.H., and Greenberg, E.P. (1994) Structure of the autoinducer required for expression of *Pseudomonas aeruginosa* virulence genes. *Proc Natl Acad Sci U S A* **91**: 197-201.

Pearson, J.P., Van Delden, C., and Iglewski, B.H. (1999) Active efflux and diffusion are involved in transport of *Pseudomonas aeruginosa* cell-to-cell signals. *J Bacteriol* **181**: 1203-1210.

Pedersen, K., and Gerdes, K. (1999) Multiple *hok* genes on the chromosome of *Escherichia coli*. *Mol Microbiol* **32**: 1090-1102.

Perna, N.T., Plunkett, G., Burland, V., Mau, B., Glasner, J.D., Rose, D.J. *et al.* (2001) Genome sequence of enterohaemorrhagic *Escherichia coli* O157: H7. *Nature* **409**: 529-533.

Pesci, E.C., Pearson, J.P., Seed, P.C., and Iglewski, B.H. (1997) Regulation of *las* and *rhl* quorum sensing in *Pseudomonas aeruginosa*. *J Bacteriol* **179**: 3127–3132.

Pfaffl, M.W. (2001) A new mathematical model for relative quantification in real-time RT-PCR. *Nucleic Acids Res* **29**: e45.

Prüß, B.M., Besemann, C., Denton, A., and Wolfe, A.J. (2006) A complex transcription network controls the early stages of biofilm development by *Escherichia coli*. *J Bacteriol* **188**: 3731-3739.

Pratt, L.A., and Kolter, R. (1998) Genetic analysis of *Escherichia coli* biofilm formation: roles of flagella, motility, chemotaxis and type I pili. *Mol Microbiol* **30**: 285-293.

Purnick, P.E.M., and Weiss, R. (2009) The second wave of synthetic biology: from modules to systems. *Nat Rev Mol Cell Biol* **10**: 410-422.

Ramage, H.R., Connolly, L.E., and Cox, J.S. (2009) Comprehensive functional analysis of *Mycobacterium tuberculosis* toxin-antitoxin systems: implications for pathogenesis, stress responses, and evolution. *PLoS Genet* **5**: e1000767.

Rasmussen, T.B., Manefield, M., Andersen, J.B., Eberl, L., Anthoni, U., Christophersen, C. *et al.* (2000) How *Delisea pulchra* furanones affect quorum sensing and swarming motility in *Serratia liquefaciens* MG1. *Microbiology* **146**: 3237-3244.

Rasouly, A., and Ron, E.Z. (2009) Interplay between the heat shock response and translation in *Escherichia coli*. *Res Microbiol* **160**: 288-296.

Ren, D., Bedzyk, L.A., Thomas, S.M., Ye, R.W., and Wood, T.K. (2004a) Gene expression in *Escherichia coli* biofilms. *Appl Microbiol Biotechnol* **64**: 515-524.

Ren, D., Bedzyk, L.A., Ye, R.W., Thomas, S.M., and Wood, T.K. (2004b) Differential gene expression shows natural brominated furanones interfere with the autoinducer-2 bacterial signalling system of *Escherichia coli*. *Biotech Bioeng* **88**: 630 - 642.

Ren, D., Bedzyk, L.A., Ye, R.W., Thomas, S.M., and Wood, T.K. (2004c) Differential gene expression shows natural brominated furanones interfere with the autoinducer-2 bacterial signaling system of *Escherichia coli*. *Biotechnol Bioeng* **88**: 630-642.

Ren, D., and Wood, T.K. (2005) Quorum-sensing antagonist (*5Z*)-4-bromo-5-(bromomethylene)-3-butyl-2(*5H*)-furanone influences siderophore biosynthesis in *Pseudomonas putida* and *Pseudomonas aeruginosa*. *Appl Microbiol Biotechnol* **66**: 689-695.

Rimsky, S. (2004) Structure of the histone-like protein H-NS and its role in regulation and genome superstructure. *Curr Opin Microbiol* **7**: 109-114.

Robertson, G.T., Doyle, T.B., Du, Q., Duncan, L., Mdluli, K.E., and Lynch, A.S. (2007) A Novel indole compound that inhibits *Pseudomonas aeruginosa* growth by targeting MreB is a substrate for MexAB-OprM. *J Bacteriol* **189**: 6870-6881.

Rodríguez, S., Nieto, J.M., Madrid, C., and Juárez, A. (2005) Functional replacement of the oligomerization domain of H-NS by the Hha protein of *Escherichia coli*. *J Bacteriol* **187**: 5452-5459.

Rui, L., Kwon, Y.-M., Fishman, A., Reardon, K.F., and Wood, T.K. (2004) Saturation mutagenesis of toluene *ortho*-monooxygenase of *Burkholderia cepacia* G4 for enhanced 1-naphthol synthesis and chloroform degradation. *Appl Environ Microbiol* **70**: 3246-3252.

Rui, L., Reardon, K.F., and Wood, T.K. (2005) Protein engineering of toluene *ortho*-monooxygenase of *Burkholderia cepacia* G4 for regiospecific hydroxylation of indole to form various indigoid compounds. *Appl Microbiol Biotechnol* **66**: 422-429.

Ryan, R.P., and Dow, J.M. (2008) Diffusible signals and interspecies communication in bacteria. *Microbiology* **154**: 1845-1858.

Sambrook, J., Fritsch, E.F., and Maniatis, T. (1989) *Molecular Cloning, A Laboratory Manual*. Cold Spring Harbor, NY: Cold Spring Harbor Laboratory Press.

Sauer, K., Cullen, M.C., Rickard, A.H., Zeef, L.A.H., Davies, D.G., and Gilbert, P. (2004) Characterization of nutrient-induced dispersion in *Pseudomonas aeruginosa* PAO1 biofilm. *J Bacteriol* **186**: 7312-7326.

Sauer, K., Rickard, A.H., and Davies, D.G. (2007) Biofilms and biocomplexity. *Microbe* **2**: 347-353.

Sayed, A.K., Odom, C., and Foster, J.W. (2007) The *Escherichia coli* AraC-family regulators GadX and GadW activate *gadE*, the central activator of glutamate-dependent acid resistance. *Microbiology* **153**: 2584-2592.

Schembri, M.A., Kjærgaard, K., and Klemm, P. (2003) Global gene expression in *Escherichia coli* biofilms. *Mol Microbiol* **48**: 253-267.

Schmidt, R., Bukau, B., and Mogk, A. (2009) Principles of general and regulatory proteolysis by AAA+ proteases in *Escherichia coli*. *Res Microbiol* **160**: 629-636.

Schwede, T., Kopp, J., Guex, N., and Peitsch, M.C. (2003) SWISS-MODEL: an automated protein homology-modeling server. *Nucl Acids Res* **31**: 3381-3385.

Seed, P., Passador, L., and Iglewski, B. (1995) Activation of the *Pseudomonas aeruginosa lasI* gene by LasR and the *Pseudomonas* autoinducer PAI: an autoinduction regulatory hierarchy. *J Bacteriol* **177**: 654-659.

Shah, D., Zhang, Z., Khodursky, A., Kaldalu, N., Kurg, K., and Lewis, K. (2006) Persisters: a distinct physiological state of *E. coli*. *BMC Microbiol* **6**: 53.

Sharma, V.K., Carlson, S.A., and Casey, T.A. (2005) Hyperadherence of an *hha* mutant of *Escherichia coli* O157:H7 is correlated with enhanced expression of LEE-encoded adherence genes. *FEMS Microbiol Lett* **243**: 189-196.

Shen, D.K., Filopon, D., Chaker, H., Boullanger, S., Derouazi, M., Polack, B., and Toussaint, B. (2008) High-cell-density regulation of the *Pseudomonas aeruginosa* type III secretion system: implications for tryptophan catabolites. *Microbiology* **154**: 2195-2208.

Singh, R., Paul, D., and Jain, R.K. (2006) Biofilms: implications in bioremediation. *Trends Microbiol* **14**: 389-397.

Smith, P.A., and Romesberg, F.E. (2007) Combating bacteria and drug resistance by inhibiting mechanisms of persistence and adaptation. *Nat Chem Biol* **3**: 549-556.

Spoering, A.L., Vulic, M., and Lewis, K. (2006) GlpD and PlsB participate in persister cell formation in *Escherichia coli*. *J Bacteriol* **188**: 5136-5144.

Srividhya, K.V., and Krishnaswamy, S. (2007) Sub classification and targeted characterization of prophage-encoded two-component cell lysis cassette. *J Biosci* **32**: 979-990.

Stamm, I., Lottspeich, F., and Plaga, W. (2005) The pyruvate kinase of *Stigmatella aurantiaca* is an indole binding protein and essential for development. *Mol Microbiol* **56**: 1386-1395.

Steinberger, R.E., Allen, A.R., Hansma, H.G., and Holden, P.A. (2002) Elongation correlates with nutrient deprivation in *Pseudomonas aeruginosa*-unsaturates biofilms. *Microb Ecol* **43**: 416-423.

Stewart, P.S., and Franklin, M.J. (2008) Physiological heterogeneity in biofilms. *Nat Rev Microbiol* **6**: 199-210.

Steyn, B., Oosthuizen, M.C., MacDonald, R., Theron, J., and Brözel, V.S. (2001) The use of glass wool as an attachment surface for studying phenotypic changes in *Pseudomonas aeruginosa* biofilms by two-dimensional electrophoresis. *Proteomics* **1**: 871-879.

Suh, S.-J., Silo-Suh, L., Woods, D.E., Hassett, D.J., West, S.E.H., and Ohman, D.E. (1999) Effect of *rpoS* mutation on the stress response and expression of virulence factors in *Pseudomonas aeruginosa*. *J Bacteriol* **181**: 3890-3897.

Tamae, C., Liu, A., Kim, K., Sitz, D., Hong, J., Becket, E. *et al.* (2008) Determination of antibiotic hypersensitivity among 4,000 single-gene-knockout mutants of *Escherichia coli*. *J Bacteriol* **190**: 5981-5988.

Tan, Q., Awano, N., and Inouye, M. (2011) YeeV is an *Escherichia coli* toxin that inhibits cell division by targeting the cytoskeleton proteins, FtsZ and MreB. *Mol Microbiol* **79**: 109-118.

Tendeng, C., and Bertin, P.N. (2003) H-NS in Gram-negative bacteria: a family of multifaceted proteins. *Trends Microbiol* **11**: 511-518.

Tomlin, K.L., Clark, S.R.D., and Ceri, H. (2004) Green and red fluorescent protein vectors for use in biofilm studies of the intrinsically resistant *Burkholderia cepacia* complex. *J Microbiol Methods* **57**: 95-106.

Tramonti, A., Visca, P., De Canio, M., Falconi, M., and De Biase, D. (2002) Functional characterization and regulation of *gadX*, a gene encoding an AraC/XylS-like transcriptional activator of the *Escherichia coli* glutamic acid decarboxylase system. *J Bacteriol* **184**: 2603-2613.

Ueda, A., and Wood, T.K. (2009) Connecting quorum sensing, c-di-GMP, Pel polysaccharide, and biofilm formation in *Pseudomonas aeruginosa* through tyrosine phosphatase TpbA (PA3885). *PLoS Pathog* **6**: e1000483.

Ueguchi, C., Kakeda, M., and Mizuno, T. (1993) Autoregulatory expression of the *Escherichia coli hns* gene encoding a nucleoid protein: H-NS functions as a repressor of its own transcription. *Mol Gen Genet* **236**: 171-178.

van Houdt, R., and Michiels, C.W. (2005) Role of bacterial cell surface structures in *Escherichia coli* biofilm formation. *Res Microbiol* **156**: 626-633.

van Houdt, R., Aertsen, A., Moons, P., Vanoirbeek, K., and Michiels, C.W. (2006) *N*-Acyl-*L*-homoserine lactone signal interception by *Escherichia coli*. *FEMS Microbiol Lett* **256**: 83-89.

Vijayakumar, S.R.V., Kirchhof, M.G., Patten, C.L., and Schellhorn, H.E. (2004) RpoS-regulated genes of *Escherichia coli* identified by random *lacZ* fusion mutagenesis. *J Bacteriol* **186**: 8499-8507.

Vilain, S., Pretorius, J.M., Theron, J., and Brozel, V.S. (2009) DNA as an adhesin: *Bacillus cereus* requires extracellular DNA to form biofilms. *Appl Environ Microbiol* **75**: 2861-2868.

Wang, L.-H., He, Y., Gao, Y., Wu, J.E., Dong, Y.-H., He, C. *et al.* (2004) A bacterial cell–cell communication signal with cross-kingdom structural analogues. *Mol Microbiol* **51**: 903-912.

Wang, X., Kim, Y., and Wood, T.K. (2009) Control and benefits of CP4-57 prophage excision in *Escherichia coli* biofilms. *ISME J* **3**: 1164-1179.

Wang, X., Kim, Y., Hong, S.H., Ma, Q., Brown, B.L., Pu, M. *et al.* (2011) Antitoxin MqsA helps mediate the bacterial general stress response. *Nat Chem Biol* **7**: 359-366.

Wang, X., and Wood, T.K. (2011) Toxin/antitoxin systems influence biofilm and persister cell formation and the general stress response. *Appl Environ Microbiol* **77**: 5577-5583.

Waterman, S.R., and Small, P.L.C. (2003) Identification of the promoter regions and σ^S-dependent regulation of the gadA and gadBC genes associated with glutamate-dependent acid resistance in Shigella flexneri. *FEMS Microbiol Lett* **225**: 155-160.

Webb, J.S., Thompson, L.S., James, S., Charlton, T., Tolker-Nielsen, T., Koch, B. *et al.* (2003) Cell death in *Pseudomonas aeruginosa* biofilm development. *J Bacteriol* **185**: 4585-4592.

White-Ziegler, C.A., and Davis, T.R. (2009) Genome-wide identification of H-NS-controlled, temperature-regulated genes in *Escherichia coli* K-12. *J Bacteriol* **191**: 1106-1110.

Williams, P., and Cámara, M. (2009) Quorum sensing and environmental adaptation in *Pseudomonas aeruginosa*: a tale of regulatory networks and multifunctional signal molecules. *Curr Opin Microbiol* **12**: 182-191.

Woo, K.M., Kim, K.I., Goldberg, A.L., Ha, D.B., and Chung, C.H. (1992) The heat-shock protein ClpB in *Escherichia coli* is a protein-activated ATPase. *J Biol Chem* **267**: 20429-20434.

Wood, T.K., and Peretti, S.W. (1991) Effect of chemically-induced, cloned-gene expression on protein synthesis in *E. coli*. *Biotechnol Bioeng* **38**: 397-412.

Wood, T.K., Barrios, A.F.G., Herzberg, M., and Lee, J. (2006) Motility influences biofilm architecture in *Escherichia coli*. *Appl Microbiol Biotechnol* **72**: 361-367.

Wood, T.K. (2008) Molecular approaches in bioremediation. *Curr Opin Biotechnol* **19**: 572-578.

Wood, T.K. (2009) Insights on *Escherichia coli* biofilm formation and inhibition from whole-transcriptome profiling. *Environ Microbiol* **11**: 1-15.

Wood, T.K., Hong, S.H., and Ma, Q. (2011) Engineering biofilm formation and dispersal. *Trends Biotechnol* **29**: 87-94.

Xavier, K.B., and Bassler, B.L. (2003) LuxS quorum sensing: more than just a numbers game. *Curr Opin Microbiol* **6**: 191 - 197.

Yamaguchi, Y., Park, J.-H., and Inouye, M. (2009) MqsR, a crucial regulator for quorum sensing and biofilm formation, is a GCU-specific mRNA interferase in *Escherichia coli*. *J Biol Chem* **284**: 28746-28753.

Yee, A., Chang, X., Pineda-Lucena, A., Wu, B., Semesi, A., Le, B. *et al.* (2002) An NMR approach to structural proteomics. *Proc Natl Acad Sci U S A* **99**: 1825-1830.

Yim, H.H., and Villarejo, M. (1992) *osmY*, a new hyperosmotically inducible gene, encodes a periplasmic protein in *Escherichia coli*. *J Bacteriol* **174**: 3637-3644.

Yoshimura, T., and Esak, N. (2003) Amino acid racemases: functions and mechanisms. *J Biosci Bioeng* **96**: 103-109.

You, L., Cox, R.S., Weiss, R., and Arnold, F.H. (2004) Programmed population control by cell-cell communication and regulated killing. *Nature* **428**: 868-871.

Zhang, A., Rimsky, S., Reaban, M.E., Buc, H., and Belfort, M. (1996) *Escherichia coli* protein analogs StpA and H-NS: regulatory loops, similar and disparate effects on nucleic acid dynamics. *EMBO J* **15**: 1340-1349.

Zhang, X.-S., García-Contreras, R., and Wood, T.K. (2007) YcfR (BhsA) influences *Escherichia coli* biofilm formation through stress response and surface hydrophobicity. *J Bacteriol* **189**: 3051-3062.

Zhang, X.-S., García-Contreras, R., and Wood, T.K. (2008) *Escherichia coli* transcription factor YncC (McbR) regulates colanic acid and biofilm formation by repressing expression of periplasmic protein YbiM (McbA). *ISME J* **2**: 615-631.

APPENDIX

RECONFIGURING THE QUORUM-SENSING REGULATOR SDIA OF *ESCHERICHIA COLI* TO CONTROL BIOFILM FORMATION VIA INDOLE AND *N*-ACYLHOMOSERINE LACTONES*

Overview

SdiA is a homolog of quorum-sensing regulators that detects *N*-acylhomoserine lactone (AHL) signals from other bacteria. *Escherichia coli* uses SdiA to reduce its biofilm formation in the presence of both AHLs and its own signal indole. Here we reconfigured SdiA (240 aa) to control biofilm formation using protein engineering. Four SdiA variants were obtained with altered biofilm formation including truncation variants SdiA1E11 (F7L, F59L, Y70C, M94K, and K153X) and SdiA14C3 (W9R, P49T, N87T, frame shift at N96, and L139X) which reduced biofilm formation by 5- to 20-fold compared to wild-type SdiA in the presence of endogenous indole. Whole-transcriptome profiling revealed that wild-type SdiA reduced biofilm formation by repressing genes related to indole synthesis and curli synthesis, compared to no SdiA, while variant SdiA1E11 induced genes related to indole synthesis compared to wild-type SdiA. These results suggested altered indole metabolism, and corroborating the DNA microarray results in regard to indole synthesis, variant SdiA1E11 produced 9-fold more indole which led to reduced swimming motility and cell density. Also, wild-type SdiA decreased curli production and *tnaA* transcription while SdiA1E11 increased *tnaA* transcription (*tnaA* encodes tryptophanase which

---

* Reprinted with permission from "Reconfiguring the quorum-sensing regulator SdiA of *Escherichia coli* to control biofilm formation via indole and *N*-acylhomoserine lactones" by Jintae Lee, Toshinari Maeda, Seok Hoon Hong, and Thomas K. Wood, 2009, *Applied and Environmental Microbiology* 75:1703-1716, Copyright 2009, American Society for Microbiology, DOI:10.1128/AEM.02081-08. S.H. Hong performed saturation mutagenesis and truncation of SdiA, biofilm assay of SdiA2D10 with various AHLs, and swimming motility assay. S.H. Hong, T. Maeda, and J. Lee performed the biofilm screening. J. Lee was responsible for the rest of the experiments.

forms indole) compared to wild-type SdiA. Hence, wild-type SdiA decreased biofilm formation by reducing curli production and motility, and SdiA1E11 reduced biofilm formation via indole. Furthermore, an AHL-sensitive variant (SdiA2D10 having four mutations at E31G, Y42F, R116H, and L165Q) increased biofilm formation 7-fold in the presence of *N*-octanoyl-*DL*-homoserine lactone and *N*-(3-oxododecatanoyl)-*L*-homoserine lactone. Therefore, SdiA can be evolved to increase or decrease biofilm formation, and biofilm formation may be controlled by altering sensors rather than signals.

Introduction

It is important to be able to control biofilms containing multiple species for engineering applications. For example, in the first engineered biofilm (a microbial consortium), we engineered a *Bacillus subtilis* biofilm to secrete the peptide antimicrobials indolicidin and bactenecin to inhibit the growth of sulfate-reducing bacteria in the biofilm (without harming the protective *B. subtilis* biofilm) and thereby decrease corrosion (Jayaraman *et al.*, 1999). We also developed the first synthetic signaling circuit to control biofilm formation and used it to control the biofilm formation of *Escherichia coli* and *Pseudomonas fluorescens* by manipulating the extracellular concentration of the signal indole (Lee *et al.*, 2007a).

To increase the toolkit for manipulating biofilm formation, we investigated here how SdiA of *E. coli* controls biofilm formation and whether this protein may be evolved to control biofilm formation through the use of extracellular signals. We chose SdiA as a tool because SdiA interacts with one of the extracellular signals produced by *E. coli*, indole (Lee *et al.*, 2007a; Lee *et al.*, 2008), as well as recognizes acylhomoserine lactones (AHLs) from other bacteria (Lindsay and Ahmer, 2005) and binds AHLs (Yao *et al.*, 2006).

SdiA of *E. coli*, named for its ability to suppress cell division inhibitors (Wang *et al.*, 1991), is a 240 amino acid protein that belongs to the LuxR family of transcriptional regulators

(Henikoff *et al.*, 1990) that induces the *ftsQAZ* locus involved in cell division (Wang *et al.*, 1991); however, its role in *E. coli* cell physiology remains enigmatic (Lindsay and Ahmer, 2005). Using SdiA, *Salmonella enterica* and *E. coli* detect the quorum-sensing signals AHLs produced from other bacteria although they do not synthesize AHLs (Lindsay and Ahmer, 2005); AHLs control social behavior like biofilm formation (Davies *et al.*, 1998) and virulence (Winson *et al.*, 1995). Also, SdiA is stabilized upon binding of AHLs (Yao *et al.*, 2006), and consists of an autoinducer-binding domain (residues 1-171) (Yao *et al.*, 2005) and a helix-turn-helix DNA binding domain (residues 197-216) (Wang *et al.*, 1991).

SdiA represses the expression of virulence factors by interacting with unknown stationary phase signals in *E. coli* O157:H7 (Kanamaru *et al.*, 2000), enhances multidrug resistance by stimulating multidrug efflux pumps in *E. coli* (Rahmati *et al.*, 2002), and increases acid-tolerance of *E. coli* upon exposure to AHLs (Van Houdt *et al.*, 2006). We found that SdiA decreases early *E. coli* biofilm formation 51-fold (Lee *et al.*, 2007a), enhances acid-resistance (Lee *et al.*, 2007a), and is required to reduce *E. coli* biofilm formation in the presence of AHLs as well as in the presence of the stationary-phase signal indole (Lee *et al.*, 2007a; Lee *et al.*, 2008). Indole is an *E. coli* quorum-sensing signal (Lee *et al.*, 2007b) that works primarily at temperatures found outside the human host (Lee *et al.*, 2008), and reduces biofilm formation (Domka *et al.*, 2006; Bansal *et al.*, 2007; Lee *et al.*, 2007b; Lee *et al.*, 2007a; Lee *et al.*, 2008). Therefore, SdiA, via direct or indirect interaction with indole and AHLs, is a key protein for intra-species and inter-species cell communication as well as for biofilm formation.

Directed evolution has been utilized to show the evolutionary pliability of the AHL response regulator LuxR of *Vibrio fischeri* by broadening its substrate range (Collins *et al.*, 2005), by increasing its sensitivity to octanoyl-*L*-homoserine lactone (Collins *et al.*, 2005), and by eliminating its response to 3-oxohexanoyl-homoserine lactone with a carbonyl substituent at the

third carbon (Collins *et al.*, 2006). Site-directed mutagenesis of the LuxR-type quorum-sensing activator TraR of *Agrobacterium tumefaciens* has been performed on the residues forming hydrogen bonds with *N*-oxooctanoyl-*L*-homoserine lactone to alter AHL specificity (Chai and Winans, 2004) and to alter AHL binding (Luo *et al.*, 2003). Also, spontaneous mutations of LasR (another LuxR family member from *Pseudomonas aeruginosa*), including a truncation mutant, cause phenotypic diversification, such as differences in colony morphology, pyocyanin and elastase production, swarming motility, and cell viability in the late stationary phase (Luján *et al.*, 2007).

Since cell communication and biofilm formation are important for bacterial survival in microbial consortia (Jayaraman and Wood, 2008), bacteria may readily evolve response regulators for enhanced fitness. We investigated here how the quorum-sensing regulator SdiA influences biofilm formation then hypothesized that SdiA may be evolved for enhanced or reduced biofilm formation in the absence or presence of cell signals such as indole and AHLs. Both indole (Wang *et al.*, 2001) and AHLs (Fuqua *et al.*, 1994) are extracellular signals so they were chosen as potential signals for reconfiguring SdiA to respond to them. Using random mutagenesis (error-prone PCR), SdiA libraries were obtained and screened for altered biofilm formation in the presence and absence of indole and two AHLs, *N*-butyryl-*DL*-homoserine lactone (C4-*DL*-HSL), and *N*-(3-oxooctanoyl)-*L*-homoserine lactone (3o-C8-*L*-HSL). After obtaining four biofilm mutants, DNA microarrays were utilized to understand the mechanism of biofilm reduction by wild-type SdiA and by the evolved SdiA variant, SdiA1E11, that was 20-fold more effective at reducing biofilm formation. In addition, site directed mutagenesis, saturation mutagenesis, double mutations, and real-time, reverse-transcription polymerase chain reaction (RT-PCR) were used to investigate the mechanism by which SdiA1E11 controls biofilm; the primary mechanism is its influence on the concentration of indole. Hence, our goals

were to discern how wild-type SdiA functions in biofilms, to control biofilm formation by evolving SdiA, and to determine how the SdiA variants function.

Materials and methods

Bacterial strains and materials.

The strains utilized are shown in Table 1. *E. coli* K-12 BW25113 and its isogenic mutants were obtained from the National of Institute of Genetics in Japan (Keio collection) (Baba *et al.*, 2006); the *sdiA* deletion in BW25113 was confirmed by DNA microarrays (Lee *et al.*, 2008). BW25113 *sdiA* was used as the host for screening plasmids containing *sdiA* alleles created via error-prone PCR (epPCR); these alleles were expressed using pCA24N-*sdiA* (Kitagawa *et al.*, 2005). The empty pCA24N plasmid does not express the green fluorescent protein (GFP) (Kitagawa *et al.*, 2005), and all the SdiA variants are not GFP fusions. All *E. coli* strains were initially streaked from −80°C glycerol stocks on Luria-Bertani (LB) agar plates (Sambrook *et al.*, 1989) containing 50 μg/mL kanamycin (for the host) and 30 μg/mL chloramphenicol (for maintaining pCA24N-*sdiA*). All experiments were performed at 30°C since SdiA (Van Houdt *et al.*, 2006) and indole (Lee *et al.*, 2008) are primarily active at this temperature in *E. coli*. SdiA was expressed using 1 mM isopropyl-β-D-thiogalactopyranoside (IPTG, Sigma, St. Louis, MO).

For cell density measurements, BW25113 *sdiA* harboring various SdiA variants was grown in LB (25 mL) containing IPTG in 250 mL flasks at 250 rpm, and the optical density was measured at 600 nm. Each experiment was performed with at least four independent cultures. The specific growth rates of each strain were determined by measuring the cell turbidity at 600 nm of two independent cultures as a function of time using turbidity values less than 0.7.

Indole was purchased from Fisher Scientific Co. (Pittsburg, PA). C4-*DL*-HSL, *N*-hexanoyl-*DL*-homoserine lactone (C6-*DL*-HSL), *N*-octanoyl-*DL*-homoserine lactone (C8-*DL*-HSL), *N*-decanoyl-*DL*-homoserine lactone (C10-*DL*-HSL), *N*-dodecanoyl-*DL*-homoserine lactone (C12-

DL-HSL), 3o-C8-*L*-HSL, and *N*-(3-oxotetradecanoyl)-*L*-homoserine lactone (3o-C14-*L*-HSL) were purchased from Sigma. *N*-butyryl-*L*-homoserine lactone (C4-*L*-HSL) and *N*-(3-oxododecanoyl)-*L*-homoserine lactone (3o-C12-*L*-HSL) were purchased from Cayman Chemical (Ann Arbor, MI). C4-*DL*-HSL, C4-*L*-HSL, C6-*DL*-HSL, and C8-*DL*-HSL were dissolved in water. Indole, 3o-C8-*L*-HSL, C10-*DL*-HSL, C12-*DL*-HSL, 3o-C12-*L*-HSL, and 3o-C14-*L*-HSL were dissolved in dimethylformamide (DMF); DMF alone was used as a control.

Error-prone PCR, saturation mutagenesis, and truncation of SdiA.

sdiA from plasmid pCA24N-*sdiA* under the control of *pT5-lac* promoter was mutated by epPCR as described previously (Fishman *et al.*, 2004) using two primers, SdiA front and SdiA reverse (Table 2). The epPCR product was cloned into pCA24N-*sdiA* using BseRI and PstI after treating the plasmid with Antarctic phosphatase (New England Biolabs, Beverly, MA). The ligation mixture was electroporated into BW25113 *sdiA* as described previously (Fishman *et al.*, 2004).

To perform saturation mutagenesis and to truncate the carboxy terminus of SdiA, site directed mutagenesis was performed using the QuikChange® XL Site-directed Mutagenesis Kit (Stratagene, La Jolla, CA). DNA primers (Table 2) were designed to substitute all possible amino acids at M94 and W95 for SdiA1E11 as a parent protein and at H28, E29, I30, E31, Y39, D40, Y41, and Y42 for SdiA2D10 as a parent protein. Also, DNA primers (Table 2) were designed to introduce a stop codon at wild-type SdiA codons R16, Q33, T53, A73, L93, A110, and L133. The resulting *sdiA* nucleotide sequences were confirmed by DNA sequencing using the ABI™ Prism BigDye Terminator Cycle Sequencing Ready Kit (PerkinElmer, Wellesley, MA).

Biofilm screening of SdiA variants.

Biofilm mutants were screened using polystyrene 96-well microtiter plates and an adapted

crystal violet assay (Pratt and Kolter, 1998). The crystal violet dye stains both the air-liquid interface and bottom liquid-solid interface biofilm, and the total biofilm formation at both interfaces was measured at 540 nm whereas cell growth was measured at 620 nm. BW25113 *sdiA* colonies expressing SdiA variants from pCA24N-*sdiA* were grown overnight in 96-well plates with 200 μL of LB at 250 rpm, the overnight cultures were diluted (1:100) in 300 μL of LB containing IPTG, and biofilm was formed for 24 h without shaking (where appropriate, 500 μM indole, 10 μM C4-*DL*-HSL, or 10 μM 3o-C8-*L*-HSL were also added). Total biofilm formation was normalized by cell growth (turbidity at 620 nm) to avoid overestimating changes due to growth effects. As controls, BW25113 *sdiA* with empty pCA24N and pCA24N-*sdiA* (wild-type *sdiA*) were used. Interesting biofilm mutants were re-analyzed by re-streaking the colonies on fresh LB plates and by performing another biofilm assay. Mutant *sdiA* alleles were sequenced with two primers, Seq primer 1 and Seq primer 2 (Table 2). Each data point was averaged from more than twelve replicate wells (six wells from two independent cultures). Protein truncations of variants SdiA1E11, SdiA14C3, and SdiA16G12 were verified using standard Laemmli discontinuous sodium dodecyl sulfate-polyacrylamide gel electrophoresis (SDS-PAGE (Sambrook *et al.*, 1989)).

Indole assay.

Extracellular and intracellular concentrations of indole were measured with reverse-phase high-performance liquid chromatography as described previously (Lee *et al.*, 2007a). BW25113 *sdiA* harboring various *sdiA* plasmids was grown in LB containing IPTG to a turbidity of 3.0 at 600 nm. The turbidity of 3.0 represents a time point when wild-type *E. coli* secretes approximately 300 μM indole. Each experiment was performed with two independent cultures.

Swimming motility and curli assays.

Swimming motility was measured as described previously (Lee *et al.*, 2007a). Exponentially

grown cells (turbidity of 1.0 at 600 nm) were used to assay motility in plates containing 1% (w/v) tryptone, 0.25% (w/v) NaCl, and 0.3% (w/v) agar. In order to test the effect of indole on motility, indole was added in the agar plate. The motility halos were measured after 20 h in the presence of IPTG. Each experiment was performed with two replicates from two independent cultures.

For curli, LB agar medium containing 20 μg/mL Congo red (Sigma), 10 μg/mL Coomassie brilliant blue (Sigma), 15 g/L agar, and IPTG was used as described previously to visualize *E. coli* curli expression after 28-h incubation at 30ºC (Reisner *et al.*, 2006). Since Congo red binds both curli and cellulose (Da Re and Ghigo, 2006), a cellulose specific assay using calcofluor (Da Re and Ghigo, 2006) was used to determine if curli or cellulose was identified by the Congo red assay. For the cellulose assay, BW25113 *adrA* was used as a negative cellulose control and BW25113 *adrA*/pCA24N-*adrA* was used as a positive cellulose control.

Total RNA isolation for DNA microarrays.

BW25113 *sdiA*/pCA24N, BW25113 *sdiA*/pCA24N-*sdiA*, and BW25113 *sdiA*/pCA24N-*sdiA1E11* were grown in 250 mL LB containing IPTG for 12 h with ten g of glass wool (Corning Glass Works, Corning, N.Y.) in 1 L Erlenmeyer shake flasks to form a robust biofilm (Ren *et al.*, 2004b). RNA was isolated from the biofilm cells as described previously using sonication and a bead beater (Ren *et al.*, 2004b).

DNA microarray analysis.

The *E. coli* GeneChip Genome 2.0 Array contains 10,208 probe sets for open reading frames, rRNA, tRNA, and intergenic regions for four *E. coli* strains: MG1655, CFT073, O157:H7-Sakai, and O157:H7-EDL933. cDNA synthesis, fragmentation, and hybridizations were as described previously (González Barrios *et al.*, 2006). Hybridization was performed for 16 h, and the total cell intensity was scaled to an average value of 500. Background values, noise

values, and scaling factors of the three arrays were examined and were comparable. The intensities of polyadenosine RNA control were used to monitor the labeling process. For each binary microarray comparison of differential gene expression, if the gene with the larger transcription rate did not have a consistent transcription rate based on the 11 probe pairs (*p*-value less than 0.05), these genes were discarded. A gene was considered differentially expressed when the *p*-value for comparing two chips was lower than 0.05 (to assure that the change in gene expression was statistically significant and that false positives arise less than 5%) and when the expression ratio was higher (4-fold) than the standard deviation for all K-12 genes of the microarrays (2.1-fold for SdiA vs. no SdiA and 2.6-fold for SdiA1E11 vs. SdiA) (Ren *et al.*, 2004a). Gene functions were obtained from the Affymetrix–NetAffx Analysis Center (https://www. affymetrix.com/analysis/netaffx/index.affx).

Double mutations.

BW25113 *tnaA sdiA* and BW25113 *mtr sdiA* were constructed as described previously using the Rapid Gene Knockout procedure with P1 transduction (Maeda *et al.*, 2008) by using plasmid pCP20 (Cherepanov and Wackernagel, 1995) to eliminate the kanamycin resistance gene (Km^R). The four mutations of the two double mutants were confirmed by PCR with six primers (Table 2): SdiA up, SdiA down, TnaA up, TnaA down, Mtr up, and Mtr down which flank each gene of interest and confirm both insertion and elimination of Km^R.

RT-PCR.

To corroborate the DNA microarray data, the transcription of *tnaA* was quantified with primers TnaA front and TnaA reverse (Table 2) using RT-PCR (Bansal *et al.*, 2007). BW25113 *sdiA* harboring pCA24N (no *sdiA* control), pCA24N-*sdiA*, or pCA24N-*sdiA1E11* was grown in LB containing IPTG to a turbidity of 1.8 at 600 nm when *E. coli* produces indole. RNA was isolated from the suspension cells as described previously (Ren *et al.*, 2004b). Housekeeping

gene *rrsG* (16S ribosomal RNA) with primers RrsG front and RrsG reverse (Table 2) was used to normalize the expression data. A total of 36 RT-PCR reactions with two independent cultures were performed based on three RT-PCR reactions for *tnaA* and the *rrsG* housekeeping gene for the three different samples (BW25113 *sdiA/*pCA24N, pCA24N-*sdiA*, and pCA24N-*sdiA1E11*) using an iCycler (Bio-Rad, Hercules, CA) and MyiQ software (Bio-Rad).

Protein modeling.

The amino acid sequences of the SdiA1E11 (residues 1-152) were modeled into the known three-dimensional structure of the *E. coli* SdiA (residues 1-171, Protein Data Bank accession code 2avx) (Yao *et al.*, 2006). The three-dimensional model was obtained using the SWISS-MODEL server (hhtp://swissmodel.expasy.org/) (Schwede *et al.*, 2003). The molecular visualization program PyMOL (http://pymol.sourceforge.net/) was utilized to make the protein image of the molecular model.

Microarray accession numbers.

The microarray data summarized in Table 3 have been deposited in the NCBI Gene Expression Omnibus (Edgar *et al.*, 2002) (http://www.ncbi.nlm.nih.gov/geo/) and are accessible through accession number GSE11779.

Results

Random mutagenesis of SdiA and biofilm screening.

To reconfigure SdiA for greater control of biofilm formation with and without external signals, epPCR mutagenesis using both manganese and an unbalanced dNTP mixture (Fishman *et al.*, 2004) was used to mutate randomly *sdiA*. The epPCR products were cloned into plasmid pCA24N-*sdiA*, and the plasmids were transformed into *E. coli* K-12 BW25113 *sdiA* so that there was no background SdiA in these cells, and all the changes in phenotype were due to plasmid-encoded SdiA variants. By sequencing five random colonies, the maximum error rate was

determined to be 0.94%. Colonies were screened (4577) for altered biofilm formation with and without extracellular signals (500 μM indole, 10 μM C4-*DL*-HSL, or 10 μM 3o-C8-*L*-HSL), which resulted in the identification of four biofilm variants (Fig. 1A). The mutations of SdiA1E11, SdiA14C3, and SdiA16G12, decreased biofilm formation at 24 h in the absence of extracellular signals (Fig. 2AB). The SdiA2D10 variant increased biofilm formation in the presence of 3o-C8-*L*-HSL in LB. Biofilm screening with C4-*DL*-HSL and indole did not lead to an interesting variant.

Unexpectedly, SdiA1E11, SdiA14C3, and SdiA16G12 (Fig. 1A) had truncations in SdiA so that they lack the carboxy DNA-binding domain (residues 196-216) (Wang *et al.*, 1991) (Fig. 1A). SdiA1E11 has five mutations at F7L, F59L, Y70C, M94K, and K153X (X indicates termination), SdiA14C3 has mutations at W9R, P49T, N87T, frame shift at N96, and L139X, and SdiA16G12 has mutation Q151X. Also, the AHL sensitive SdiA2D10 variant has four mutations at E31G, Y42F, R116H, and L165Q (Fig. 1A). In order to eliminate any possible chromosomal mutation effects, all the pCA24N-*sdiA* plasmids identified during the first- and second- screens were re-transformed into BW25113 *sdiA*, and the changes in biofilm formation were confirmed; hence, the changes in biofilm formation are due to the changes in the *sdiA* gene on the plasmid.

SdiA variants decrease E. coli biofilm formation.

Previously, we discovered that the deletion of *sdiA* causes a 51-fold increase in biofilm formation in LB at 30°C after 8 h (Lee *et al.*, 2007a); hence, SdiA reduces biofilm formation. Consistently, deleting *sdiA* resulted in an 18-fold increase in biofilm formation in LB after 8 h (Fig. 2A). As expected, overexpressing wild-type SdiA from pCA24N-*sdiA* reduced biofilm formation 3.5-fold after 8 h compared to no SdiA (empty vector pCA24N) (Fig. 2A). Similar results were observed in LB glu after 8 h (Fig. 2A); hence, the biofilm phenotype due to SdiA

could be partially complemented (full complementation probably was not achieved because of expression differences due to the non-native promoter and differences in copy number).

Biofilm formation in the presence of the SdiA variants was compared at both 8 h and 24 h since the differences in biofilm formation upon deleting wild-type *sdiA* gradually decreases with time (Lee *et al.*, 2007a) (Fig. 2AB). Two truncation variants, SdiA1E11 and SdiA16G12, lacking the carboxy-terminus DNA-binding domain of SdiA, resulted in a significant reduction of biofilm formation (5- to 10-fold) in both LB and LB glu after 8 h (Fig. 2A). After 24 h, SdiA1E11 further decreased biofilm (5- to 20-fold) in both LB and LB glu, SdiA14C3 decreased biofilm formation (4- to 6-fold) in both LB and LB glu, and SdiA16G12 decreased biofilm (8-fold) primarily in LB glu (Fig. 2B). Biofilm formation via the evolved SdiA variants was more reduced in LB glu probably because of the catabolite repression of *tnaA* (Botsford and DeMoss, 1971) which should reduce indole concentrations. These results show that the quorum-sensing regulator SdiA may be evolved to alter dramatically *E. coli* biofilm and may be altered to keep biofilm formation low for long periods.

The modeled protein structure of SdiA1E11 is shown in Fig. 1B and is based on the known structure of *E. coli* SdiA (residues 1-171, the autoinducer-binding domain) (Yao *et al.*, 2006). The K153X truncation of SdiA1E11 causes it to lose most of the long α5 alpha helix (residues 148-168, shown as a blue ribbon in Fig. 1B).

Reconfiguring SdiA to alter biofilm formation with AHLs.

Previously we reported that the addition of exogenous AHLs (10 μM of *N*-butyryl-, *N*-hexanoyl-, and *N*-octanoyl-*DL*-homoserine lactones) inhibited *E. coli* biofilm formation up to 27% without inhibiting growth (Lee *et al.*, 2007a). Also, *N*-hexanoyl-*L*-homoserine lactone significantly decreases *E. coli* biofilm in mixed culture with *Serratia plymuthica* (Moons *et al.*, 2006). Here, the SdiA2D10 variant was identified, and the mutations of SdiA2D10 increased

biofilm formation 1.9-fold in the presence of 10 μM 3o-C8-*L*-HSL in LB (normalized biofilm, 0.69 ± 0.02 vs. 1.31 ± 0.05) while 3o-C8-*L*-HSL addition to wild-type SdiA reduced biofilm formation by 6% under these conditions (normalized biofilm, 1.00 ± 0.06 vs. 0.94 ± 0.02) in LB after 24 h; hence, the four mutations of SdiA2D10 reversed the impact of this AHL on biofilm formation. Both biofilm variants SdiA1E11 and SdiA14C3 did not change biofilm formation upon adding 10 μM 3o-C8-*L*-HSL (normalized biofilm, 0.22 ± 0.03 vs. 0.26 ± 0.03 for SdiA1E11 and 0.23 ± 0.09 vs. 0.25 ± 0.09 for SdiA14C3) in LB after 24 h.

Moreover, the AHL sensitive SdiA2D10 and wild-type SdiA were tested with nine different *N*-acylhomoserine lactones with four to 14 carbons for the variable side chain at 10 μM in LB and LB glu. The mutations of SdiA2D10 increased biofilm formation (4- to 7-fold) in the presence of six AHLs (C4-*L*-HSL, C6-*DL*-HSL, C8-*DL*-HSL, 3o-C8-*L*-HSL, C10-*DL*-HSL, C12-*DL*-HSL, and 3o-C12-*L*-HSL) in LB glu after 24 h (Fig. 3), while the wild-type SdiA decreased biofilm formation less than 1.3-fold with the same AHLs compared to no AHLs (data not shown). Also, these AHLs increased biofilm formation maximally 2-fold with SdiA2D10 in LB (data not shown). Hence, AHLs enhanced biofilm formation via the evolved SdiA2D10 primarily in LB glu in which indole production is reduced due to catabolite repression of *tnaA* (Botsford and DeMoss, 1971). The results show SdiA may be altered to enhance biofilm formation of *E. coli* in the presence of AHLs produced from other bacteria.

Whole transcriptome analysis of SdiA and SdiA1E11 in biofilm cells.

To understand how overexpression of SdiA regulates gene expression in biofilm cells, DNA microarrays were used to determine differential gene expression for biofilm cells with overexpression of SdiA vs. biofilm cells without SdiA (empty plasmid) in LB for 12 h. It was found that 208 genes were regulated significantly (more than 4-fold) with SdiA vs. no SdiA; 37 genes were induced and 171 genes were repressed (Table 3). Most notable was that two indole-

related genes (*tnaAB*) and the *tna* leader region (*tnaC*) were highly repressed (7.5- to 23-fold) upon overexpressing SdiA. Hence, indole-related genes are repressed by wild-type SdiA. Also, genes were repressed related to curli synthesis (*csgDEFG* and *csgBAC*), the AI-2 uptake operon (*lsrACDBFG*), acid-resistance (*gadA*, *gadBC*, *gadX*, *hdeAB*, and *hdeD*), and a newly found acid resistance regulator *ariR* (Lee *et al.*, 2007c), while five cold shock protein genes (*cspH*, *cspG*, *cspI*, *cspB*, and *cspF*) were induced in biofilm cells with SdiA (Table 3). These results indicate that SdiA influences the regulation of many genes including genes related to cell communication. However, the transcriptional level of the cell division regulator of *ftsQAZ* and the AI-2 synthesis gene of *luxS* were not changed by overexpression of SdiA.

Another whole-transcriptome study was used to determine differential gene expression for biofilm cells with overexpression of the SdiA1E11 variant (the most important biofilm mutant) vs. biofilm cells with overexpression of wild-type SdiA grown in LB for 12 h. It was found that 60 genes were regulated significantly (more than 4-fold) with SdiA1E11 vs. wild-type SdiA; 46 genes were induced and 14 genes were repressed (Table 3). In contrast to the comparison of wild-type SdiA vs no SdiA, most notable was that two indole-related genes (*tnaAB*) and the *tna* leader region (*tnaC*) were highly induced (6.5- to 16-fold) upon overexpressing SdiA1E11. Hence, indole genes are preferentially induced with SdiA1E11. Also, genes were induced in biofilm cells with SdiA1E11 related to curli synthesis, acid-resistance (*gadA*, *gadBC*, *hdeB*, and *ariR*), and the AI-2 uptake operon (*lsrKRACDBFG*) while five cold shock protein genes (*cspH*, *cspG*, *cspI*, *cspB*, and *cspF*) were repressed (Table 3). The results indicate that the evolved SdiA1E11 differentially regulates gene expression from wild-type SdiA.

RT-PCR.

RT-PCR was used to corroborate the whole-transcriptome results with wild-type SdiA and SdiA1E11. As expected, overexpression of wild-type SdiA repressed *tnaA* transcription by 48-

fold ($\Delta\Delta C_T = 5.6 \pm 2.5$, where Ct is the threshold cycle of the target genes) compared to no SdiA which is consistent with the previous report (Wei *et al.*, 2001b). In contrast, overexpression of SdiA1E11 induced (226-fold, $\Delta\Delta C_T = 7.8 \pm 2.3$) *tnaA* transcription compared to overexpression of wild-type SdiA; hence, the mutations that lead to SdiA1E11 alter regulation of *tnaA* by SdiA.

Wild-type SdiA decreases curli production.

Since curli fibers are required both for adhesion and biofilm formation (Prigent-Combaret *et al.*, 2000) and overexpression of SdiA most repressed (11- to 37-fold) curli genes (*csgDEFG* and *csgBAC*) (Table 3), curli production was measured upon overexpressing SdiA and SidA1E11 using a Congo red plate assay. SdiA decreased dramatically curli production while SdiA1E11 decreased curli to a small extent (Fig. 4A); these data corroborate well the microarray data (Table 3). Since Congo red binds both curli and cellulose (Da Re and Ghigo, 2006), and CsgD controls the production of curli as well as cellulose (Da Re and Ghigo, 2006), a cellulose specific assay using calcofluor was also used to investigate cellulose production upon expression of SdiA. Unlike curli production in colonies, cellulose production with planktonic cells increased slightly upon overexpressing both SdiA (1.3 ± 0.1 fold) and SdiA1E11 (1.8 ± 0.3 fold) compared to no SdiA. These results suggest that the reduction of Congo red binding is due to a decrease in curli production (Fig. 4A). Moreover, three curli mutants (*csgB*, *csgE*, and *csgF*) formed 2- to 3-fold less biofilm compared to wild-type strain (Fig. 4B) as expected. The results suggest that wild-type SdiA inhibits curli production, which partially explains the decrease in biofilm formation.

Evolved SdiA variants alter indole production.

Since the whole-transcriptome and RT-PCR analysis showed that the most differentially-expressed genes due to the mutations of variant SdiA1E11 vs. wild-type SdiA were indole-related genes that were induced (*tnaAB* and *tnaC*) (Table 3), extracellular indole concentrations

were measured with the SdiA variants. Corroborating the microarray data (induction of indole-producing *tnaA*), SdiA1E11 produced 9-fold more extracellular indole than wild-type SdiA at the same cell turbidity of 3 at 600 nm (Fig. 5), and SdiA1E11 also produced 9.6-fold more intracellular indole than wild-type SdiA (3.2 ± 0.5 vs. 0.33 ± 0.09 nmol/mg total protein). Note the chromosomal deletion of *sdiA* (*sdiA*/pCA24N vs. BW25113/pCA24N) did not change indole production (Fig. 5). In contrast, overexpression of full length SdiA (SdiA2D10 and wild-type SdiA) decreased (5-fold) indole production, which was expected since a previous microarray result indicated overexpression of SdiA repressed *tnaA* by 4-fold (Wei *et al.*, 2001b) and our RT-PCR results indicated the same repression. Therefore, evolving SdiA to reduce biofilm formation via variant SdiA1E11 resulted in induction of *tnaA* which leads to more indole, which has been shown by us to reduce biofilm formation with 11 *E. coli* strains (Domka *et al.*, 2006; Lee *et al.*, 2007b; Lee *et al.*, 2007a; Zhang *et al.*, 2007; Lee *et al.*, 2008).

Also, the whole-transcriptome analysis showed that wild-type SdiA repressed (5- to 14-fold) the AI-2 uptake gene operon (*lsrKRACDBFG*) and SdiA1E11 induced (3- to 4-fold) those genes compared to wild-type SdiA (Table 3) although the expression of the gene which encodes the AI-2 synthesis protein (*luxS*) was not changed by overexpression of SdiA. Hence, these results also support that SdiA is associated with multiple signals, AHLs, AI-2, and indole (Lee *et al.*, 2008).

SdiA1E11 functions via indole as evidenced by cell density, motility, and biofilm formation with double mutants.

Since the mutations of SdiA1E11 decreased biofilm formation dramatically (Fig. 2AB) and increased indole concentrations dramatically (Fig. 5), we hypothesized that SdiA1E11 may function through indole. To test this hypothesis, cell density and motility were evaluated for SdiA1E11. Cell density was chosen since quorum sensing signals allow bacteria to monitor their

own population density to coordinate the expression of specific genes (Fuqua *et al.*, 1994), conditioned medium with unknown extracellular signals influences the final cell density of *E. coli* (Yang *et al.*, 2006), and indole prevents cell division (Chant and Summers, 2007). Also, motility was examined since it positively influences biofilm formation in *E. coli* (Pratt and Kolter, 1998; Wood *et al.*, 2006), and indole reduces both biofilm formation and motility in *E. coli* (Lee *et al.*, 2007a). In order to confirm these two phenotypes are related to indole and SdiA, cell growth and motility were measured in the presence of indole.

As shown in Fig. 6A, both of the two most-distinctive biofilm inhibition mutants, SdiA1E11 and SdiA14C3, reached a different final cell density, while the deletion of *sdiA* itself did not significantly change cell density; the mutations of SdiA1E11 decreased cell density by 18 ± 4%, and SdiA14C3 increased cell density by 16 ± 5% (note the specific growth rates were nearly unchanged, Table 4A). These results indicate that the quorum-sensing regulator SdiA may be evolved to control cell density. Also, the growth curves and the final cell density of the other two biofilm mutants SdiA16G12 and SdiA2D10 were similar to that of wild-type SdiA (data not shown). Indole is clearly linked to final cell density as it decreases the cell density of the wild-type strain in a dose-dependent manner (Fig. 6B).

For cell motility, overexpression of wild-type SdiA decreased (2-fold) motility (*sdiA*/pCA24N vs. *sdiA*/pCA24N-*sdiA*, Fig. 7A), which is consistent with previous results (Kanamaru *et al.*, 2000), and overexpression of wild-type SdiA completely complemented the *sdiA* deletion (*sdiA*/pCA24N-*sdiA* vs. BW25113/pCA24N, Fig. 7A). Also, the three low biofilm-forming variants (SdiA1E11, SdiA16G12, and SdiA14C3) showed 1.5- to 1.7-fold less motility, which partially explains the biofilm reduction of these mutants. For SdiA1E11, motility was decreased probably due to high indole concentration (Fig. 5) since the addition of exogenous indole decreased motility in a dose-dependent manner (Fig. 7B).

Moreover, two double mutants, BW25113 *tnaA sdiA* and BW25113 *mtr sdiA* (Mtr is involved in indole import (Yanofsky *et al.*, 1991)) were constructed to investigate the effect of indole on biofilm formation with SdiA and SdiA1E11. As expected, BW25113 *tnaA sdiA* did not produce indole. In the *tnaA sdiA* strain, wild-type SdiA decreased biofilm formation compared to no SdiA (Fig. 2C) as observed in the *sdiA* strain (Fig. 2B); however, SdiA1E11 increased rather than decreased biofilm formation compared to wild-type SdiA (Fig. 2C). Also, with *tnaA sdiA*, SdiA1E11 did not appreciably decrease the final cell density compared to wild-type SdiA, while both wild-type SdiA and SdiA1E11 increased the final cell density compared to no SdiA (Fig. 6C). Therefore, indole synthesis via *tnaA* is required for SdiA1E11 to alter cell phenotypes.

Mtr is less important for the mechanism of SdiA1E11; SdiA1E11 did not change biofilm formation compared to wild-type SdiA in the *mtr sdiA* mutant (not shown), but decreased the final cell density (not shown) as observed in the *sdiA* strain (Fig. 6A). For wild-type SdiA, both TnaA (Fig. 2C) and Mtr were not required for SdiA activity as SdiA decreased biofilm formation in the two double mutants. We also tried to construct double mutants of *sdiA luxS* and *sdiA lsrB* to investigate the mechanism of SdiA associated with AI-2 since SdiA most repressed AI-2 transport genes (Table 3). However, both double mutations were lethal which shows the importance of SdiA and AI-2 and their interdependence.

Saturation mutagenesis and truncation of SdiA.

Since two SdiA variants (SdiA1E11 and SdiA2D10) have a truncation along with additional mutations at E31G, Y42F, and M94K (Fig. 1A) and since the amino acid residues of Y41 and W95 are highly conserved throughout the LuxR family (Yao *et al.*, 2006), we investigated the importance of these and related positions of SdiA by substituting all possible amino acids via saturation mutagenesis using SdiA variants SdiA1E11 and SdiA2D10 as parent proteins (saturation mutations at M94 and W95 for SdiA1E11 and saturation mutations at H28, E29, I30,

E31, Y39, D40, Y41, and Y42 for SdiA2D10). After screening 1762 colonies to ensure with a probability of 99% that all possible codons were utilized (Rui *et al.*, 2004), we could not identify better variants that show a significant change of biofilm formation with and without 3o-C8-*L*-HSL than SdiA1E11 and SdiA2D10. For example, about 10% of the variants from saturation mutagenesis at positions M94 and W95 of SdiA1E11 reduced biofilm similar to the parent SdiA1E11.

Since three of the biofilm mutants (SdiA1E11, SdiA16G12, and SdiA14C3) contained truncations at the C-terminus of SdiA (Fig. 1), we investigated the relationship between the length of SdiA and biofilm formation. Seven truncation mutants were constructed using site directed mutagenesis to introduce a stop codon at R16, Q33, T53, A73, L93, A110, and L133 of SdiA. Four truncation variants (SdiAL133, SdiAA110, SdiAL93, and SdiAA73) lacking the carboxy-terminus DNA-binding domain of SdiA had a significant reduction in biofilm formation (3- to 10-fold) in both LB and LB glu for 8 h (data not shown). Also, SdiAL133X decreased biofilm formation (10-fold) in LB glu compared to wild-type SdiA after 24 h, which is comparable with the 20-fold reduction in biofilm formation by SdiA1E11 having five mutations at F7L, F59L, Y70C, M94K, and K153X (Fig. 2B). Overall, these results confirm that deletion of the C-terminus of SdiA results in a reduction in biofilm formation.

Discussion

Here we demonstrate that the quorum sensing regulator SdiA may be evolved to control biofilm formation of *E. coli*. Two main phenotypes were found: with SdiA1E11, biofilm is reduced an additional 20-fold primarily due to increased indole concentrations, and with SdiA2D10, biofilm is increased 7-fold in the presence of C8-*DL*-HSL and 3o-C12-*L*-HSL. These results show the cell's genetic circuitry may be re-wired internally to both increase and decrease biofilm formation. Unlike where we controlled biofilm formation by manipulating indole extracellular concentrations by cloning a monooxygenase in a second bacterium (Lee *et al.*, 2007a), the current results are important for controlling biofilm formation with a single strain by controlling a sensor rather than the signal. Previous efforts to control biofilm formation by using synthetic circuits utilized induction of *traA*, the conjugation plasmid pilin gene, upon exposure to UV light (Kobayashi *et al.*, 2004). Others have coordinated cell communication via quorum-sensing molecules and synthetic circuits but not controlled biofilm formation (Brenner *et al.*, 2007).

We determined the mechanism by which SdiA1E11 reduces biofilm formation is through increased indole concentrations. The lines of evidence for this conclusion are that (i) the whole-transcriptome analysis shows *tnaA* is induced (Table 3), (ii) extracellular (Fig. 5) and intracellular indole concentrations were increased, (iii) motility is decreased (Fig. 7A) and indole addition to the host reduced motility in a dose-dependent manner (Fig. 7B), (iv) cell density was decreased (Fig. 6A) and indole addition to the host reduced cell density in a dose-dependent manner (Fig. 6B), and (v) SdiA1E11 did not affect biofilm formation (Fig. 2C) or cell density in a *tnaA sdiA* double mutant (Fig. 6C).

Several physiological roles of SdiA have been determined along with the structure of the N-terminal AHL binding domain of SdiA (residues 1-171); however, identification of endogenous

signal(s) from *E. coli* that bind to SdiA has been difficult. It is known that unidentified extracellular factors from conditioned medium are titrated by the N-terminal part of SdiA and prevent induction of *E. coli* O157:H7 virulence factors (Kanamaru *et al.*, 2000), that the extracellular factors (even from AI-2 deficient strains) regulate the *ftsQ2p* cell division promoter via SdiA (García-Lara *et al.*, 1996; Sitnikov *et al.*, 1996), and that the extracellular factors decrease cell growth when the multidrug efflux pumps AcrAB are overexpressed (Yang *et al.*, 2006); note overexpression of SdiA increases AcrAB expression (Rahmati *et al.*, 2002). In all three cases, it is highly possible that indole is part of the unidentified extracellular component of the conditioned media in these previous SdiA studies since it is abundant in the conditioned medium of stationary-phase cells (up to 600 μM in LB medium (Domka *et al.*, 2006)) and since indole affects two of these phenotypes: indole decreases *ftsQ2p* cell division promoter via SdiA (Lee *et al.*, 2007a) and indole reduces cell growth (Chant and Summers, 2007; Lee *et al.*, 2007a). Since some of these SdiA-mediated effects occur in LuxS-minus strains and since the synthesis of AI-2 and AI-3 depends on the presence of LuxS (Sperandio *et al.*, 2003), AI-2 and AI-3 are unlikely to be the extracellular factors that interact with SdiA.

Additional evidence shows indole and SdiA are related. Indole biofilm signaling requires SdiA (Lee *et al.*, 2008), and indole signaling occurs primarily at 30°C (Lee *et al.*, 2008) in a manner similar to SdiA responsiveness occurring mainly at 30°C but not at 37°C in *E. coli* (Van Houdt *et al.*, 2006). Both indole and SdiA decrease biofilm formation and motility (Lee *et al.*, 2007a), enhance antibiotic resistance (Rahmati *et al.*, 2002; Hirakawa *et al.*, 2005; Lee *et al.*, 2008), influence acid-resistance (indole decreases and SdiA increases acid-resistance) (Van Houdt *et al.*, 2006; Lee *et al.*, 2007a), and regulate cell division (indole decreases and SdiA increases cell division) (Wang *et al.*, 1991; Chant and Summers, 2007; Lee *et al.*, 2008). In the current study, mutation of SdiA significantly altered biofilm formation, cell density, indole

production, and motility. However, how indole and SdiA are related and control cell physiology is unknown and should be investigated further since SdiA (like LasR and TraR (Bottomley *et al.*, 2007)) is insoluble without AHLs binding it (Yao *et al.*, 2006); yet, AHLs are not readily available (since *E. coli* does not produce them) and SdiA alters phenotypes in the absence of AHLs.

In this study, through the whole-genome analysis (Table 3), we also found a new role for wild-type SdiA that explains its role in reducing early biofilm formation (Fig. 2A): SdiA decreases curli production via repression of *csgDEFG* and *csgBAC* (Table 3). These DNA microarray results were corroborated with a curli assay (Fig. 4A). In addition, three curli *csgB*, *csgE*, *csgF* mutants were used to show the proteins encoded by these genes are directly related to biofilm formation (Fig. 4B). Curli fibers from *E. coli* show biochemical and biophysical properties of amyloid proteins that are associated with debilitating human ailments including Alzheimer's and prion diseases (Chapman *et al.*, 2002), and curli fibers function as a major structure of adherence that is essential for biofilm formation of *E. coli* (Prigent-Combaret *et al.*, 2000).

In contrast, we previously reported that in suspension cells, SdiA (wild-type strain vs. *sdiA* deletion mutant) induces curli genes (*csgDEFG* and *csgBAC*) (Lee *et al.*, 2008). Also, SdiA most represses genes involved in uridine monophosphate (UMP) biosynthesis (*carAB*, *pyrLBI*, *pyrF*, and *uraA*) in suspension cells (Lee *et al.*, 2008) while in biofilm cells (this study), SdiA did not change the gene expression of these genes. Therefore, SdiA has distinctive roles for cells in suspension vs. cells in biofilms.

In the current study, truncation of the C-terminal DNA-binding domain of SdiA (K153X) and additional mutations (F7L, F59L, Y70C, and M94K) in SdiA1E11 dramatically increase indole production (Fig. 5) which leads to decreased biofilm formation (Fig. 2AB) and decreased

motility (Fig. 7), as indole decreases these two phenotypes (Lee *et al.*, 2007a). Notably three mutations (F59L, Y70C, and M94K) in SdiA1E11 are adjacent to the residues involved in the binding of *N*-octanoyl-homoserine lactones (Y63, W67, Y72, D80, and W95) (Yao *et al.*, 2006), and three of the four mutations in SdiA1E11 (F7L F59L, and Y70C) result in the lost of aromatic side chains. The truncation of the C-terminus, which should abolish the DNA-binding activity of SdiA and retain the ligand-binding domain (Yao *et al.*, 2006), enhances the control of SdiA over biofilm formation and should be investigated further. Since the overproduced N-terminal part of SdiA inhibits the expression of virulence factors in wild-type *E. coli* O157:H7 and negatively affects on the activity of the full-length SdiA (Kanamaru *et al.*, 2000), it is interesting to investigate if truncated SdiA variants such as SdiA1E11 alter the expression of virulence genes.

Overexpression of SdiA from a plasmid showed significant effects on cell division (Wang *et al.*, 1991), increased mitomycin C resistance (Wei *et al.*, 2001a), and increased multi-drug resistance (Rahmati *et al.*, 2002), while the chromosomal deletion of *sdiA* had no effect or reduced effects on these phenotypes (Wang *et al.*, 1991; Wei *et al.*, 2001a; Rahmati *et al.*, 2002). We also observed that overexpression of wild-type SdiA led to a significant decrease of *tnaA* expression (whole-transcriptome and RT-PCR results) along with reduced indole production (Fig. 5), while the chromosomal *sdiA* deletion did not affect indole production (Fig. 5) although the *sdiA* deletion itself significantly influenced biofilm formation, motility, and acid-resistance (Lee *et al.*, 2007a). It was previously proposed that SdiA has very low levels of activity in pure culture (in the absence of AHLs) (Ahmer, 2004), that overexpression of SdiA may override normal regulation (Ahmer, 2004), and that overexpression of SdiA from a plasmid results in a large pleiotropic response (Lindsay and Ahmer, 2005). Most importantly though, we were able to find SdiA mutations that allow us to increase or decrease biofilm formation even if the role of SdiA remains incompletely characterized.

Natural bacterial biofilms are heterogeneous communities. Hence, many bacteria utilize quorum-sensing circuits to sense their own population density as well as to eavesdrop on quorum-sensing signals from other bacteria so that bacteria readily coordinate group behavior (such as biofilm formation and pathogenesis) in multispecies communities (Case *et al.*, 2008). Previously, it was suggested both *Salmonella enterica* and *E. coli* utilize SdiA to eavesdrop on AHL from other strains (Michael *et al.*, 2001) since the SdiA-regulated, outer membrane protein promoter p*rck* responded to several AHLs (*N*-butyryl, *N*-oxobutyryl-, *N*-hexanoyl-, *N*-oxohexanoyl-, *N*-octanoyl-, *N*-oxooctanoyl-, *N*-decanoyl-, and *N*-oxodecanoyl-homoserine lactones). In the current study, an evolved SdiA variant (SdiA2D10) increased the biofilm formation of *E. coli* the most in the presence of C8-*DL*-HSL and 3o-C12-*L*-HSL while wild-type SdiA decreases *E. coli* biofilm formation up to 51-fold in short term experiments (Lee *et al.*, 2007a), and three AHLs signals (*N*-butyryl-, *N*-hexanoyl-, and *N*-octanoyl-homoserine lactones) decrease biofilm formation with wild-type *E. coli* but not with the *sdiA* mutant (Lee *et al.*, 2007a). Therefore, we show here that *E. coli* can evolve SdiA to control biofilm formation in the presence of the signals of other microbial species. Similarly, indole and 7-hydroxyindole, which have been termed promiscuous biofilm signals (Wood, 2009), increase the biofilm formation of *P. aeruginosa* (which does not synthesize indole), decrease its production of virulence factors by repressing quorum-sensing related genes, and enhance multidrug resistance by inducing efflux pump genes (Lee *et al.*, 2009). *P. aeruginosa* was also found to degrade indole and 7-hydroxyindole (Lee *et al.*, 2009). Hence, *E. coli* may use indole to reduce the virulence of other bacteria while other bacteria have acquired a defense system to cope with indole. Therefore, competition and adaptation are prevalent, and SdiA may play an important role in multispecies consortia.

Many bacteria contain more than one quorum-sensing circuit to adapt to diverse

environmental conditions (Case *et al.*, 2008), and LuxR has been rapidly evolved for increased sensitivity to a broad range of AHLs (Collins *et al.*, 2005). Similarly, *E. coli* has SdiA associated with multiple signals (e.g., indole, AHLs, and AI-2) (Lee *et al.*, 2008). In this study, we demonstrate that the LuxR homolog SdiA may be readily evolved; as a result, evolved SdiA variants alter biofilm formation, cell density, indole concentration, and motility in *E. coli*. The mechanism of how pathogenic bacteria evolve such traits as antibiotic resistance within a short time is still unclear (Aharoni *et al.*, 2005) and how strains interact with multiple species in natural biofilms is also unclear. This study implies that bacteria have the capability to evolve a quorum sensing protein that is related to detecting other bacteria and that quorum sensing proteins can be a target for biofilm control.

Reference

Aharoni, A., Gaidukov, L., Khersonsky, O., Gould, S.M., Roodveldt, C., and Tawfik, D.S. (2005) The 'evolvability' of promiscuous protein functions. *Nat Genet* **37**: 73-76.

Ahmer, B.M. (2004) Cell-to-cell signalling in *Escherichia coli* and *Salmonella enterica*. *Mol Microbiol* **52**: 933-945.

Baba, T., Ara, T., Hasegawa, M., Takai, Y., Okumura, Y., Baba, M. et al. (2006) Construction of *Escherichia coli* K-12 in-frame, single-gene knockout mutants: the Keio collection. *Mol Syst Biol* **2**: 2006 0008.

Bansal, T., Englert, D., Lee, J., Hegde, M., Wood, T.K., and Jayaraman, A. (2007) Differential effects of epinephrine, norepinephrine, and indole on *Escherichia coli* O157:H7 chemotaxis, colonization, and gene expression. *Infect Immun* **75**: 4597-4607.

Botsford, J.L., and DeMoss, R.D. (1971) Catabolite repression of tryptophanase in *Escherichia coli*. *J Bacteriol* **105**: 303-312.

Bottomley, M.J., Muraglia, E., Bazzo, R., and Carfi, A. (2007) Molecular insights into quorum sensing in the human pathogen *Pseudomonas aeruginosa* from the structure of the virulence regulator LasR bound to its autoinducer. *J Biol Chem* **282**: 13592-13600.

Brenner, K., Karig, D.K., Weiss, R., and Arnold, F.H. (2007) Engineered bidirectional communication mediates a consensus in a microbial biofilm consortium. *Proc Natl Acad Sci U S A* **104**: 17300-17304.

Case, R.J., Labbate, M., and Kjelleberg, S. (2008) AHL-driven quorum-sensing circuits: their frequency and function among the Proteobacteria. *ISME J* **2**: 345-349.

Chai, Y., and Winans, S.C. (2004) Site-directed mutagenesis of a LuxR-type quorum-sensing transcription factor: alteration of autoinducer specificity. *Mol Microbiol* **51**: 765-776.

Chant, E.L., and Summers, D.K. (2007) Indole signalling contributes to the stable maintenance of *Escherichia coli* multicopy plasmids. *Mol Microbiol* **63**: 35-43.

Chapman, M.R., Robinson, L.S., Pinkner, J.S., Roth, R., Heuser, J., Hammar, M. et al. (2002) Role of *Escherichia coli* curli operons in directing amyloid fiber formation. *Science* **295**: 851-855.

Cherepanov, P.P., and Wackernagel, W. (1995) Gene disruption in *Escherichia coli*: TcR and KmR cassettes with the option of Flp-catalyzed excision of the antibiotic-resistance determinant. *Gene* **158**: 9-14.

Collins, C.H., Arnold, F.H., and Leadbetter, J.R. (2005) Directed evolution of *Vibrio fischeri* LuxR for increased sensitivity to a broad spectrum of acyl-homoserine lactones. *Mol Microbiol* **55**: 712-723.

Collins, C.H., Leadbetter, J.R., and Arnold, F.H. (2006) Dual selection enhances the signaling specificity of a variant of the quorum-sensing transcriptional activator LuxR. *Nat Biotechnol* **24**: 708-712.

Da Re, S., and Ghigo, J.M. (2006) A CsgD-independent pathway for cellulose production and biofilm formation in *Escherichia coli*. *J Bacteriol* **188**: 3073-3087.

Davies, D.G., Parsek, M.R., Pearson, J.P., Iglewski, B.H., Costerton, J.W., and Greenberg, E.P. (1998) The involvement of cell-to-cell signals in the development of a bacterial biofilm. *Science* **280**: 295-298.

Domka, J., Lee, J., and Wood, T.K. (2006) YliH (BssR) and YceP (BssS) regulate *Escherichia coli* K-12 biofilm formation by influencing cell signaling. *Appl Environ Microbiol* **72**: 2449-2459.

Edgar, R., Domrachev, M., and Lash, A.E. (2002) Gene Expression Omnibus: NCBI gene expression and hybridization array data repository. *Nucleic Acids Res* **30**: 207-210.

Fishman, A., Tao, Y., Bentley, W.E., and Wood, T.K. (2004) Protein engineering of toluene 4-monooxygenase of *Pseudomonas mendocina* KR1 for synthesizing 4-nitrocatechol from nitrobenzene. *Biotechnol Bioeng* **87**: 779-790.

Fuqua, W.C., Winans, S.C., and Greenberg, E.P. (1994) Quorum sensing in bacteria: the LuxR-LuxI family of cell density-responsive transcriptional regulators. *J Bacteriol* **176**: 269-275.

García-Lara, J., Shang, L.H., and Rothfield, L.I. (1996) An extracellular factor regulates expression of *sdiA*, a transcriptional activator of cell division genes in *Escherichia coli*. *J Bacteriol* **178**: 2742-2748.

González Barrios, A.F., Zuo, R., Hashimoto, Y., Yang, L., Bentley, W.E., and Wood, T.K. (2006) Autoinducer 2 controls biofilm formation in *Escherichia coli* through a novel motility quorum-sensing regulator (MqsR, B3022). *J Bacteriol* **188**: 305-316.

Henikoff, S., Wallace, J.C., and Brown, J.P. (1990) Finding protein similarities with nucleotide sequence databases. *Methods Enzymol* **183**: 111-132.

Hirakawa, H., Inazumi, Y., Masaki, T., Hirata, T., and Yamaguchi, A. (2005) Indole induces the expression of multidrug exporter genes in *Escherichia coli*. *Mol Microbiol* **55**: 1113-1126.

Jayaraman, A., and Wood, T.K. (2008) Bacterial quorum sensing: Signals, circuits, and implications for biofilms and disease. *Annu Rev Biomed Eng* **10**: 145-167.

Jayaraman, A., Mansfeld, F.B., and Wood, T.K. (1999) Inhibiting sulfate-reducing bacteria in biofilms by expressing the antimicrobial peptides indolicidin and bactenecin. *J Indust Microbiol Biotechnol* **22**: 167-175.

Kanamaru, K., Kanamaru, K., Tatsuno, I., Tobe, T., and Sasakawa, C. (2000) SdiA, an *Escherichia coli* homologue of quorum-sensing regulators, controls the expression of virulence factors in enterohaemorrhagic *Escherichia coli* O157:H7. *Mol Microbiol* **38**: 805-816.

Kitagawa, M., Ara, T., Arifuzzaman, M., Ioka-Nakamichi, T., Inamoto, E., Toyonaga, H., and Mori, H. (2005) Complete set of ORF clones of *Escherichia coli* ASKA library (A Complete Set of *E. coli* K-12 ORF Archive): Unique Resources for Biological Research. *DNA Res* **12**: 291-299.

Kobayashi, H., Kaern, M., Araki, M., Chung, K., Gardner, T.S., Cantor, C.R., and Collins, J.J. (2004) Programmable cells: interfacing natural and engineered gene networks. *Proc Natl Acad Sci U S A* **101**: 8414-8419.

Lee, J., Jayaraman, A., and Wood, T.K. (2007a) Indole is an inter-species biofilm signal mediated by SdiA. *BMC Microbiol* **7**: 42.

Lee, J., Bansal, T., Jayaraman, A., Bentley, W.E., and Wood, T.K. (2007b) Enterohemorrhagic *Escherichia coli* biofilms are inhibited by 7-hydroxyindole and stimulated by isatin. *Appl Environ Microbiol* **73**: 4100-4109.

Lee, J., Attila, C., Cirillo, S.L., Cirillo, J.D., and Wood, T.K. (2009) Indole and 7-hydoxyindole diminish *Pseudomonas aeruginosa* virulence. *Microb Biotechnol* **2**: 75-90.

Lee, J., Zhang, X.S., Hegde, M., Bentley, W.E., Jayaraman, A., and Wood, T.K. (2008) Indole cell signaling occurs primarily at low temperatures in *Escherichia coli*. *ISME J* **2**: 1007-1023.

Lee, J., Page, R., García-Contreras, R., Palermino, J.M., Zhang, X.S., Doshi, O. et al. (2007c) Structure and function of the *Escherichia coli* protein YmgB: a protein critical for biofilm formation and acid-resistance. *J Mol Biol* **373**: 11-26.

Lindsay, A., and Ahmer, B.M. (2005) Effect of *sdiA* on biosensors of *N*-acylhomoserine lactones. *J Bacteriol* **187**: 5054-5058.

Luján, A.M., Moyano, A.J., Segura, I., Argaraña, C.E., and Smania, A.M. (2007) Quorum-sensing-deficient (*lasR*) mutants emerge at high frequency from a Pseudomonas aeruginosa mutS strain. *Microbiology* **153**: 225-237.

Luo, Z.-Q., Smyth, A.J., Gao, P., Qin, Y., and Farrand, S.K. (2003) Mutational analysis of TraR. Correlating function with molecular structure of a quorum-sensing transcriptional activator. *J Biol Chem* **278**: 13173-13182.

Maeda, T., Sanchez-Torres, V., and Wood., T.K. (2008) Metabolic engineering to enhance bacterial hydrogen production. *Microb Biotechnol* **1**: 30-39.

Michael, B., Smith, J.N., Swift, S., Heffron, F., and Ahmer, B.M. (2001) SdiA of *Salmonella enterica* is a LuxR homolog that detects mixed microbial communities. *J Bacteriol* **183**: 5733-5742.

Moons, P., Van Houdt, R., Aertsen, A., Vanoirbeek, K., Engelborghs, Y., and Michiels, C.W. (2006) Role of quorum sensing and antimicrobial component production by *Serratia plymuthica* in formation of biofilms, including mixed biofilms with *Escherichia coli*. *Appl Environ Microbiol* **72**: 7294-7300.

Pratt, L.A., and Kolter, R. (1998) Genetic analysis of *Escherichia coli* biofilm formation: roles of flagella, motility, chemotaxis and type I pili. *Mol Microbiol* **30**: 285-293.

Prigent-Combaret, C., Prensier, G., Le Thi, T.T., Vidal, O., Lejeune, P., and Dorel, C. (2000) Developmental pathway for biofilm formation in curli-producing *Escherichia coli* strains: role of flagella, curli and colanic acid. *Environ Microbiol* **2**: 450-464.

Rahmati, S., Yang, S., Davidson, A.L., and Zechiedrich, E.L. (2002) Control of the AcrAB multidrug efflux pump by quorum-sensing regulator SdiA. *Mol Microbiol* **43**: 677-685.

Reisner, A., Krogfelt, K.A., Klein, B.M., Zechner, E.L., and Molin, S. (2006) In vitro biofilm formation of commensal and pathogenic *Escherichia coli* strains: impact of environmental and genetic factors. *J Bacteriol* **188**: 3572-3581.

Ren, D., Bedzyk, L.A., Ye, R.W., Thomas, S.M., and Wood, T.K. (2004a) Differential gene expression shows natural brominated furanones interfere with the autoinducer-2 bacterial signaling system of *Escherichia coli*. *Biotechnol Bioeng* **88**: 630-642.

Ren, D., Bedzyk, L.A., Thomas, S.M., Ye, R.W., and Wood, T.K. (2004b) Gene expression in *Escherichia coli* biofilms. *Appl Microbiol Biotechnol* **64**: 515-524.

Rui, L., Kwon, Y.M., Fishman, A., Reardon, K.F., and Wood, T.K. (2004) Saturation mutagenesis of toluene *ortho*-monooxygenase of *Burkholderia cepacia* G4 for enhanced 1-naphthol synthesis and chloroform degradation. *Appl Environ Microbiol* **70**: 3246-3252.

Sambrook, J., Fritsch, E.F., and Maniatis, T. (1989) *Molecular Cloning: A Laboratory Manual*. Cold Spring Harbor, NY: Cold Spring Harbor Laboratory Press.

Schwede, T., Kopp, J., Guex, N., and Peitsch, M.C. (2003) SWISS-MODEL: An automated protein homology-modeling server. *Nucleic Acids Res* **31**: 3381-3385.

Sitnikov, D.M., Schineller, J.B., and Baldwin, T.O. (1996) Control of cell division in *Escherichia coli*: regulation of transcription of *ftsQA* involves both *rpoS* and SdiA-mediated autoinduction. *Proc Natl Acad Sci U S A* **93**: 336-341.

Sperandio, V., Torres, A.G., Jarvis, B., Nataro, J.P., and Kaper, J.B. (2003) Bacteria-host communication: the language of hormones. *Proc Natl Acad Sci U S A* **100**: 8951-8956.

Van Houdt, R., Aertsen, A., Moons, P., Vanoirbeek, K., and Michiels, C.W. (2006) *N*-acyl-*L*-homoserine lactone signal interception by *Escherichia coli*. *FEMS Microbiol Lett* **256**: 83-89.

Wang, D., Ding, X., and Rather, P.N. (2001) Indole can act as an extracellular signal in *Escherichia coli*. *J Bacteriol* **183**: 4210-4216.

Wang, X.D., de Boer, P.A., and Rothfield, L.I. (1991) A factor that positively regulates cell division by activating transcription of the major cluster of essential cell division genes of *Escherichia coli*. *Embo J* **10**: 3363-3372.

Wei, Y., Vollmer, A.C., and LaRossa, R.A. (2001a) In vivo titration of mitomycin C action by four *Escherichia coli* genomic regions on multicopy plasmids. *J Bacteriol* **183**: 2259-2264.

Wei, Y., Lee, J.M., Smulski, D.R., and LaRossa, R.A. (2001b) Global impact of *sdiA* amplification revealed by comprehensive gene expression profiling of *Escherichia coli*. *J Bacteriol* **183**: 2265-2272.

Winson, M.K., Camara, M., Latifi, A., Foglino, M., Chhabra, S.R., Daykin, M. et al. (1995) Multiple *N*-acyl-*L*-homoserine lactone signal molecules regulate production of virulence determinants and secondary metabolites in *Pseudomonas aeruginosa*. *Proc Natl Acad Sci U S A* **92**: 9427-9431.

Wood, T.K. (2009) Insights on *Escherichia coli* biofilm formation and inhibition from whole-transcriptome profiling. *Environ Microbiol* **11**: 1-15.

Wood, T.K., González Barrios, A.F., Herzberg, M., and Lee, J. (2006) Motility influences biofilm architecture in *Escherichia coli*. *Appl Microbiol Biotechnol* **72**: 361-367.

Yang, S., Lopez, C.R., and Zechiedrich, E.L. (2006) Quorum sensing and multidrug transporters in *Escherichia coli*. *Proc Natl Acad Sci U S A* **103**: 2386-2391.

Yanofsky, C., Horn, V., and Gollnick, P. (1991) Physiological studies of tryptophan transport and tryptophanase operon induction in *Escherichia coli*. *J Bacteriol* **173**: 6009-6017.

Yao, Y., Martinez-Yamout, M.A., and Dyson, H.J. (2005) Backbone and side chain ^{1}H, ^{13}C and ^{15}N assignments for *Escherichia coli* SdiA1-171, the autoinducer-binding domain of a quorum sensing protein. *J Biomol NMR* **31**: 373-374.

Yao, Y., Martinez-Yamout, M.A., Dickerson, T.J., Brogan, A.P., Wright, P.E., and Dyson, H.J. (2006) Structure of the *Escherichia coli* quorum sensing protein SdiA: activation of the folding switch by acyl homoserine lactones. *J Mol Biol* **355**: 262-273.

Zhang, X.S., García-Contreras, R., and Wood, T.K. (2007) YcfR (BhsA) influences *Escherichia coli* biofilm formation through stress response and surface hydrophobicity. *J Bacteriol* **189**: 3051-3062.

Table 1 Strains and plasmids used in this study. Km^R, Cm^R, and Ap^R are kanamycin, chloramphenicol, and ampicillin resistance, respectively.

Strains and plasmids	Genotype/relevant characteristics	Source
Strain		
E. coli K-12 BW25113	*lacI*^{q} *rrnB*$_{T14}$ Δ*lacZ*$_{WJ16}$ hsdR514 Δ*araBA*-D$_{AH33}$ Δ*rhaBAD*$_{LD78}$	(Baba *et al.*, 2006)
E. coli K-12 BW25113 Δ*sdiA*	K-12 BW25113 Δ*sdiA* Ω Km^R	(Baba *et al.*, 2006)
E. coli K-12 BW25113 Δ*tnaA*	K-12 BW25113 Δ*tnaA* Ω Km^R	(Baba *et al.*, 2006)
E. coli K-12 BW25113 Δ*mtr*	K-12 BW25113 Δ*mtr* Ω Km^R	(Baba *et al.*, 2006)
E. coli K-12 BW25113 Δ*csgB*	K-12 BW25113 Δ*csgB* Ω Km^R	(Baba *et al.*, 2006)
E. coli K-12 BW25113 Δ*csgE*	K-12 BW25113 Δ*csgE* Ω Km^R	(Baba *et al.*, 2006)
E. coli K-12 BW25113 Δ*csgF*	K-12 BW25113 Δ*csgF* Ω Km^R	(Baba *et al.*, 2006)
E. coli K-12 BW25113 Δ*adrA*	K-12 BW25113 Δ*adrA* Ω Km^R	(Baba *et al.*, 2006)
E. coli K-12 BW25113 Δ*tnaA* Δ*sdiA*	K-12 BW25113 Δ*tnaA* Δ*sdiA* Ω Km^R	this study
E. coli K-12 BW25113 Δ*mtr* Δ*sdiA*	K-12 BW25113 Δ*mtr* Δ*sdiA* Ω Km^R	this study
Plasmids		
pCA24N	Empty vector; Cm^R	(Kitagawa *et al.*, 2005)
pCA24N-*sdiA*	pCA24N *pT5-lac*::*sdiA*; expresses SdiA derived from *E. coli*	(Kitagawa *et al.*, 2005)
pCA24N-*adrA*	pCA24N *pT5-lac*::*adrA*; expresses AdrA derived from *E. coli*	(Kitagawa *et al.*, 2005)
pCP20	Ap^R and Cm^R plasmid with temperature-sensitive replication and thermal induction of FLP synthesis	(Chant and Summers, 2007)

Table 2 Primers used for error prone PCR, DNA sequencing, RT-PCR, and confirmation of the double mutants, saturation mutagenesis (SM), and truncation of *sdiA*. The positions mutated by saturation and site-directed mutagenesis are underlined.

Purpose	Primer	Sequence (5' to 3')
error-prone PCR of *sdiA*	SdiA front	AGGCGTATCACGAGGCCCTTTC
	SdiA reverse	CAGTCACGATGAATTCCCCTAG
DNA Sequencing	Seq primer 1	CACCGATCGCCCTTCCCAACAGTTGC
	Seq primer 2	GCAGTTACTGGTGCGCGAAAG
RT-PCR for *tnaA*	TnaA front	TGAAGAAGTTGGTCCGAATAACGTG
	TnaA reverse	CTTTGTATTCTGCTTCACGCTGCTT
RT-PCR for house-keeping gene *rrsG*	RrsG front	TATTGCACAATGGGCGCAAG
	RrsG reverse	ACTTAACAAACCGCCTGCGT
confirmation of the *sdiA* mutation	SdiA up	AATGCGATGGCTTGCAAAAGTAATT
	SdiA down	AGCAAATTAAACAAGCCTACCGTCA
confirmation of the *tnaA* mutation	TnaA up	CTGGCGAATTAATCGGTATAGCAGA
	TnaA down	GATCAGTCATGATGCCACCTTTAGA
confirmation of the *mtr* mutation	Mtr up	GTACTCGTGTACTGGTACAGTGCAA
	Mtr down	TCCTACATAGACCTGATAAGCGAAG
SM at H28 E29	SdiAf H28 E29	GGAGACCGCAGAAGAGGTCTACNNSNNSATTGAGCTTCAG GCTCAGCAGC
	SdiAr H28 E29	GCTGCTGAGCCTGAAGCTCAATSNNSNNGTAGACCTCTTCT GCGGTCTCC
SM at I30 E31	SdiAf I30 E31	CCGCAGAAGAGGTCTACCATGAANNSNNSCTTCAGGCTCAG CAGCTGGAG
	SdiAr I30 E31	CTCCAGCTGCTGAGCCTGAAGSNNSNNTTCATGGTAGACCT CTTCTGCGG
SM at Y39 D40	SdiAf Y39 D40	TTGAGCTTCAGGCTCAGCAGCTGGAGNNSNNSTACTATTCG TTATGTGTC
	SdiAr Y39 D40	GACACATAACGAATAGTASNNSNNCTCCAGCTGCTGAGCCT GAAGCTCAA
SM at Y41 D44	SdiAf Y41 D44	CTTCAGGCTCAGCAGCTGGAGTACGATNNSNNSTCGTTATG TGTCCGCCA
	SdiAr Y41 D44	TGGCGGACACATAACGASNNSNNATCGTACTCCAGCTGCTG AGCCTGAAG

Table 2 Continued.

Purpose	Primer	Sequence (5' to 3')
SM at M94 W95	SdiAf M94 W95	AACTTTAGTCAGGGCCATTTANNSNNSAATGATGACTTATT CAGCGAAGC
	SdiAr M94W95	GCTTCGCTGAATAAGTCATCATTSNNSNNTAAATGGCCCTG ACTAAAGTT
Truncation at R16	SdiAf R16	GCGTCGCACGATGCTGTTGTAATTTCAGAGGATGGAGACCG
	SdiAr R16	CGGTCTCCATCCTCTGAAATTACAACAGCATCGTGCGACGC
Truncation at Q33	SdiAf Q33	GGTCTACCATGAAATTGAGCTTTAAGCTCAGCAGCTGGAG
	SdiAr Q33	CTCCAGCTGCTGAGCTTAAAGCTCAATTTCATGGTAGACC
Truncation at T53	SdiAf T53	CCGCCACCCGGTACCATTCTAACGACCTAAAGTGGC
	SdiAr T53	GCCACTTTAGGTCGTTAGAATGGTACCGGGTGGCGG
Truncation at A73	SdiAf A73	GAGGCGTGGGTTAGTTATTATCAGTAAAAAAACTTTCTCGC
	SdiAr A73	GCGAGAAAGTTTTTTTACTGATAATAACTAACCCACGCCTC
Truncation at L93	SdiAf L93	CTTTAGTCAGGGCCATTAAATGTGGAATGATGAC
	SdiAr L93	GTCATCATTCCACATTTAATGGCCCTGACTAAAG
Truncation at A110	SdiAf A110	CAGCCGTTATGGGAAGCCTAACGCGCACATGGTTTACGC
	SdiAr A110	GCGTAAACCATGTGCGCGTTAGGCTTCCCATAACGGCTG
Truncation at L133	SdiAf L133	CAAACCGGGCGCTGGGCTTTTAATCCTTTTCCCGTTG
	SdiAr L133	CAACGGGAAAAGGATTAAAAGCCCAGCGCCCGGTTTG

Table 3 Partial whole-transcriptome profiles to determine the impact of SdiA1E11 and wild-type SdiA on biofilm formation. Partial list of the most differentially-expressed genes for biofilm cells of BW25113 *sdiA*/pCA24N-*sdiA* vs. BW25113 *sdiA*/pCA24N and BW25113 *sdiA*/pCA24N-*sdiA1E11* vs. BW25113 *sdiA*/pCA24N-*sdiA* grown in LB with 30 μg/mL chloramphenicol and 1 mM IPTG for 12 h at 30°C. Raw data for the two DNA microarrays are available using GEO series accession number GSE 11779. Primarily, genes differentially-expressed above 4-fold are shown although some related genes are shown for completeness.

		Fold change		
Gene	**b #**	**SdiA vs. no SdiA**	**SdiA1E11 vs. SdiA**	**Description**
sdiA	b1916	5043.0	-2.3	LuxR/UhpA family, regulation of cell division *ftsQAZ* genes, sensing AHLs and required for indole signaling.
Indole related genes				
tnaC	b3707	-22.6	16.0	tryptophanase leader peptide
tnaA	b3708	-7.5	6.5	tryptophanase
tnaB	b3709	-16.0	9.8	low affinity tryptophan permease
Fimbriae and curli genes				
sfmH	b0533	-2.3	4.6	fimbrial assembly protein
csgG	b1037	-21.1	3.2	curli production assembly/transport component
csgF	b1038	-36.8	4.3	curli production assembly/transport component
csgE	b1039	-24.3	3.7	curli production assembly/transport component, 2nd curli operon
csgD	b1040	-17.1	3.0	2-component transcriptional regulator for 2nd curli operon, family of LuxR/UhpA
csgB	b1041	-29.9	2.8	minor curlin subunit precursor
csgA	b1042	-17.1	2.6	curlin major subunit, coiled surface structures, cryptic
csgC	b1043	-10.6	3.2	putative curli production protein
yfcV	b2339	-2.0	4.0	putative fimbrial-like protein
AI-2 uptake genes				
lsrA	b1513	-7.0	3.0	autoinducer-2 (AI-2) uptake
lsrC	b1514	-4.9	3.0	autoinducer-2 (AI-2) uptake
lsrD	b1515	-5.3	3.5	autoinducer-2 (AI-2) uptake
lsrB	b1516	-13.9	3.2	autoinducer-2 (AI-2) uptake
lsrF	b1517	-9.8	4.0	function unknown, involved in AI-2 catabolism
lsrG	b1518	-7.5	3.0	function unknown, involved in AI-2 catabolism
Acid-resistance genes				
ariR	b1166	-4.9	3.7	AriR, regulator of acid-resistance influenced by indole
ymgC	b1167	-4.0	3.7	hypothetical protein in AriR operon
gadC	b1492	-14.9	3.0	glutamic acid decarboxylase
gadB	b1493	-32.0	3.5	glutamate decarboxylase isozyme
gadX	b3516	-5.7	2.5	putative ARAC-type regulatory protein
gadA	b3517	-21.1	3.5	glutamate decarboxylase A, isozyme, PLP-dependent
hdeB	b3509	-19.7	3.2	acid resistance protein HdeB
hdeA	b3510	-14.9	3.2	10K-L protein, periplasmic protein related to acid resistance protein
hdeD	b3511	-11.3	2.6	acid resistance protein HdeD

Table 3 Continued.

		Fold change		
Gene	**b #**	**SdiA vs. no SdiA**	**SdiA1E11 vs. SdiA**	**Description**
Cold shock and stress genes				
cspH	b0989	8.0	-4.0	cold shock protein CspH
cspG	b0990	4.9	-3.5	cold shock protein CspG
cspI	b1552	2.8	-4.0	cold shock protein CspI
cspB	b1557	5.3	-4.0	cold shock protein CspB
cspF	b1558	10.6	-4.9	cold shock protein CspF
rtT	b1228	8.0	-4.6	rtT RNA; may modulate the stringent response
katE	b1732	-5.7	2.1	catalase HPII
csiE	b2535	-7.0	4.0	stationary phase inducible protein
csiD	b2659	-14.9	3.7	carbon starvation-induced (*csi*) gene
uspB	b3494	-6.5	2.3	universal stress protein B
ibpB	b3686	4.0	1.1	16 kDa heat shock protein B
ibpA	b3687	5.3	-1.6	16 kDa heat shock protein A
oxyS	b4458	4.9	-4.0	global regulatory RNA OxyS
Metabolism and transport genes				
psiF	b0384	-7.5	2.5	phosphate starvation-inducible protein psiF precursor
queA	b0405	4.3	-2.6	S-adenosylmethionine:tRNA ribosyltransferase-isomerase
poxB	b0871	-6.1	1.6	pyruvate dehydrogenase/oxidase: FAD- and thiamine PPi-binding
agp	b1002	-6.1	4.9	acid glucose-1-phosphatase
potB	b1125	4.0	-2.5	spermidine/putrescine transport system permease protein
potA	b1126	4.6	-2.5	spermidine/putrescine transport ATP-binding protein
narY	b1467	-6.1	3.2	cryptic nitrate reductase 2 beta subunit
narZ	b1468	-8.0	4.3	cryptic nitrate reductase 2 alpha subunit
narU	b1469	-5.3	3.2	nitrite extrusion protein 2
osmC	b1482	-6.1	1.9	osmotically inducible protein C
osmE	b1739	-8.0	2.1	osmotically inducible lipoprotein E precursor
rnfB	b1628	4.0	-2.5	electron transport complex protein
astE	b1744	-8.6	4.6	succinylglutamate desuccinylase
astB	b1745	-12.1	4.3	succinylarginine dihydrolase
astD	b1746	-8.0	4.0	succinylglutamic semialdehyde dehydrogenase
astA	b1747	-13.9	4.6	arginine succinyltransferase
cstC	b1748	-12.1	4.9	succinylornithine transaminase
flu	b2000	-1.4	7.0	antigen 43 (Ag43) phase-variable biofilm formation autotransporter
fbaB	b2097	-8.6	2.8	fructose-bisphosphate aldolase class I
yojH	b2210	5.7	-2.6	malate:quinone oxidoreductase
tktB	b2465	-6.5	1.7	transketolase 2
gabD	b2661	-13.0	2.6	succinate-semialdehyde dehydrogenase [NADP+]
gabT	b2662	-13.0	3.5	4-aminobutyrate aminotransferase
gabP	b2663	-8.6	3.5	GABA permease

Table 3 Continued.

		Fold change		
Gene	**b #**	**SdiA vs. no SdiA**	**SdiA1E11 vs. SdiA**	**Description**
hycB	b2724	-3.5	4.6	formate hydrogenlyase subunit 2
hyuA	b2873	-2.6	4.0	phenylhydantoinase
ravA	b3012	-5.3	2.3	2,5-diketo-D-gluconic acid reductase A
glgS	b3049	-7.0	2.5	glycogen synthesis protein
secG	b3175	4.0	-2.6	protein-export membrane protein
rpsI	b3230	4.6	-2.6	30S ribosomal protein S9
rpsQ	b3311	4.6	-2.6	30S ribosomal protein S17
glpD	b3426	5.7	-4.9	sn-glycerol-3-phosphate dehydrogenase (aerobic)
ggt	b3447	-6.5	2.6	gamma-glutamyltranspeptidase
ugpB	b3453	-5.7	2.1	glycerol-3-phosphate-binding periplasmic protein precursor
ddpX	b1488	-7.5	3.0	D-Ala-D-Ala dipeptidase, Zn-dependent
dppF	b3540	-8.0	3.5	dipeptide transport ATP-binding protein
dppD	b3541	-8.0	3.5	dipeptide transport ATP-binding protein
dppC	b3542	-8.6	4.0	dipeptide transport system permease protein
aldB	b3588	-12.1	4.0	aldehyde dehydrogenase B (lactaldehyde dehydrogenase)
rnpA	b3704	4.3	-3.0	ribonuclease P protein component
bglF	b3722	4.3	2.6	glucoside PTS transporter
qor	b4051	-6.5	1.9	quinone oxidoreductase
actP	b4067	-17.1	5.3	acetate permease
acs	b4069	-10.6	4.6	acetyl-coenzyme A synthetase
melA	b4119	-6.1	2.6	alpha-galactosidase
blc	b4149	-6.1	2.1	outer membrane lipoprotein blc precursor
aidB	b4187	-6.1	2.0	AidB protein
ytfQ	b4227	-6.1	2.1	putative D-ribose transport protein (ABC superfamily, peri_bind)
treA	b1197	-7.5	2.8	periplasmic trehalase precursor
treC	b4239	4.3	-3.0	trehalose-6-phosphate hydrolase
treB	b4240	4.3	-3.0	PTS system, trehalose-specific IIBC component
Other genes				
rhlE	b0797	6.5	-3.7	putative ATP-dependent RNA helicase
rmf	b0953	9.8	2.6	hypothetical protein
sfa	b0991	4.9	-3.5	Sfa protein
wrbA	b1004	-16.0	3.2	flavoprotein WrbA
ftsT	b1569	-2.3	4.0	transcriptional repressor of cell division inhibition protein
hisL	b2018	2.3	-9.8	His operon leader peptide
fis	b3261	4.3	-2.3	DNA-binding protein Fis
slp	b3506	-14.9	1.9	outer membrane protein slp precursor
spf	b3864	4.9	-3.7	spot 42 RNA
phnB	b4107	-9.8	2.8	PhnB protein
mutL	b4170	-1.3	-4.3	MutHLS complex, enzyme in methyl-directed mismatch repair

Table 3 Continued.

		Fold change		
Gene	**b #**	**SdiA vs. no SdiA**	**SdiA1E11 vs. SdiA**	**Description**
isrB	b4434	6.1	-6.1	intergenic sequence sRNA
isrC	b4435	-1.3	4.0	intergenic sequence sRNA
micF	b4439	-7.0	2.1	regulatory antisense RNA affecting ompF expression
Hypothetical genes				
yahK	b0325	-5.7	2.6	hypothetical zinc-type alcohol dehydrogenase-like protein
yahO	b0329	-7.0	2.8	hypothetical protein
ybaS	b0485	-7.5	2.3	probable glutaminase YbaS
ybaT	b0486	-6.5	2.5	hypothetical transport protein
ybcL	b0545	-5.3	2.6	DLP12 prophage
ybgA	b0707	-5.3	2.3	hypothetical protein
ybgS	b0753	-9.2	2.8	hypothetical protein
ybhB	b0773	-5.3	2.1	hypothetical protein
ybiY	b0824	-2.5	4.3	putative pyruvate formate-lyase 3 activating enzyme
ybjP	b0865	-7.0	1.7	putative lipoprotein
ycaC	b0897	-9.8	4.9	hypothetical protein
ycgB	b1188	-9.8	2.8	hypothetical protein
ychH	b1205	-6.5	2.5	hypothetical protein
yciD	b1256	-9.8	2.5	hypothetical protein
yciL	b1269	4.0	-2.8	hypothetical protein
ydfK	b1375	6.1	-4.0	hypothetical protein
ynaF	b1376	-5.7	1.7	hypothetical protein
ydbC	b1406	-5.7	3.0	hypothetical protein
ydcJ	b1423	-8.6	4.0	hypothetical protein
ydcS	b1440	-13.9	4.6	putative ABC transporter Periplasmic binding protein
ydcT	b1441	-11.3	5.7	putative ABC transporter ATP-binding protein
ydcU	b1442	-7.5	3.2	hypothetical ABC transporter permease protein
ydcV	b1443	-8.0	3.7	hypothetical ABC transporter
ydcW	b1444	-12.1	5.7	putative betaine aldehyde dehydrogenase
yddJ	b1470	-2.6	4.6	hypothetical protein
yddS	b1487	-6.1	3.0	putative ABC transport system periplasmic binding protein
ydeI	b1536	-5.7	3.5	hypothetical protein
ydgN	b1629	4.6	-2.6	electron transport complex protein
ydiM	b1690	-3.2	4.3	putative transport protein (MFS family)
ydjN	b1729	4.6	-2.1	hypothetical symporter
yeaH	b1784	-8.6	2.8	hypothetical protein
yedP	b1955	-5.3	2.3	hypothetical protein
yedU	b1967	-8.6	2.5	hypothetical protein
yeeF	b2014	5.7	-2.1	hypothetical protein
yegP	b2080	-6.5	2.3	hypothetical protein
yehE	b2112	-6.1	1.6	hypothetical protein

Table 3 Continued.

		Fold change		
Gene	**b #**	**SdiA vs. no SdiA**	**SdiA1E11 vs. SdiA**	**Description**
yohC	b2135	-5.7	2.8	hypothetical protein
yeiN	b2165	-3.0	4.3	hypothetical protein
ygaF	b2660	-9.8	2.6	hypothetical protein
ygaQ	b2654	-2.6	4.0	hypothetical protein
ygaR	b2655	-2.3	4.0	hypothetical protein
yqaD	b2658	-2.3	4.0	hypothetical protein
ygaM	b2672	-7.5	2.1	hypothetical protein
ygdI	b2809	-6.1	1.7	hypothetical protein
ygeL	b2856	-1.4	4.0	predicted DNA-binding transcriptional regulator
ygeN	b2857	-2.1	4.0	hypothetical protein
yqjE	b3099	-5.7	-1.5	hypothetical protein
yhbC	b3170	3.5	-4.0	hypothetical protein
yhbE	b3184	4.6	-3.5	hypothetical protein
yhdG	b3260	4.3	-2.5	hypothetical protein
yhiE	b3512	-12.1	2.8	hypothetical protein
yjcH	b4068	-24.3	5.7	hypothetical protein
yjdI	b4126	-6.5	1.5	hypothetical protein
yjdJ	b4127	-5.3	2.0	hypothetical protein

Table 4A 96-well plate biofilm raw data of Fig. 2A and specific growth rates in LB medium in shake flasks. Bacterial cell growth (turbidity at 620 nm) and total biofilm formation (OD at 540 nm) for BW25113 *sdiA* cells expressing the SdiA variants in LB and LB glu medium after 8 h at 30°C. Biofilm/cell growth was normalized with data of BW25113 *sdiA* cells expressing wild-type SdiA. WT indicates wild-type. Specific growth rates were found in LB at 30°C.

Specific growth rates, cell growth, and total biofilm in LB after 8 h							
Strains	WT /pCA24N	*sdiA* /pCA24N	*sdiA* /WTSdiA	*sdiA* /SdiA1E11	*sdiA* /SdiA16G12	*sdiA* /SdiA14C3	*sdiA* /SdiA2D10
specific growth rate*, h^{-1}	0.94 ± 0.01	0.97 ± 0.05	0.76 ± 0.05	0.87 ± 0.02	0.89 ± 0.02	0.90 ± 0.02	0.82 ± 0.02
cell growth	0.49 ± 0.01	0.54 ± 0.02	0.39 ± 0.01	0.25 ± 0.02	0.40 ± 0.01	0.36 ± 0.07	0.43 ± 0.01
total biofilm	0.03 ± 0.01	0.55 ± 0.07	0.11 ± 0.02	0.02 ± 0.01	0.02 ± 0.01	0.12 ± 0.01	0.06 ± 0.01
biofilm/cell	0.06 ± 0.02	1.02 ± 0.13	0.29 ± 0.05	0.06 ± 0.01	0.04 ± 0.01	0.34 ± 0.02	0.14 ± 0.03
relative normalized biofilm	0.19 ± 0.06	3.5 ± 0.5	1.0 ± 0.2	0.20 ± 0.05	0.14 ± 0.05	1.16 ± 0.07	0.5 ± 0.1
Cell growth and total biofilm in LB glu after 8 h							
Strains	WT /pCA24N	*sdiA* /pCA24N	*sdiA* /WTSdiA	*sdiA* /SdiA1E11	*sdiA* /SdiA16G12	*sdiA* /SdiA14C3	*sdiA* /SdiA2D10
cell growth	0.75 ± 0.02	0.81 ± 0.02	0.47 ± 0.02	0.40 ± 0.02	0.64 ± 0.02	0.52 ± 0.09	0.57 ± 0.03
total biofilm	0.03 ± 0.01	0.48 ± 0.04	0.09 ± 0.01	0.01 ± 0.01	0.01 ± 0.01	0.10 ± 0.02	0.06 ± 0.01
biofilm/cell	0.03 ± 0.01	0.59 ± 0.05	0.19 ± 0.03	0.03 ± 0.01	0.02 ± 0.00	0.20 ± 0.05	0.11 ± 0.03
relative normalized biofilm	0.18 ± 0.03	3.1 ± 0.2	1.0 ± 0.2	0.15 ± 0.03	0.10 ± 0.02	1.1 ± 0.2	0.6 ± 0.2

Table 4B 96 well plate biofilm raw data of Fig. 2B. Bacterial cell growth (turbidity at 620 nm) and total biofilm formation (OD at 540 nm) for BW25113 *sdiA* cells expressing the SdiA variants in LB and LB glu medium after 24 h at 30°C. Biofilm/cell growth was normalized with data of BW25113 *sdiA* cells expressing wild-type SdiA. WT indicates wild-type.

Cell growth and total biofilm in LB after 24 h							
Strains	WT /pCA24N	*sdiA* /pCA24N	*sdiA* /WTSdiA	*sdiA* /SdiA1E11	*sdiA* /SdiA16G12	*sdiA* /SdiA14C3	*sdiA* /SdiA2D10
cell growth	0.79 ± 0.02	1.06 ± 0.01	0.89 ± 0.01	0.56 ± 0.04	0.83 ± 0.05	1.08 ± 0.15	0.95 ± 0.03
total biofilm	0.52 ± 0.02	1.12 ± 0.04	1.02 ± 0.08	0.15 ± 0.02	0.53 ± 0.07	0.28 ± 0.04	0.76 ± 0.02
biofilm/cell	0.66 ± 0.03	1.06 ± 0.04	1.15 ± 0.09	0.26 ± 0.04	0.63 ± 0.09	0.26 ± 0.05	0.80 ± 0.04
relative normalized biofilm	0.57 ± 0.02	0.92 ± 0.04	1.00 ± 0.07	0.22 ± 0.03	0.55 ± 0.07	0.23 ± 0.03	0.70 ± 0.07
Cell growth and total biofilm in LB glu after 24 h							
Strains	WT /pCA24N	*sdiA* /pCA24N	*sdiA* /WTSdiA	*sdiA* /SdiA1E11	*sdiA* /SdiA16G12	*sdiA* /SdiA14C3	*sdiA* /SdiA2D10
cell growth	0.64 ± 0.05	0.84 ± 0.03	0.83 ± 0.04	0.68 ± 0.02	0.86 ± 0.02	0.64 ± 0.02	0.85 ± 0.03
total biofilm	0.11 ± 0.02	0.43 ± 0.09	0.52 ± 0.02	0.02 ± 0.01	0.09 ± 0.06	0.06 ± 0.02	0.15 ± 0.03
biofilm/cell	0.16 ± 0.03	0.50 ± 0.09	0.63 ± 0.02	0.03 ± 0.01	0.08 ± 0.09	0.10 ± 0.05	0.18 ± 0.03
relative normalized biofilm	0.25 ± 0.05	0.8 ± 0.1	1.00 ± 0.02	0.05 ± 0.02	0.1 ± 0.1	0.16 ± 0.08	0.29 ± 0.05

Table 5. 96 well plate biofilm raw data of Fig. 3. Bacterial cell growth (turbidity at 620 nm) and total biofilm formation (OD at 540 nm) for BW25113 *sdiA* cells expressing the SdiA2D10 in LB glu medium in the presence of nine AHLs after 24 h at 30°C. Biofilm/cell growth was normalized based on variant SdiA2D10 without AHLs (either with addition of water or dimethylformamide, DMF, depending on the diluent used for the AHL). C4-*DL*-HSL, C6-*DL*-HSL, C8-*DL*-HSL, and C4-*L*-HSL were dissolved in water. C10-*DL*-HSL, C12-*DL*-HSL, 3o-C8-*L*-HSL, 3o-C12-*L*-HSL, and 3o-C14-*L*-HSL were dissolved in DMF.

AHLs	H_2O	C4-*DL*-HSL	C6-*DL*-HSL	C8-*DL*-HSL	C4-*L*-HSL
cell growth	0.85 ± 0.03	0.64 ± 0.03	0.60 ± 0.04	0.72 ± 0.06	0.67 ± 0.02
total biofilm	0.15 ± 0.03	0.10 ± 0.02	0.5 ± 0.2	0.9 ± 0.2	0.58 ± 0.09
biofilm/cell	0.18 ± 0.03	0.16 ± 0.03	0.8 ± 0.2	1.3 ± 0.2	0.9 ± 0.1
relative normalized biofilm	1.0 ± 0.2	0.9 ± 0.2	4.7 ± 1.4	7.3 ± 1.6	4.9 ± 1.1

AHLs	DMF	C10-*DL*-HSL	C12-*DL*-HSL	3o-C8-*L*-HSL	3o-C12-*L*-HSL	3o-C14-*L*-HSL
cell growth	0.89 ± 0.05	0.87 ± 0.04	0.83 ± 0.03	0.63 ± 0.03	0.96 ± 0.02	0.82 ± 0.03
total biofilm	0.22 ± 0.03	1.25 ± 0.08	1.1 ± 0.1	0.4 ± 0.1	1.59 ± 0.06	0.73 ± 0.06
biofilm/cell	0.24 ± 0.04	1.43 ± 0.08	1.3 ± 0.1	0.7 ± 0.1	1.66 ± 0.07	0.88 ± 0.08
relative normalized biofilm	1.0 ± 0.2	5.9 ± 1.1	5.3 ± 1.0	2.7 ± 0.7	6.8 ± 1.2	3.6 ± 0.7

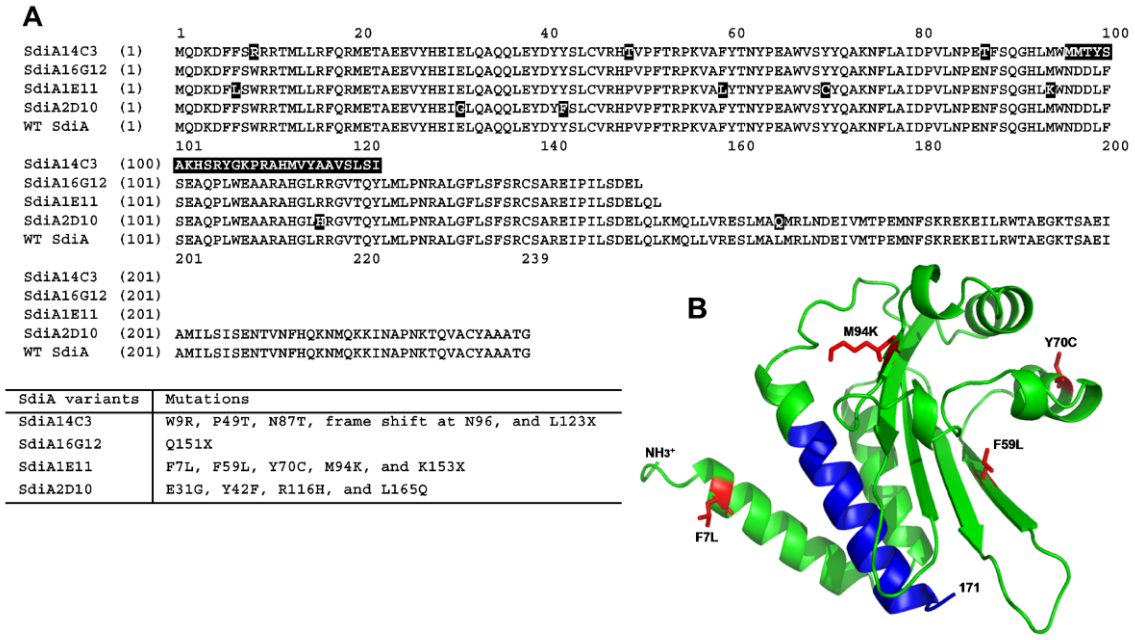

SdiA variants	Mutations
SdiA14C3	W9R, P49T, N87T, frame shift at N96, and L123X
SdiA16G12	Q151X
SdiA1E11	F7L, F59L, Y70C, M94K, and K153X
SdiA2D10	E31G, Y42F, R116H, and L165Q

Figure 1 Protein sequence and structure of SdiA variants. Protein sequences of the SdiA error-prone PCR variants (A). Amino acid changes are indicated by black highlight. SdiA14C3 has a frame shift at N96 due to the deletion of one base pair. Modeled protein structure of SdiA1E11 (B). Truncated region (residues 153-171) is shown as a blue ribbon, and the mutations (F7L, F59L, Y70C, and M94K) are shown in red. WT indicates wild-type.

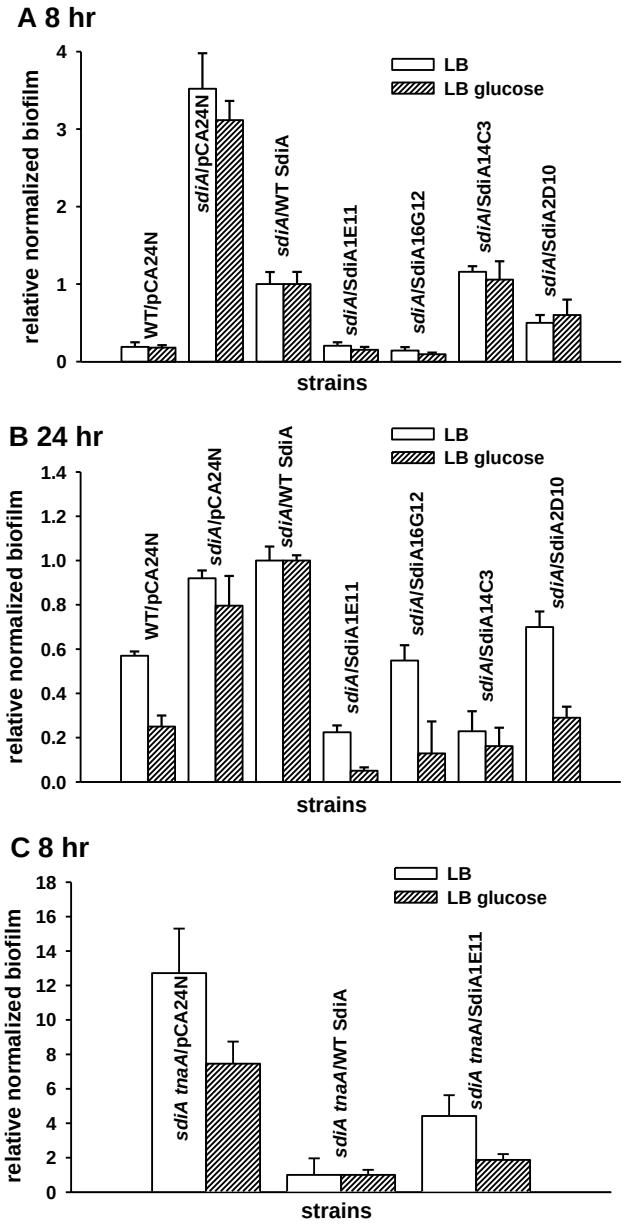

Figure 2 Biofilm formation with SdiA variants. Relative biofilm formation in the presence of endogenous indole and normalized by bacterial growth (turbidity at 620 nm) for BW25113 *sdiA* cells expressing the SdiA variants in LB and LB glu medium after 8 h (A) and after 24 h (B) (raw data are shown in Table 4A and 4B), and relative biofilm formation normalized by bacterial growth (turbidity at 620 nm) for BW25113 *sdiA tnaA* cells expressing wild-type SdiA and SdiA1E11 after 8 h (C) at 30°C. No extracellular signal was added. Normalized biofilm data are relative to BW25113 *sdiA*/pCA24N-*sdiA*. Each data point is the average of at least twelve replicate wells from two independent cultures, and one standard deviation is shown. SdiA was expressed using 1 mM IPTG.

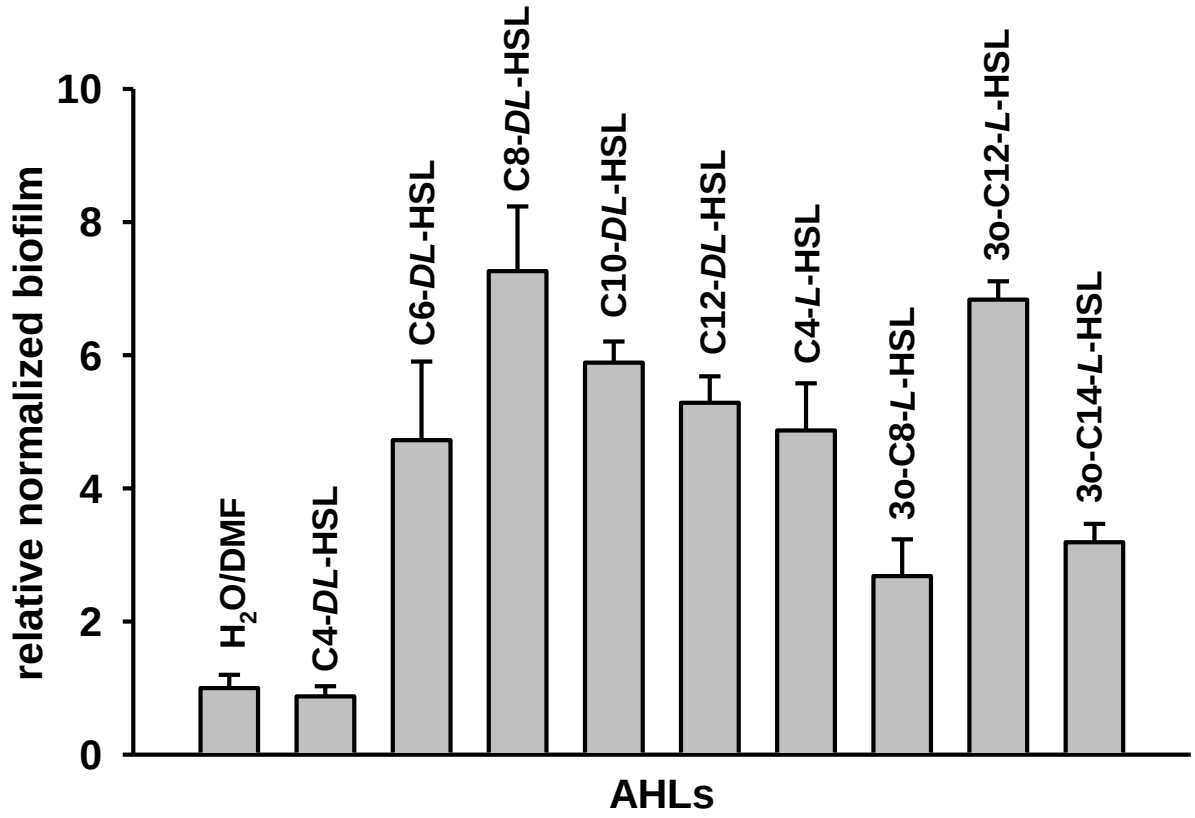

Figure 3 Biofilm formation with SdiA2D10 in the presence of AHLs. Relative biofilm formation in LB glu medium after 24 h at 30°C for BW25113 *sdiA* cells expressing SdiA2D10 in the presence of added AHLs and with endogenous indole. Biofilm formation was normalized by bacterial growth (turbidity at 620 nm) and is relative to cells without added AHLs. C4-*DL*-HSL, C4-*L*-HSL, C6-*DL*-HSL, and C8-*DL*-HSL were dissolved in water, and C10-*DL*-HSL, C12-*DL*-HSL, 3o-C8-*L*-HSL, 3o-C12-*L*-HSL, and 3o-C14-*L*-HSL were dissolved in DMF. AHLs were added at the beginning of culturing. Raw data are shown in Table 5. Each data point is the average of at least twelve replicate wells from two independent cultures, and one standard deviation is shown. SdiA2D10 was expressed using 1 mM IPTG.

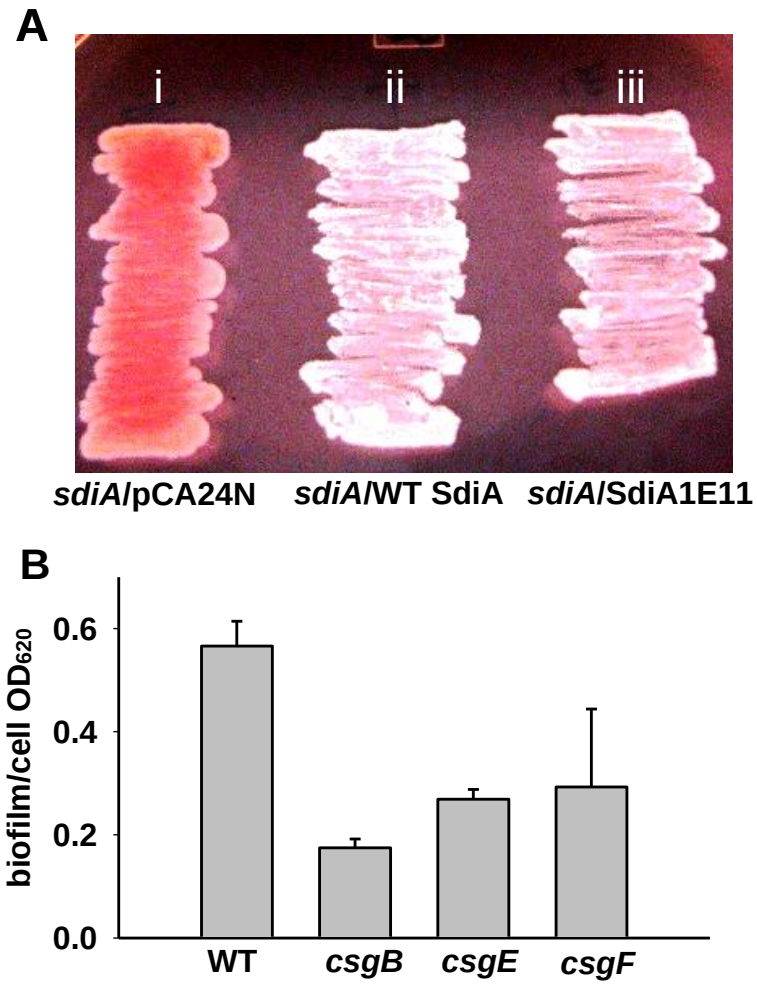

Figure 4 Curli production with SdiA1E11 and biofilm formation of csgB, csgE, and csgF knockout mutants. BW25113 *sdiA* cells expressing no SdiA (empty vector) (i), wild-type SdiA (ii), and SdiA1E11 (iii) on a Congo red plate after 28 h in LB at 30ºC (A). Biofilm formation of BW25113, BW25113 *csgB*, BW25113 *csgE*, BW25113 *csgF* in LB at 30ºC after 24 h (B).

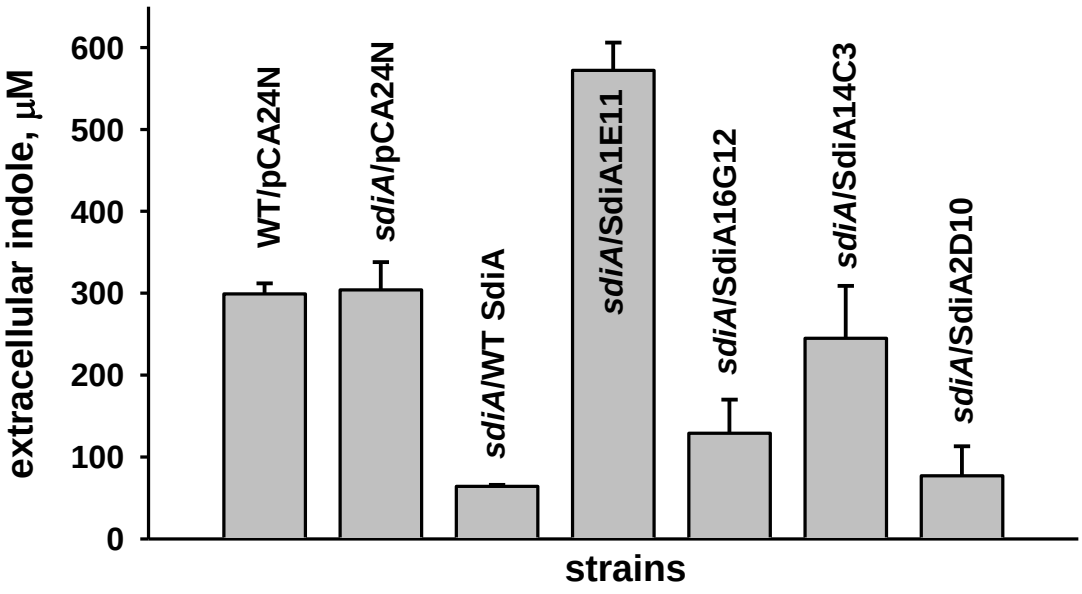

Figure 5 Production of extracellular indole with SdiA variants. BW25113 *sdiA* cells expressing the SdiA variants were grown at a cell density of 3.0. Each experiment was repeated at least two times, and one standard deviation is shown. SdiA was expressed using 1 mM IPTG.

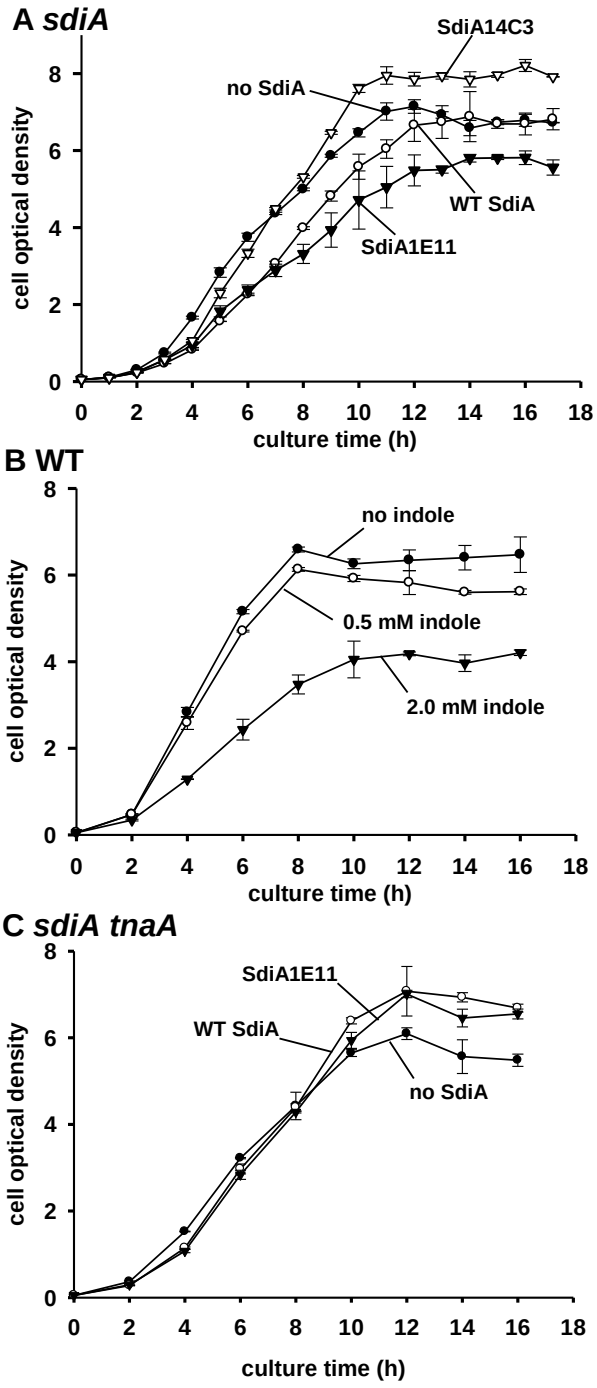

Figure 6 G**rowth of cells producing SdiA variants**. Growth in LB at 30°C for BW25113 *sdiA* cells expressing the SdiA variants (A), BW25113 cells in the presence of indole (0, 0.5, and 2.0 mM) (B), and BW25113 *sdiA tnaA* cells expressing wild-type SdiA and SdiA1E11 (C). Each data point is the average of at least two independent cultures. SdiA was expressed using 1 mM IPTG.

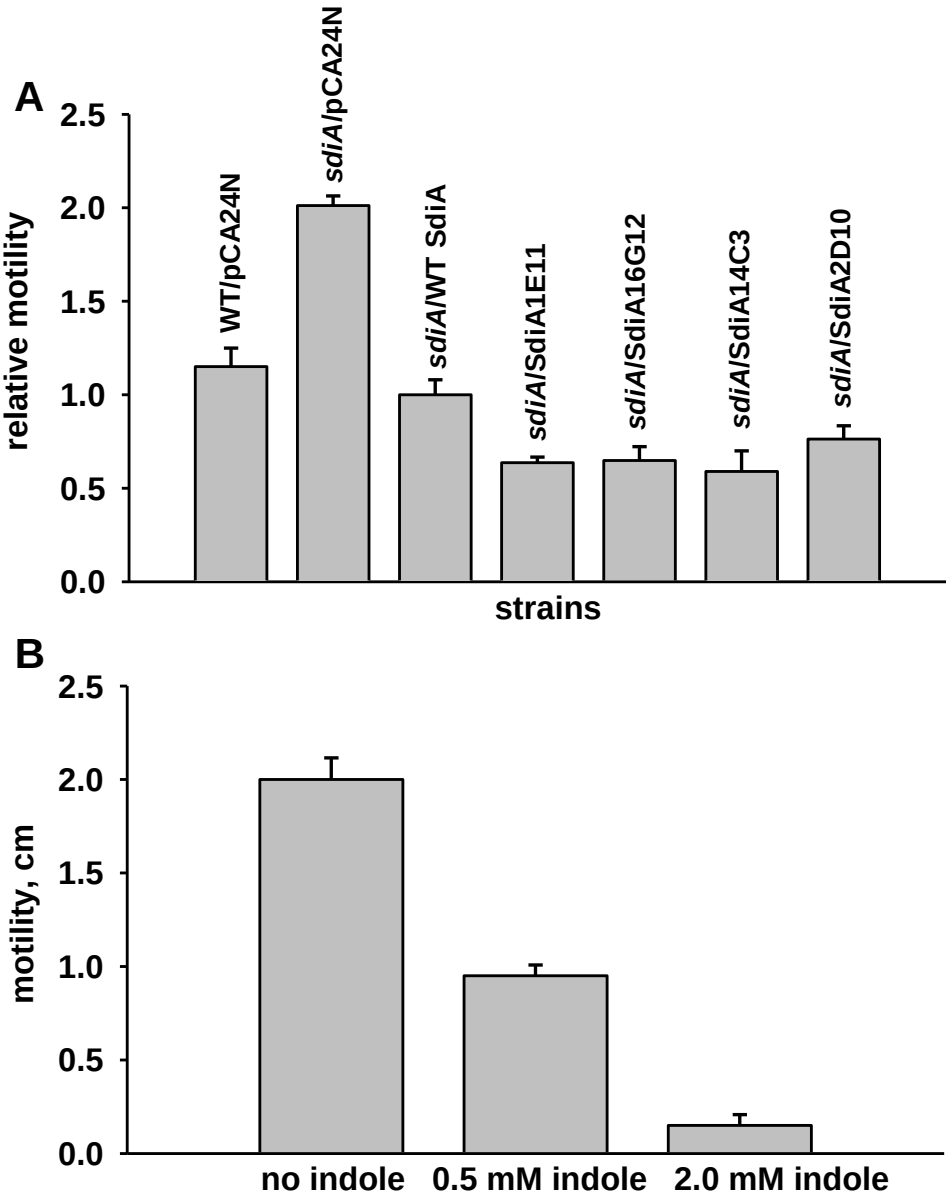

Figure 7 Swimming motility of cells producing SdiA variants. Swimming motility of BW25113 *sdiA* cells expressing the SdiA variants (A) and BW25113 cells in the presence of indole (0, 0.5, and 2.0 mM) (B) after 20 h at 30^{o}C. Each experiment was repeated two times, and one standard deviation is shown. SdiA was expressed using 1 mM IPTG.

VITA

Name: Seok Hoon Hong

Address: Texas A&M University, Department of Chemical Engineering, 3122 TAMU, College Station, TX 77843-3122

Email: s98hong@neo.tamu.edu

Education: B.S., Chemical and Biological Engineering, Seoul National University, 2005

M.S., Chemical and Biological Engineering, Seoul National University, 2007

Ph.D., Chemical Engineering, Texas A&M University, 2011